UNIVERSITY OF CALIFORNIA SAN DIEGO

Clicks and Currents: Leveraging Passive Acoustic Data to Advance Understanding of Toothed Whale Ecology Relative to the Gulf Stream

A dissertation submitted in partial satisfaction of the requirements
for the degree Doctor of Philosophy
in

Oceanography

by

Rebecca Cohen

Committee in charge:

John Hildebrand, Co-Chair
Kaitlin Frasier, Co-Chair
Andrew Barton
Simone Baumann-Pickering
Elsa Cleland
Bruce Cornuelle

2022

The Dissertation of Rebecca E. Cohen is approved, and it is acceptable in quality and form for publication on microfilm and electronically.

University of California San Diego

2022

DEDICATION

For my daughter, Samara.

EPIGRAPH

"All models are wrong, but some are useful."

George Box

TABLE OF CONTENTS

LIST OF FIGURES

LIST OF TABLES

ACKNOWLEDGEMENTS

Pursuing a PhD has been a truly formative experience, and would not have been possible without the guidance, expertise, love, support and patience of a diverse host of people. Many thanks to my primary scientific advisors, mentors, and models – John Hildebrand, Kait Frasier, and Simone Baumann-Pickering. The work you do has been, and continues to be, an inspiration to me, both personally and professionally. Thanks also to the remainder of my committee – Andrew Barton, Bruce Cornuelle, and Elsa Cleland – who took a lot of time to provide feedback and suggestions on my work at all stages, and contribute their highly-valued perspectives and expertise. And to David Holway, who acted as a committee member for three years, and would've been on my final defense committee if circumstances had allowed. I was also lucky enough to work alongside and learn from a number of highly skilled researchers and engineers who make our lab's work possible: Sean Wiggins, Ally Rice, Jenny Trickey, Bruce Thayre, John Hurwitz, Erin O'Neill, and Ryan Griswold. These folks exposed me to many practical aspects of device development, testing, deployment, and retrieval, data collection and processing, data analysis, and scientific cruise logistics, all of which gave me a greater appreciation for the collaborative nature of marine bioacoustics research and made me a more well-rounded scientist.

I didn't realize what an important role post-doctoral scholars play in supervising doctoral students until I got the chance to interact with a number of brilliant postdocs as they moved through my lab and adjacent labs. Jack Butler, Goldie Philips, Alba Solsona Berga, and Annebelle Kok – thanks for always being open to discussions of bioacoustics, marine acoustics, and statistics at the very limits of my understanding, and somehow never once making me feel stupid for not already knowing something. I hope to do the same for others as I transition into a postdoc role myself. Many thanks to my predecessors and peers in the Scripps Whale Acoustics Lab, Scripps Acoustic Ecology Lab, and Scripps Machine Listening Lab: Josh Jones, Anne Simonis, Regina Guazzo, Camille Pagniello,

Ashlyn Giddings, Natalie Posdaljian, Eric Snyder, Morgan Ziegenhorn, Vanessa Zobell, Michaela Alksne, Ella Kim, Eva Hidalgo Pla, Shelby Bloom, and Catalina Aguilar. I was so lucky to learn with and from you all, and to work alongside such a wonderful group of people, and I look forward to many future collaborations. And to my two undergraduate interns – Amanda Leu and Lauren Baggett – both of whom went on to the Master's program: thanks for letting me learn by teaching, and for all that you contributed to my dissertation research. I can't wait to see where both of you take your careers.

Outside my immediate lab group, I benefitted enormously from the brilliant and supportive SIO community. Thanks to Peter Franks for being a mentor and guide during those first rocky years of grad school (in addition to teaching the best courses!). To Brett Pickering for letting me tag along on some small boat and ship operations and creating great learning opportunities for me and so many other students. To everyone who participated in the SIO Machine Learner's Group and embraced my idea of a forum for discussion and learning about shared ML techniques. And to all of the SIO Department administrators who keep our programs running, especially Gilbert Bretado, who works tirelessly for us students year in and year out.

My path to a PhD was not very direct, but it was always interesting. So much of what I've accomplished is a direct product of the steadfast support and encouragement of my parents, Marie and Martin Cohen. Their unflappable certainty that I would find my own path gave me the confidence to do just that. And of course Vladimir, my partner, cheerleader, support, advisor, comic relief, reality check, advocate, co-parent, and love. Thank you for sustaining me through this marathon degree, and for so fully embracing my career aspirations. I'm so excited and grateful to be on this journey with you.

Chapter 2, in full, is a reprint of the material as it appears in Cohen, R.E., K.E. Frasier, S. Baumann-Pickering, S.M. Wiggins, M.A. Rafter, Baggett, L.M., J.A. Hildebrand. (2022). Identification of western North Atlantic odontocete echolocation click types using machine learning and spatiotemporal correlates. PLOS One 17(3): e0264988. The dissertation author was the primary investigator and author of this paper.

Chapter 3, in full, has been submitted for publication of the material as it may appear in Science Advances. Cohen, R.E., Frasier, K.E., Baumann-Pickering, S., Hildebrand, J.A. Spatial and temporal separation of toothed whales in the western North Atlantic. The dissertation author was the primary researcher and author of this paper.

Chapter 4, in full, is currently being prepared for submission for publication of the material. Cohen, R.E., Baggett, L.M., Frasier, K.E., Baumann-Pickering, S., Hildebrand, J.A. The role of the Gulf Stream in niche partitioning of toothed whales in the western North Atlantic. The dissertation author was the primary researcher and author of this material.

VITA

2007 Bachelor of Arts in Italian Literary and Cultural Studies, University of Connecticut
2016 Bachelor of Science in Biology, CUNY Brooklyn College
2019 Master of Science in Marine Biology, University of California San Diego
2022 Doctor of Philosophy in Oceanography, University of California San Diego

PUBLICATIONS

Cohen, RE, KE Frasier, S Baumann-Pickering, SM Wiggins, MA Rafter, JA Hildebrand. (2022). Identification of western North Atlantic odontocete echolocation click types using machine learning and spatiotemporal correlates. PLOS One 17(3): e0264988. https://doi.org/10.1371/journal.pone.0264988.

Cohen, RE, CC James, A Lee, MM Martinelli, WT Muraoka, M Ortega, R Sadowski, L Starkey, AR Szesciorka, SE Timko, EL Weiss and PJS Franks. (2018). Marine host-pathogen dynamics: influences of global climate change. Oceanography 31(2), DOI: https://doi.org/10.5670/oceanog.2018.201.

Frasier, KE, **RE Cohen**, JS Trickey, SM Wiggins, A Solsona Berga, MS Soldevilla, L Garrison, S Baumann-Pickering, JA Hildebrand. (2017). Echolocation for restoration: Odontocete monitoring in the Gulf of Mexico. The Journal of the Acoustical Society of America 142(4):2533-2533. DOI: 10.1121/1.5014257.

ABSTRACT OF THE DISSERTATION

Clicks and Currents: Leveraging Passive Acoustic Data to Advance Understanding of Toothed Whale Ecology Relative to the Gulf Stream

by

Rebecca E. Cohen

Doctor of Philosophy in Oceanography

University of California San Diego, 2022

Professor John A, Hildebrand, Co-Chair
Dr. Kaitlin E. Frasier, Co-Chair

The western North Atlantic is a dynamic region characterized by the Gulf Stream western boundary current and inhabited by a diverse host of odontocete, or toothed whale, top predators. Their habitats are highly exploited by commercial fisheries, shipping, marine energy extraction, and naval exercises, subjecting them to a variety of potentially harmful interactions. Many of these species remain poorly understood due to the difficulties of observing them in the pelagic environment. Their habitat utilization and the impacts of anthropogenic activities are not well known. Over the past decade, passive acoustic data has become increasingly utilized for the study of a wide variety of marine animals, and offers several advantages over traditional line-transect visual survey methods. Passive acoustic devices can be deployed at offshore monitoring sites for long periods of time, enabling detection of even rare and cryptic species across seasons and sea states, and without altering animal behaviors. Here we utilized a large passive acoustic data set collected across a latitudinal

habitat gradient in the western North Atlantic to address fundamental knowledge gaps in odontocete ecology. I approached the problem of discriminating between species based on spectral and temporal features of echolocation clicks by using machine learning to identify novel click types, and then matching these click types to species using spatiotemporal correlates. I was able to identify novel click types associated with short-beaked common dolphins, Risso's dolphins, and short-finned pilot whales in this way. Next I characterized temporal patterns in presence and activity for ten different species across our monitoring sites at three different temporal scales: seasonal, lunar, and diel. I observed spatiotemporal separation of apparent competitors, and complex behavioral patterns modulated by interactions between the seasonal, lunar, and diel cycles. Finally I investigated the relationships between species presence and oceanographic covariates to predict habitat suitability across the region, and explored niche partitioning between potentially competitive species. The insights gained here significantly advance our understanding of toothed whale ecology in this region, and can be used for more effective population assessments and management in the face of anthropogenic threats and climate change.

1 INTRODUCTION

For centuries whales have captured human interest and imagination as monstrous leviathans, symbols of cultural and religious significance, valuable commercial resources, entertaining acrobatic performers, irksome competitors for fisheries resources, and more. Public perception of whales underwent a fundamental shift in the early 1970's when the complex acoustic repertoires of humpback whales were first described [1], earning them an additional reputation as mysterious singers of the deep, but it had long been known among seafarers that whales produce a variety of sounds [2]. Acoustic studies of whales only became possible beginning in the 1950's thanks to improvements in underwater sound acquisition technology pioneered by the U.S. Navy as part of ongoing efforts to detect enemy submarines [3,4]. Since then much work has been done to advance both the technology enabling marine bioacoustics studies, and our understanding of the use and importance of sound to marine organisms from many taxa (see [5,6] for examples). Given this long-standing fascination with whales and sound, it's surprising how much remains to be learned about the fundamental ecology of so many cetacean species.

Cetaceans can be divided into two broad groups, Mysticeti and Odontoceti, based on divergent evolutionary pathways [7]. Mysticetes are commonly known as "baleen whales" for their unique filter feeding apparatus, while odontocetes, distinguished by retention of the ancestral toothed condition, are known as "toothed whales". Odontocetes are additionally distinguished by their complex social structures [8–10], sophisticated foraging strategies [11–19], and, perhaps most importantly, the development of biosonar [13,20]. Biosonar consists of the emission of sound pulses (termed "clicks" when referring to odontocete echolocation) and subsequent reception and interpretation of the echoes resulting from incidence of those sound pulses upon surfaces with differing acoustic impedance than the surrounding media. Light attenuates quickly in water due to absorption and scattering, but water's characteristic high density makes it an excellent medium for transmission of sound pressure. All

odontocete species exploit this characteristic of their marine environment by using echolocation for foraging and environmental sensing [13,21], and some species use clicks for communicatory purposes as well [22–25]. Since odontocetes and bats are the only animals known to echolocate, detection of echolocation clicks in marine acoustic data can be used to infer odontocete presence. Much work has been done on discriminating between odontocete species based on the spectral (frequency content) and temporal characteristics of their clicks, uncovering species-specific click types for a number of beaked whales, sperm whales, pygmy and dwarf sperm whales, porpoises, and a few dolphins (e.g. [26–34]). But many dolphin species still remain acoustically indistinguishable due to high levels of intra-individual and intraspecific variability, and interspecific overlap, which has limited the utilization of passive acoustic data for the detection and assessment of dolphins at the species level.

The western North Atlantic hosts a particularly large and diverse array of cetaceans, including six mysticete species and more than two dozen odontocete species. All odontocete species are top predators, and their large body sizes, thermoregulation, and active lifestyles necessitate calorically-rich diets [35–38]. Combined with large populations, odontocetes are responsible for the consumption of huge quantities of mid- and upper-trophic level organisms, estimated at 33-54 million tons annually in the North Atlantic [39]. Just in the southern New England and mid-Atlantic Bight regions, toothed whales are estimated to consume >225,000 tons of squid each year [40]. It has been posited that, as a function of their large populations and enormous consumption of biomass, whales also contribute to nutrient recycling, upper ocean productivity, and ultimately carbon sequestration in a process dubbed "the whale pump" [41–43].

While these estimates of the ecological importance of toothed whales are certainly impressive, they are only rough sketches based on a small handful of species for which we have sufficient data to characterize foraging ecology and estimate population sizes and energetic needs. Most odontocete species are data deficient owing to the difficulty of observing highly mobile species with low densities over their vast pelagic ranges, seasonally variable distribution patterns, and often prolonged diving

behavior and cryptic surface presence. For many species of dolphin and beaked whales we know little about distribution or abundance, habitat suitability, foraging ecology, acoustic behavior, etc. In the US these data gaps are of practical concern in light of the Marine Mammal Protection Act (1972), which mandated assessment, management, and protection of all cetacean species inhabiting US exclusive economic zone (EEZ) waters. The National Marine Fisheries Service (NMFS), an office of the National Oceanic and Atmospheric Administration (NOAA), invests substantial resources to regularly assess all marine mammal stocks, including estimates of abundance and mortality and identification of threats to each stock. For odontocete species these assessments are often based on sparse data aggregated over many years, and lack the temporal resolution to identify seasonal patterns in distribution or interannual trends in population size. Additionally, owing to the difficulties of visually distinguishing between species with similar morphologies, most of the beaked whale species are unable to be resolved to the species level, leaving these species to be managed as a homogeneous group.

The oceanography of the western North Atlantic is dominated by the Gulf Stream, a powerful western boundary current responsible for high volume transport of warm equatorial waters to higher latitudes [44], balancing global heat budgets and moderating the climate of western Europe [45]. In the western half of the basin, the Gulf Stream acts as a dynamic frontal boundary delineating two distinct ecoregions, and contributes to the formation of surface and intermediate water masses [46–49]. The Gulf Stream also constitutes the final surface leg of the Atlantic meridional overturning circulation (AMOC); variability in the AMOC has been correlated with variability in the transport and position of the Gulf Stream north wall [50,51]. Ecological communities differ across the frontal wall, and variability in Gulf Stream position has been observed to translate directly to changes in the distributions of organisms tracking particular oceanic conditions [52–54]. This region is also highly exploited by humans for fisheries, commercial shipping, and marine energy extraction. Natural habitat variability driven by the Gulf Stream, changes in global circulation and Gulf Stream dynamics as a

result of anthropogenically-induced climate change, and interactions with anthropogenic exploitation of marine resources are all likely to impact the odontocete species which inhabit the western North Atlantic. Management in the face of such threats requires better knowledge of the status and ecology of these populations. Thanks to the advances in marine bioacoustics outlined above, we are now poised to uncover such knowledge.

In this dissertation I address several aspects of odontocete ecology in the western North Atlantic, starting with the most basic of questions: who's who? In second chapter I utilized a large passive acoustic data set collected from 11 shelf break and slope monitoring sites over a 3-year study period to identify novel odontocete click types and expand the catalog of known species-specific click types. The time series of odontocete species presence derived in this chapter set the stage for ecological studies of these species across a larger region, and with finer temporal resolution and species resolution, than has previously been possible in this study area. In Chapter 3 I characterized temporal patterns in odontocete species presence at our monitoring sites at three spatial scales: seasonal, lunar, and diel. I additionally investigate complex interactions between these cycles with differing periods to uncover previously un-described variability in diel activity patterns. Finally, in Chapter 4 I explored the relationships between species presence and a number of environmental covariates to gain new insights into niche partitioning of this large guild of top predators, and generate predictive maps of habitat suitability with improved seasonal coverage. Taken together, these studies substantially advance our understanding of odontocete species ecology in this dynamic region, and offer tools for further research.

2 IDENTIFICATION OF WESTERN NORTH ATLANTIC ODONTOCETE ECHOLOCATION CLICK TYPES USING MACHINE LEARNING AND SPATIOTEMPORAL CORRELATES

2.1 ABSTRACT

A combination of machine learning and expert analyst review was used to detect odontocete echolocation clicks, identify dominant click types, and classify clicks in 32 years of acoustic data collected at 11 autonomous monitoring sites in the western North Atlantic between 2016 and 2019. Previously-described click types for eight known odontocete species or genera were identified in this data set: Blainville's beaked whales (*Mesoplodon densirostris*), Cuvier's beaked whales (*Ziphius cavirostris*), Gervais' beaked whales (*Mesoplodon europaeus*), Sowerby's beaked whales (*Mesoplodon bidens*), and True's beaked whales (*Mesoplodon mirus*), *Kogia* spp., Risso's dolphin (*Grampus griseus*), and sperm whales (*Physeter macrocephalus*). Six novel delphinid echolocation click types were identified as "unidentified delphinid" (UD) and named according to their median peak frequencies (e.g. a type with peak frequency at 36 kHz would be dubbed UD36). Consideration of the spatiotemporal distribution of these unidentified click types, and comparison to historical sighting data, enabled assignment of the probable species identity to three of the six types, and group identity to a fourth type. UD36, UD26, and UD28 were attributed to Risso's dolphin (*G. griseus*), short-finned pilot whale (*G. macrorhynchus*), and short-beaked common dolphin (*D. delphis*), respectively, based on similar regional distributions and seasonal presence patterns. UD19 was attributed to one or more species in the subfamily *Globicephalinae* based on spectral content and signal timing. UD47 and UD38 represent distinct types for which no clear spatiotemporal match was apparent. This approach leveraged the power of big acoustic and big visual data to add to the catalog of known species-specific acoustic signals and yield new inferences about odontocete spatiotemporal distribution patterns. The tools and call types described here can be used for efficient analysis of other existing and future passive acoustic data sets from this region.

2.2 INTRODUCTION

Odontocetes, or toothed whales, are vocal species which use sound for social communication, foraging, and navigation [21,55], making them prime targets for passive acoustic monitoring. Although the acoustic repertoire of some odontocete species have been well-studied, many remain understudied, have yet to be acoustically characterized, and cannot be distinguished to the species level in passive acoustic recordings. This limits the utilization of passive acoustic data sets for odontocete population assessments and ecological studies. Echolocation clicks, short in duration and mostly broadband biosonar impulses, are produced by odontocete species across a range of behavioral contexts. Species-specific echolocation click types, exhibiting characteristic spectral and temporal features, have been discovered for a broad range of odontocete species including sperm whales [33], Kogia spp. [32], beaked whales [28], and Risso's dolphins [29]. Discriminating features typically include spectral peaks and/or notches, and clicking rate. The challenge of identifying robust patterns within naturally variable signals is considerable when working with echolocation clicks due to the substantial signal variability observed in response to both environmental conditions and behavioral state [56–61]. Additionally, these signals are abundant—tens of millions of clicks from a dozen or more species can easily be recorded over the course of a year of recording effort at a monitoring site—making them good candidates for automated signal discovery.

The analysis of marine acoustic data has traditionally been highly labor intensive, with expert analysts manually logging individual encounters, calls, or even clicks of their target species. Such approaches are severely limited by the rate at which the data can be thus analyzed, and in recent years the rate and volume of passive acoustic data collection has outstripped the pace of manual analysis. These expert analyst methods are also less than ideal in terms of reproducibility and objectivity [62]. Over the past decade the development of machine learning tools, and their applications to ecological data, has resulted in a proliferation of automated methods for analyzing large marine acoustic datasets. Both unsupervised and supervised learning frameworks, most notably clustering and deep learning

algorithms, have become standard tools in the analysis of marine acoustic data [63–73]. These approaches require initial time investment to develop the models, and for some applications this investment may be substantial. For example, the creation of labeled training and testing sets for supervised learning is a notably time- and labor-intensive process. But once a model has been adequately trained, analysis of large datasets can be readily accomplished. Automated signal discovery, detection, and classification algorithms (with the latter two sometimes occurring in a single step) have demonstrated good success for a number of marine mammal species [see, e.g., Refs 64,65,67,68,71–74] with improved objectivity and reproducibility compared to manual analysis.

As underwater autonomous passive acoustic recordings are collected without associated species presence metadata, species-level attribution of novel signals found in these data require drawing on other data sources. Traditional marine mammal line-transect visual surveys provide high confidence species presence and group size data, and in some regions such surveys have been carried out regularly for years or even decades. These two modalities are highly complementary, with passive acoustic devices providing high temporal resolution long-term time series of acoustic presence at discrete sampling points, and visual surveys providing snapshots of animal presence over survey track lines or grids. When aggregated over years and across sites, both can give an indication of long-term species range and distribution patterns over large regions. By combining these disparate data streams, it may be possible to gain insights about which species are producing a newly identified acoustic signal type. Simultaneous passive acoustic recordings and visual sightings can be especially valuable as such instances may provide explicit labels for encounters within the acoustic data set.

In this work, we identify novel species-specific odontocete echolocation click types, and determine the species most likely responsible for producing them. This was accomplished using an unsupervised signal discovery and labeling approach on a large autonomous passive acoustic data set from the U.S. eastern seaboard. By combining machine learning techniques with expert analyst review, we identified recurring signal types that exhibited the characteristics of odontocete

echolocation clicks. The spatiotemporal distribution patterns exhibited by these signals were compared to the historical distribution of sighting data for each odontocete species known to be present in the region to correlate species presence with click types. Opportunistic encounters captured in both the acoustic and the historical sighting data were used where available to build evidence for species attributions. This approach yielded six novel delphinid click types; likely species assignments were identified for three types (UD36, UD26, and UD28), and a group-level assignment was identified for a fourth type (UD19), with two click types remaining unidentified. These novel species assignments will enable further study of these species' spatiotemporal distribution patterns and ecology using passive acoustic recordings collected in this region, and may be an indication of the signals attributable to the same species in other regions.

2.3 METHODS

2.3.1 Data Collection

Passive acoustic data were collected using High-frequency Acoustic Recording Packages (HARPs) [75] deployed at 11 continental shelf break and slope sites between 30° N and 42° N in the western North Atlantic (Figure 2.1). The devices were deployed at depths of approximately 450 m to 1,350 m and recorded continuously with a sampling rate of 200 kHz and 16-bit analog-to-digital conversion. Most devices were equipped with a single omnidirectional sensor (International Transducer Corporation's ITC-1042). Seven deployments used devices with separate low frequency (Teledyne Benthos AQ-1) and high-frequency (ITC1042) sensors. Both devices had well-characterized combined frequency response between 10 Hz and 100 kHz. A bandpass filter reduced low-frequency noise and high-frequency aliasing. Devices recorded for between 4 months and 14.5 months per deployment; repeated redeployments at each site enabled almost uninterrupted recording from Spring 2016 to Spring 2019 (Table 2.1), totaling just over 32 years of recording effort across sites.

Publicly available historical visual survey data were accessed on Duke University's OBIS-SEAMAP database [76] (individual data set citations are found in the Supporting Information) to compile a record of odontocete species sightings in the western North Atlantic. A total of 58,320 sightings were compiled for 27 odontocete species, ~52% from shipboard surveys, ~40% from aerial surveys, and the remainder from shore stations. The geographical limits of 63° - 82° W and 24° - 46° N were chosen to bound the study area, and sightings outside these limits were excluded. Rare data from as far back as 1913 were included in the analysis, but ~94% of the sightings occurred during 1980-2019.

2.3.2 Signal Detection & Classification

All analyses were carried out in MATLAB (Mathworks, Inc., Natick, MA, USA) using custom routines and a combination of automated methods and manual analysis developed by Frasier et al. [63,67,77]. This combined approach enables efficient signal detection, signal type discovery, and classification of large numbers of echolocation clicks with consistent, objective criteria, while simultaneously incorporating analyst review to ensure the resultant detections, signal types, and classifications are meaningful and not simply artifacts of the automated algorithms.

Echolocation clicks were identified using a 2-step automated detection routine [77]. In the first step, acoustic data were filtered with a 5-pole Butterworth filter with a passband between 5 kHz and 100 kHz, and then waveform samples exceeding a peak-to-peak threshold of 118 dB re:1 μPa were identified; areas of interest were expanded to include all samples within 2.5 ms of each high amplitude peak, and high-amplitude events separated by <2.5 ms were merged. In the second step, individual impulsive signals were located within these high-amplitude events by identifying samples exceeding the amplitude threshold; individual signal start and end times were then defined as the first and last sample on either side of the main peak which exceeded the 70th percentile of energy for the entire high-energy event. Individual signals separated by <100 μs were merged, and clipped signals were discarded. Descriptive parameters were calculated for each candidate click (duration, spectrum (400-

point FFT yielding a 500 Hz spectral resolution, Hann window, 50% overlap), peak frequency, peak-to-peak amplitude at the peak frequency, -3dB bandwidth, and envelope shape) and compared to user-defined thresholds to determine whether to retain or discard the impulse. The goal was to capture as many odontocete echolocation clicks as possible, particularly previously undescribed types; therefore, thresholds were set to span the range of variability of known odontocete click types based on previous works [26–33,78,79]. This approach was anticipated to also capture many non-click signals, which would be classified as non-target events in the subsequent steps. The detector was run on each deployment independently, yielding time series of putative clicks and their parameters from each site. Detected clicks in this analysis were not evaluated to identify on-axis arrivals, but rather all detected clicks were retained for the clustering and classification steps, to identify dominant signal types across detections.

To identify dominant click types at each site the unsupervised clustering approach developed by Frasier et al. [67], also a 2-step process, was used to cluster each deployment independently. Identical settings were used to cluster all deployments to allow direct comparison of the final clusters across deployments. In the first step, deployments were divided into 5-minute time bins and the Chinese whispers algorithm [80] was used to cluster detections in each bin based on pairwise spectral distances; only clicks with peak-to-peak sound pressure levels $\geqq$120 dB re:1μPa were clustered. 5-minute bin durations were selected as a trade-off between maintaining high temporal resolution while considering a time period within which there were likely to be sufficient clicks for the clustering algorithm to identify meaningful groupings, and simultaneously reducing the large volume of data of each deployment down to a more tractable size for the second clustering step. This determination was made based upon the slowest odontocete clicking rate in our analysis, that of sperm whales, which may click as slowly as once per second [81], and the expectation that some clicks would have been excluded by the detector during low-amplitude encounters (distant animals). Additionally, this bin duration was considered short enough to capture possible evolutions in click characteristics over the

course of a given encounter (typically tens of minutes to several hours). An edge pruning parameter p_e = 0.95 was used for the first clustering iteration, consistent with the approach of Frasier et al. [67] resulting in the formation of on average 1.2 clusters per bin. Multiple clusters formed in a bin if there were sufficient clicks representing two or more distinctly different signal types. Mean spectrum, inter-click-interval (ICI) distribution, and mean waveform envelope were calculated for each cluster formed in each 5-minute bin. In the second step, the same algorithm was used to cluster a subsample of 40,000 bin-level spectra per deployment by comparing spectral shape as well as mean waveform envelope. This step was memory-limited, and selecting a subset of the bin-level averages was necessary due to the computational demands of the clustering algorithm. To improve the robustness of the clusters formed by this second step, clusters consisting of fewer than 25 bin-level averages representing a minimum of 50 individual detections each were discarded. These requirements reduced the formation of clusters based on short-lived noise events, or a small number of randomly similar noises, but likely also resulted in rare click types not being represented in the final clusters. A pruning parameter p_e = 0.98 was selected for this step by comparing several clustering iterations run with varying parameter values ($0.95 \leq p_e \leq 0.99$) and considering cluster consistency versus unnecessary separation of highly similar clusters. As with the detector, consistent settings were used for all deployments to allow meaningful comparison of the clusters formed across deployments. Mean summary spectra per cluster, ICI distributions, concatenations of contributing bin-level spectra, and concatenations of contributing bin-level mean waveform envelopes, along with information about which bin-level spectra contributed to each cluster, were saved for the output from this step.

Clusters arising from this second step were manually compared across sites to identify recurring signal types. Clusters were compared on spectral shape and ICI distribution, with consideration given to the self-similarity of a cluster (i.e., the consistency of apparent spectral features across all contributing bins, an indication of cluster quality), the number of bins contributing to each cluster, the number of sites an apparent type was present at, and the consistency of an apparent type at

those sites across the three-year study period. Multiple clusters from a given site were allowed to contribute to an apparent type, on the premise that click types show substantial natural variability and the stringency of the clustering process may have led to overzealous cluster separation. Eighteen (18) distinct recurring impulse types were identified, each of which was classified as either: 1) a previously-described click type attributable to a known species; 2) a recurrent signal which appeared to be an odontocete click type, but whose species of origin was unknown; or 3) a non-odontocete impulse from a noise source such as anthropogenic sonar or cavitation bubbles. Sonar was easily identified by the concentration of energy in narrow spectral bands, long-duration signal envelopes compared to echolocation clicks, and multi-modal inter-signal-interval histograms which arose from pooling data from sonar operating with different ping rates. Differentiation between odontocete click types and cavitation bubbles (e.g. ship propellers, snapping shrimp) was based largely on signal timing, relying on the tendency of odontocetes to produce click trains with fairly regular and species-specific timing [28,82], while cavitation bubbles are produced at random. Descriptive parameters (mean power spectrum, peak frequencies, 3dB bandwidth) were calculated for each type based on 2,000 representative clicks. The ICI median of modes for each type based on the ICI distributions from 1,000 5-minute bins containing clicks from that type was computed. In the modal ICI distribution plots below, values <0.02 s have been suppressed to reduce the contribution of high density encounters in which ICIs values are saturated with near-zero values due to the interleaving of click trains from many individuals clicking simultaneously.

The final 18 types selected from the clustering process, as well as a class representing Gulf of Mexico Gervais' beaked whales [83] and another class from the same Gulf of Mexico data representing snapping shrimp [84], which have been previously observed in acoustic data from the JAX site, were used to establish training classes for a deep neural network-based classifier. We hypothesized that the Gulf of Mexico Gervais' population, which may or may not migrate between the Gulf of Mexico and the Atlantic, might be distinct and acoustically identifiable; therefore, Gulf of

Mexico Gervais' clicks were included as a separate class to test whether their presence was detected at the Atlantic monitoring sites. Five noise classes accounting for several of the common noise types were included so that these signals would not end up incorrectly labeled as odontocete clicks for lack of an outgroup: ship noise, snapping shrimp, and 3 classes of sonar separated by frequency content. Another important consideration was the maximum number of classes a classifier can be realistically expected to discriminate between with an acceptable level of error, as the likelihood of correct classification is inversely proportional to the number of classes.

Several different types of training data and neural network architectures were tested to tune the hyperparameters of the model and optimize performance. Examples for each class were either subsampled (for well-represented classes) or augmented via simulation (for minority classes) to obtain a balanced set of 5,500 examples per class. Augmentation was carried out by adding Gaussian noise to existing examples, resulting in new examples which retained the defining characteristics of their target classes while avoiding redundancy. Examples were randomly subdivided for training (5000 examples) and testing (500 examples); training data were further randomly subdivided for training and validation using an 80/20 split: 80% for training and 20% for validating performance. Final network architecture consisted of four 512-node fully connected layers with rectified linear unit (ReLU) [85] activation, 50% dropout between fully connected layers, batch normalization after the last two dropout layers, and a softmax [86] output layer. Highest test accuracy was attained by training on spectral shape, click rate, and waveform envelope shape (Table 2.2).

The trained model was run on all HARP deployments, yielding labels and associated probabilities for each 5-minute bin-level mean spectrum. Classifier performance on novel data was expected to have different accuracy than that which was achieved on the training and testing sets due to the occurrence of intermediate and noisy clicks and signal types which do not belong to any of the available classes. To account for this, a high-level review of the bin-level labels for each deployment was carried out to remove obviously incorrect labels. For each deployment, spectra assigned to each

class were sorted by peak frequency and concatenated for visual comparison; spectra whose frequency content was highly inconsistent with the characteristics of their labeled class were manually flagged for removal. This step was carried out conservatively to remove blatantly incorrect labels while leaving untouched both good and questionable labels, in hopes of retaining all bins which seemed to possibly indicate presence for each class. Residual classifier error was then estimated by calculating the false positive rate (FPR) for a stratified random subset of the retained labels. This approach was favored over the quantification of confusion due to the uncertainty involved in the assignment of noisy and intermediate clicks to a "true" class. The effects of enforcing increasingly high received level and number-clicks-per-bin thresholds were explored as approaches to minimize FPR by attempting to exclude poor quality clicks.

2.3.3 Spatiotemporal Correlation

To assess regional and temporal patterns in the distribution of the click types, average seasonal acoustic presence of respective click types across acoustic monitoring site were plotted as scaled bubble maps. Hours of acoustic presence were first summed within each season and normalized by recording effort to account for gaps between deployments, and then seasons were averaged across the three-year study period. Seasons were defined as: Spring: March-May; Summer: June-August; Fall: September-November; Winter: December-February. Classifier error (FPR, averaged across repeated deployments at each site) was used to scale bubbles to avoid misleading bubble sizes at sites where error was high for a given click type.

Maps of historical sighting data were similarly plotted for each odontocete species (the exception being the two Kogia species, breviceps and sima, which were grouped by genus as Kogia spp. due to the challenges of discriminating between these species at sea) to allow direct comparison to the click type bubble maps. Seasonal sightings were pooled for each season across all years of data for each species, rather than averaged, due to large interannual differences in survey effort and

sighting rates. Survey track lines traveled in each season were plotted when available (138 of 197 total datasets), to give a sense of where lack of sightings may be confounded by lack of visual survey effort.

To further support species-specific click type identifications based on matches between acoustic and visual distributions and seasonal patterns, delphinid sightings occurring within the estimated recording radius (~2 km)[87] of the acoustic mooring sites were identified and the acoustic data collected during these known species encounters was examined to identify associated echolocation events. Sightings recorded within close proximity of any acoustic mooring were rare due to a lack of coordinated visual and acoustic monitoring effort, but 4 qualifying encounters were identified.

2.4 RESULTS

Of the 20 classes established based on the clustering output and used to train the neural network, nine represented known odontocete species or genera: Blainville's beaked whale (M. densirostris), Cuvier's beaked whale (Z. cavirostris), Atlantic Gervais' beaked whale (M. europaeus), Gulf of Mexico Gervais' beaked whale (M. europaeus), Sowerby's beaked whale (M. bidens), True's beaked whale (M. mirus), Kogia spp., Risso's dolphin (G. griseus), sperm whale (P. macrocephalus). Six appeared to be delphinid clicks whose species of origin were unknown. The remaining five classes represented a variety of noise sources which were included in the classifier to reduce the incidence of false positives: snapping shrimp, ship cavitation, high-, mid-, and multi-frequency sonar. The unidentified click types were presumed to be generated by delphinids and not beaked whales based on their waveforms with few oscillations, and short, delphinid-like ICIs [59,88–90]. These delphinid click types were named "UD" for "unidentified delphinid," followed by the approximate value of the median peak frequency in kHz (e.g. "UD36"). They can be differentiated by their signal parameters peak frequency, 3dB bandwidth, and modal ICI (Table 2.3). An overview of the results for the noise classes is available in the Supporting Information (S1 Text, Figure 2.17).

All odontocete click types exhibited distinct regional and seasonal patterns in distribution and acoustic density. Absolute magnitude of acoustic presence, in terms of average seasonal hours per site (scaled by FPR), varied substantially between click types. UD28 exhibited a maximum presence at NFC each spring, averaging 901 hours, while Kogia presence peaked at an average of 9.5 hours at GS in the winter.

2.4.1 Risso's Dolphin (*Grampus griseus*)

Description: This click type, known to be generated by Risso's dolphins based on previous works [29,59], is characterized by a multi-peaked structure (Figure 2.2a). The Risso's clicks in our analysis exhibited lower-amplitude peaks at 23.5 kHz and 27 kHz, and a narrow main peak reaching maximum amplitude at a median frequency of 33 kHz. The modal ICI value of ~0.145 s was on the longer side for delphinids, and was consistent with the relatively large body size of Risso's dolphins.

Spatiotemporal distribution: The Risso's click type showed a predominantly northerly distribution, although it was present at every acoustic monitoring site in every season (Figure 2.2b). A clear seasonal pattern was visible, with highest presence at WC, BC, and NC in the spring shifting northward to highest presence at NC, OC, and HZ in the summer and into the fall; winter presence was lower at all of the northern sites. JAX exhibited the highest levels of acoustic presence of the southern sites, with a distinct maximum in the spring and summer and minimum in the fall and winter. Historical sightings of Risso's dolphins map quite well to the acoustic presence of the Risso's click type (Figure 2.2c).

2.4.2 Sowerby's Beaked Whale (*Mesoplodon bidens*)

Description: Sowerby's beaked whales produce clicks with energy distributed across a wide band from 50 kHz to 90 kHz [30,91] (Figure 2.3a). We found the median peak frequency to be 67 kHz. The median modal ICI value, ~0.135 s, was surprisingly short for a large-bodied species, but was consistent with previous findings.

Spatiotemporal distribution: Overall acoustic presence of Sowerby's was quite low at our monitoring sites, but an interesting distribution pattern was visible with maxima in presence in two distinct regions - one in the WC area and another further north at HZ (Figure 2.3b). Highest levels of presence in both regions were seen in the spring, while presence was lowest in the fall, although the amplitude of this seasonal fluctuation was not very large. Sightings of Sowerby's beaked whales were rare, and most commonly occurred near the shelf break of Georges Bank in the summer (Figure 2.3c); this pattern was not mirrored in the acoustic presence, although the pattern of a northerly distribution is visible in both sets of maps.

2.4.3 Blainville's Beaked Whale (*Mesoplodon densirostris*)

Description: This click type, known to be attributable to Blainville's beaked whale [28,92], exhibited a sharp onset of energy around 25 kHz and a single peak which, in our analysis, attained highest amplitude at a median frequency of 31.5 kHz (Figure 2.4a) . The median modal ICI value was 0.325 s.

Spatiotemporal distribution: Blainville's exhibited the greatest acoustic presence at BS, where a slight summer decline in presence was visible (Figure 2.4b). Presence was negligible across the other monitoring sites, but a very slight increase at GS, BP, and JAX was visible in the spring. Sightings of Blainville's were rare and occurred mostly near the Bahamas (Figure 2.4c).

2.4.4 Gervais' Beaked Whale (*Mesoplodon europaeus*)

Very few clicks were classified as Gulf of Mexico Gervais' (maximum 1.9 hours at JAX in spring), and the clicks classified as Atlantic Gervais did not appear meaningfully different from those classified as Gulf of Mexico Gervais'. Therefore we concluded that these types are not currently differentiable using our methods, and have combined the two classes here. It remains unclear whether this is because there is no acoustic distinction to be made between the two, or because the Gulf of Mexico whales do not migrate to the Atlantic, providing no true Gulf of Mexico Gervais' encounters for the classifier to identify.

Description: The type attributed to Gervais' beaked whale was characterized by a sharp onset of energy at around 30 kHz [34] (Figure 2.5a). The Gervais' clicks in our analysis reached peak amplitude at a median frequency of 46.5 kHz, with a much lower amplitude peak present at 23.5 kHz. We observed that the rate of energy drop-off above 50 kHz seemed to be a function of received level, with higher amplitude clicks exhibiting only a small diminishment in amplitude at the higher frequencies, and lower-amplitude clicks exhibiting a much steeper rate of drop-off. The median modal ICI value was ~0.275 s.

Spatiotemporal distribution: The acoustic presence of the Gervais' click type lived up to this species' moniker of "Gulf Stream beaked whale", with highest presence at the Gulf Stream monitoring site (Figure 2.5b). Overall distribution was strictly southerly and mostly focused at the GS and BP sites, with lower levels of presence at HAT and BS and no presence at JAX. There was a distinct seasonal pattern apparent, with an increase in presence at GS and BP beginning in the fall and reaching a maximum in the winter, and lower levels of presence in the spring and summer. Sightings of Gervais' beaked whales were very rare, with just 34 sightings reported in all the years of visual survey data included in this analysis (Figure 2.5c). These sightings suggest Gervais' presence much further north than indicated by our acoustic data, though northerly sightings were located much farther offshore than our recording devices, which may explain why there was no meaningful acoustic presence of Gervais' north of Hatteras. Alternatively, some of these putative Gervais' sightings may be mislabeled due to the difficulty of visually discriminating between mesoplodont beaked whales at sea, and potential misidentification of True's beaked whales.

2.4.5 True's Beaked Whale (*Mesoplodon mirus*)

Description: True's beaked whales produce clicks with a spectral shape similar to those of Gervais' beaked whales, with a sharp onset of energy around 30 kHz [26]; the True's clicks in our analysis reached peak amplitude at a median frequency of 48 kHz, with a much lower amplitude peak

present at 24.5 kHz (Figure 2.6a). True's beaked whale clicks can be distinguished from Gervais' by a shorter median modal ICI value of ~0.185 s.

Spatiotemporal distribution: True's beaked whale clicks were detected at very low levels at all monitoring sites north of Hatteras (Figure 2.6b). A clear seasonal pattern was visible, with increased presence in both the summer and the winter compared to the fall and the spring, and lowest overall presence in the fall. Highest acoustic presence was seen at NC in all seasons but the fall. Sightings of True's beaked whales were exceedingly rare, with just 10 records in all the years of visual survey data included in this analysis (Figure 2.6c), all of which occurred north of Hatteras.

2.4.6 Cuvier's Beaked Whale (*Ziphius cavirostris*)

Description: The click type attributable to Cuvier's beaked whale is distinctively multi-peaked [28,93] (Figure 2.7a). The median peak frequency of Cuvier's clicks in our analysis (38 kHz) doesn't adequately describe the complex spectral shape, in which most of the click's energy is focused in the main peak, but auxiliary peaks of successively decreasing amplitudes at ~23.5 kHz, ~19 kHz, and ~72 kHz were also consistently present. In our analysis this species exhibited a median modal ICI of ~0.465 s.

Spatiotemporal distribution: The acoustic presence of Cuvier's across our monitoring sites was focused at HAT, with low levels of presence north of this point and negligible presence at the southern sites (Figure 2.7b). A slight increase in presence at WC and HZ was visible in the winter. Sightings of Cuvier's occurred mostly in the summer, with the majority of sightings along the shelf break and in deep offshore waters from Cape Hatteras north to Georges Bank (Figure 2.7c).

2.4.7 *Kogia* spp.

Description: This high frequency click type is generated by both species in the genus Kogia [32,94,95]. The frequency content of these clicks was only partially captured by our sampling frequency of 200 kHz, and resultant Nyquist frequency of 100 kHz, but the energy distribution

exclusively >60 kHz makes even a partial spectrum of this click type easily identifiable (Figure 2.8a). The median modal ICI value for Kogia clicks in our analysis was ~0.085 s.

Spatiotemporal distribution: The overall acoustic presence of Kogia spp. at our monitoring sites was the lowest of all click types in our analysis and the distribution of this click type was strongly southerly, with highest presence at the four sites in the South Atlantic Bight (Figure 2.8b). A seasonal signal was visible at GS, with increased presence in the winter and spring compared to the summer and fall, but presence at the other southern sites was fairly consistent across seasons. Very low levels of true presence were coupled with high levels of error at the northern sites; the apparent increase in presence at NC was mostly due to a persistent high-frequency noise source occurring throughout the 2016-2017 deployment, which was misclassified as Kogia spp. Sightings of Kogia spp. occurred mostly in the summer, with the majority of sightings occurring along the shelf break and in deep offshore waters from Cape Hatteras north to Georges Bank (Figure 2.8c).

2.4.8 Sperm Whale (Physeter macrocephalus)

Description: Sperm whale clicks are characterized by their low frequency content [33] (Figure 2.9a). The median peak frequency for sperm whale clicks in our study was 8.5 kHz, but it should be noted that this may have been skewed by our choice of a bandpass filter with passband from 5 kHz – 100 kHz, and the decision within the detector to exclude impulses with peak frequency <5 kHz. The median modal ICI value of 0.485 s was similar to what has been previously reported for female sperm whales [81,82].

Spatiotemporal distribution: Sperm whales were the second most abundant click type in our analysis and were detected at all of our monitoring sites, with most presence detected from HAT northward (Figure 2.9b). An increase in presence was apparent across the northern sites in the spring, and lowest overall presence was seen in the winter. This pattern of acoustic presence was a good match for the distribution of historical sightings of sperm whales, which occurred primarily along the

shelf break and in deep offshore waters, and were more numerous north of Cape Hatteras in the spring and summer months (Figure 2.9c).

2.4.9 UD36 - Risso's dolphin (*Grampus griseus*)

Description: This click type was established based on clusters from several of the northern HARP sites which exhibited spectra with a main peak at 36 kHz characterized by a small trough, a lower amplitude peak at 26 kHz, and a shoulder at 23 kHz (Figure 2.10a). The median modal ICI value was 0.155 s. The UD36 click type shared several features, such as the location of spectral peaks and the ICI, with the click type identified in this dataset which was attributable to Risso's dolphin (Fig 1.2a). The key difference was that the lower-frequency peaks of UD36 were not as pronounced as those present in the Risso's click type.

Spatiotemporal distribution: UD36 exhibited a distinctive northerly distribution with highest presence at the WC, BC, and NC monitoring sites (Figure 2.10b). There was a marked increase in presence during the spring months which seemed to carry slightly into summer, with much lower levels of presence in the fall and winter. The distribution and seasonal pattern were very similar to the distribution of historical sightings of Risso's dolphin (Figure 2.10c). During manual review of the automated labels we observed that UD36 was mostly confused with the Risso's click type, and to a much lesser extent with UD38. We also observed that UD36 predominantly occurred interspersed throughout encounters with the Risso's click type; high-quality encounters solely with UD36 did occur, however. This may suggest that UD36 is an alternative Risso's click type, or that it is generated by a species which is often, but not always, associated with Risso's dolphins. Due to the similarities in spectral shape and click rate we believe UD36 is likely an alternative Risso's click type. Multiple click types have previously been reported for a single odontocete species [30,31,56,78]; use of different click types may be determined by behavioral state, or may be a function of angle of arrival at the receiver or of regional variation [56,96,97].

2.4.10 UD26 - Short-finned pilot whale (*Globicephala macrorhynchus*)

Description: This click type had substantial low-frequency (<20 kHz) energy, with a double peaked structure characterized by a deep notch whose minimum fell between 20 kHz - 23 kHz (Figure 2.11a). The narrow lower peak reached maximum amplitude typically around 19 kHz, while the broader upper peak extended from 25 kHz – 35 kHz. The median modal ICI value was 0.165 s. The low frequency content and relatively long ICI were consistent with a larger-bodied delphinid, such as the species in the subfamily *Globicephalinae*, commonly referred to as "blackfish".

Spatiotemporal distribution: UD26 was predominantly found at and north of Cape Hatteras, between the HAT and BC monitoring sites (Figure 2.11b). This type exhibited a seasonal shift in presence, with higher presence at NFC and WC beginning in the summer and peaking in the fall, which gave way to higher presence at HAT beginning in the fall, peaking in the winter, and carrying into the spring. The regional distribution and seasonal presence of UD26 were a good match for the historical distribution of short-finned pilot whale sightings in this region (Figure 2.11c). The low overall acoustic presence of this click type was also in line with the relatively small number of sightings of short-finned pilot whales across all years of visual survey data. The only anomalous feature in this match was the presence of UD26 detections with relatively low error rates at HZ, as short-finned pilot whales are not thought to be present this far north. The detections labeled as UD26 at HZ showed a slight upwards shift in frequency content relative to the UD26 detections from the US mid-Atlantic region, but otherwise had a similar spectral shape and modal ICI. It may be that this northern variant of UD26 is in fact distinct from the UD26 encountered further south, and should be studied separately.

Supporting observations: We identified three short-finned pilot whale sightings in close proximity to an acoustic device and looked at the concurrent acoustic data to identify any acoustic encounters which might be attributed to the sighted species. Acoustic encounters associated with two of the three sightings exhibited features consistent with those of UD26; one of these encounters, from

JAX, is shown in Figure 2.12. The third encounter, which was very low amplitude, did not exhibit the characteristics of UD26. There was also a fourth sighting, just 0.63 km from NFC in October of 2017, which was associated with a high-amplitude encounter which strongly exhibited the characteristics of UD26; however, this visual sighting was only identified to the genus level. The scarcity of long-finned pilot whale sightings near NFC in the fall (Figure 2.18) suggests that the species sighted during this fourth encounter was most likely short-finned pilot whale. Examination of acoustic encounters labeled as UD26 also revealed the consistent presence of low-frequency whistles (<10 kHz) and buzz-type calls previously reported for pilot whales [98,99]. Additionally, a similar click type has been reported for short-finned pilot whales from Hawaii [79], the Gulf of Mexico [67], the western North Atlantic [100], and the eastern North Atlantic [90].

Manual review of a subset of the automated labels revealed that at sites where this type was more abundant, most of the classification error could be attributed to misclassification as UD19, which we believe may be another *Globicephalinae* spp. type. Such confusion occurred when the lower-frequency peak of UD26 was much higher-amplitude than the higher-frequency peak, resulting in a spectral shape quite similar to that of UD19. Our observations of clicks with a spectrum intermediate between UD26 and UD19 may indicate that short-finned pilot whales produce a variety of clicks describing a continuum between these two types. Alternatively, the frequent co-occurrence of these two types may tell us that the short-finned pilot whales producing UD26 sometimes co-occur with other *Globicephalinae* species producing UD19.

2.4.11 UD28 - Short-beaked common dolphin (*Delphinus delphis*)

Description: This click type had a simple spectral structure with a single peak around 28 kHz (Figure 2.13a) and a short median modal ICI value of 0.075 s. Based on this generic shape, and the ubiquity of this click type across sites, UD28 seemed likely attributable to bottlenose or short-beaked common dolphins, both of which were common in the study area.

Spatiotemporal distribution: This click type was the most abundant type detected in our analysis and exhibited the lowest classification error across sites of all the novel types (Figure 2.13b). UD28's distribution predominantly north of Cape Hatteras, with increased presence between HAT and BC in the winter and spring months, was highly similar to the historical distribution of short-beaked common dolphin sightings in this region (Figure 2.13c). Similarly generic click spectra have also been previously reported for bottlenose dolphins [27,96], but the abundance of UD28 at the northern sites in the winter does not mirror the distribution of bottlenose dolphin sightings in this region (S5 Fig).

Supporting observations: A click type similar to UD28 has been previously reported for short-beaked common dolphin clicks in the Pacific [29]. Additionally, the long duration and dense clicking activity typical of UD28 bouts in this study region suggests large group sizes. According to the sighting data we compiled, this is more in keeping with what has been observed for short-beaked common dolphins (mean group size: 30.7 individuals, 10^{th} & 90^{th} percentiles: [1,60]; from 5183 sightings with group size data recorded) than for bottlenose dolphins (mean group size: 7.6 individuals, 10^{th} & 90^{th} percentiles: [1,18]; from 26,086 sightings with group size data recorded).

2.4.12 UD19 - *Globicephalinae* spp.

Description: UD19 had a simple spectral shape similar to UD28, but with the peak centered at a lower frequency of 19 kHz (Figure 2.14a). The modal ICI value for this click type was 0.135 s. Similar to UD26, the low frequency and slow click rate may be indicative of a large-bodied species within the subfamily *Globicephalinae*.

Spatiotemporal distribution: This click type was the third most abundant in our analysis, after UD28 and sperm whales, and was present at all sites at least part of the year (Figure 2.14b). UD19 showed a pronounced seasonal pattern with highest presence at NFC and WC in the summer and fall, and much lower levels of presence everywhere in the winter and spring. However, the distribution and seasonal pattern of this click type were not good matches for the distribution of sighting data for any single dolphin species found in this region, *Globicephalinae* spp. or otherwise. There were some

similarities in the seasonal distribution of UD19 to that of UD26, suggesting at first glance a match for short-finned pilot whales, but this may to some extent have been due to confusion between UD26 and UD19. As described above, clicks spanning a continuum between these two spectral shapes were often observed during bouts with both UD26 and UD19, resulting in confusion consistent with what was seen during classifier testing (S1 Table). There was some ambiguity as to the best choice of "true" class for clicks with a pronounced main peak at 19 kHz in addition to a much lower amplitude auxiliary peak between 25 kHz - 30 kHz. Even after accounting for the incidence of false positive UD19 detections, the abundance of UD19 was incongruous with the low number of short-finned pilot whale sightings in this area (Figure 2.11c). The more numerous *Globicephalinae* species in the study region was the long-finned pilot whale, but the distribution of UD19 did not reproduce the distribution or seasonal patterns visible in long-finned pilot whale sightings (Figure 2.18). One possible explanation for this ambiguity is that UD19 does not represent a single species but may in fact be attributable to several *Globicephalinae* species which produce similar clicks and which have been inadvertently grouped into a single class in this analysis. In addition to long-finned pilot whales, short-finned pilot whales, orcas, false killer whales, pygmy killer whales, and melon-headed whales are also known to be present in the study area. The pooling of species with markedly different spatial distribution patterns may have resulted in a generalized distribution of this click type which obscures the distinct patterns of each species included.

Supporting observations: Similar to UD26, examination of encounters with UD19 revealed the consistent presence of low-frequency whistles (<10 kHz) and buzz-type calls typical of *Globicephalinae* species [98,99].

2.4.13 UD47 – distinctive type without a clear spatiotemporal match

Description: This click type was characterized by its distinctive spectral banding pattern, with well-defined low-amplitude peaks at 20 kHz and 28 kHz and a broad main peak between 40 kHz - 55 kHz (Figure 2.15a). The modal ICI (0.065 s) was typical of smaller-bodied delphinids, of which there

are several species in this region which have yet to be matched with a characteristic click type: bottlenose dolphins, Atlantic white-sided dolphin, white-beaked dolphin, Fraser's dolphin, Atlantic spotted dolphin, pantropical spotted dolphin, spinner dolphin, Clymene dolphin, striped dolphin, rough-toothed dolphin.

Spatiotemporal distribution: UD47 exhibited negligible presence at the shelf break sites south of HAT, low levels of presence at JAX in the spring and summer, highest presence at HAT, and low levels of presence at the northern sites (Figure 2.15b). Very little seasonal pattern was apparent, though there was a slight increase in presence at HAT in the winter and spring months. This distribution was not a good match for the distribution of historical sighting data for any dolphin species in this region.

2.4.14 UD38 - distinctive type without a clear spatiotemporal match

Description: UD38 had a relatively narrow main peak with most energy between 38 kHz – 45 kHz, and two lower-amplitude auxiliary peaks at 16 kHz and 19 kHz; both lower-frequency peaks were not always apparent (Figure 2.16a). The modal ICI value was 0.065 s (Table 2); as with UD47, this may suggest a small-bodied delphinid.

Spatiotemporal distribution: UD38 exhibited a predominantly northerly distribution with highest presence always at HAT (Figure 2.16b). Presence at HAT peaked in the winter, while a slight increase in presence at the northern sites could be seen in the spring. There were low levels of acoustic presence of UD38 at the southern sites with variable error rates. Like UD47, there was no clear species match based on the distribution and seasonal pattern for this click type.

2.5 DISCUSSION

Our two-pronged approach leveraged big acoustic data and many decades of visual survey efforts to yield new inferences about odontocete acoustic identity, and was made possible by the combined power of automated algorithms and expert analyst review. Identification of six novel

delphinid click types, and attribution of four of the six to a particular species/genus, substantially expands our ability to identify delphinid species presence in passive acoustic data from this region, and thereby pursue ecological studies. This approach can be applied for signal type discovery and identification in any region where large passive acoustic and visual survey data sets have been collected, and will enable improved utilization of large marine passive acoustic data sets. The catalog of impulsive signal types presented here in the form of our neural network training classes is, to the best of our knowledge, the first of its kind for this area and represents a comprehensive overview of the dominant odontocete species and impulsive noise sources commonly found at deep water acoustic monitoring sites spanning the region.

Odontocetes produce directional clicks with greater amplitudes on-axis (forward of the rostrum) and lower amplitudes off-axis (lateral from the rostrum)[55]. Since our detector output did not discriminate between on-axis and off-axis clicks, the click types presented in this analysis may represent both on-axis and off-axis arrivals at our sensors. Previous works have suggested that most delphinid clicks arriving at a seafloor sensor are off-axis [87], while those of beaked whales are likely on-axis when the animals are more than a few hundred meters from the sensor [83]. Clicks which arrive at a sensor from an off-axis path are typically distorted relative to their on-axis counterparts, with complex waveforms, amplitude and peak frequency decreasing as a function of off-axis angle, and spectral notches often being introduced [56,96,101–103]. Angle of off-axis is also an important consideration, as click which are only slightly off-axis may appear very similar to on-axis clicks. In a passive acoustic monitoring paradigm it is reasonable to assume that a large proportion of clicks arriving on a sensor are off-axis, but this did not appear to be a reason, in and of itself, to discard these clicks from analysis. Off-axis click have generally not been as well-studied as on-axis clicks but their distortions may carry a signature of the acoustic anatomy of the generating species, and therefore there may be species-specific features of off-axis clicks which make them equally well suited to species classifications as on-axis clicks [29]. If some of the click types presented here represent off-axis

arrivals, this may explain why the species to click type correspondence is not always one to one, both in this work and in previous works [30,31,78]. A better understanding of the relationship between on-axis and off-axis click features as they are received by a seafloor sensor would be valuable for improved interpretation of large passive acoustic data sets. This could perhaps be obtained through studies combining body-mounted orientation-recording tags and seafloor acoustic sensors.

The distribution patterns exhibited by the known click types we identified represent two distinct cases: in the case of Risso's dolphins and sperm whales, the acoustic presence mirrors the distribution and seasonal patterns of sightings along the shelf break (Figures 2.2 b-c, 2.9 b-c), whereas in the case of the beaked whales and *Kogia* spp., the acoustic data reveals presence patterns which are not represented in the sighting data (Figures 2.3-2.8 b-c). The former case is an encouraging proof-of-concept for our approach of matching acoustic presence patterns to the distribution of historical sighting data in order to attribute novel click types to species. For species which are readily available for both visual detection and acoustic detection, the two approaches should generate comparable presence maps, and we see this in the result for both Risso's dolphins and sperm whales. In the latter case we see a mismatch between the presence patterns captured by the two methodologies, which suggests that one of these approaches is not well-suited to detecting the species of interest. Indeed, beaked whales and *Kogia* spp. are known to be cryptic species which exhibit inconspicuous surface behaviors and undertake prolonged deep dives, complicating the task of inferring species presence patterns from ship-based and aerial sighting data. Autonomous passive acoustic data collection captures animals throughout the water column and is thought to have no effect on animal presence or behavior, so the acoustic presence recorded via this methodology may be a better indicator of the true spatiotemporal presence patterns of these elusive species. This is likely the case for Sowerby's, Blainville's, Gervais', and True's beaked whales, as the acoustic presence maps suggest that they are present at more sites and throughout more seasons than is shown by the historical sighting data (Figures 2.3-2.6 b-c). In each case there are, however, some offshore sightings which represent

animals which would not have been available to be captured in the acoustic data due to their distance from the acoustic monitoring sites, demonstrating the limitations of point sampling compared to data collection along far-reaching track lines. For Cuvier's beaked whales and *Kogia* spp. these missed presence points are fairly numerous in the summer months (Figures 2.7c, 2.8c). However, the fact that there is no corresponding increase in acoustic presence of either species in the northern region during the summer may suggest that the increase in sightings is due to disproportionate summer survey effort, rather than a true increase in presence. The fullest understanding of the distribution and seasonal presence patterns for these two species could likely be attained by combining passive acoustic and visual survey data.

Matching acoustic presence maps to historical sighting maps requires consideration of the differences between these two approaches to observing species presence. UD36, the novel click type assigned to Risso's dolphin, exhibited a clear increase in acoustic presence in the spring, which mirrored the increased density in Risso's sightings tightly clustered along the shelf break north of Hatteras in the spring compared to the winter and fall (Figure 2.10b-c). However, in absolute terms there were more Risso's individuals sighted in the summer. These summer sightings were somewhat more widely distributed on the shelf and offshore, meaning many individuals were too far from our devices to be acoustically detected, which may explain why this increase was not as clearly reflected in the summertime acoustic presence of UD36 at our monitoring sites. Increased summer Risso's sightings may also be a function of increased sighting effort, as opposed to increased species presence, while acoustic monitoring effort was uniform throughout seasons. Similar to UD36, the acoustic presence of UD28, assigned here to short-beaked common dolphins, exhibited increased presence in the winter and spring, while short-beaked common dolphin sightings peak in the summer (Figure 2.13b-c). This may be due to the apparent shift in distribution of short-beaked common dolphins, from the outer shelf and shelf break during the winter and spring northward onto Georges Bank and inshore during the summer and fall. Many of the animals sighted in the summer and fall were not available to

be captured on our acoustic devices for this reason. The distribution of short-finned pilot whale sightings (Figure 2.11c) may underestimate their true presence due to missing data points, as many Globicephala sightings are identified only to the genus level (2701 *Globicephala* spp. records in our analysis, compared to 566 *G. macrorhynchus* and 1361 *G. melas* records). In areas where the ranges of the two pilot whale species overlap, high probabilities of sighting either species may lead to lower confidence in species level identifications, and more sightings reported simply as *Globicephala* spp. (Figure 2.18). The predominance of UD26 clicks during multiple encounters with visually-confirmed short-finned pilot whales complements the possibly-incomplete sighting data to support this species assignment.

UD19 exhibited a very strong summer and fall presence at the mid-Atlantic sites, but it is unclear from this analysis where these individuals, which we believe may represent more than one species, spend the winter and spring months (Figure 2.14b). It may be that the individuals accounting for the high levels of acoustic presence at HAT, NFC, and WC in the summer and fall are a different species than the individuals accounting for the lower levels of presence across all sites in the winter and spring. Further study of the variability within this type may reveal subtypes with varying seasonal presence which could be linked to the presence of particular species. UD47 and UD38 may be attributable to species whose distribution and seasonal presence patterns are not well-elucidated by historical sighting data, and identification of these click types to species may necessitate additional data types.

The oceanography in this region is dominated by the influence of the Gulf Stream, a high-volume current which transports warm, high-salinity equatorial water along the shelf break of the southeastern U.S. until its separation point at Cape Hatteras, where it turns eastward towards northern Europe. The Gulf Stream front is a steep gradient in temperature and salinity which delineates a boundary between two very different habitats: warm oligotrophic waters of the Gulf Stream to the south and east, and cold, lower-salinity, productive sub-polar waters to the north and west. It is not

surprising, therefore, that the distributions of many species in this region reflect the presence of this boundary. Most of our unidentified click types exhibited little to no presence at the three monitoring sites situated directly in the path of the Gulf Stream: GS, BP and BS. As can be seen by the presence of Blainville's and Gervais' beaked whales and *Kogia* spp. acoustic encounters at these sites (Figures 2.4c, 2.5c, 2.8c), this was not likely a result of poor acoustic propagation conditions or low detectability at these sites, but rather a clear species preference regarding the conditions of the Gulf Stream waters. The distinct regional and temporal patterns exhibited by the distributions of each of the unidentified click types may provide us with insights into the ecology of the species to which they are attributed.

2.5.1 Clustering and click type identification

Even with the help of the automated signal discovery pipeline, the process of identifying recurring signal types across so many sites and years of data was not a trivial matter. A consideration when using an automated clustering approach is the tradeoff between cluster separation and the proportion of nodes (5-minute bin average spectra, in this analysis) which are isolated by user-defined thresholds. By tuning the parameters of the clustering process we are able to impose arbitrary requirements of cluster size and self-similarity, yielding types which describe highly consistent and commonly present signals. This comes at the expense of types which exhibit greater natural variability or are present in lower numbers. The first case may be acceptable for our purposes, which rely upon consistently present spectral and temporal features to discriminate between species. The loss of rare types, however, undermines our efforts to identify characteristic click types for these species. When comparing clusters across sites, the requirement for apparent click types to exhibit presence at multiple sites and across the years of recording effort (in order to avoid establishing types based on site-specific noise sources or atypical species presence phenomena) likely further excluded species with low or intermittent presence in this region, even if they did have highly distinctive and recognizable clicks which formed robust clusters. This is an issue worth exploring further, as rare species are often the

most data deficient, and methods of collecting information on their presence and distribution are sorely lacking. Further study of the clusters excluded from our training set may reveal types which correlate well with the presence of rare species. Future work should explore approaches to identifying rare click types in these large data sets and differentiating them from random noise events.

After acceptably self-similar clusters had been formed, the issue of signal variability was still highly pertinent when comparing clusters and making decisions about which should be deemed examples of a single type, and which warranted separate consideration. As with all manual signal identification, this step involved subjective judgement calls guided by knowledge of previously documented signal types and the characteristics of our monitoring sites. Due to the lack of supporting data justifying subdivisions of similar clusters, an approach favoring simplicity over hyper-fragmentation of types was chosen. This may have resulted in signal categories which obscured some species-level differences, such as may be the case for UD19. We did not, however, choose to merge UD36 with the Risso's click type despite their apparent similarity for two reasons: 1) while these types often co-occurred in our data, high quality encounters with solely UD36 were also present, and, 2) UD36 has not been observed in click clusters generated from HARP data from the Gulf of Mexico [67] or southern California (analyses underway), where Risso's are regularly acoustically detected. This suggested to us that UD36 might actually be generated by a species other than Risso's dolphin, or might be a regionally-specific click type indicative of stock delineations [97]. For these reasons we initially chose to analyze UD36 independent of the previously established Risso's click type. An alternative to this manual approach to establishing click types would be to carry out a third clustering step, comparing clusters across deployments and sites in an automated fashion as opposed to manually. It should be noted that at sites where multiple odontocete species frequently co-occur (most notably HAT and NFC), the clusters themselves may not always have been single-species. In cases of the co-occurrence of species with similar click types, multiple spectra may have been separated within each 5-minute bin by the first step of clustering, but then any combination of those bin-level spectra

may have been included in a final cluster with characteristics spanning two or more highly similar species. Such an occurrence would mean that the different species were not effectively available to be separated during manual review of the clusters from that site (and neither would they be separated by a third pass of clustering).

2.5.2 Classification error

During the classification step, the neural network was required to distinguish both highly divergent signals and quite similar signals, likely resulting in lower success in discriminating between similar signals. This could muddy the waters when looking at the geographic distribution of each click type. An iterative approach to labeling, where broad classes are first separated (i.e. sperm whale, beaked whales, dolphins) and then individual classifiers tuned to the more nuanced distinctions within each class are run in a second step, might show improved discriminatory ability. We did observe, however, that our classifier was resilient to small shifts in frequency content when the overall spectral shape was conserved, as seen in the classification of UD26 at mid-Atlantic versus northern sites. This is a useful quality when looking to discriminate to the species level, as regional differences in frequency content for a given species have been previously described [97], and these differences may be accommodated by the kind of classifier used here.

We found that classification error, quantified by the false positive rate for the novel click types, varied greatly between click types, and also between sites within some of the types. One of the challenges with multi-class classification is that the probability of successful classification is inversely proportional to the number of classes. For a classifier choosing between 20 classes, the probability of random success is just 5%; training data improves those odds substantially, but the model is still challenged by discriminating between so many classes, some of which are quite similar. The error rates reported here are typically much lower than would be expected from random guessing, except when presence of a click type at a given site is very low. Manual review of a subset of the labels, and observation of the presence of many intermediate and noisy clicks, drove home the impracticality of

attempting manual labeling from scratch. Especially at sites where many species are present and acoustic bouts overlap, such as HAT and NFC, distinguishing intra-type variability from inter-type variability can perplex even highly specialized analysts, and requires a prodigious time investment. These are important factors to keep in mind when evaluating classifier accuracy and considering the tradeoff between accuracy and time required to generate labeled time series. The approach to signal classification used here is fast, objective, and repeatable, and there are many options available for continuing to improve the classifier, such as multi-step classification and model ensembles.

A recurring feature across many of our click types was higher levels of classifier error at sites with low levels of presence for that type. This is to be expected when there is a mismatch between the probability distribution of classes learned by the neural network and the probability distribution of species present in the data. This phenomenon, known as dataset shift, has recently gained attention in the literature on machine learning applications in ecological studies, along with some proposed solutions [104–107]. The insights gained here regarding the presence of different click types across our sites could be applied in future to create a training set which more accurately reflects the true probability distribution of each type.

We sought to minimize our classifier error by enforcing increasingly strict minimum peak-to-peak receive level and number-clicks-per-bin thresholds in order to weed out low-quality clicks. In the end, we found that this approach did not have much impact on the patterns in distribution and seasonal presence visible in the acoustic presence maps, though it did dramatically reduce the number of clicks retained for analysis. In light of this we decided to use fairly relaxed thresholds in order to retain more of the detected clicks in our analysis. Due to the number of classes evaluated here, the size of the acoustic data set, and the uncertainty involved in "true" class selection for intermediate clicks when quantifying confusion, we calculated a single FPR for each novel click type at each site, and used that single value to scale the acoustic presence in all seasons. Development of efficient and objective approaches to quantification of confusion in such large data sets when out-of-distribution signals are

present could lead to more accurate time series adjustments, as well as an opportunity to improve future classifiers by identifying the particular features a classifier had difficulty separating.

2.6 CONCLUSION

Our findings illustrate the complementary nature of marine passive acoustic and visual survey data, and provide a means of ascertaining species identity for novel acoustic signals within existing and forthcoming acoustic data sets based on spatiotemporal correlations. The workflow described here provides a highly objective, repeatable, and fast approach to signal discovery and classification for large acoustic data sets. Identification of two unidentified click types from this region as short-beaked common dolphins and short-finned pilot whales, as well as attribution of a second click type to Risso's dolphin, expands our knowledge of species-specific click types and sets the stage for ecological studies of these species using passive acoustic data. Assignment of UD19 to the *Globicephalinae* subfamily is a first step in species identification, though more work remains to disentangle the ambiguity remaining around this click type. Species identities were not forthcoming for UD47 or UD38 in this analysis, but the recognition of these recurring signal types as likely delphinid click types will enable further study of their occurrence patterns, which may lead to future species identifications.

2.7 FIGURES

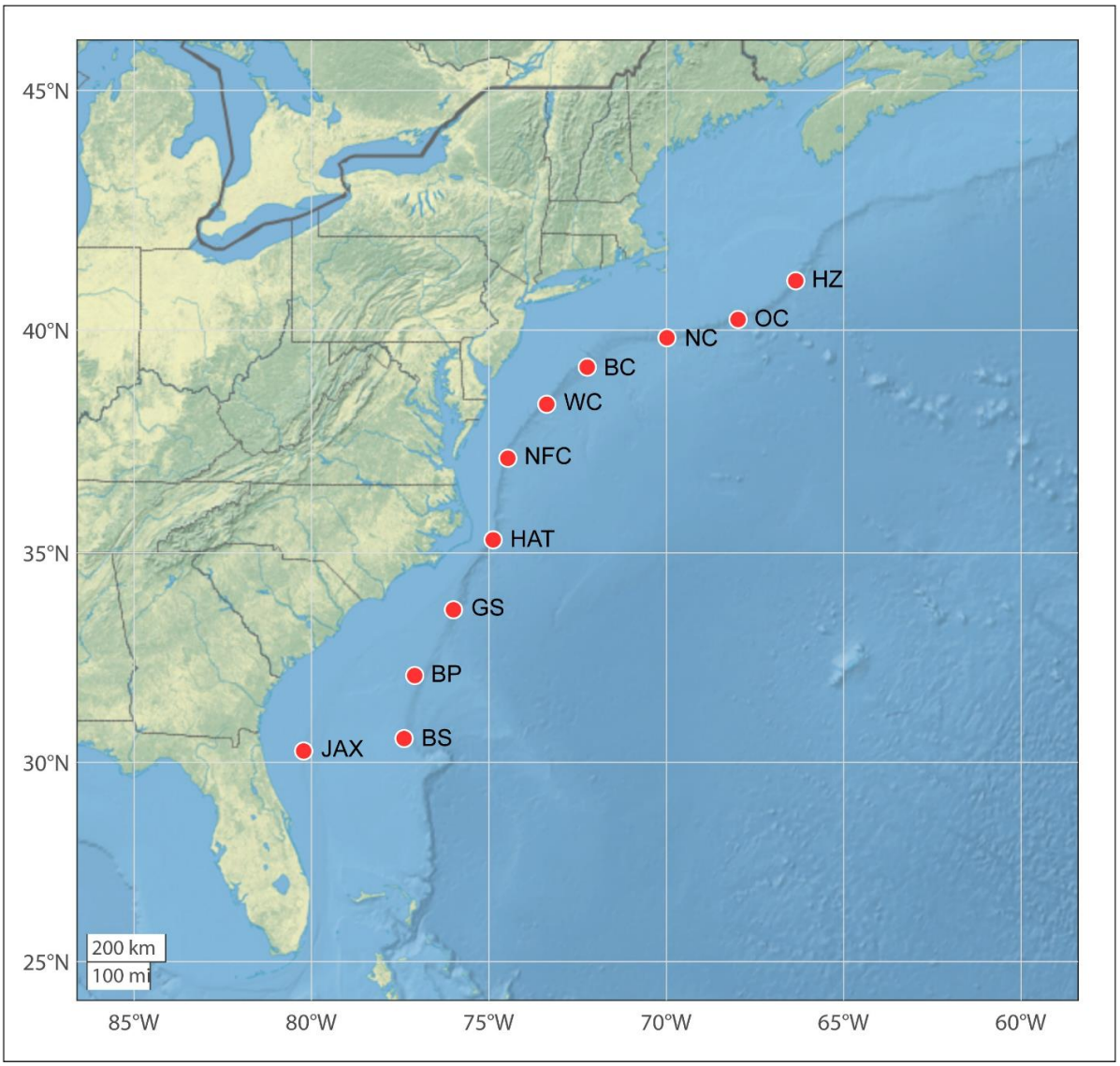

Figure 2.1: Western North Atlantic study area with long-term autonomous passive acoustic monitoring sites (red circles) and associated site name abbreviations. HZ = Heezen Canyon; OC = Oceanographer's Canyon; NC = Nantucket Canyon; BC = Babylon Canyon; WC = Wilmington Canyon; NFC = Norfolk Canyon; HAT = Hatteras; GS = Gulf Stream; BP = Blake Plateau; BS = Blake Spur; JAX = Jacksonville.

Table 2.1: HARP deployment information for repeated deployments at the acoustic monitoring sites shown in Fig 2.1.

Site		Latitude	Longitude	Depth (m)	Data Start Date & Time		Data End Date & Time	
Heezen Canyon (HZ)	1	41° 03.71' N	66° 21.10' W	883	4/22/2016	18:00:00	6/19/2017	7:05:06
	2	41° 03.70' N	66° 21.09' W	885	7/9/2017	0:00:00	1/13/2018	15:25:06
	3	41° 03.70' N	66° 21.09' W	885	6/11/2018	17:59:59	5/10/2019	6:33:44
Oceanographer's Canyon (OC)	1	40° 15.80' N	67° 59.17' W	448	4/24/2016	5:59:59	5/18/2017	6:37:35
	2	40° 15.80' N	67° 59.18' W	447	7/6/2017	23:59:59	4/16/2018	5:56:18
	3	40° 13.80' N	67° 58.68' W	882	6/10/2018	6:00:00	5/19/2019	4:33:45
Nantucket Canyon (NC)	1	39° 49.94' N	69° 58.93' W	894	4/21/2016	18:00:00	5/24/2017	14:53:51
	2	39° 49.96' N	69° 58.92' W	894	7/16/2017	18:00:00	6/9/2018	13:02:36
	3	39° 49.98' N	69° 58.92' W	894	6/10/2018	0:00:00	6/3/2019	4:43:45
Babylon Canyon (BC)	1	39° 11.46' N	72° 13.72' W	999	4/20/2016	18:00:00	6/10/2017	23:04:05
	2	39° 11.43' N	72° 13.63' W	1003	6/30/2017	12:00:00	6/3/2018	11:31:21
	3	39° 11.52' N	72° 13.64' W	997	6/3/2018	12:00:00	5/19/2019	19:30:00
Wilmington Canyon (WC)	1	38° 22.45' N	73° 22.24' W	1028	4/20/2016	6:00:00	6/29/2017	20:57:36
	2	38° 22.43' N	73° 22.21' W	1036	6/30/2017	0:00:00	6/2/2018	20:42:36
	3	38° 22.40' N	73° 22.19' W	1045	6/2/2018	22:00:00	5/19/2019	8:32:30
Norfolk Canyon (NFC)	1	37° 09.99' N	74° 20.00' W	1028	4/30/2016	12:00:00	6/28/2017	18:38:51
	2	37° 10.04' N	74° 27.98' W	992	6/30/2017	0:00:00	6/2/2018	16:15:06
	3	37° 09.87' N	74° 27.95' W	1111	6/2/2018	12:00:00	5/18/2019	17:46:40
Hatteras (HAT)	1	35° 18.11' N	74° 52.74' W	1194	4/29/2016	12:00:00	2/6/2017	8:56:03
	2	35° 35.05' N	74° 44.99' W	1128	5/9/2017	12:02:54	10/25/2017	14:11:45
	3	35° 35.01' N	74° 44.58' W	1222	10/26/2017	12:00:00	6/1/2018	0:54:59
	4	35° 35.39' N	74° 44.86' W	1327	6/1/2018	4:00:00	12/14/2018	14:42:36
	5	35° 35.36' N	74° 45.27' W	1208	12/14/2018	0:00:00	5/17/2019	18:17:30

Table 2.1 Continued: HARP deployment information for repeated deployments at the acoustic monitoring sites shown in Fig 1.1.

Site		Latitude	Longitude	Depth (m)	Data Start Date & Time	Data End Date & Time	Site	Latitude
Gulf Stream (GS)	1	33° 39.94' N	76° 00.08' W	926	4/29/2016	0:00:00	6/27/2017	18:35:06
	2	33° 40.02' N	75° 59.97' W	932	6/28/2017	0:00:00	6/26/2018	11:31:21
	3	33° 40.20' N	75° 59.86' W	933	6/28/2018	23:59:59	6/18/2019	14:17:09
Blake Plateau (BP)	1	32° 06.36' N	77° 05.66' W	953	4/28/2016	12:00:00	6/27/2017	4:57:36
	2	32° 06.42' N	77° 05.41' W	951	6/27/2017	12:00:00	6/28/2018	13:08:51
	3	32° 06.32' N	77° 05.44' W	950	6/28/2018	0:00:00	5/28/2019	4:01:15
Blake Spur (BS)	1	30° 35.03' N	77° 23.44' W	1047	4/27/2016	18:00:00	6/26/2017	15:22:05
	2	30° 34.98' N	77° 23.43' W	1047	6/26/2017	18:00:00	6/23/2018	7:32:33
	3	30° 34.98' N	77° 23.40' W	1047	6/28/2018	0:00:00	6/16/2019	20:13:45
Jacksonville (JAX)	1	30° 09.11' N	79° 46.21' W	748	4/26/2016	18:00:00	6/25/2017	19:23:35
	2	30° 09.16' N	79° 46.19' W	748	6/25/2017	18:03:57	10/28/2017	17:27:48
	3	30° 09.14' N	79° 46.24' W	746	6/27/2018	0:00:00	6/15/2019	11:03:45

Table 2.2: Neural network test performance on a balanced test set of 500 examples per class. Names for known-type classes are abbreviations of the species/genus names: *Gg: Grampus griseus; Mb: Mesoplodon bidens; Md*: *Mesoplodon densirostris; Me: Mesoplodon europaeus;* GoM *Me:* Gulf of Mexico *Mesoplodon europaeus; Mm: Mesoplodon mirus; Pm: Pyseter macrocephalus; Zc: Ziphius cavirostris.*

	Gg	*Kogia* spp.	*Mb*	*Md*	*Me*	GoM *Me*	*Mm*	*Pm*	*Zc*	UD36	UD26	UD28	UD19	UD47	UD38	Ships	High-freq Sonar	Mid-freq Sonar	Multi-freq Sonar	Snap Shrimp
Gg	91.8	0	0	0	0	0	0	0	0	8.2	0	0	0	0	0	0	0	0	0	0
***Kogia* spp.**	0	100	0	0	0	0	0	0	0	0	0	0	0	0	0	0	0	0	0	0
Mb	0	0	99.4	0	0	0	0.2	0	0	0	0	0	0	0.2	0	0	0.2	0	0	0
Md	0	0	0	100	0	0	0	0	0	0	0	0	0	0	0	0	0	0	0	0
Me	0	0	0	0	99.8	0	0.2	0	0	0	0	0	0	0	0	0	0	0	0	0
GoM *Me*	0	0	0	0	0	100	0	0	0	0	0	0	0	0	0	0	0	0	0	0
Mm	0	0	0	0	0	0	100	0	0	0	0	0	0	0	0	0	0	0	0	0
Pm	0	0	0	0	0	0	0	96	0	0	0	0	0	0	0	3.4	0.2	0.4	0	0
Zc	0	0	0	0	0	0	0	0	99.6	0	0	0	0	0	0.4	0	0	0	0	0
UD36	0.4	0	0	0	0	0	0	0	0	99.6	0	0	0	0	0	0	0	0	0	0
UD26	0	0	0	0	0	0	0	0	0	0	99.8	0	0.2	0	0	0	0	0	0	0
UD28	1	0	0	0	0	0	0	0	0	0.4	0.2	97.8	0.4	0	0.2	0	0	0	0	0
UD19	0	0	0	0	0	0	0	0	0	0	6.8	0.8	92.4	0	0	0	0	0	0	0
UD47	0	0	0	0	0	0	0	0	0	0	0	0	0	99.8	0.2	0	0	0	0	0
UD38	0	0	0	0	0	0	0	0	0.2	0	0	0	0	1	98.8	0	0	0	0	0
Ships	0	0	0	0	0	0	0	4.2	0	0	0	0	0	0	0	95.8	0	0	0	0
High-freq Sonar	0	0	0	0	0	0	0	0	0	0	0	0	0	0	0	0	100	0	0	0
Mid-freq Sonar	0	0	0	0	0	0	0	0	0	0	0	0	0	0	0	0.4	0	99.6	0	0
Multi-freq Sonar	0	0	0	0	0	0	0	0	0	0	0	0	0	0	0	0	0	0	100	0
Snap Shrimp	0	0	0	0	0	0	0	0	0	0	0	0	0	0	0	0	0	0	0	100

Table 2.3: Signal parameters peak frequency, 3dB bandwidth, and modal ICI for known species and novel click types given as median with 10th and 90th percentile in brackets. Names for known-type classes are abbreviations of the species/genus names: Gg: *Grampus griseus*; Mb: *Mesoplodon bidens*; Md: *Mesoplodon densirostris*; Me: *Mesoplodon europaeus*; Mm: *Mesoplodon mirus*; Zc: *Ziphius cavirostris*; *Kogia*: *Kogia* spp.; Pm: *Physeter macrocephalus*.

Click Type	Peak Frequency (kHz)	3dB Bandwidth (kHz)	Modal ICI (s)
Gg	32.5 [23.5,38.0]	4.5 [2,10]	0.145 [0.085,0.195]
Mb	67.0 [59.5,73.5]	13.5 [6.5,21.0]	0.135 [0.125,0.185]
Md	31.5 [28.5,35.5]	7.5 [3,11]	0.325 [0.225,0.375]
Me	46.5 [38.0,74.5]	11.5 [4.5,20.5]	0.285 [0.245,0.305]
Mm	47.5 [41.0,75.0]	11.3 [3.50,21.5]	0.185 [0.165,0.205]
Zc	38.5 [31.0,42.5]	7.0 [3.5,13.5]	0.465 [0.085,0.535]
Kogia	99.5 [93.0,99.5]	7.0 [4.0,12.5]	0.085 [0.065,0.115]
Pm	8.5 [6.5,13.0]	3.0 [1.5,5.5]	0.475 [0.035,0.655]
UD36	36.5 [30.0,47.0]	5.5 [2.5,13.0]	0.155 [0.135,0.177]
UD26	26 .5 [12.0,39.0]	4 [2.0,9.5]	0.165 [0.085,0.195]
UD28	28.5 [23.0,34.3]	9 [3.0,15.0]	0.075 [0.045,0.105]
UD19	19 .0 [15.0,26.5]	9 [3.5,15.0]	0.135 [0.035,0.225]
UD47	47 .0 [19.5,57.0]	6.5 [2.5,15.5]	0.065 [0.055,0.085]
UD38	38.5 [29.3,46.5]	8 [4.0,14.5]	0.065 [0.055,0.085]

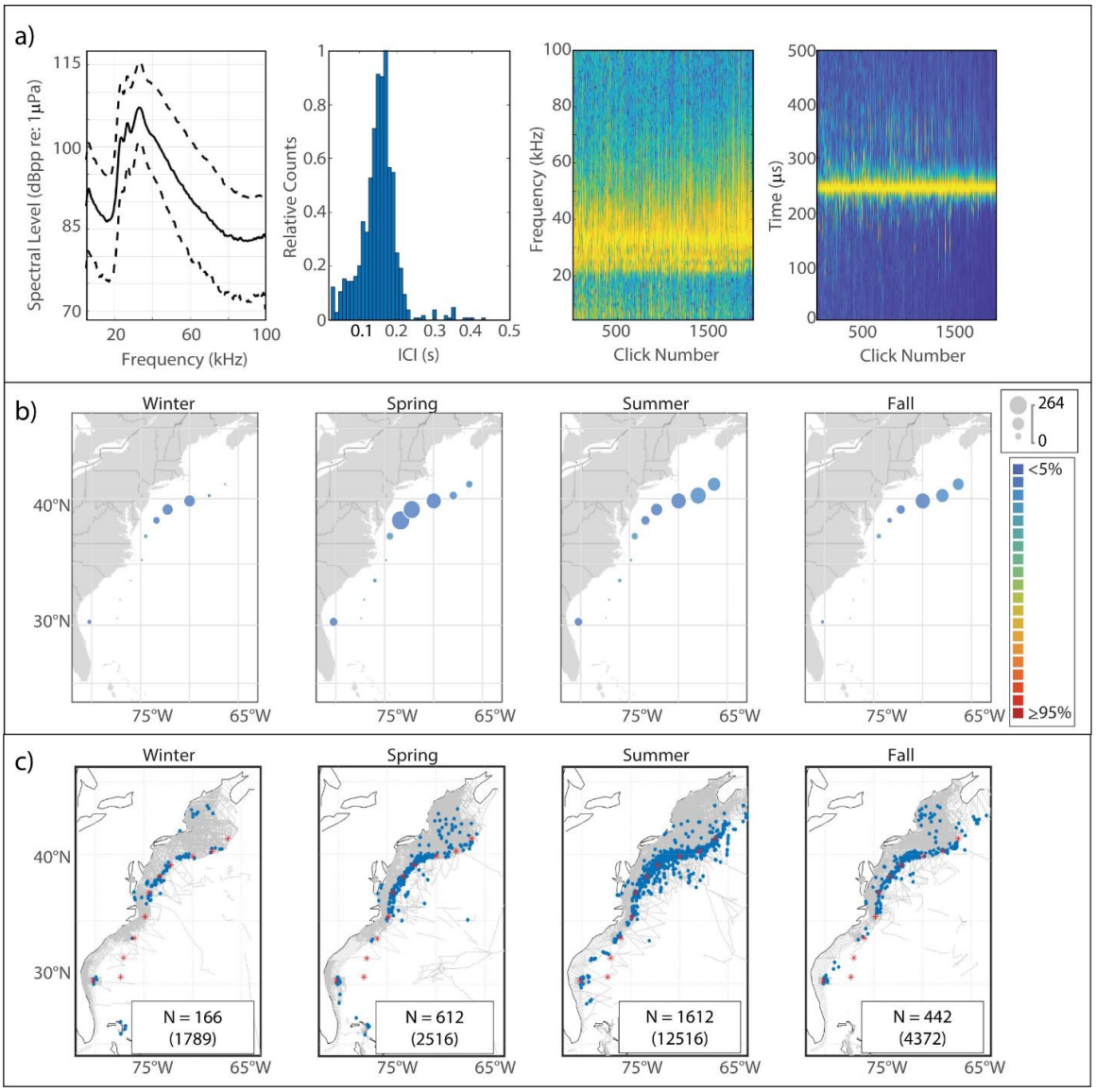

Figure 2.2: Results for Risso's dolphin showing click type (a), acoustic presence (b), and historical sightings (c). Click type plots, from left to right: median power spectrum (solid line) with 10th and 90th percentiles (dashed lines); distribution of modal ICI values from 1,000 5-minute bins; concatenation of normalized click spectra, sorted by received level; concatenation of normalized waveform envelopes, sorted by received level. For the concatenated spectra and waveform envelopes, the normalized magnitude of the frequency/pressure is represented by color such that warmer colors show greater magnitude. Acoustic presence shown as scaled circles depicting cumulative hours at each acoustic monitoring site per season, averaged across three years of data; classifier error given by color per legend in (b). Historical sightings per season (blue dots), shown relative to acoustic monitoring sites (red stars) and track lines of surveys undertaken in each season (grey lines). Inset within each sighting map shows number of sightings (N); total number of individuals summed across all sightings for which group size data was available is shown in parentheses.

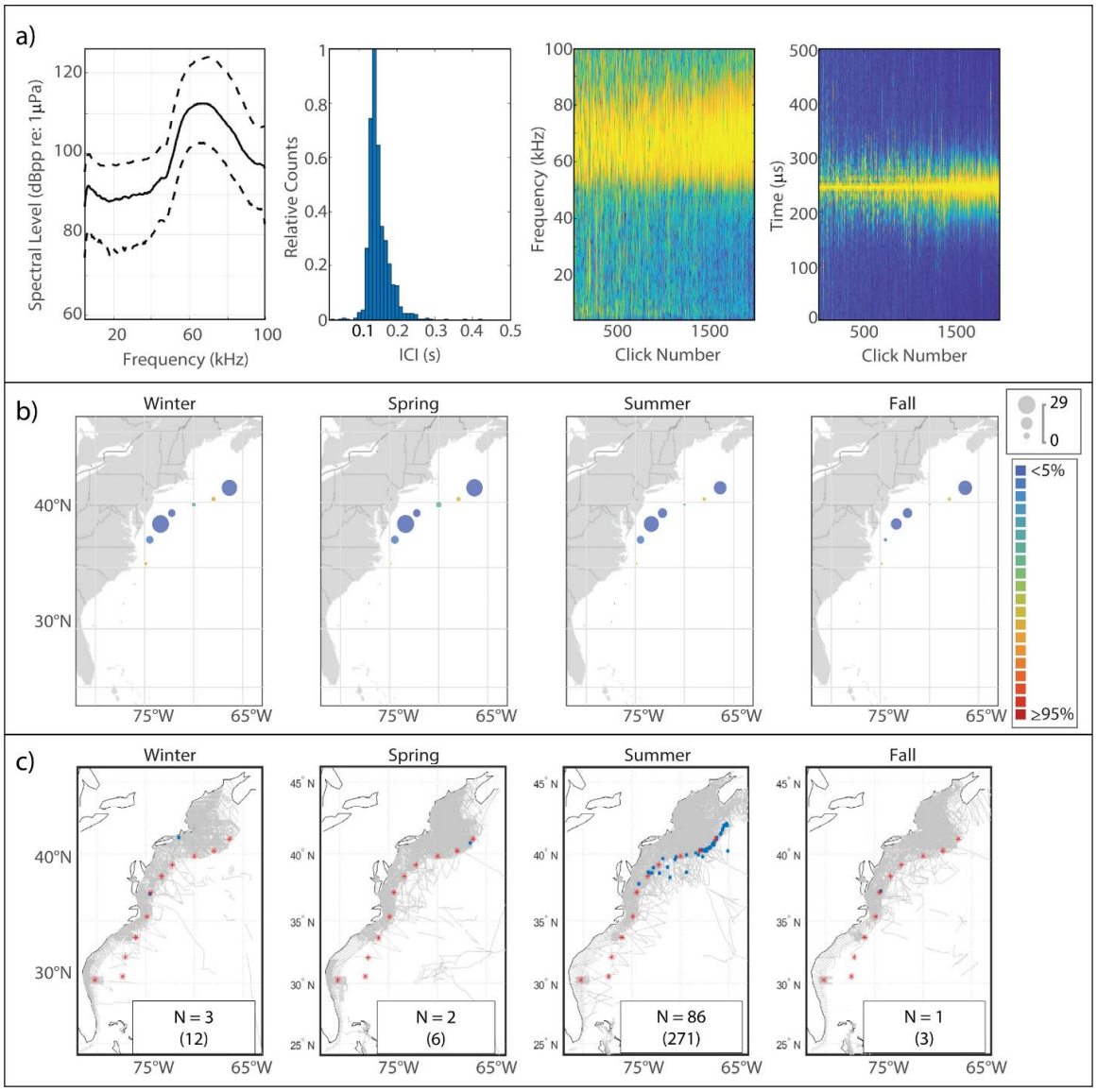

Figure 2.3 Results for Sowerby's beaked whale showing click type (a), acoustic presence (b), and historical sightings (c). Subplots as in Fig 1.2.

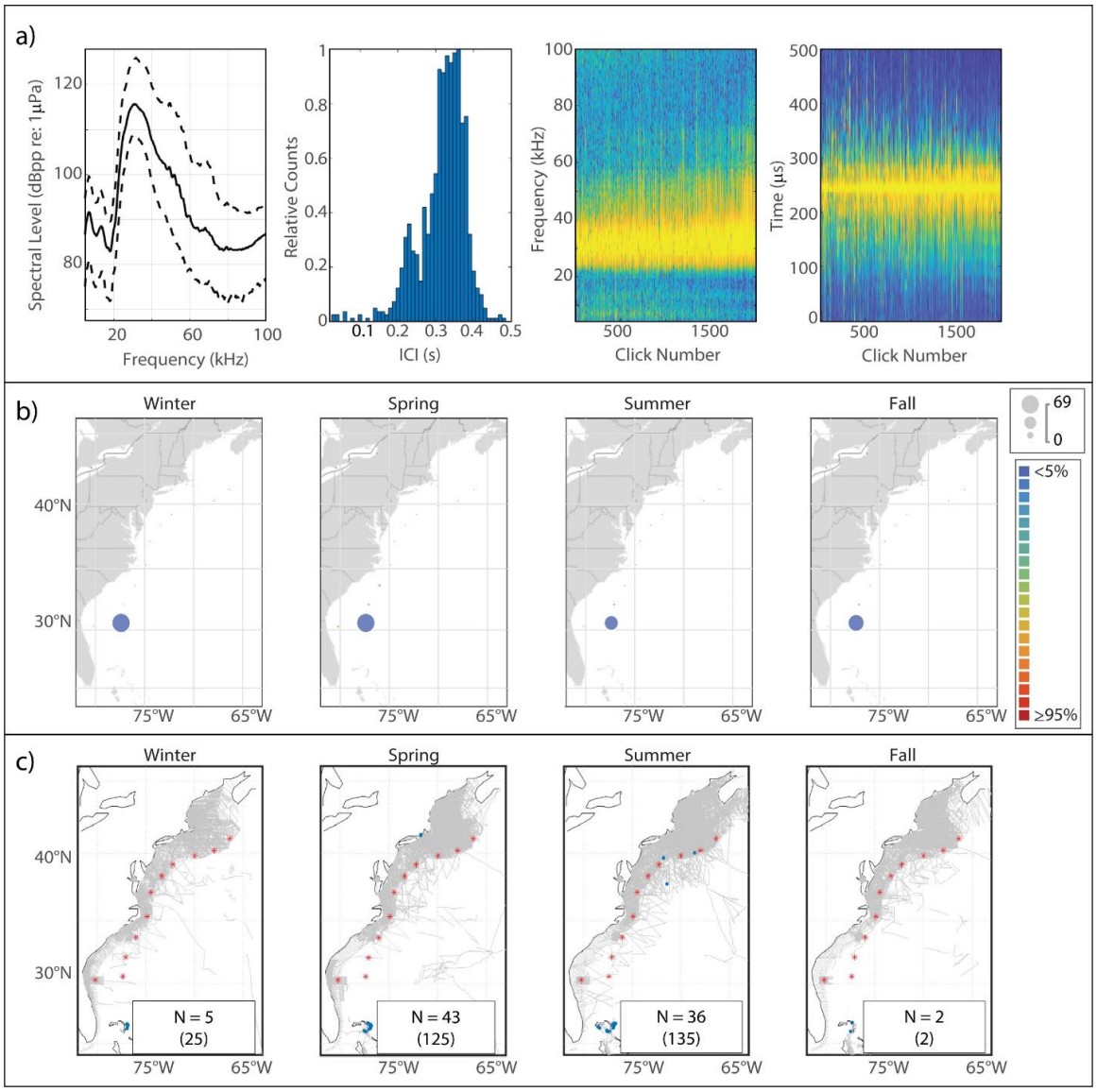

Figure 2.4: Results for Blainville's beaked whale showing click type (a), acoustic presence (b), and historical sightings (c). Subplots as in Fig 1.2.

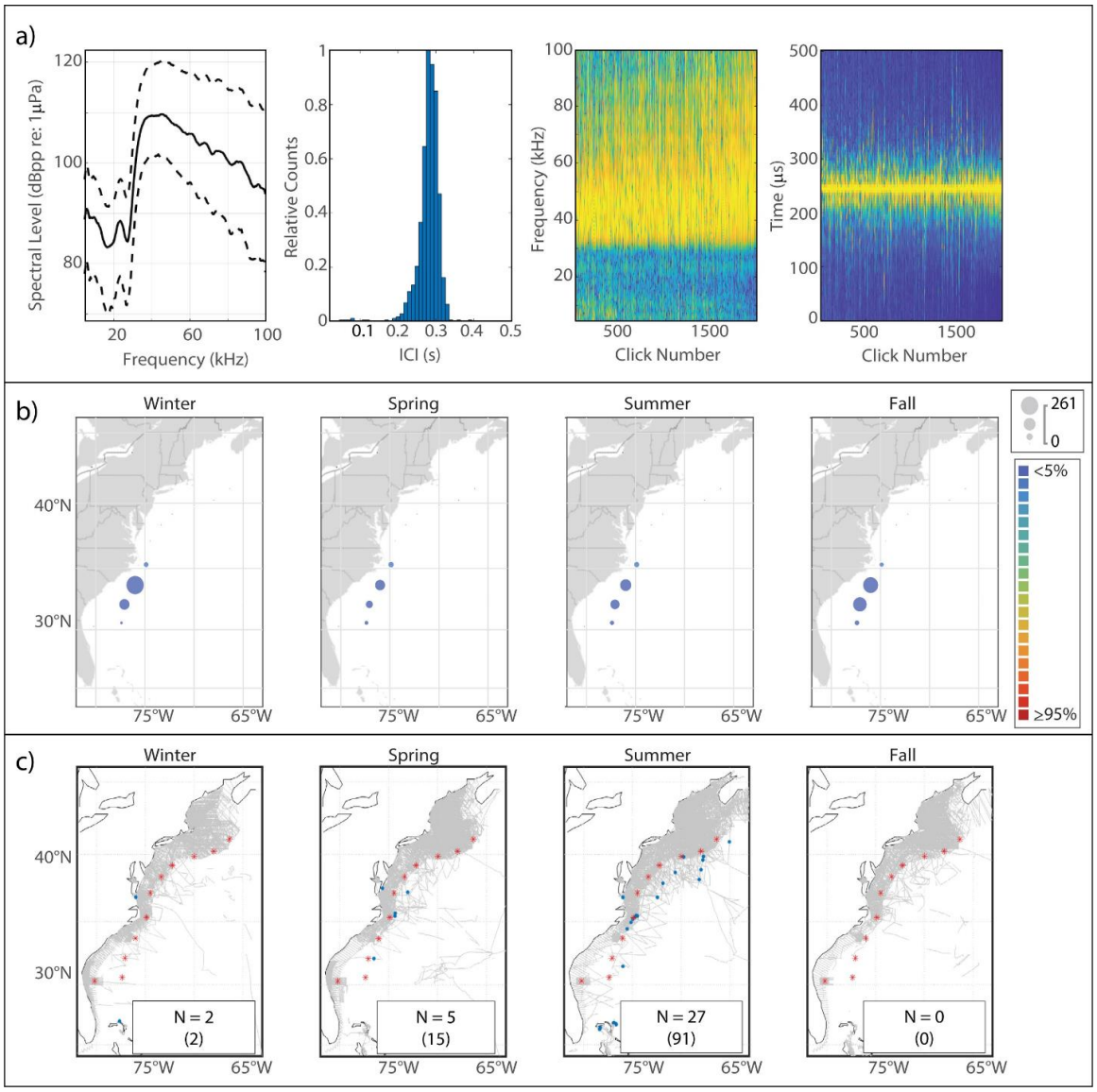

Figure 2.5: Results for Gervais' beaked whale showing click type (a), acoustic presence (b), and historical sightings (c). Subplots as in Fig 1.2.

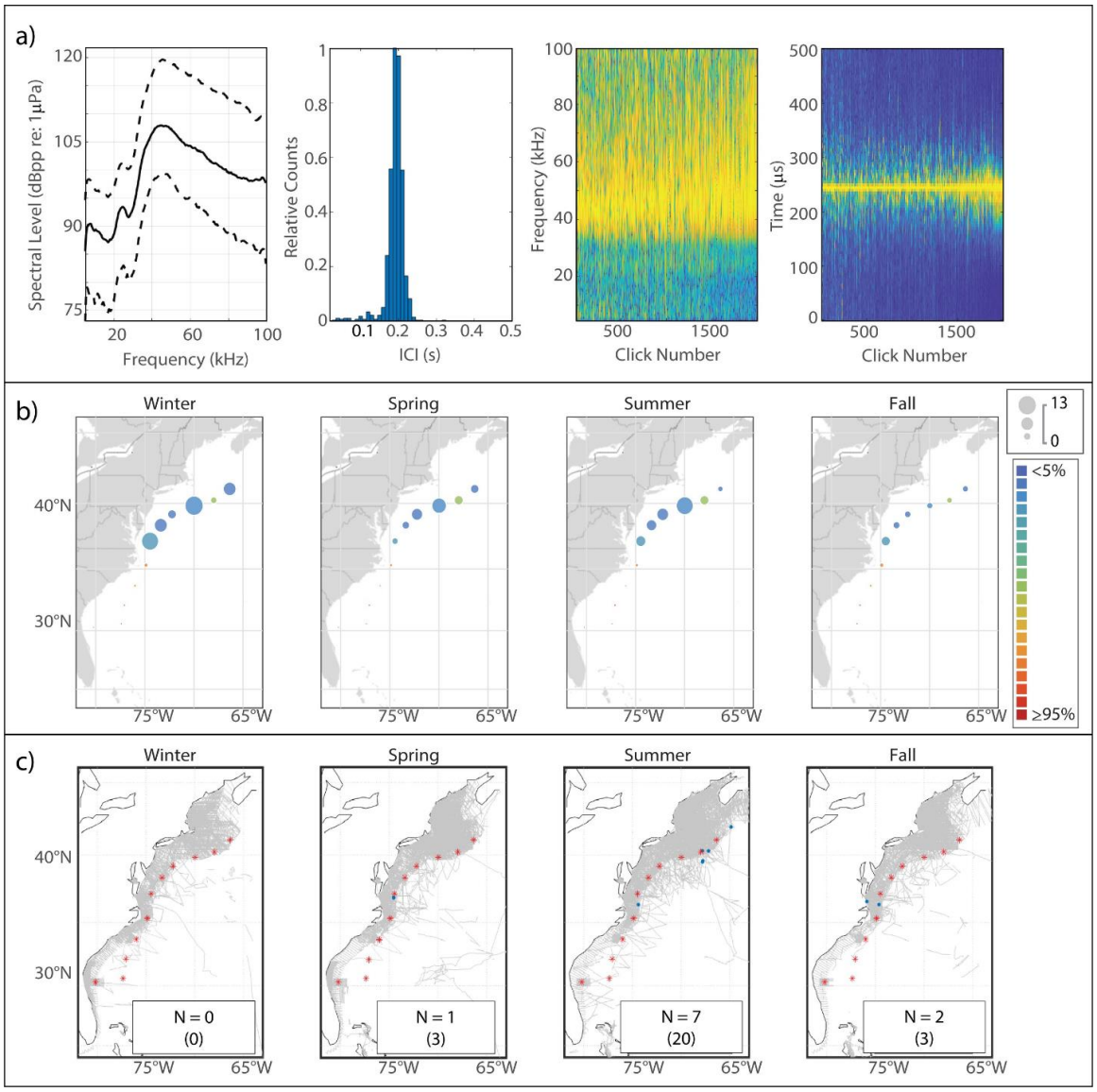

Figure 2.6: Results for True's beaked whale showing click type (a), acoustic presence (b), and historical sightings (c). Subplots as in Fig 1.2.

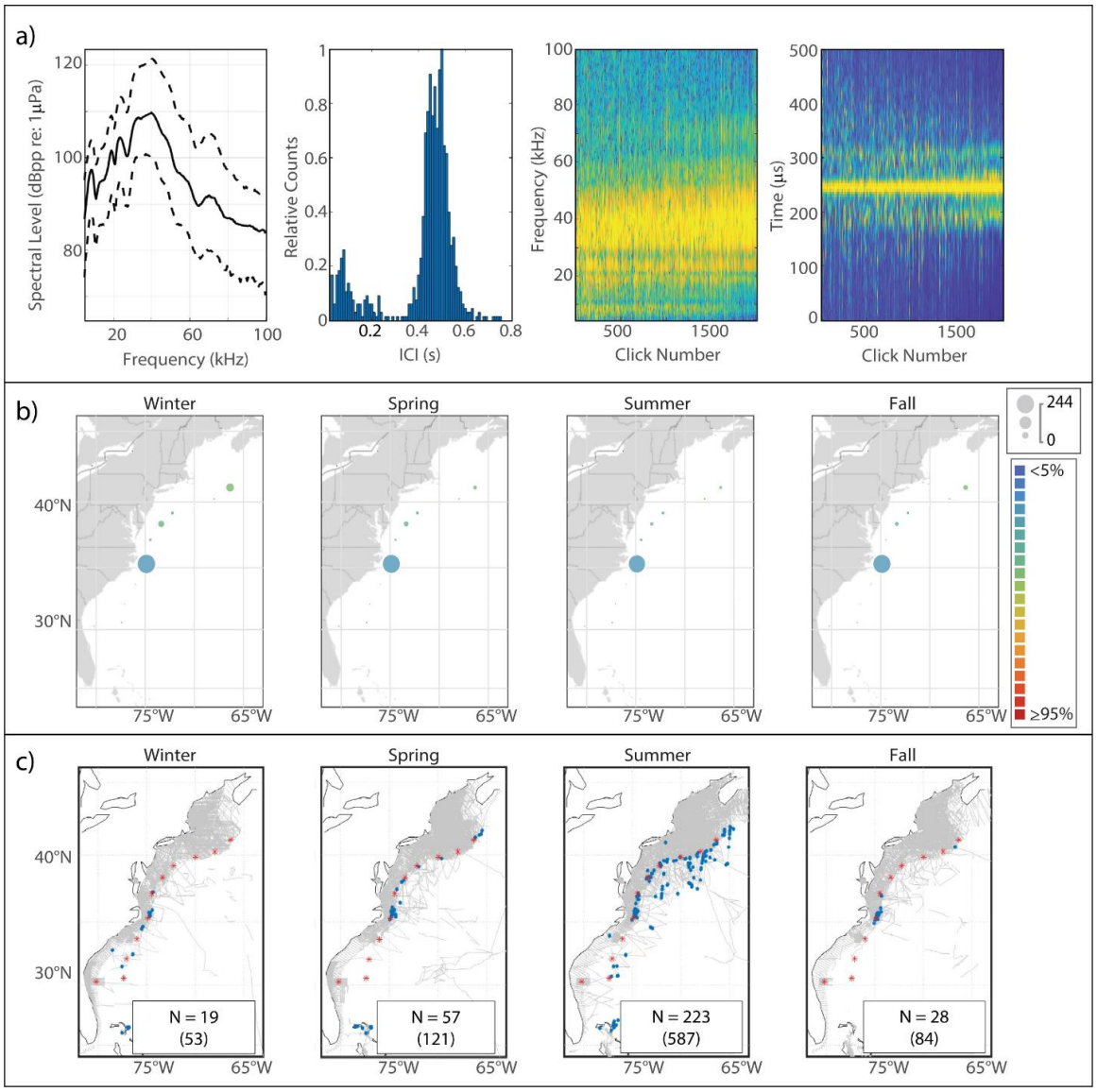

Figure 2.7: Results for Cuvier's beaked whale showing click type (a), acoustic presence (b), and historical sightings (c). Subplots as in Fig 1.2.

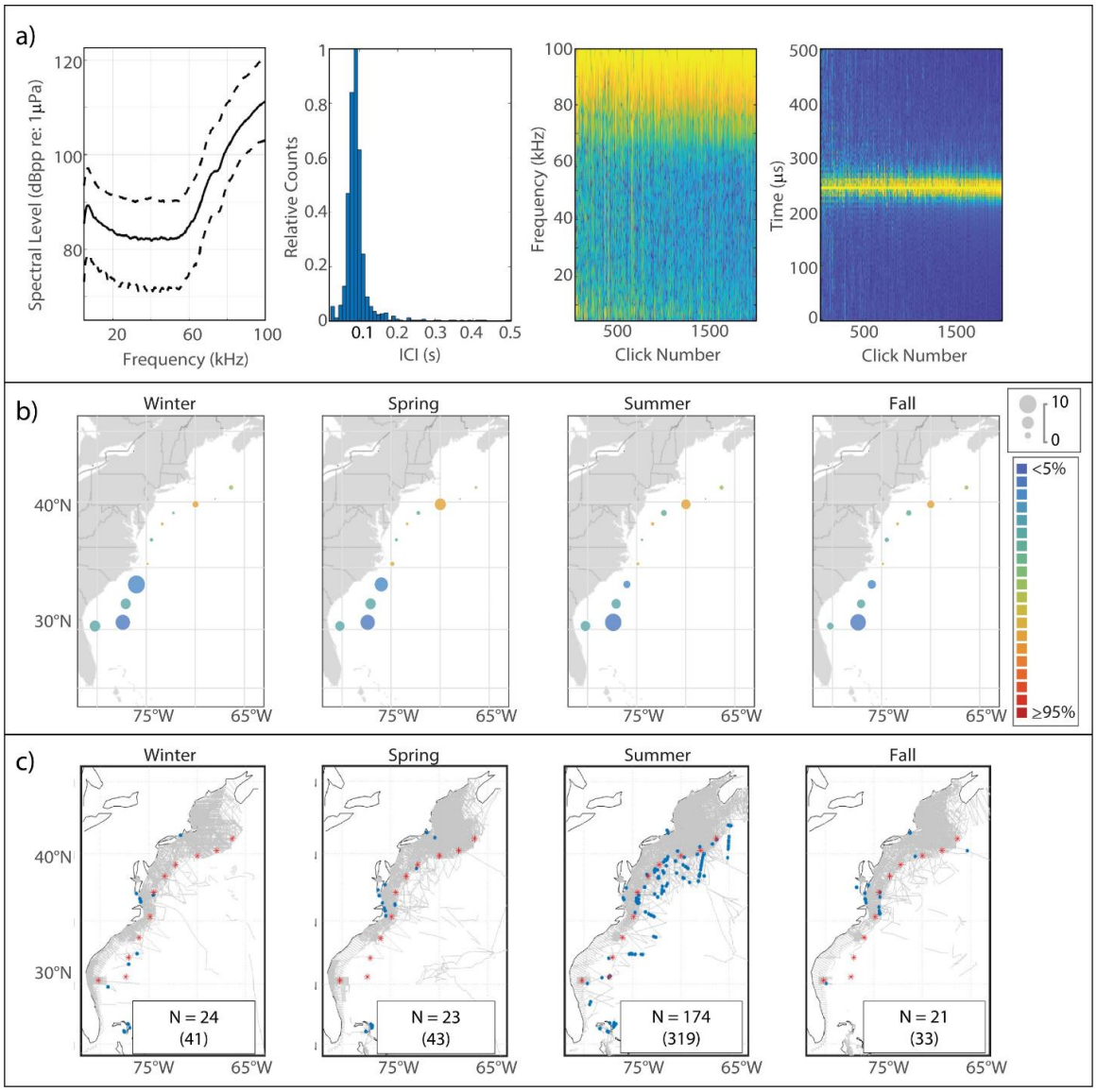

Figure 2.8: Results for *Kogia* spp. showing click type (a), acoustic presence (b), and historical sightings (c). Subplots as in Fig 1.2.

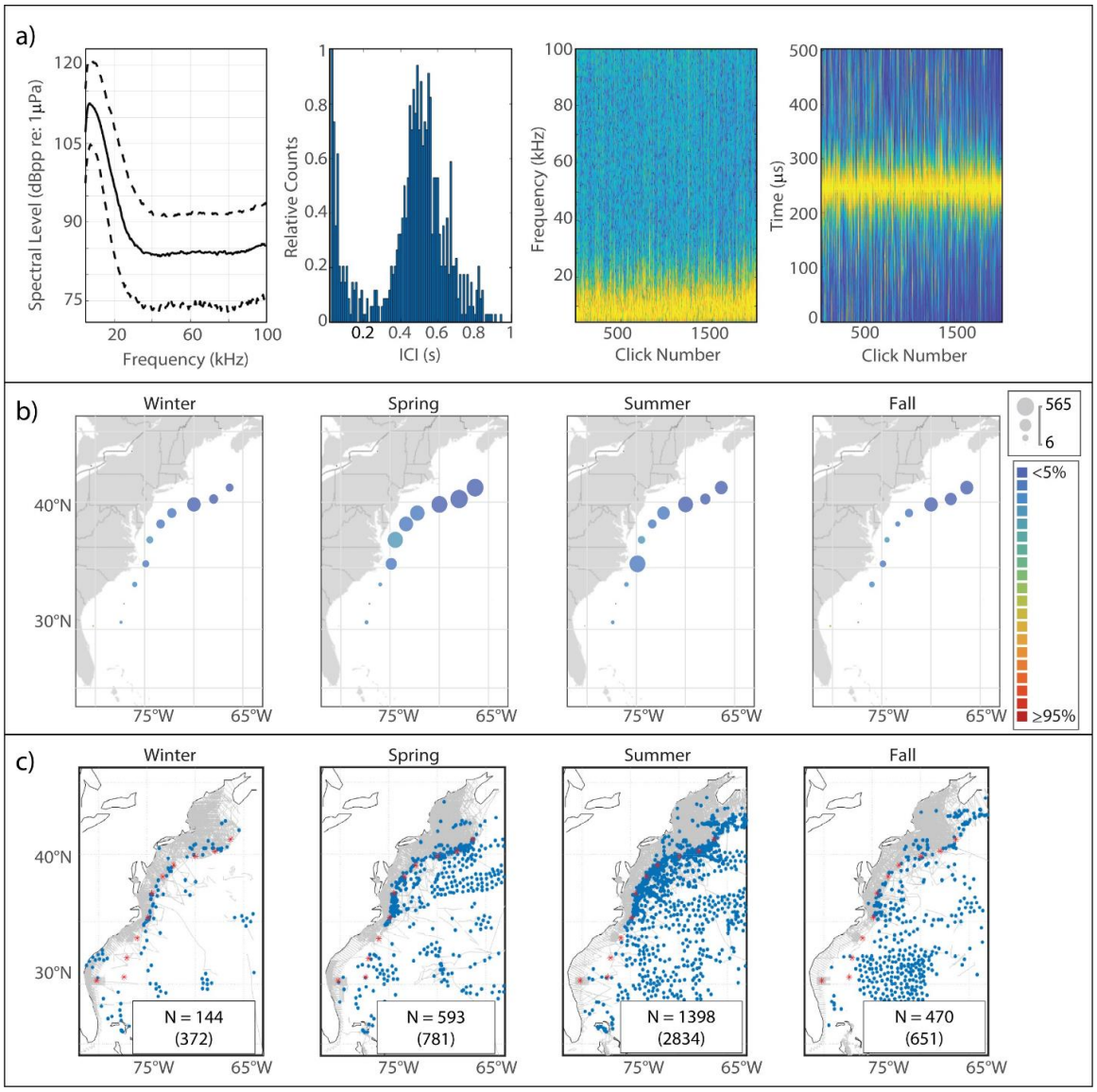

Figure 2.9: Results for sperm whale showing click type (a), acoustic presence (b), and historical sightings (c). Subplots as in Fig 1.2.

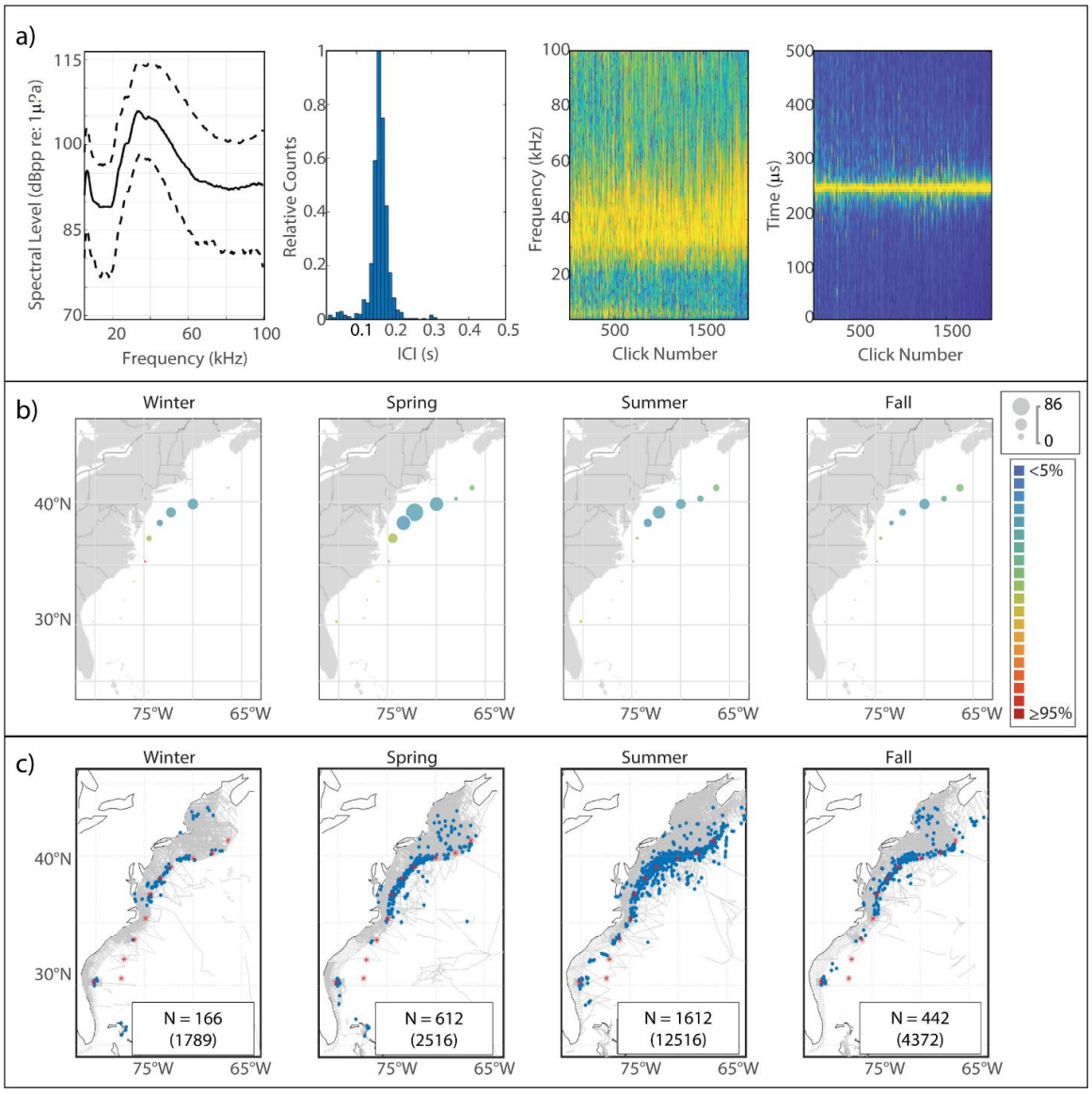

Figure 2.10: Results for UD36 showing click type (a), acoustic presence (b), and historical sightings of probable species match, Risso's dolphin (c). Subplots as in Fig 1.2.

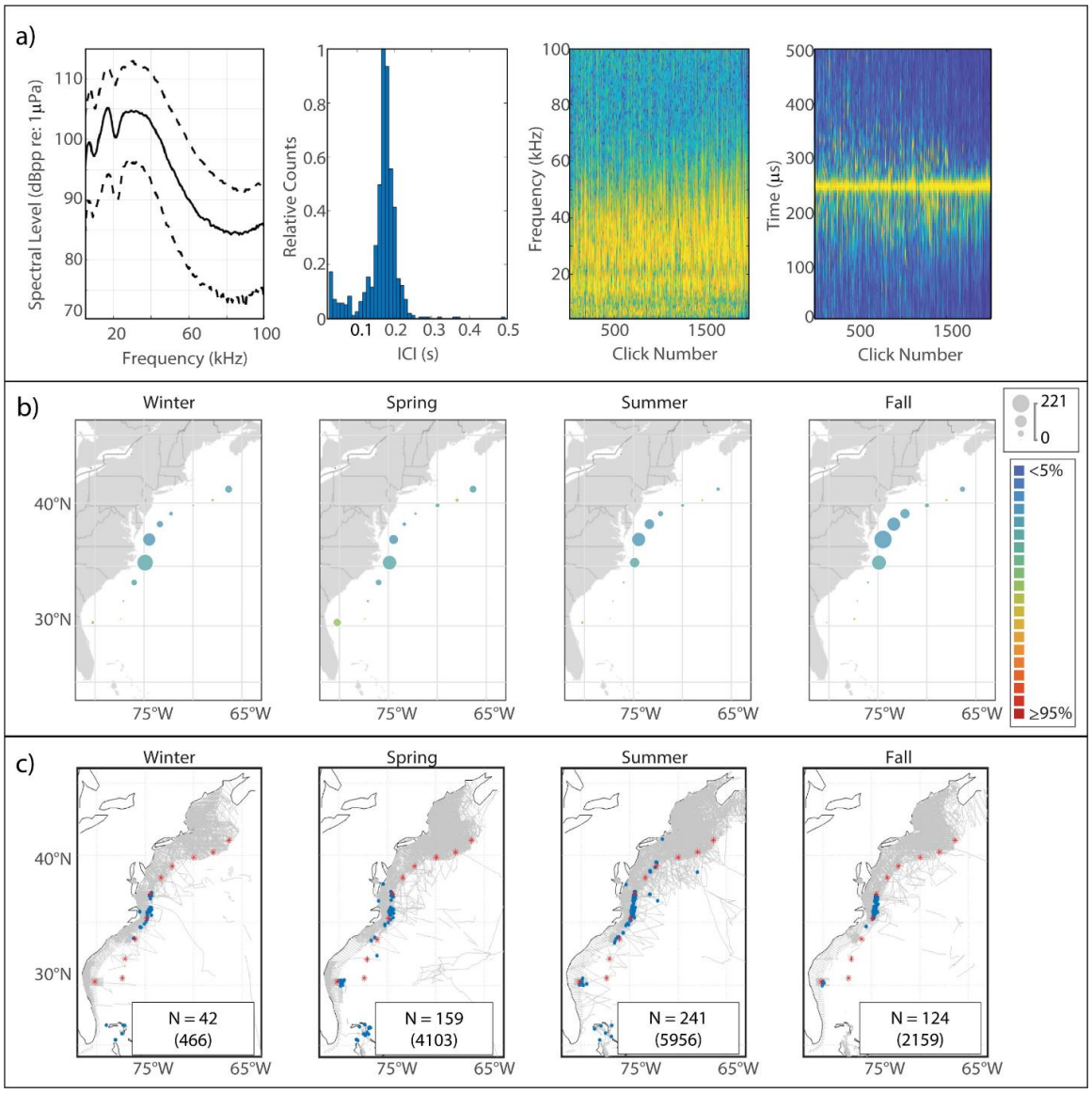

Figure 2.11: Results for UD26 showing click type (a), acoustic presence (b), and historical sightings of probable species match, short-finned pilot whales (c). Subplots as in Fig 1.2.

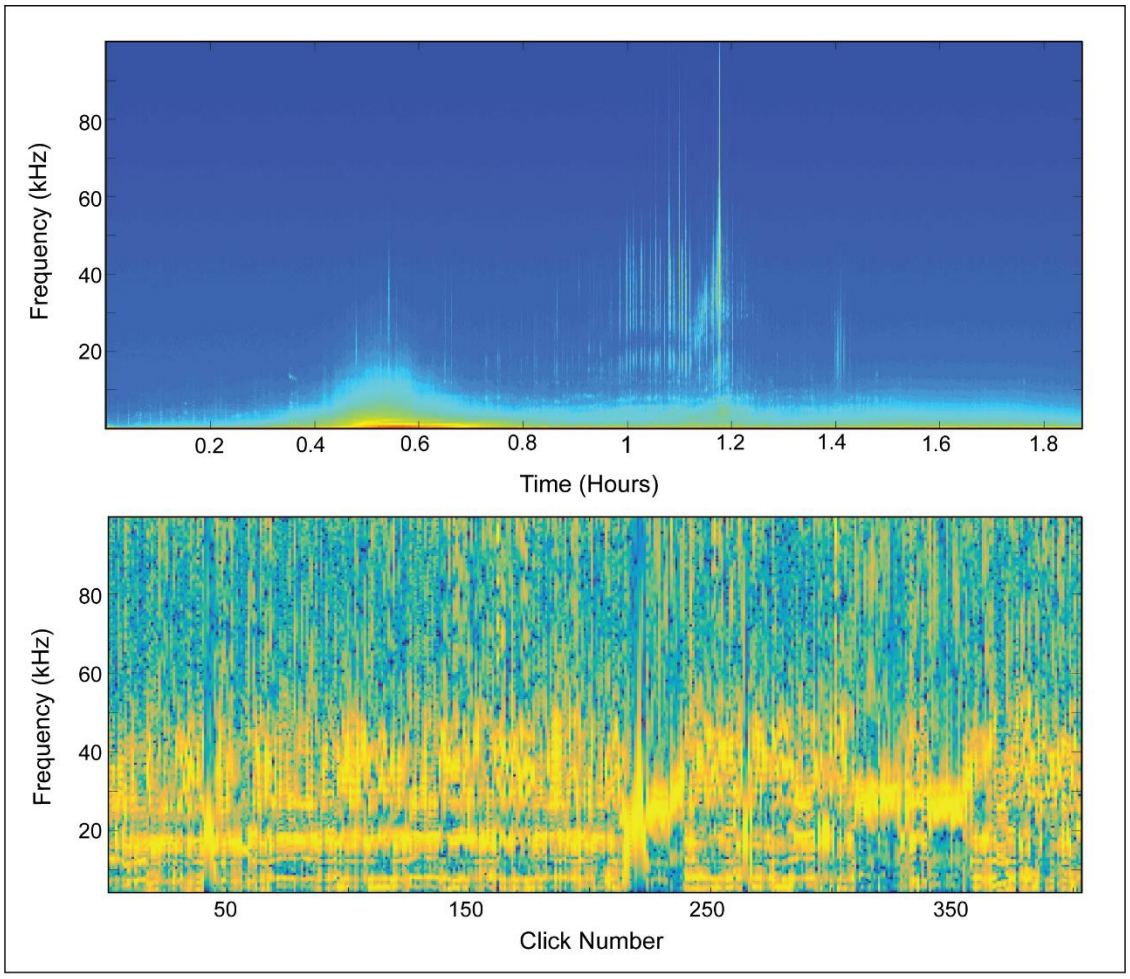

Figure 2.12: Visually confirmed short-finned pilot whale bout. Top panel: long-term spectrogram showing an acoustic encounter with visually-identified short-finned pilot whales at the JAX acoustic monitoring site. Bottom panel: concatenated spectra of clicks detected between 00:59 and 01:07. Most of these clicks exhibit spectral features consistent with UD26, though some natural variability is visible. In both plots the magnitude of the frequency is represented by color such that warmer colors show greater magnitude.

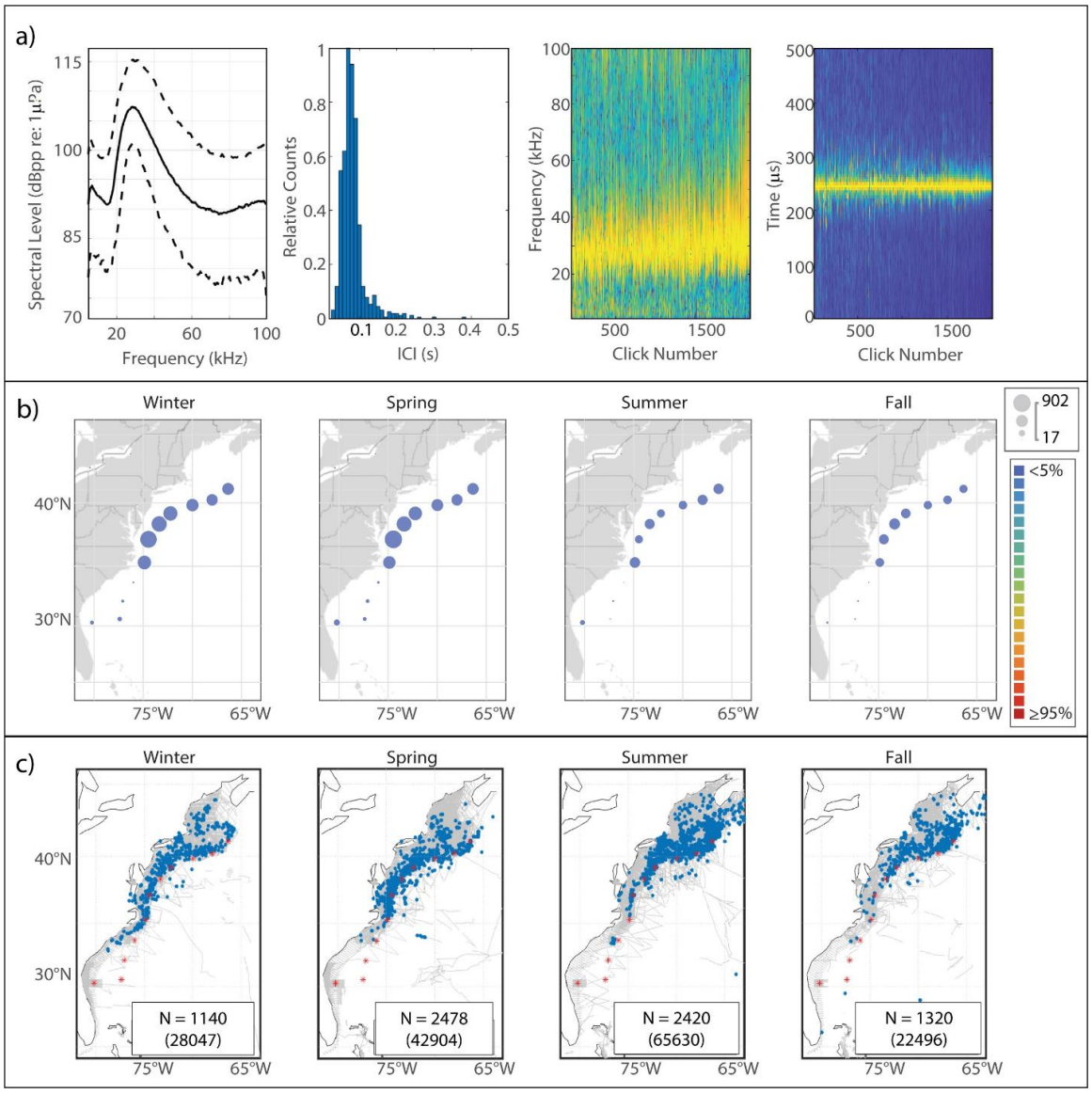

Figure 2.13: Results for UD28 showing click type (a), acoustic presence (b), and historical sightings of probable species match, short-beaked common dolphin (c). Subplots as in Fig 1.2.

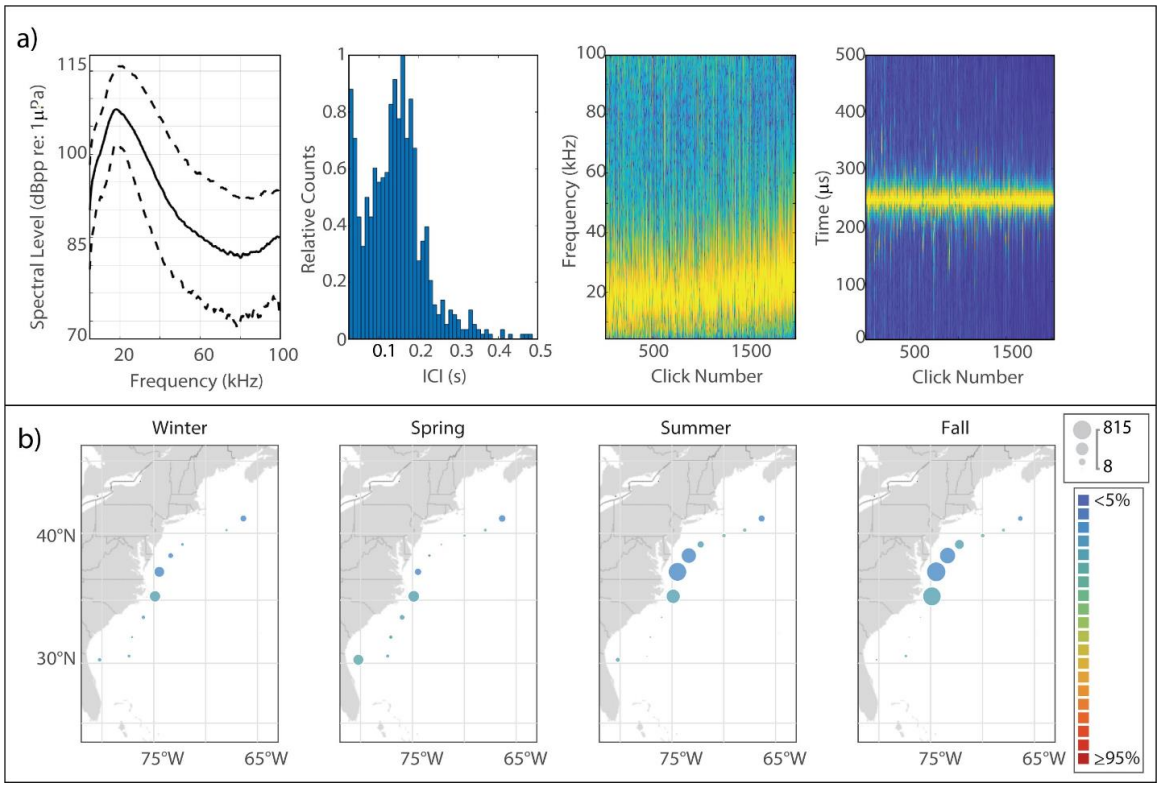

Figure 2.14: Results for UD19 showing click type (a), and acoustic presence (b). Subplots as in Fig 1.2(a-b).

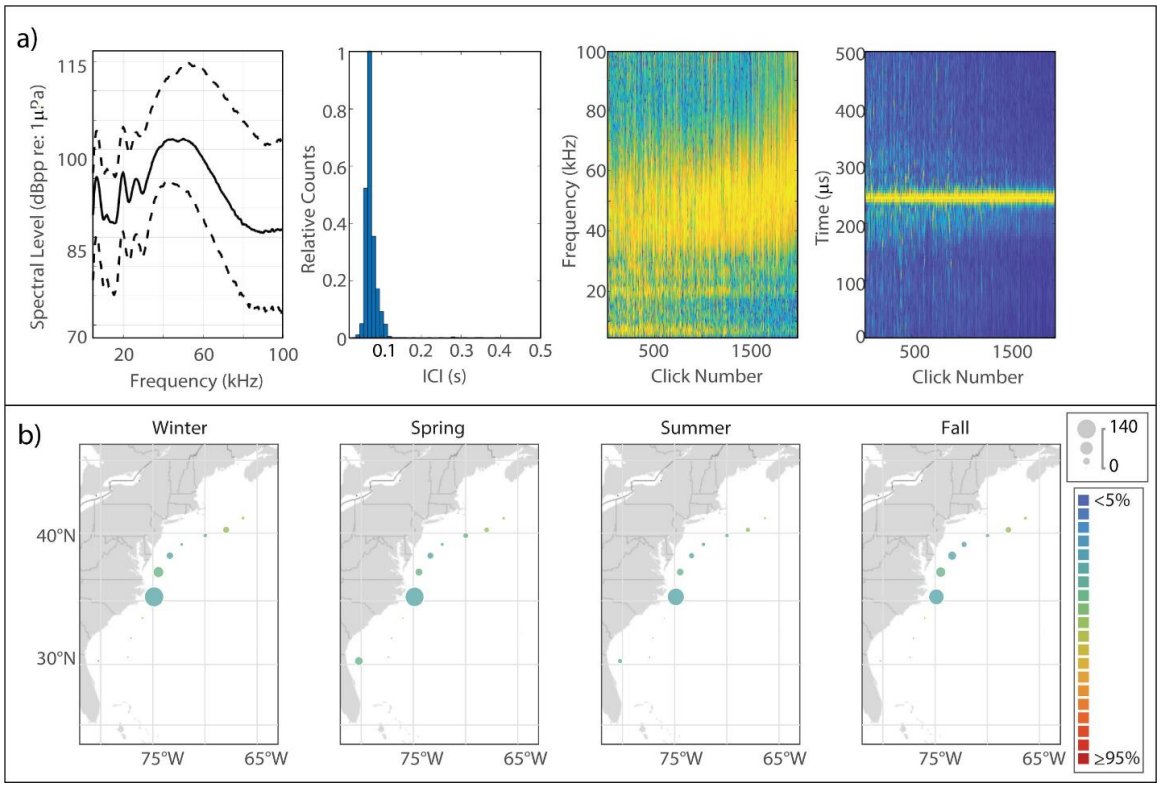

Figure 2.15: Results for UD47 showing click type (a), and acoustic presence (b). Subplots as in Fig 1.2(a-b).

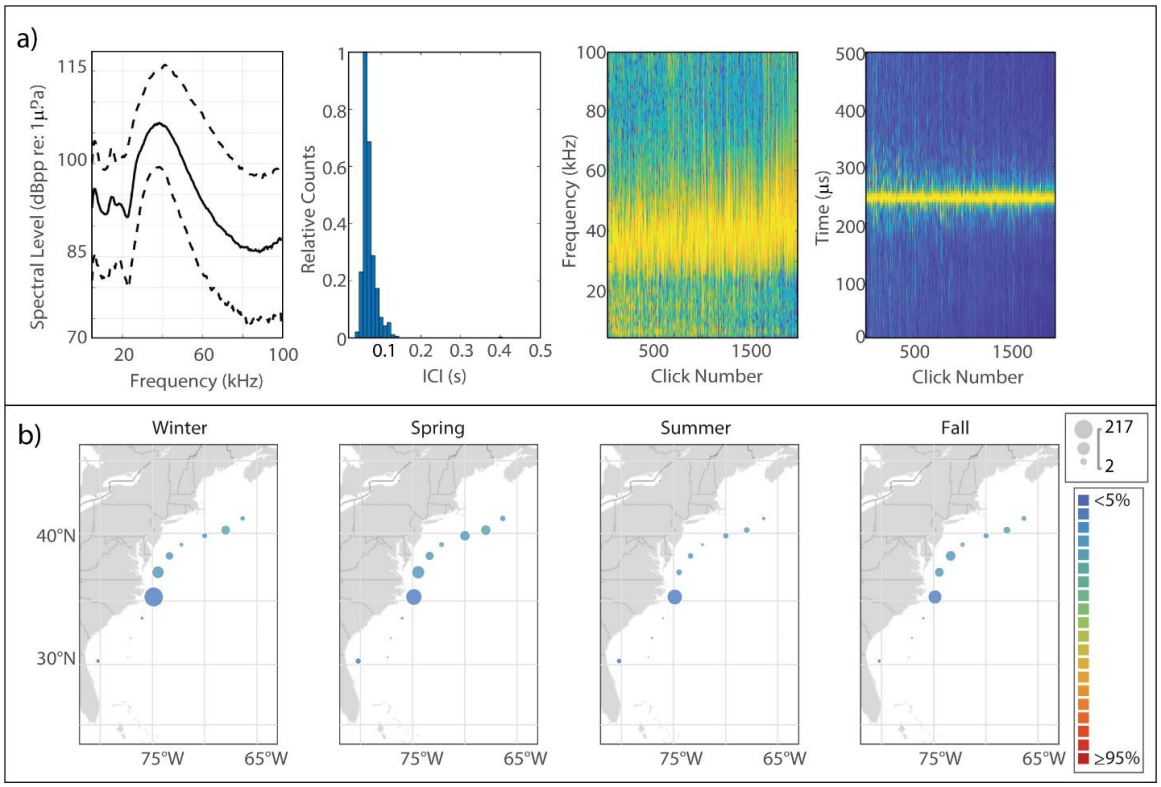

Figure 2.16: Results for UD38 showing click type (a), and acoustic presence (b). Subplots as in Fig 1.2(a-b).

Figure 2.17: Characteristics of noise classes; a) ships; b) mid-frequency sonar; c) high-frequency sonar; d) multi-frequency sonar; e) snapping shrimp. Columns are: median power spectrum (solid line) with 10^{th} and 90^{th} percentiles (dashed lines); distribution of modal IPI values from 1000 5-minute bins; concatenation of normalized impulsive signal spectra, sorted by received level; concatenation of normalized waveform envelopes, sorted by received level. For the concatenated spectra and waveform envelopes, the normalized magnitude of the frequency/pressure is represented by color such that warmer colors show greater magnitude.

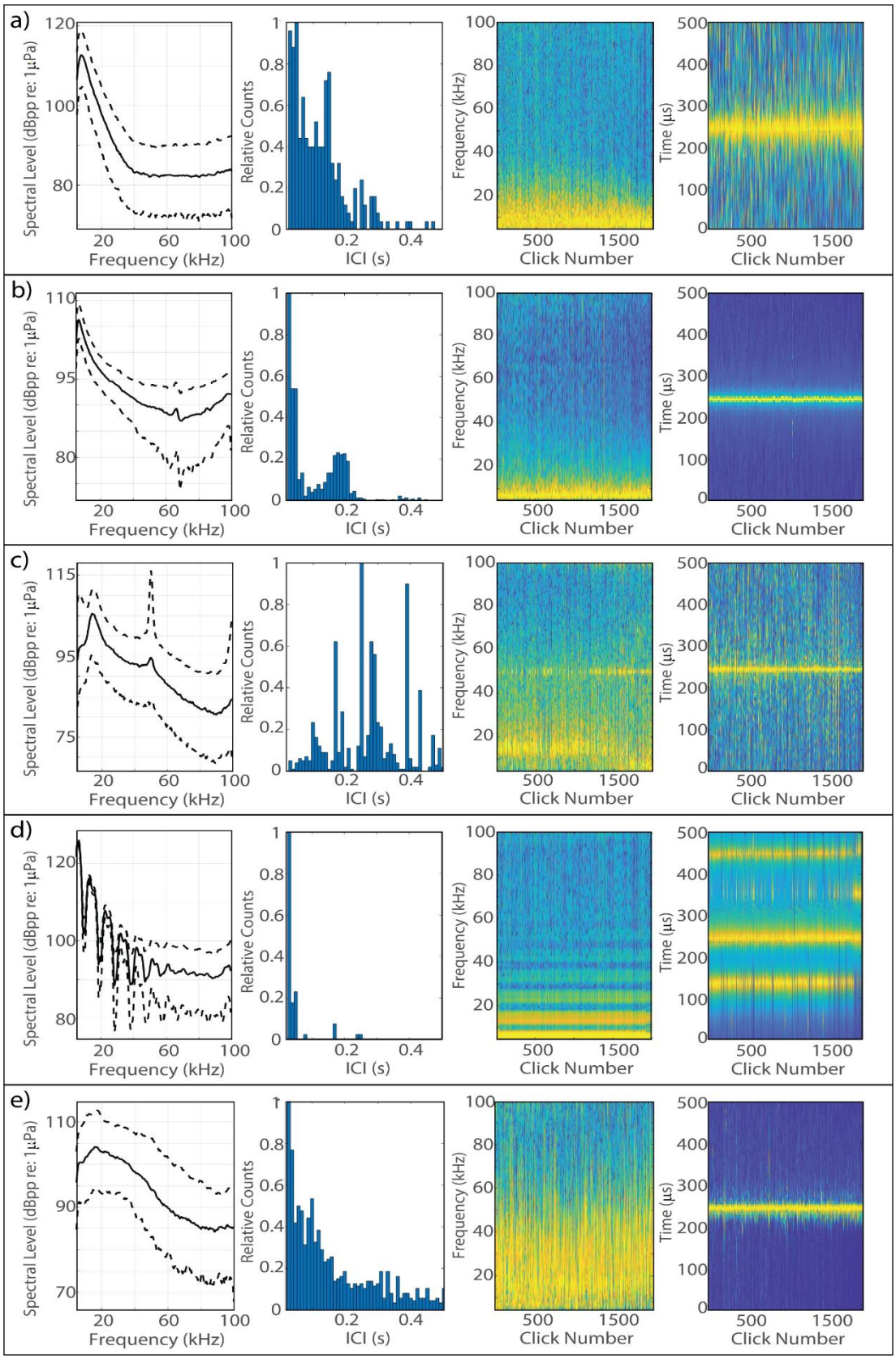
a)
b)
c)
d)
e)
Spectral Level (dBpp re: 1µPa)
Frequency (kHz)
Relative Counts
ICI (s)
Frequency (kHz)
Click Number
Time (µs)
Click Number

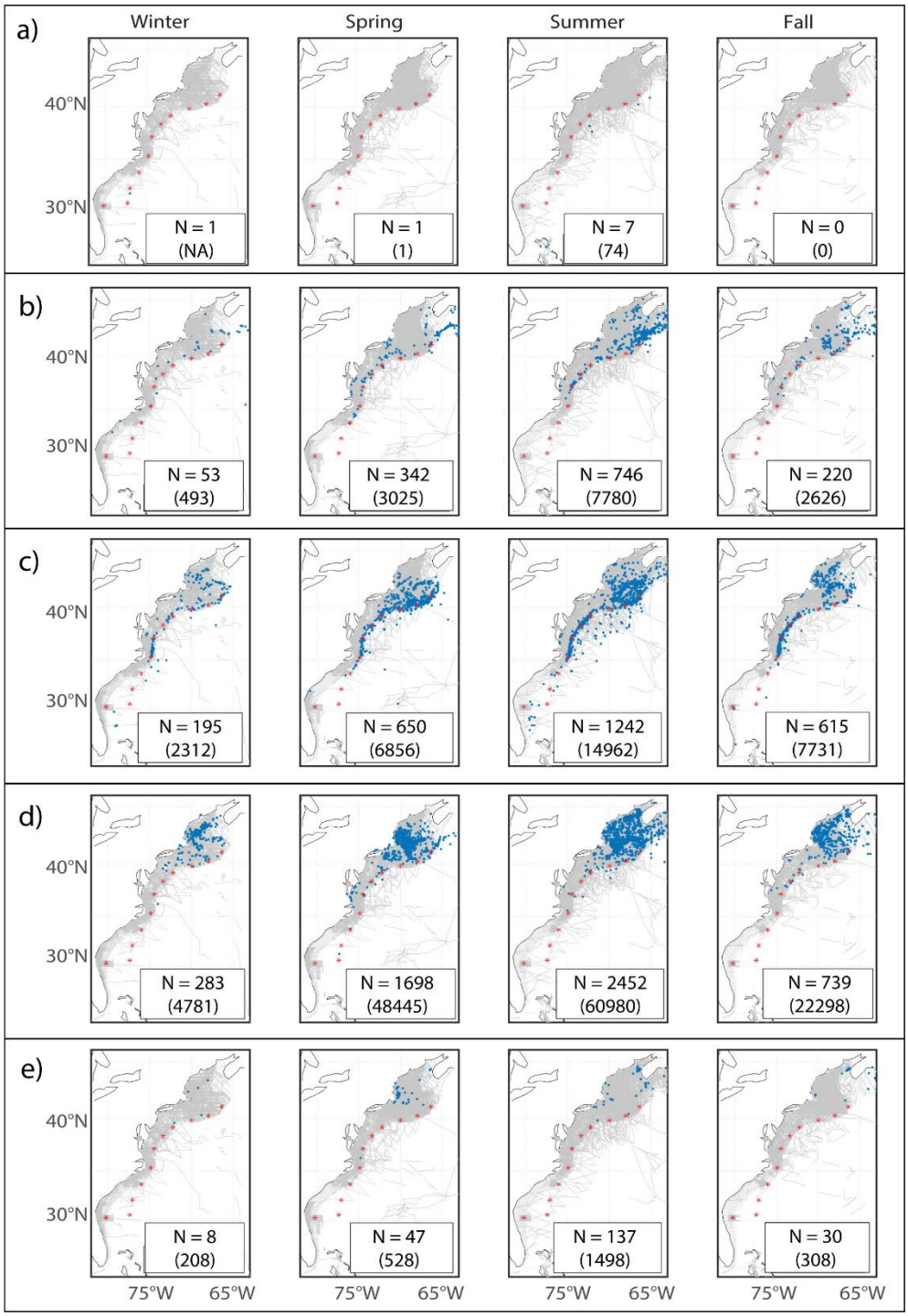

Figure 2.18: Historical sighting maps of a) pygmy killer whales (*Feresa attenuata*); b) long-finned pilot whales (*Globicephala melas*); c) *Globicephalinae* spp.; d) Atlantic white-sided dolphins (*Lagenorhynchus acutus*); e) white-beaked dolphins (*Lagenorhynchus albirostris*). Sightings are plotted per season (blue dots), shown relative to acoustic monitoring sites (red stars) and track lines of surveys undertaken in each season (grey lines). Inset within each sighting map shows number of sightings; total number of individuals summed across all sightings for which group size data was available is given in parentheses.

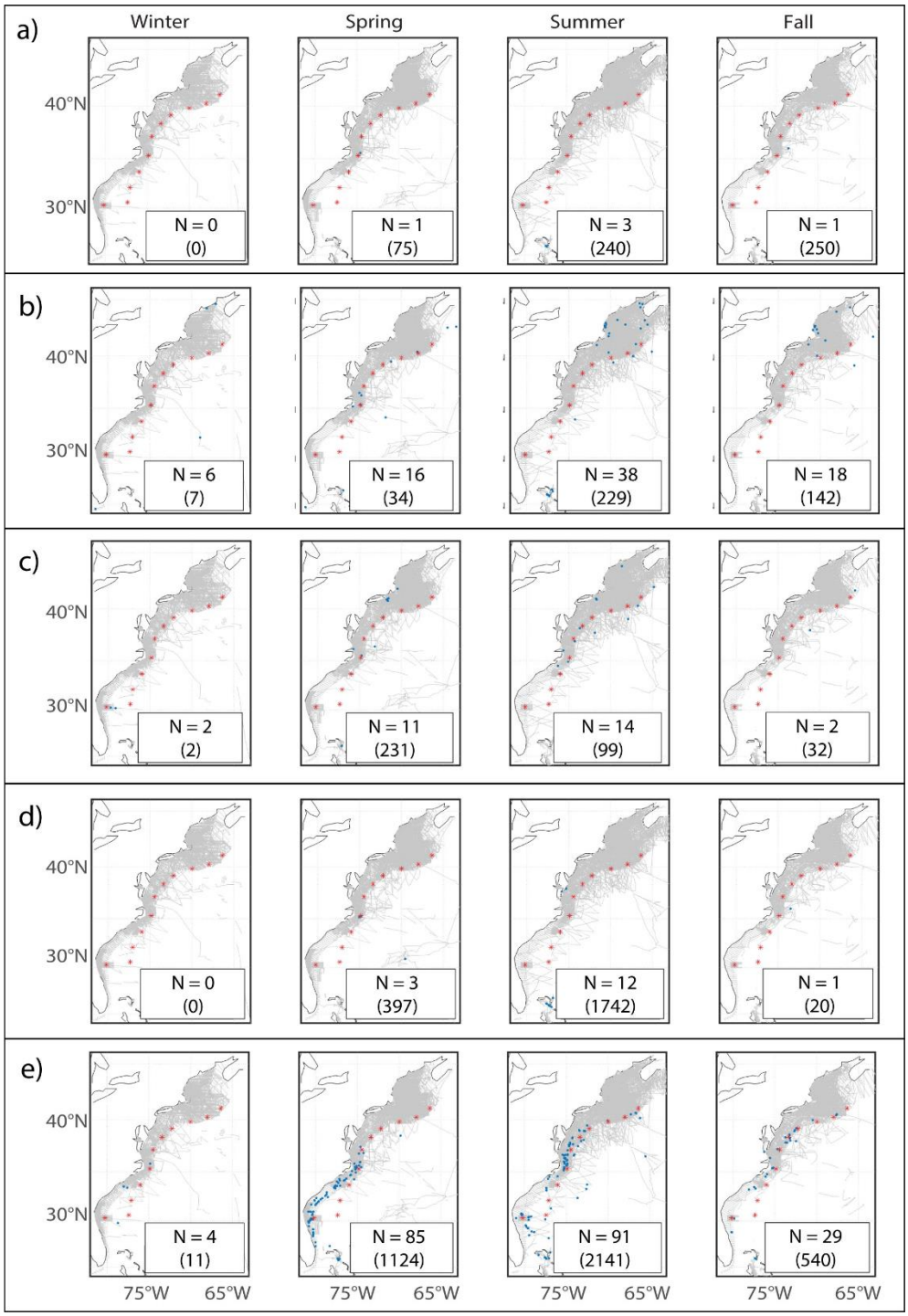

Figure 2.19: Historical sighting maps of a) Fraser's dolphin (*Lagenodelphis hosei*); b) killer whales (*Orcinus orca*); c) false killer whale (*Pseudorca crassidens*); d) melon-headed whale (*Peponocephala electra*); e) pantropical-spotted dolphins (*Stenella attenuata*). Sightings are plotted per season (blue dots), shown relative to acoustic monitoring sites (red stars) and track lines of surveys undertaken in each season (grey lines). Inset within each sighting map shows number of sightings; total number of individuals summed across all sightings for which group size data was available is given in parentheses.

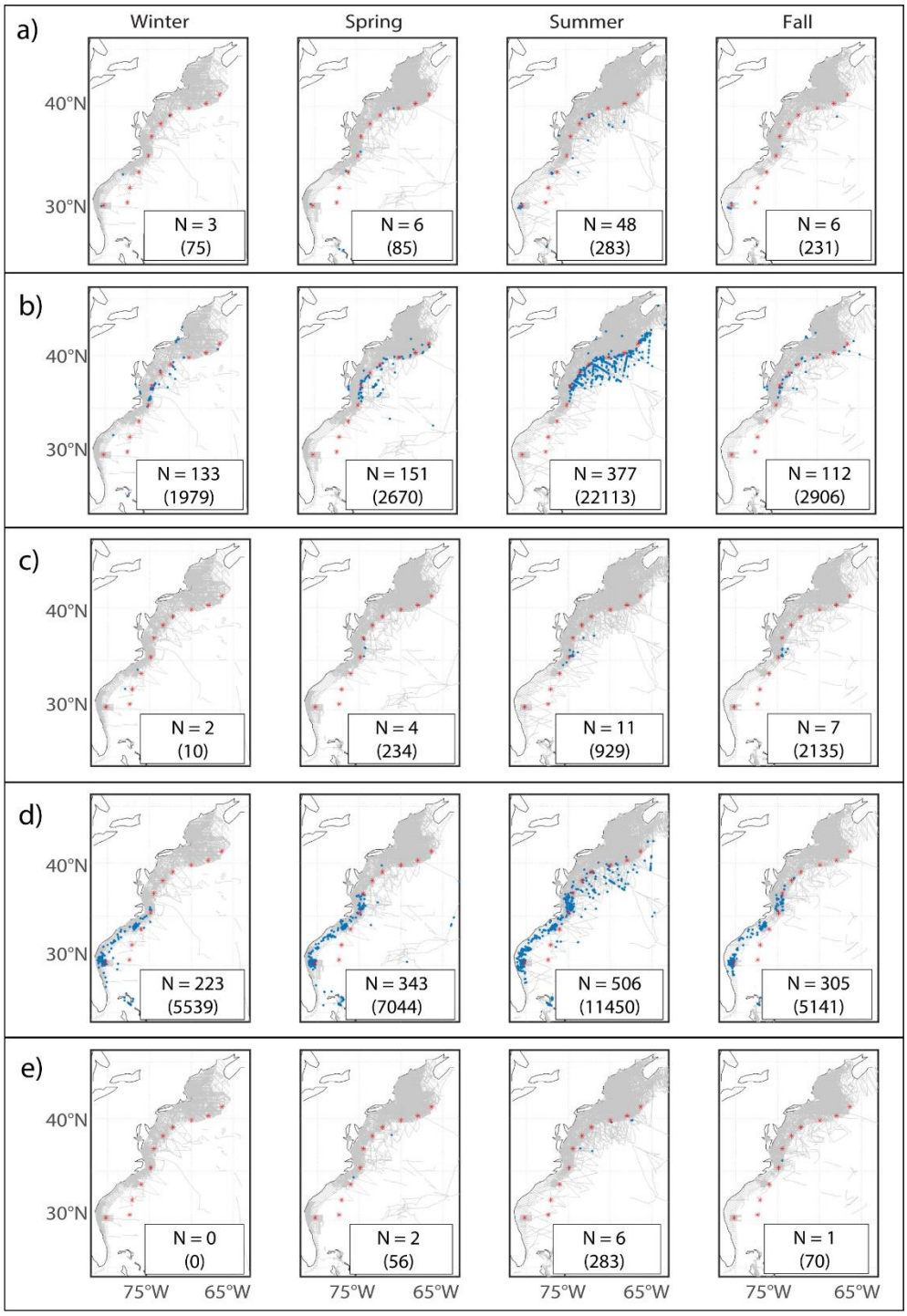

Figure 2.20: Historical sighting maps of a) rough-toothed dolphins (*Steno bredanensis*); b) striped dolphins (*Stenella coeruleoalba*); c) Clymene dolphins (*Stenella clymene*); d) Atlantic-spotted dolphins (*Stenella frontalis*); e) spinner dolphins (*Stenella longirostris*). Sightings are plotted per season (blue dots), shown relative to acoustic monitoring sites (red stars) and track lines of surveys undertaken in each season (grey lines). Inset within each sighting map shows number of sightings; total number of individuals summed across all sightings for which group size data was available is given in parentheses.

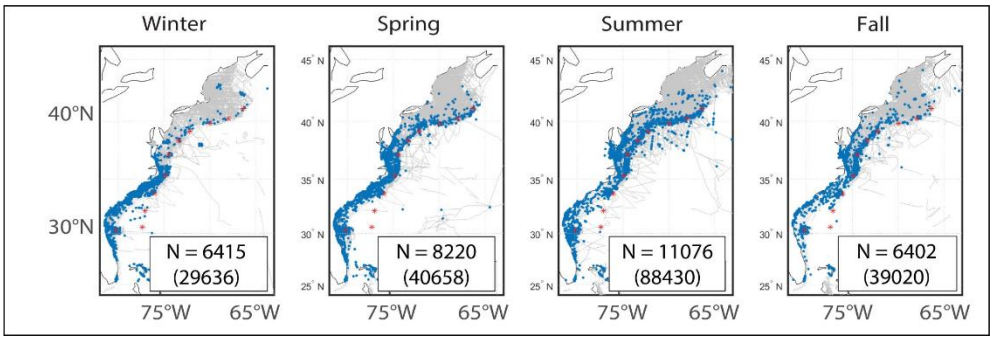

Figure 2.21: Historical sighting map of bottlenose dolphins (*Tursiops truncatus*). Sightings are plotted per season (blue dots), shown relative to acoustic monitoring sites (red stars) and track lines of surveys undertaken in each season (grey lines). Inset within each sighting map shows number of sightings; total number of individuals summed across all sightings for which group size data was available is given in parentheses.

2.8 APPENDIX

Noise Class Descriptions

Ships - Ship noise, produced through propeller cavitation and, to a lesser extent, mechanical noise from the operation of components such as engines, generators, fans, power plants, etc., exhibits a power spectrum with most energy in the 10-100Hz range, though energy may extend as high as 10kHz [108,109] (Figure 2.17a). Since cavitation bubbles are not produced at a regular rate, the inter-impulse-interval distribution for boat noise is right-skewed.

Mid-Frequency Sonar - This class accounts for the presence of mid-frequency (1 kHz – 10 kHz) sonar at several of our southern sites (Figure 2.17b). The inter-pulse-interval histogram for this class is likely multimodal due to the use of variable ping rates across different instances of the use of this sonar.

High-Frequency Sonar - This class was created as a catchall for a few types of high-frequency (>10 kHz) sonar observed in our data; the training examples included signals with peak frequencies at 14 kHz, 50 kHz, and 69 kHz (Figure 2.17c). The inter-pulse-interval histogram for this class is likely multimodal due to the use of variable ping rates across different instances of the use of this sonar.

Multi-Frequency Sonar - This class accounts for the presence of what may be multi-beam sonar at some of our types; in the training examples for this class, multiple energy peaks are present simultaneously (Figure 2.17d).

Snapping Shrimp - Snapping shrimp produce broadband impulses which look spectrally similar to echolocation clicks ([84][110], Figure 2.17e). However, there is no coherent snapping rate, and so the inter-pulse-interval histogram exhibits a right-skewed distribution.

2.9 ACKNOWLEDGEMENTS

This project used data collected through collaborations between the Marine Bioacoustics Research Collective (MBARC) and both the National Oceanic and Atmospheric Administration (NOAA) and the US Navy. Many thanks to Sofie Van Parijs and Danielle Cholewiak of NOAA Northeast Fisheries Science Center (NEFSC), Joel Bell of Naval Facilities Engineering Command (NAVFAC) Atlantic, Michael Richlen of HDR, and Andrew Read (Duke University) for project support and sampling design development. Thanks also to Eric Matzen of NEFSC, and Drexel "Stormy" Harrington, Drex Harrington, and Bev Harrington of the Tiki XIV, for fieldwork support enabling instrument deployment and recovery. Several members of the SIO Whale Acoustics Laboratory and the Scripps Acoustic Ecology Lab made substantial contributions to this project: thanks to Bruce Thayre, John Hurwitz, Jennifer Trickey, and Ryan Griswold for acoustic device development, testing, deployment, and recovery; to Erin O'Neill for acoustic data pre-processing and quality control; and to Morgan Ziegenhorn for discussions which contributed to the development of the neural network classifier, the evaluation of classifier performance, and the establishment of the click types presented here.

Chapter 2, in full, is a reprint of the material as it appears in Cohen, R.E., K.E. Frasier, S. Baumann-Pickering, S.M. Wiggins, M.A. Rafter, Baggett, L.M., J.A. Hildebrand. (2022). Identification of western North Atlantic odontocete echolocation click types using machine learning and spatiotemporal correlates. PLOS One 17(3): e0264988. The dissertation author was the primary investigator and author of this paper.

3 SPATIAL AND TEMPORAL SEPARATION OF TOOTHED WHALES IN THE WESTERN NORTH ATLANTIC

3.1 ABSTRACT

A diverse group of odontocetes inhabits the pelagic habitats of the western North Atlantic, a region characterized by the dynamic Gulf Stream western boundary current. As top predators targeting mid-trophic level fish and squid, this co-occurrence would seem to give rise to competition for prey resources. A variety of spatial, temporal, and behavioral separation strategies have been observed among predator guilds in both marine and terrestrial systems, but little is known about the life histories of many of these odontocete species and how they mitigate direct competition. Historically, visual survey data has been relied upon to gain insights into the ecology of these species, but large ranges, low densities, and at times cryptic surface behaviors have resulted in a paucity of sightings for most. These data deficits have limited our ability to carry out fundamental research, such as establishing baselines of distribution and abundance, much less addressing higher-level ecological questions about interspecies interactions. More recently, passive acoustic data has been successfully exploited to monitor pelagic species continuously, and with improved detection and species resolution in the case of some cryptic species. Here we utilized a long-term passive acoustic data set collected at eleven shelf break and slope monitoring sites spanning the region to quantify presence and characterize seasonal, lunar, and diel activity patterns for ten odontocete species. Our results demonstrated strong regional preferences, with most species exhibiting higher levels of presence north of the Gulf Stream front. Additionally, we found clear patterns of spatiotemporal separation between species with similar foraging ecology when they occurred in the same areas. The dolphin species exhibited much stronger diel activity patterns than the deep diving beaked whales, sperm whales, and *Kogia* spp. We also observed substantial variability in diel activity patterns, which were modulated both by the seasonal cycle and lunar cycles, and sometimes also varied between sites. We situate these findings in the context of the foraging ecology of each species. This is the first study characterizing year-round, day-

and-night temporal activity patterns for many of these species in this region, and reveals new insights into the complex behavior patterns arising in response to natural cycles playing out over three different temporal scales (seasonal, lunar, diel).

3.2 INTRODUCTION

Marine predators in the pelagic environment are challenged to find prey that are often low-density, patchy, and transient. They must maximize foraging efficiency while simultaneously minimizing competitive interactions between species. For mobile species a variety of spatial, temporal, and behavioral separation strategies, have been observed, such as differing diel activity patterns, depth distributions, seasonal changes in site occupancy or habitat use, and prey specialization [111–115]. These are generally thought to be means of reducing interspecies competition.

More than two dozen odontocete, or toothed whale, species inhabit the western North Atlantic. All odontocetes are top predators and can be loosely divided into two groups based on their diving and foraging ecology: shallow divers, such as small-bodied delphinids, feed primarily on epi- and mesopelagic fish and squid in surface waters, while deep divers, such as beaked whales, Kogia spp., and sperm whales are specialized for pursuit of meso-, bathy-, and benthopelagic prey. Species within each of these groups target similar prey, increasing the potential for interspecific competition, but the radiation and success of this large group argues for effective means of managing such competition.

The western North Atlantic is characterized by the Gulf Stream current, which bisects the region and acts as a frontal boundary between two different oceanic regimes, as well as a driver of mixing between very different water masses [46]. South of Cape Hatteras, North Carolina, warm, high-salinity, low-nutrient Gulf Stream waters originating in the Sargasso Sea dominate the water column; to the north the primary water masses are all comparatively cool, fresh, and productive, with Coastal Water and Slope Water in the upper layers on and off the shelf, respectively, and Labrador Sea Water, including the deep western boundary current, at depth between the shelf break and the northern

wall of the Gulf Stream [47–49]. The ecological communities present in these distinct regions differ substantially [52,116,117].

In oceanic food webs the distribution and abundance of highly mobile top predators are thought to be driven by prey availability [35,118–120]. The distribution and abundance of these prey are driven by oceanic conditions operating on a range of temporal and spatial scales: diel vertical migration in response to sunlight and moonlight [121,122]; mesoscale features which can input nutrients, entrap and transport water parcels, and act as particle aggregators [123,124]; and seasonal changes in primary and low trophic level productivity in response to differential nutrient and light availability [125–127]. Optimal foraging theory posits that cetacean predators must balance the energetic expenditures and oxygenic requirements of foraging behaviors (e.g. transit between widely distributed food patches, dive depth and rate, prey pursuit/capture strategies) against the calories gained, integrated over time, determined by metabolic rate, energy stores, and other factors [128,129]. Odontocetes have developed several behaviors and foraging strategies enabling them to exploit mid- and upper-trophic level prey which are heterogeneously distributed over large spatiotemporal scales (weeks-months, and 10s-1000s km), and which may form dense patches over much smaller spatiotemporal scales (hours-days, and 10s-100s m) [130–133]. These strategies include biosonar, social behaviors including cooperative feeding and associations with other top predators, and temporally variable behaviors such as prey switching, seasonal movements, and diel and lunar foraging cycles [11–19].

The distributions of odontocetes in the western North Atlantic have traditionally been estimated by aggregating visual survey data over many years, revealing large-scale differences in habitat preference [134–136]. This approach can provide high-level insights, but is confounded by seasonally biased and spatially inconsistent visual survey effort, and is not sensitive to fine temporal-scale changes in site occupancy or habitat use. Odontocetes are difficult to observe in the open ocean due to their pelagic lifestyles and at times cryptic behavior, but as highly soniferous species they lend

themselves well to acoustic studies. All odontocete species use biosonar for foraging, environmental sensing, and sometimes communication, and these impulsive signals can readily be identified in passive acoustic data [28,29,32,33]. The increasing popularity of marine passive acoustic monitoring over the past decade has led to the accumulation of large passive acoustic data sets on the order of hundreds of terabytes, with potential for novel insights into the acoustic ecology of many offshore and cryptic species with limited visual observation records [87,137–141].

In this study, we examine one such data set, spanning three consecutive years (May 2016 - April 2019) and collected at eleven (11) acoustic monitoring sites arranged across a latitudinal habitat gradient in the western North Atlantic (Figure 1a), to characterize temporal patterns in acoustic activity for ten (10) odontocete species at a variety of temporal scales. Included in this analysis were Risso's dolphins (Grampus griseus), identified by two different click types, short-beaked common dolphins (*Delphinus delphis*), short-finned pilot whales (*Globicephala macrorhynchus*), Blainville's beaked whales (*Mesoplodon densirostris*), Sowerby's beaked whales (*Mesoplodon bidens*), Gervais' beaked whales (*Mesoplodon europaeus*), True's beaked whales (*Mesoplodon mirus*), Cuvier's beaked whales (*Ziphius cavirostris*), sperm whales (*Physeter macrocephalus*), and *Kogia* spp. analyzed as a genus-level group. The two Risso's dolphin click types are denoted here as "Gg1" (canonical click type described by [29]) and "Gg2" (novel click type UD36 attributed to Risso's dolphins by [142]). Time series of acoustic presence were derived for these species by [142] using a combination of automated algorithms and expert analyst review.

In the present study, we modeled acoustic presence/absence of each species in 5-minute bins relative to four temporal covariates: Julian day (JD), normalized time of day (NT), moon phase (MPh), and study year (Yr); interaction terms between JD and NT, and between NT and MPh were included to account for potential changes in diel patterns over the course of the seasonal and lunar cycles. Here we report on interspecies, inter-site, and temporal differences in acoustic activity patterns, and discuss our

findings in light of what is known of each species' foraging ecology and the oceanographic conditions across the study region.

3.3 METHODS

3.3.1 Acoustic Presence Data

For this study we used time series of labeled odontocete echolocation clicks from [142], which were derived from a large passive acoustic data set collected through repeated mooring deployments at eleven monitoring sites in the western North Atlantic over the course of three years. Clicks were detected and classified to species using a machine learning workflow, and then classification error was quantified by manual verification of a subset of the labeled data. The species included in this analysis were: Risso's dolphins (*Grampus griseus*), short-beaked common dolphins (*Delphinus delphis*), short-finned pilot whales (*Globicephala macrorhynchus*), Blainville's beaked whales (*Mesoplodon densirostris*), Sowerby's beaked whales (*Mesoplodon bidens*), Gervais' beaked whales (*Mesoplodon europaeus*), True's beaked whales (*Mesoplodon mirus*), Cuvier's beaked whales (*Ziphius cavirostris*), sperm whales (*Physeter macrocephalus*), and *Kogia* spp. analyzed as a genus-level group. We also included UD36, a click type identified by [142] and attributed to Risso's dolphin; here the canonical Risso's dolphin click type established [29] will be denoted "Gg1", and UD36 will be denoted "Gg2". We analyzed these two Risso's cues independently to characterize similarities or differences in temporal occurrence. For each species/group we binned the time series of labeled clicks into 5-minute time bins, then scaled the number of clicks per bin by recording effort as well as the classifier error rates which had been calculated on a per-species per-deployment basis. Since some clicks were isolated by the clustering algorithm, and therefore were unavailable to be labeled by the classifier, we considered binomial presence/absence in each 5-minute bin to be a more reliable metric of species presence than the actual number of clicks labeled to that species. To remove spurious presence bins based on very few detections, we set a minimum number of clicks per bin threshold to be considered

"presence": ≥50 clicks per 5-minute bin for delphinid species, and ≥20 clicks per 5-minute bin for beaked whales, sperm whales, and *Kogia* spp. These values were selected based on consideration of the click-production rates and group sizes of these species, but are essentially arbitrary.

3.3.2 Temporal Covariates

To quantify the significance of apparent patterns in seasonal, lunar, and diel activity, we modeled acoustic presence for each species as a response to Julian day, moon phase, and normalized time of day using the statistical computing software R [143]. Moon phase data was calculated based on location and date using the *getMoonIllumination* function in the R package *suncalc* [144]. Since our sites span a wide latitudinal range, normalized time of day was used instead of hour of day to account for differences in diel phase length between sites over the course of each year. Study year was included as a factor to account for differences between years, though the small sample size at this temporal scale (N=3) undermines statistical power, and therefore we did not attempt to characterize interannual differences or trends.

3.3.3 Statistical Modeling

We selected the multivariate generalized additive model (GAM) framework [145], commonly used in cetacean habitat modeling [136,146–151], to model a smooth function of acoustic presence (binomial data with a logit link) as a linear combination of smooth functions of our temporal covariates. The GAM approach is popular for its ability to accommodate non-normally distributed response data, such as binomially-distributed presence/absence data or Poisson-distributed count data, as well as its interpretability. However, one of the fundamental assumptions underlying GAMs is independence of observations, a condition which is often violated by temporal or spatial autocorrelation in animal presence observations. Rather than reducing the temporal resolution of our analysis, and thereby perhaps our ability to discern diel cycles, we chose to use generalized estimating equations (GEEs) [152] to model the temporal autocorrelation structure directly from the data and use that structure to provide more reliable standard error estimates, an approach that has been successfully

used in a number of cetacean modeling studies [153–155]. The *geeglm* function of the *geepack* package in R [156] was used. This approach requires a grouping variable indicating blocks within which data is known to be correlated, and between which independence is assumed. To determine the most appropriate block size for each species at each site we calculated the autocorrelation function of our presence time series using the *acf* function in the base R package *stats.* A first-order autoregressive ("ar1") correlation structure was used for all models based upon inspection of the autocorrelation function plots.

Julian day, moon phase, and normalized time of day were supplied to the models as cyclic splines using the *mSpline* function in the R package *splines2* [157], extending the GEEGLM framework to a GEEGAM. Cyclicity was desired to coerce continuity between, e.g., December and January. To determine the optimal number of knots to use in the splines we fit simple univariate models with a range of knot values, from 4 (minimum required for a cyclic variable in *mSpline*) to 8, and compared the quasilikelihood information criterion (QIC). The QIC is an analog of the Akaike information criterion (AIC) which is more suitable for GEEs, which use quasilikelihood rather than maximum likelihood [158]. We found that for all three smooth covariates, splines with 5 knots had the lower QIC values for the majority of our models, indicating the most favorable tradeoff between model fit and complexity. We also noted that Julian day splines with just 4 knots didn't allow enough flexibility to capture the bimodality in presence which we observed in some of our histograms of presence versus Julian day. Rather, such inflexible splines would overly smooth the two peaks, resulting in an estimated single peak in presence right at the time of an actual trough presence. Therefore we chose to use 5 knots for all three smooth terms in all models, both for consistency and to allow sufficient flexibility.

An interaction term was included between Julian day and normalized time of day to account for the possibility of changes in diel patterns over the course of the seasonal cycle. We believed this interaction to have ecological relevance given the variable availability of prey species throughout the

year and the likely necessity for plasticity in foraging behavior. An interaction term between normalized time of day and moon phase was also included. Lunar cycles have been shown to be significant for some odontocete species [16,159,160], though it is uncertain whether these patterns are driven by the magnitude of lunar illumination and its impact on the depth distribution of diel vertically migrating prey [121,161,162], or if the patterns are the result of endogenous circadian rhythms. If lunar cycles are driven by lunar illuminance we might expect to see the most pronounced impact on cetacean activity at night, as lunar illuminance during the day is negligible compared to solar illuminance. By including this interaction we were able to consider lunar cycles exhibited during the nighttime independent of any patterns present during the daytime.

Full models with all four temporal predictors, plus two interactions, were initially run for all species at all sites meeting a minimum presence criterion of ≥100 presence bins across the entire study period (Table 3.1). For each model, marginal significance of each term was calculated by fitting repeated ANOVAs with each model term in the last position; non-significant terms were removed and models re-run in a stepwise fashion until only significant terms remained in each model (Table 3.2). If one or both terms contributing to an interaction were not significant on their own, but the interaction was significant, both contributing terms were retained. At HAT, the deployment location shifted northward by about 33 km after the first study year. This shift moved our device mostly out of the direct flow of the Gulf Stream, resulting in quite obvious changes in species presence between the first study year and the second two. We therefore judged that the deployments spanning this move could not be considered contiguous or representative of the same habitat. Data from the first study year at HAT were not utilized; models were only constructed at HAT for those species which exhibited sufficient presence in the second and third study years. *Kogia* spp. were also not modeled at any of the northern sites because the sampling frequency of 200 kHz limited the acoustic analysis of Cohen *et al.* [142] to a Nyquist frequency of 100 kHz, making *Kogia* spp. identifiable only by click spectra with highest amplitudes above 90 kHz, resulting from aliased energy [163]. Since the full click spectra

could not be resolved, we had no way of differentiating apparent *Kogia* spp. clicks from similarly narrow-bandwidth high-frequency harbor porpoise (*Phocoena phocoena*) clicks in the northern region where these species co-occur along the shelf break [164].

To assess model fit we examined binned residual plots, which compare the actual vs. model predicted probability of presence for blocks of observations [165]. Inspection of the binned residual plots showed that model performance was highly variable, with the quality of fit tightly correlated with the level of presence the model was fitted to; models based on fewer than about a thousand presence bins generally performed quite poorly. As these models contained simple explanatory variables capturing only temporal cycles, we did not expect them to account for all of the variability in animal presence, but good model fit is required to have confidence in the patterns estimated by the model. Therefore we chose to set a minimum threshold of ≥60% of binned residuals within the 95% confidence intervals and discard models which did not meet this criterion in order to avoid drawing spurious conclusions from ill-fitting models. About two thirds of our models (57/82) satisfied this criterion and were retained, while the remaining third (26) were considered too unreliable to interpret. Of the models retained, about half (29/57) had ≥80% of binned residuals within the 95% confidence interval. Partial residual plots of the smooth functions of significant terms were also compared to histograms of presence binned across observed values of our covariates to verify that the patterns estimated by the models were reflective of the underlying data.

Study year was significant in 50/57 of the retained models (Table 3.2), but as our data only represented an N of 3 at this temporal scale we cannot make any robust estimates of interannual trends.

3.4 RESULTS

Using echolocation clicking as a proxy for animal presence, ten species of odontocetes were examined at eleven sites distributed along the shelf break of the Western North Atlantic (Figure 3.1).

Acoustic recording effort was almost continuous at each site, except for brief gaps between deployments; larger gaps resulted when devices failed at Heezen Canyon (HZ) and Jacksonville (JAX) (Table 2.1). Species presence varied across sites by three orders of magnitude (Table 3.1). Distinct patterns of spatial distribution and activity were observed as detailed below.

3.4.1 Regional Differentiation

The acoustic presence of all species exhibited clear preferences either for or against Gulf Stream waters (Figure 3.2). Most species had higher levels of presence in the north; only Blainville's and Gervais' beaked whales and *Kogia* spp. primarily occupied the southern stations, which are characterized by the strong influence of the Gulf Stream.

Within the northern and southern regions, the beaked whales also exhibited distinctly different patterns of primary site occupancy: In the south, Blainville's beaked whales were present almost exclusively at the southernmost site, Blake Spur (BS), while Gervais' beaked whales were present at all sites south of Cape Hatteras (HAT), with a marked peak at the Gulf Stream site (GS) and lower presence at BS. In the north Cuvier's, Sowerby's, and True's beaked whales occupied many of the same sites, but their sites of primary occupancy were non-overlapping. Cuvier's beaked whales were most abundant at HAT, with presence one or two orders of magnitude lower in the north. Sowerby's beaked whales exhibited two preferred loci of presence, one at Heezen Canyon (HZ) and another at Wilmington Canyon (WC). Detections of True's beaked whales were strongest at Nantucket Canyon (NC), where both Cuvier's and Sowerby's were conspicuously absent despite occupying neighboring sites.

The three dolphin species all had higher levels of presence at the northern sites, but their distribution patterns were dissimilar. Common dolphins were consistently present across the study area, with a bias towards the northern region. Risso's dolphins exhibited a stronger preference for northern sites, shown by negligible presence of both click types in the south, except at Jacksonville (JAX). Short finned pilot whales had their strongest occurrence at HAT and Norfolk Canyon (NFC),

with lower presence at the more northerly sites and at JAX, and negligible occupation of Blake Plateau (BP) and BS. Sperm whales exhibited a similar regional distribution to common dolphins, with presence at all sites but a bias towards the northern sites. *Kogia* spp. exhibited low levels of presence at all sites south of HAT, and negligible presence in the north.

3.4.2 Seasonal Fluctuations in Presence are Apparent Across Species

The seasonal cycle, represented by Julian day (JD), was highly significant ($p < 0.001$) in almost all of the retained models (Table 3.2). Most JD patterns were unimodal, with a peak in presence during one particular season; season of peak presence varied across species (Figure 3.2). However, in some cases bimodal patterns with two distinct seasonal peaks in presence occurred (e.g. Figure 3.2b).

The JD patterns for common dolphins were consistent across most sites, with presence peaking in the spring between BS and NC, though the peaks fell later in the summer at OC and HZ in the north, and at JAX in the south (Figure 3.3). This was similar to the Risso's dolphin seasonal patterns at the sites where both species occurred. Common dolphins did not appear to meaningfully occupy any of the sites during the fall.

The two Risso's dolphin click types present in the dataset showed similar seasonal patterns per site across sites north of HAT (Figure 3.3): in spring they were found in the mid-Atlantic Bight, whereas in fall they were more present at the northernmost sites, such as Heezen Canyon. A clear boundary occurred between NC and Oceanographer's Canyon (OC), with spring presence below and fall presence above. The Gg1 click type exhibited a spring/fall bimodality at both NFC and NC, which was indistinct or absent for Gg2. Presence of both Risso's click types was quite low from HAT southward and was not possible to model, except for Gg1 at the JAX site. Risso's dolphins were absent from all sites in the winter.

Short finned pilot whales were most abundant at HAT, where they exhibited peak presence in the winter (Figure 3.2). At the northern sites, short-finned pilot whales exhibited peak presence in fall

and early winter from NFC to Babylon Canyon (BC), and bimodal spring/fall peaks at NC giving way to a winter peak at HZ; this pattern was dissimilar from the seasonal presence of the other delphinid species at the same sites (Figure 3.3). An apparent incongruity at these northern sites, the spring peak in short-finned pilot whale presence at OC, was actually the continuation of elevated presence beginning in the fall and continuing through winter and into the spring; wider confidence intervals for this estimated seasonal pattern show that spring and fall peaks may not be truly different. We observed that Risso's dolphins and short-finned pilot whales had staggered seasonal peaks at sites where their ranges overlap, and did not generally occupy a given site at the same time.

A clear temporal separation was seen for the southern beaked whale species at BS, where Blainville's beaked whale presence peaked in the late winter, while Gervais' beaked whale presence peaked in the fall (Figure 3.4). Cuvier's and Sowerby's beaked whales both occupied the sites from NFC to HZ (Table 3.1, Figure 3.2), but available seasonal patterns suggested that they were temporally non-overlapping at these sites (Figure 3.4). At BC and WC Sowerby's beaked whale presence peaked in the fall and summer, respectively, while Cuvier's beaked whales peaked in the spring and late winter, respectively. At HZ Sowerby's and Cuvier's beaked whales peaked in early spring and winter, respectively, which suggests some co-occurrence. At NC, their site of primary occupancy, True's beaked whales exhibited summer and winter peaks in presence. Most beaked whale species exhibited a winter peak in presence at their sites of highest occupancy, regardless of whether those sites were in the south or north (Figures 3.2 & 3.4).

Peak presence of sperm whales occurred during the spring and summer at most sites (Figure 3.4). At HZ and OC bimodality was apparent, with a higher peak in the spring and a lower peak in the fall. GS was the only site where sperm whale presence peaked in the winter. While the JD smooth for *Kogia* spp. at BS suggested a summer peak in presence, the confidence intervals were wide. Examination of the raw data showed that the summer peak in presence was inconsistent: it was

particularly pronounced during July of the first study year, was lower amplitude and shifted earlier to June in the second study year, and no clear summer peak was discernible in the third study year. The strong pattern in the first year may be driving the significant p-value for JD in this model, while the interannual variability likely underlies the parameter estimate variability.

3.4.3 Lunar Cycles Were Most Impactful for Delphinids

Moon phase (MPh) was significant in most of the models, and often interacted significantly with normalized time of day (NT); most of the instances of non-significance were in models for deep divers (Table 3.2). The interaction between MPh and NT was included to enable consideration of the lunar patterns exhibited at night, when we would expect the influence of lunar illumination to be most pertinent, versus in the daytime. Despite being a significant interaction in many cases, the lunar patterns did not always appear different between daytime and nighttime. This may indicate that the interaction was one way (moon phase influenced diel pattern, but diel phase didn't influence lunar pattern).

The most coherent lunar patterns were seen for the dolphin species (Figure 3.5). Common dolphins exhibited a preference against the full moon at night at most of the sites; daytime lunar preferences were more variable. Short-finned pilot whales, on the other hand, exhibited a consistent preference for the full moon at night, and against the full moon during the day. Neither of the Risso's dolphin click types exhibited lunar patterns which were consistent across sites, or in keeping with the light preferences suggested by their diel cycles (discussed below).

Among the beaked whales there was some preference for the waxing moon, though this pattern was not consistent either across or within species (see Appendix). A lower proportion of the beaked whale models indicated an interaction between MPh and NT than was seen for the dolphin models (45% compared to 87%) and in four of five such models the confidence intervals were wide and overlapping, indicating that parameter estimates contained a lot of variability. Differences

between the daytime and nighttime lunar patterns in these cases may not be reliable or ecologically meaningful. Sperm whales exhibited variable lunar patterns across the sites for which the term was significant, but a preference for the full moon at night could be seen (see Appendix). The pattern for *Kogia* spp. had wide confidence intervals, similar to the JD and NT patterns for this group (see Appendix).

3.4.4 Diel Patterns Change Across the Seasonal and Lunar Cycles

Normalized time of day (NT) was significant in all retained models, and usually interacted significantly with JD and/or moon phase (MPh) (Table 3.2). The interaction between NT and JD revealed substantial changes in diel patterns throughout the year for some species. Diel patterns did not vary as much across the lunar cycle, suggesting the lunar influence is less important in driving odontocete diel activity patterns than the seasonal influence. However, when there was modulation of the diel pattern across the lunar cycle, variability in activity was almost exclusively confined to nighttime hours. This supports the hypothesis that the impact of the lunar cycle on odontocetes is a function of lunar illumination, which is only relevant at night. We focus here primarily on diel patterns exhibited by each species during their periods of peak presence at a given site.

Figure 3.6 provides a summary of the partitioning of presence between diel phases for each species at each site during the 90-day period centered on their seasonal peak in presence; this partitioning was calculated based on the raw presence data, not model output. A selection of illustrative partial smooth plots from the temporal models, showing diel patterns at different points in the seasonal and lunar cycles, is shown below; the remaining partial smooth plots can be seen in the Appendix.

Common dolphin diel patterns showed a preference for dark conditions, with highest levels of acoustic activity at night; occasionally a slight preference for dusk or dawn was visible (Figure 3.7). Differences in diel patterns at different points in the lunar cycle were mostly trivial (e.g. Figure 3.7a),

but were more pronounced at HAT and JAX: in spring at HAT a crepuscular pattern of dawn and dusk preference was apparent during new, waxing, and full moons, but during the waning moon a simple nocturnal pattern was estimated (Figure3.7b). A similar modulation was seen at JAX in summer, though less pronounced. At sites where the NT:MPh interaction was significant, highest levels of nighttime activity were generally during new and/or waxing moons, though in many cases, the differences in diel patterns across the lunar cycle appeared negligible.

During their seasons of peak presence, Risso's dolphins exhibited varying diel patterns across sites; within sites, diel patterns changed across the seasonal cycle (e.g. Figure 3.8a). Considering only diel patterns exhibited during seasons of peak presence, Gg1 showed a nocturnal pattern at the northernmost sites, HZ and OC; a crepuscular pattern at the mid-Atlantic Bight sites NC, BC (Figure 3.8a), and, less so, WC; and a nocturnal pattern in the south at JAX. Gg2 had distinctly different diel patterns during the same seasons at the same sites: crepuscular with some nocturnal activity at the northernmost sites, HZ and OC; diurnal at NC, BC (Figure 3.8b), and WC. Both the Risso's dolphin click types exhibited some variability in diel pattern which was modulated by the lunar cycle, though at most sites the overall shape of the diel pattern was conserved across the lunar cycle. A notable exception occurred during the Gg2 spring presence peak at NFC, when the pattern was most strongly diurnal during the waning moon, with little diel preference and wide and overlapping confidence intervals predicted at other points in the lunar cycle (Figure 3.8c).

Short-finned pilot whales exhibited a preference for well-illuminated conditions with generally diurnal echolocation behavior across seasons at HAT and NFC, their sites of peak presence (Figure 3.6). At the northern sites, pilot whales exhibited crepuscular behavior during their seasons of peak presence, often with a dawn preference. Nighttime activity levels from HAT to NC were highest during periods of lunar illumination, e.g. at HAT in the spring nighttime activity during the full moon rivaled daytime activity (Figure 3.9). At OC and HZ this pattern changed, with highest levels of nighttime activity around the waning and waxing moons in all seasons.

Diel patterns for the beaked whales in their seasons of peak presence were often quite flat, or had wide and overlapping confidence intervals when looking across points in the lunar and seasonal cycles (see Appendix). Anti-crepuscular patterns were sometimes present, with dips in activity at sunrise and sunset. Sowerby's beaked whales were anticrepuscular at HZ across the lunar cycle, and had some nocturnal preference at WC and at BC in the summer. Gervais' beaked whale exhibited a very slight dip in activity around sunset at BP in the fall, and a nocturnal preference at BP in the summer and BS in the spring. The True's model at NFC showed an anti-crepuscular pattern. Cuvier's exhibited diurnal preference during the summer peak in presence at HAT, with higher nighttime activity around the full moon; in the winter the pattern was more evenly split between daytime and nighttime, except around the waning moon, when diurnal activity dominated.

The diel pattern for *Kogia* spp. suggested an anti-dusk preference, but as with the other smooth terms for this species, confidence intervals were wide and the true pattern may not be different from a flat line. Sperm whales were the only deep divers to exhibit convincing diel patterns across sites, but these patterns were highly variable between sites and seasons and included diurnal, nocturnal, dawn preference, dusk avoidance, and dawn avoidance patterns. At HAT and BS sperm whale nighttime activity was always highest around the full moon.

3.5 DISCUSSION

The long-duration, continuously-sampled data utilized here allowed us to analyze toothed whale presence at a range of temporal scales - yearly, lunar monthly, and daily. Use of this large acoustic data set provided novel insights into temporal patterns in acoustic activity throughout the entire seasonal, lunar, and diel cycles, and as such can address some of the knowledge gaps associated with visual survey data which is largely focused on summer months for this region. Most of the species in this analysis were present primarily from HAT northwards; only 3 of the 10 species analyzed (Blainville's and Gervais' beaked whales, and *Kogia* spp.) mainly occupied the southern

sites. The acoustic monitoring sites used here are point sampling locations with limited monitoring volumes, so species which were apparently absent from one of our sites may indeed be present at that latitude, either further inshore or offshore, and simply not captured by our sampling design. But within each instrument's recording radius, the ubiquitous use of echolocation for foraging, environmental sensing, and communication makes it a good proxy for detecting odontocete species occurrence. [142] showed good alignment between the distributions of visually-detected and acoustically detected animals for species which are amenable to visual surveys, while acoustic methods have been shown to detect higher levels of presence of cryptic species than visual surveys [166]. The regional differences in species distributions shown here are also consistent with previous findings that dolphin species exhibit preferences for particular temperature and salinity ranges [136,167–170].

3.5.1 Temporal patterns vary between species, sites, and through time

We found substantial interspecific variability, as well as intraspecific regional variation, in seasonal, lunar, and diel patterns in odontocete acoustic activity. Such patterns in odontocete presence and acoustic activity are generally thought to be driven largely by the availability of prey species, which is dictated by oceanographic conditions[121–127]. This assumption is particularly relevant to this analysis since echolocation clicks were used as the indication of presence, and biosonar is known to be the primary mode of sensing prey for all odontocete species. Indeed, some of the patterns observed here seem to be well-aligned with current knowledge of foraging ecology for these species. Echolocation may also be utilized for communicatory purposes [22–25], but manual review of the raw data showed that the overwhelming majority of clicks detected on our devices were regular echolocation trains believed to be used primarily in foraging, although they may also be used for environmental sensing and orientation. Interspecies differences in site occupancy or activity patterns may be a means of minimizing competitive interactions [111,113–115]. Intraspecies variability in lunar and diel preferences may be a response to seasonally and/or regionally variable prey behavior and density, and may also be an indication of prey switching.

3.5.2 Beaked whales and deep-diving delphinids are spatially and temporally separated.

Each beaked whale species exhibited a specific locus of highest presence, distinct from the other species. Apparent spatial overlap between Cuvier's and Sowerby's beaked whales was mitigated by temporal separation at WC, BC, and HZ. A similar separation was noted between the two deep diving dolphin species, Risso's dolphins and short-finned pilot whales: from NFC northwards, the seasonal peaks in short-finned pilot whale presence fell generally during the seasonal dips in Risso's dolphin presence (also during the seasonal absence of short-beaked common dolphins at most of these sites). The non-overlapping pattern of beaked whale site occupancy, achieved through both spatial and temporal separation between species, is consistent with what has been previously reported from this region and others [171–174], though few works have identified habitat partitioning among dolphin species [175].

Risso's dolphins, pilot whales, and beaked whales are all primarily teuthophagus, with the dolphins foraging on mesopelagic species [176–185] and the beaked whales targeting meso-, bathy-, and benthopelagic species [36,186–188]. This spatiotemporal separation of site occupancy may be a means of minimizing direct competition for similar prey through behavioral differentiation [111,115,189–192], and may also reveal subtle differences in realized niche between species with highly overlapping fundamental niches. Consideration of biotic and abiotic oceanographic conditions experienced at each of these sites through time may shed some light on the prey species and/or life stages of prey likely available, and the drivers of habitat selection for these odontocete species.

3.5.3 Possible evidence of seasonal north-south and onshore-offshore movements.

The latitudinal shifts in seasonal peak presence for both Risso's click types suggest seasonal migrations between the central and northern sites; the seasonal bimodality at NC may arise from the movement of animals through this site on their way to and from their spring and fall habitats. For short-finned pilot whales we can similarly speculate about seasonal movements between north-central spring grounds (NFC, WC, BC) and either central (HAT, GS) or northern (OC, HZ) winter grounds.

As noted in [142], the click type identified as short-finned pilot whales exhibits an upwards frequency shift at HZ; this could potentially be indicative of acoustic differentiation between distinct populations, which may overlap at the mid-Atlantic bight sites. Common dolphins, on the other hand, exhibited a highly consistent seasonal pattern across almost all of the sites. The low predicted presence of both Risso's and common dolphins at all of our sites in the winter and fall, respectively, begs the question of what constitutes their cool weather habitat in this region. One explanation for the absence of these species at all of our sites during a portion of the year could be onshore-offshore movements which take them out of the sensing range of our shelf break-situated instruments. Zonal movements have been previously observed for dolphins on both seasonal and diel cycles [193–195]. A study incorporating sensors deployed along an onshore-offshore gradient could help address this knowledge gap.

3.5.4 Lunar and diel cycles differentially impact species according to their diving/foraging ecology.

Variability in lunar and diel cycles was observed across sites and seasons for many of the species, with consistent and ecologically coherent patterns only apparent for the dolphin species. Based on these findings it does not appear practical to average such patterns across sites to come up with a behavioral "rule". Rather, consideration of differences in prey fields and oceanographic conditions across our sites may provide more meaningful insights into the drivers of this apparent behavioral plasticity. Diel and lunar cycles in odontocete behavior are generally thought to be driven by light-mediated changes in prey depth distributions [121,122] and the energetic costs of, or physiological limitations on, foraging in different depth layers. Such variability in diel and lunar activity patterns may indicate adaptability to fine-scale temporal and spatial differences in prey fields. For example, [196] and [197] both reported such sub-daily and daily scale foraging responsiveness of short-finned pilot whales to changes in the micronekton scattering layers which constitute prey for the whale's own forage species.

Our findings of primarily nocturnal and crepuscular activity for Risso's dolphin click type Gg1 are consistent with current understanding of this species' foraging ecology, while the diurnal occurrence of the Gg2 click type was surprising. Risso's dolphins represent something of an intermediate between common dolphins and pilot whales in terms of foraging ecology. Risso's forage in the upper 200 m during the night, but are also known to undertake deep foraging dives during the daytime and around dusk to access prey below 400 m and meet scattering layers on their ascent [198–201]. They prey almost exclusively on cephalopods [176,178,179,181,182]. We speculate that Gg1 may be primarily associated with nighttime foraging at epigelagic depths, while Gg2 may correspond to different foraging strategies or behavioral states. Another possible explanation is that the two click types correspond to distinct Risso's populations with different foraging strategies, as suggested previously for the two distinct Pacific white-sided dolphin click types [202], but this seems less likely given the spatial and seasonal co-occurrence of the two Risso's click types.

The deep divers considered here exhibited a variety of lunar and diel patterns in acoustic activity, but no well-defined or consistent light/dark preferences were apparent either across species or within species for those modeled at multiple sites. Some diel and lunar patterns have been previously reported for some of these species: sperm whale have been reported to exhibit deeper and faster daytime swimming [203] and also to have a higher nocturnal acoustic detection rate [155]; [204] observed no differences in daytime versus nighttime foraging for Blainville's or Cuvier's based on tag data, while [159] reported a full moon preference for Blainville's, and [186] reported nocturnal foraging of Cuvier's. Diel vertical migration (DVM) is known to occur even at depths where no light penetrates [162,205,206], so it is likely that the deep-dwelling, mid-trophic level organisms targeted by these mammals undertake some sort of regular vertical displacements in pursuit of their own prey species. These odontocete species are, however, highly specialized for extended dives to great depths and it might simply be the case that their extreme diving abilities enable them to access high-quality prey items irrespective of vertical prey displacements on the scale of a few hundred meters.

3.5.5 Lunar illumination modulates dolphin diel activity patterns

For short-finned pilot whales and common dolphins, observed lunar preferences were complementary to their respective diel patterns in terms of apparent light preferences, and well-aligned with each species' foraging ecology. This suggests that illumination, as opposed to an endogenous circadian rhythm, drives these observed lunar activity cycles. Short-beaked common dolphins exhibited highly consistent nocturnal activity patterns across sites and seasons and preferred darker nighttime conditions, with reduced nighttime acoustic activity around the full moon; daytime lunar patterns were variable between sites. Extremely limited work suggests that this species is a shallow diver, capable of attaining maximum depths of about 260 m [207]. Offshore populations of short-beaked common dolphins are known to forage mainly on mesopelagic fish and, to a much lesser extent, squid [169,208], and primarily forage at night [209]. Presumably these dolphins can only access such deep-dwelling prey species when they undergo nocturnal diel migration into the epipelagic zone, a behavior which is suppressed by intense lunar illumination around the full moon [16,122]. The common dolphin diel and lunar patterns evident in this analysis are in keeping with nocturnal foraging on diel vertical migrators when they are most abundant in the surface waters.

Short-finned pilot whales, on the other hand, are known to be deep-divers capable of accessing prey at depths >1000 m [210,211]; time spent at depth is generally presumed to be engaged in foraging, when other methods of determining behavioral state are not available. [210] reported a combination of daytime and nighttime foraging behavior: fewer but deeper dives during the day, often with sprints and echolocation buzzes thought to be associated with prey pursuit and capture attempts, as well as shallower dives with a higher rate of buzzes at night. [212] also reported deepest dives during the day, with a higher rate of diving, but to somewhat shallower depths (300-500 m), at night. Some papers tracking stranded and released animals have reported longer and deeper dives and a higher proportion of time spent below 50 m at night [213,214], but given that these animals were recently stranded they may not be reliable indicators of normal behavior. [160] reported that during the

full moon, nighttime deep dives of short-finned pilot whales were deeper and longer, though there was a reduction in the proportion of nighttime dives, while there were no changes in mean depth or duration of daytime deep dives.

At HAT, our site with the most acoustic presence of short-finned pilot whales, we observed a primarily diurnal pattern in acoustic activity, and an increase in nighttime acoustic activity around the full moon, with no meaningful changes in daytime acoustic activity over the course of the lunar cycle. This bias towards diurnal and nighttime full moon acoustic activity does not align with either the primarily nocturnal, or the nocturnal-with-occasional-daytime foraging, patterns previously reported. At the northern sites short-finned pilot whales were primarily crepuscular. This may indicate that pilot whales at HAT are targeting different prey than at the northern sites, which would not be surprising given the oceanographic differences between HAT and the northern sites, particularly in terms of vicinity to and influence of the Gulf Stream. Observations for both short-beaked common dolphins and short-finned pilot whales suggest that their lunar cycles are driven by the influence of lunar illumination on the depth distribution of prey species, as opposed to endogenous circadian rhythms within the odontocete species themselves.

Previous work has demonstrated the importance of lunar influences on Risso's dolphin foraging in southern California, with reduced acoustic activity around the full moon, and more nighttime echolocation prior to moonrise than while the moon was present in the night sky or after moonset [198]. In this analysis, Risso's dolphin lunar patterns were highly variable across sites, and between the two click types analyzed. This may suggest ocean basin differences in Risso's populations, optimization of foraging strategies based on site-varying prey fields in our region, or both. It may also suggest that Risso's lunar patterns are externally forced, similar to what we observed here for short-beaked common dolphins and short-finned pilot whales, as endogenous circadian cycles would not be expected to vary by site for a species believed to traverse the entire region.

3.6 CONCLUSION

The data presented here demonstrate spatial and temporal separation of potentially competitive odontocete species in the western North Atlantic. We found that among the dolphins, seasonal, diel, and lunar patterns in acoustic activity largely broke down along the lines of foraging ecology, with shallow-diving common dolphins exhibiting quite different patterns than deep-diving pilot whales, and intermediate-diving Risso's dolphins showing some similarities to each. Beaked whales exhibited distinctly non-overlapping site occupancy, achieved through both spatial and temporal separation of peak presence, while Risso's dolphins and short-finned pilot whales were temporally non-overlapping at the northern sites. For sperm whales and beaked whales, lunar and diel patterns were highly variable between sites, and for beaked whales often appeared ecologically inconsequential in light of wide and overlapping confidence intervals. *Kogia* spp. in our analysis did not exhibit strong temporal patterns at any of the scales analyzed. Altogether, at scales finer than seasonal, the extreme deep divers (beaked whales, sperm whales, *Kogia* spp.) seemed less affected by external temporal covariates, possibly as a result of specialized foraging in the much less dynamic deep-sea environment. The variable temporal activity patterns presented here may illustrate behavioral approaches to minimizing direct prey competition among closely related species, and provide new insights into the habitat use, behavioral plasticity, and foraging patterns of odontocete species.

3.7 FIGURES

Table 3.1: HARP sites and species presence. Effort across the 3-year study period is given as cumulative days of acoustic data at each monitoring site; presence of each species is given as a percent of effort with presence. Species are: Dd: short-beaked common dolphin; Gg1 and Gg2: Risso's dolphin click types; Gm: short-finned pilot whales; Md: Blainville's beaked whale; Me: Gervais' beaked whale; Zc: Cuvier's beaked whale; Mb: Sowerby's beaked whale; Mm: True's beaked whale; Kg: Kogia spp.; Pm: sperm whale.

Site	Lat Lon	Depth (m)	Effort (days)	Percent Species Presence										
				Dd	Gg1	Gg2	Gm	Md	Me	Zc	Mb	Mm	Kg	Pm
Heezen Canyon (HZ)	41.06N 66.35W	890	926.2	16.7	3.9	0.7	1.4	0	0	1.7	1	0.1	0	14.3
Oceanographer's Canyon (OC)	40.23N 67.98W	450/ 880	990.3	16	5	0.5	0.4	0	0	0.2	0.2	0.2	0	13.2
Nantucket Canyon (NC)	39.83N 69.98W	900	1041.4	16.4	8.2	2.3	0.6	0	0	0.1	0.1	0.4	0	18.9
Babylon Canyon (BC)	39.19N 72.23W	1000	1075.4	20.6	6	2.5	1.5	0	0	0.4	0.4	0.2	0.1	12
Wilmington Canyon (WC)	38.37N 73.37W	1040	1094.8	24.7	4.3	1.4	3.1	0	0	1.5	1.1	0.2	0	9
Norfolk Canyon (NFC)	37.16N 74.47W	1110	1093.8	26	1.4	0.9	6.7	0	0	0.3	0.2	0.3	0	9.9
Hatteras (HAT)	35.30N 74.88W	1210	1001.8	21	0.4	0.1	8	0	1	13.3	0.1	0	0	12.4

Table 3.1 Continued: HARP sites and species presence. Effort across the 3-year study period is given as cumulative days of acoustic data at each monitoring site; presence of each species is given as a percent of effort with presence. Grey shading indicates presence was too low for patterns to be effectively modeled. Species are: Dd: short-beaked common dolphin; Gg1 and Gg2: Risso's dolphin click types; Gm: short-finned pilot whales; Md: Blainville's beaked whale; Me: Gervais' beaked whale; Zc: Cuvier's beaked whale; Mb: Sowerby's beaked whale; Mm: True's beaked whale; Kg: *Kogia* spp.; Pm: sperm whale.

Site	Lat Lon	Depth (m)	Effort (days)	Percent Species Presence										
				Dd	Gg1	Gg2	Gm	Md	Me	Zc	Mb	Mm	Kg	Pm
Gulf Stream (GS)	33.67N 76.00W	930	1092.3	1.3	0.4	0.1	0.8	0	7.8	0	0	0	0.3	3
Blake Plateau (BP)	32.11N 77.09W	950	1094.7	2.1	0.1	0	0.1	0	4.6	0	0	0	0.2	0.5
Blake Spur (BS)	30.58N 77.39W	1050	1090.2	2.4	0.1	0	0.1	2.8	0.8	0.1	0	0	0.4	1.7
Jacksonville (JAX)	30.28N 80.22W	750	853.7	4	1.8	0.1	0.9	0	0	0	0	0	0.2	1.1

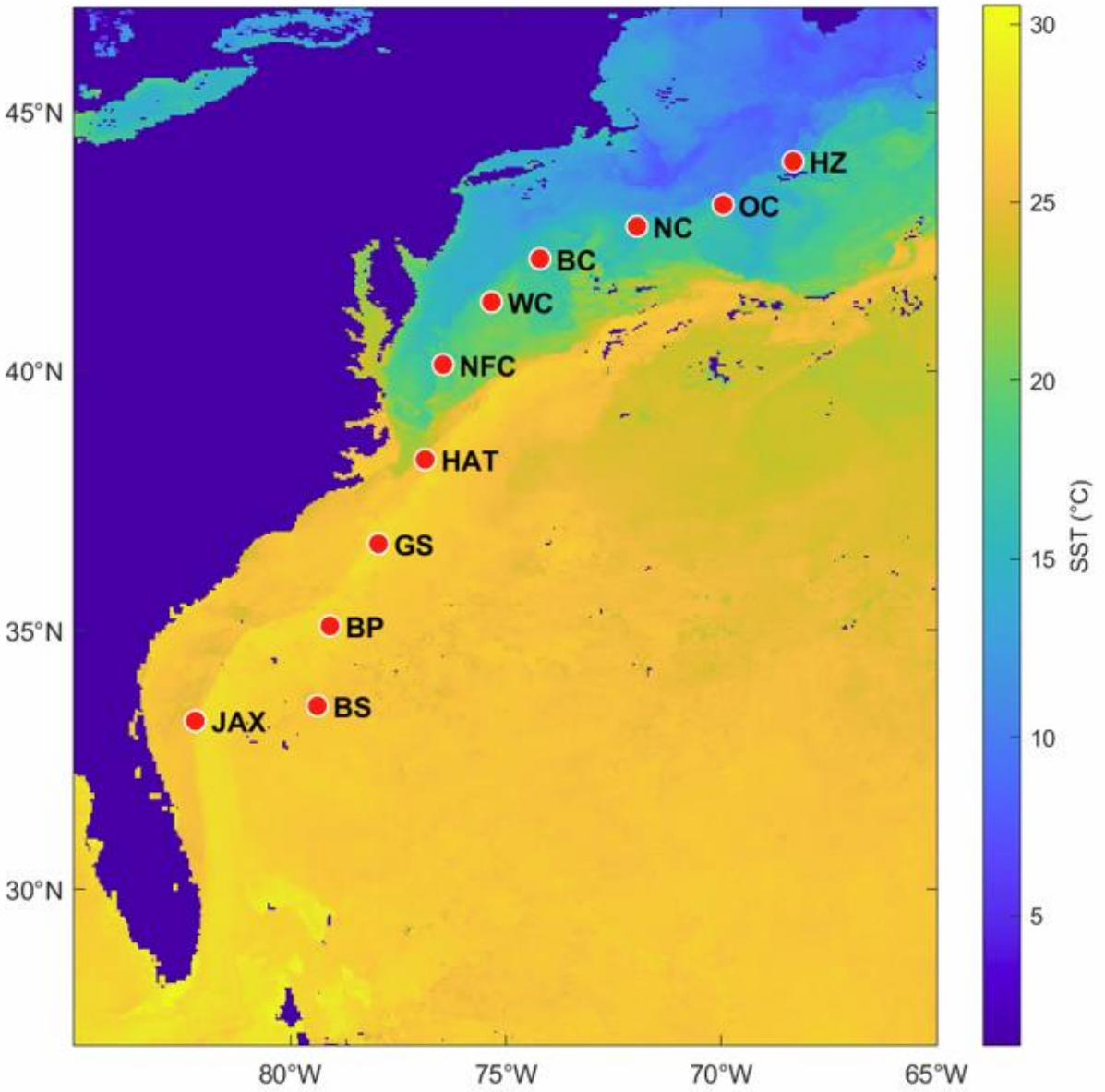

Figure 3.1: Study region in the North Atlantic with the influence of the Gulf Stream current shown by sea surface temperature. Acoustic monitoring sites displayed by red circles and site name abbreviations; full site names given in Table 3.1.

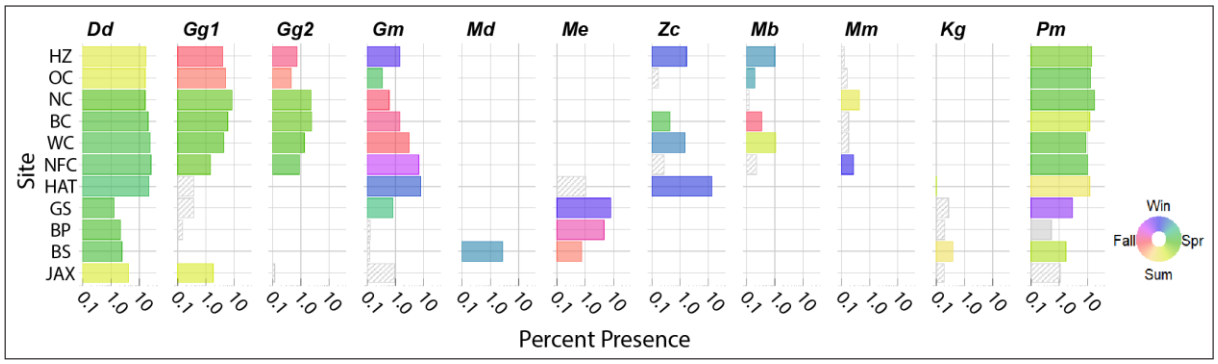

Figure 3.2: Site occupancy and seasonal peak presence by species and site. Bar length gives presence bins per thousand effort bins. Color shows the Julian day value of peak presence in models for which Julian day was significant; gray fill indicates that Julian day was not significant; stripes indicate no model due to insufficient presence or poor model performance. Site and species abbreviations as in Table 3.1.

Table 3.2: Term significance for each model by species and site; abbreviations as in Table 3.1. Terms are: Yr – study year; JD – Julian day; MPh – moon phase; NT – normalized time of day. *** = p<0.001; ** = p<0.01; * = p<0.05, NS = not significant; '-' denotes models with poor fit; blank cells indicate modeling was not undertaken due to low presence.

	Dd						***Gm***					
	Yr	**JD**	**MPh**	**NT**	**NT:JD**	**NT:MPh**	**Yr**	**JD**	**MPh**	**NT**	**NT:JD**	**NT:MPh**
HZ	***	***	**	***	***	*	***	***	NS	***	***	***
OC	***	***	***	***	***	***	***	***	***	***	***	***
NC	***	***	***	***	***	***	***	***	**	***	***	***
BC	***	***	***	***	***	**	***	***	*	***	***	***
WC	***	***	***	***	***	***	***	***	***	***	***	***
NFC	***	***	**	NS	***	***	***	***	NS	***	***	***
HAT	***	***	***	***	***	***	***	***	***	***	***	***
GS	***	***	*	NS	*	NS	***	***	***	***	***	***
BP	***	***	***	***	***	NS	-	-	-	-	-	-
BS	***	***	**	***	***	***	-	-	-	-	-	-
JAX	***	***	NS	***	***	***	-	-	-	-	-	-
	Gg1						***Md***					
	Yr	**JD**	**MPh**	**NT**	**NT:JD**	**NT:MPh**	**Yr**	**JD**	**MPh**	**NT**	**NT:JD**	**NT:MPh**
HZ	***	***	***	***	***	NS						
OC	***	***	NS	***	***	NS						
NC	***	***	***	***	***	***						
BC	***	***	***	NS	***	**						
WC	***	***	***	***	***	***						
NFC	***	***	NS	***	***	***						
HAT	-	-	-	-	-	-						
GS	-	-	-	-	-	-	-	-	-	-	-	-
BP	-	-	-	-	-	-	-	-	-	-	-	-
BS	-	-	-	-	-	-	***	***	***	***	**	NS
JAX	***	***	NS	***	**	***						
	Gg2						***Me***					
	Yr	**JD**	**MPh**	**NT**	**NT:JD**	**NT:MPh**	**Yr**	**JD**	**MPh**	**NT**	**NT:JD**	**NT:MPh**
HZ	***	***	NS	***	***	**						
OC	***	***	*	***	***	***						
NC	***	***	***	***	***	NS						
BC	***	***	NS	***	***	*						
WC	***	***	***	***	***	**						
NFC	***	***	NS	***	***	***						
HAT												
GS	-	-	-	-	-	-	***	***	***	***	NS	*
BP							***	***	***	***	***	NS
BS							**	***	**	***	**	NS
JAX	-	-	-	-	-	-						

Table 3.2 Continued: Term significance for each model by species and site; abbreviations as in Table 3.1. Terms are: Yr – study year; JD – Julian day; MPh – moon phase; NT – normalized time of day. *** = p<0.001; ** = p<0.01; * = p<0.05, NS = not significant; '-' denotes models with poor fit; blank cells indicate modeling was not undertaken due to low presence.

	Zc						***Kogia* spp.**					
	Yr	**JD**	**MPh**	**NT**	**NT:JD**	**NT:MPh**	**Yr**	**JD**	**MPh**	**NT**	**NT:JD**	**NT:MPh**
HZ	*	***	***	***	**	NS						
OC	-	-	-	-	-	-						
NC	-	-	-	-	-	-						
BC	NS	***	NS	***	NS	*						
WC	NS	***	***	***	**	NS						
NFC	-	-	-	-	-	-						
HAT	***	***	**	***	***	***						
GS	-	-	-	-	-	-	-	-	-	-	-	-
BP							-	-	-	-	-	-
BS	-	-	-	-	-	-	*	*	***	***	NS	NS
JAX							-	-	-	-	-	-
	Mb						**Pm**					
	Yr	**JD**	**MPh**	**NT**	**NT:JD**	**NT:MPh**	**Yr**	**JD**	**MPh**	**NT**	**NT:JD**	**NT:MPh**
HZ	***	***	***	***	NS	*	***	***	***	***	***	NS
OC	***	***	NS	***	***	*	***	***	***	***	***	*
NC	-	-	-	-	-	-	***	***	NS	***	***	*
BC	***	***	NS	***	***	NS	***	***	X	***	***	X
WC	***	***	***	***	NS	NS	***	***	**	***	**	NS
NFC	-	-	-	-	-	-	***	***	***	***	***	*
HAT							***	***	NS	NS	***	**
GS							NS	***	NS	NS	*	NS
BP							NS	NS	NS	NS	**	NS
BS							NS	***	***	***	**	*
JAX							-	-	-	-	-	-
	Mm											
	Yr	**JD**	**MPh**	**NT**	**NT:JD**	**NT:MPh**						
HZ	-	-	-	-	-	-						
OC	-	-	-	-	-	-						
NC	***	***	NS	***	**	NS						
BC	-	-	-	-	-	-						
WC	-	-	-	-	-	-						
NFC	***	***	NS	***	NS	NS						
HAT												
GS												
BP												
BS												
JAX												

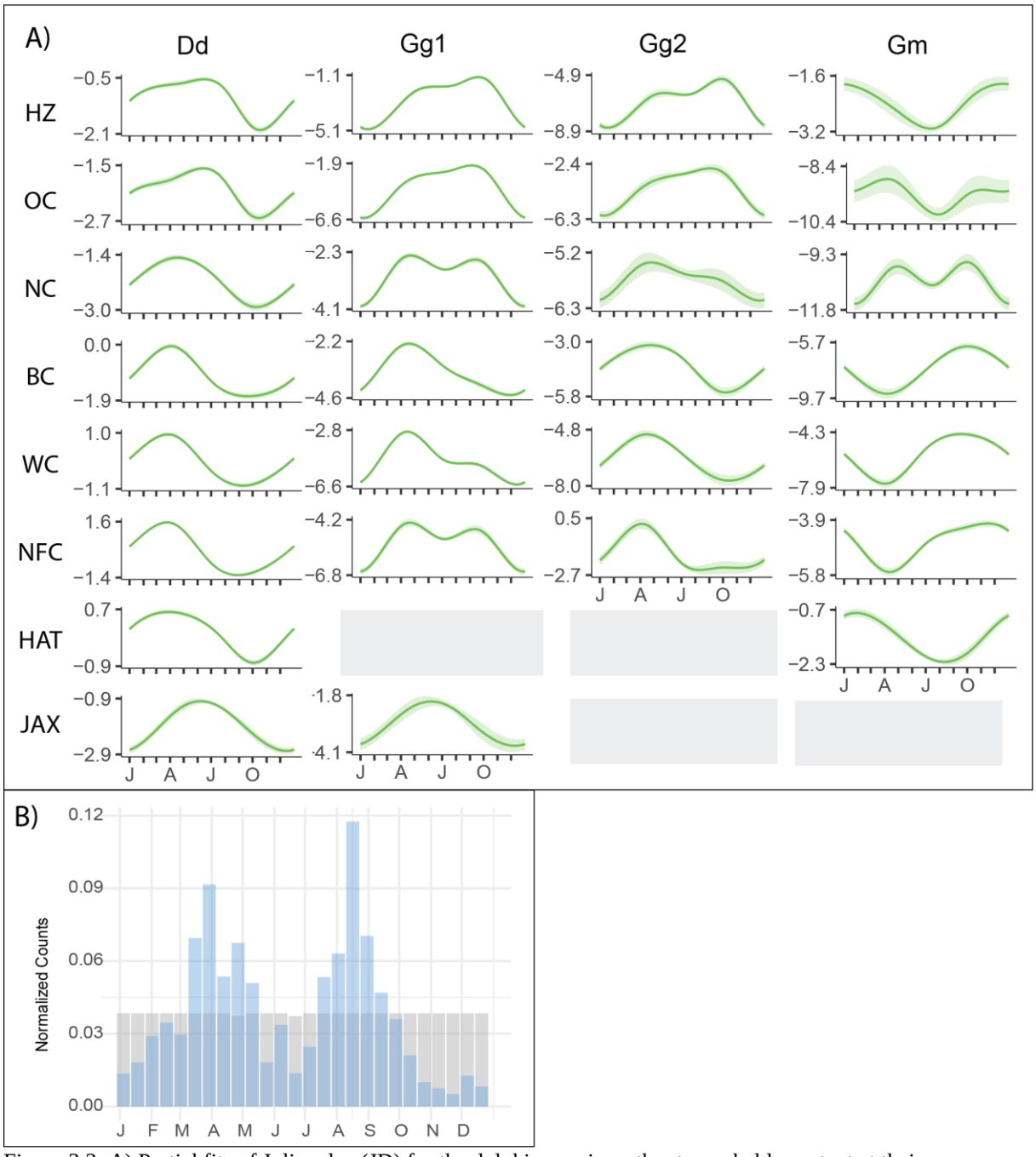

Figure 3.3: A) Partial fits of Julian day (JD) for the dolphin species; other terms held constant at their mean values. Shaded regions give 95% confidence intervals; gray blocks indicate no model due to low presence and/or poor performance. To account for the significant JD:NT (normalized time of day) interaction, JD fits were averaged across all values of NT. B) Risso's dolphin Gg1 click type presence as normalized counts (blue bars) at NFC showing clear bimodal pattern; gray bars show the distribution of effort across the year. Site and species abbreviations as in Table 3.1.

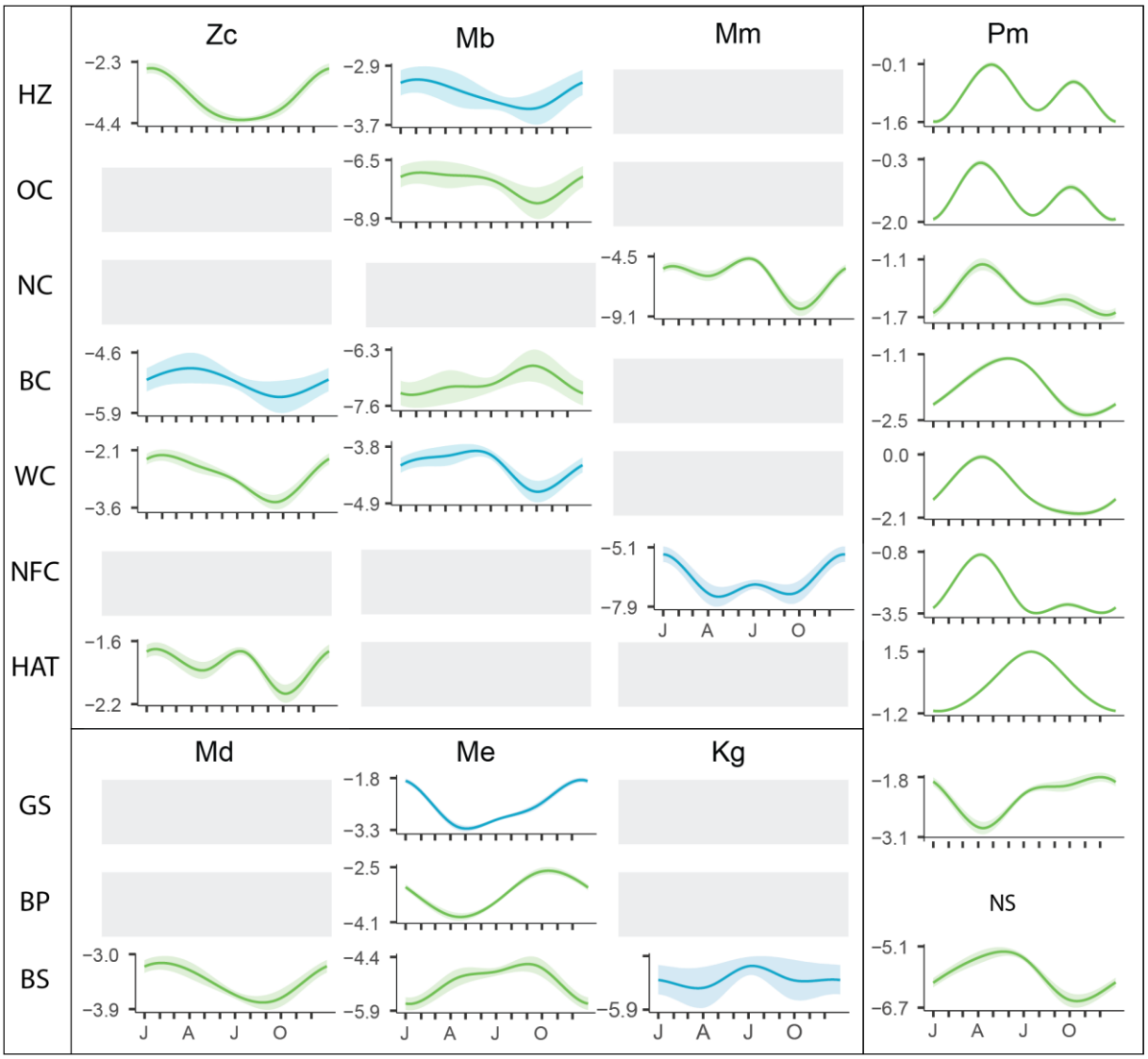

Figure 3.4: Partial fits of Julian day (JD) for the beaked whales, *Kogia* spp., and sperm whales; other terms held constant at their mean values. Shaded regions give 95% confidence intervals; gray blocks indicate no model due to low presence and/or poor performance; NS = JD was not significant. Blue lines indicate no significant interaction between JD and NT (normalized time of day); green lines indicate a significant JD:NT interaction, for which JD fits were averaged across all values of NT. Site and species abbreviations as in Table 3.1.

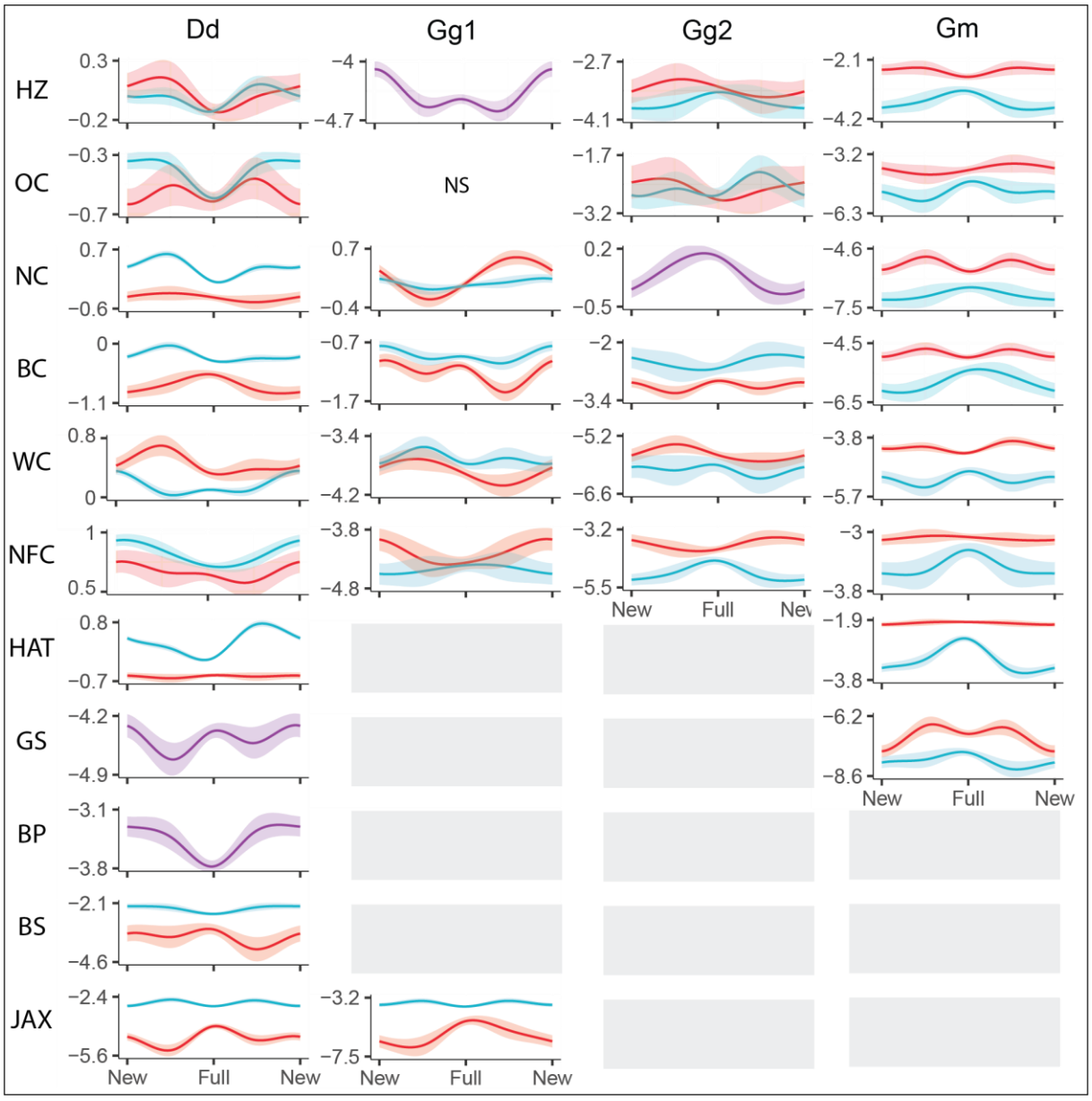

Figure 3.5: Partial fits of moon phase (MP) for the dolphin species; other terms held constant at their mean values. Shaded regions give 95% confidence intervals; gray blocks indicate no model due to low presence and/or poor performance. Plots showing a single curve (purple) depict the lunar pattern in the absence of significant interactions; plots with two curves depict the lunar patterns in the daytime (red) and nighttime (blue) when there was a significant interaction between MP and normalized time of day (NT). Site and species abbreviations as in Table 3.1.

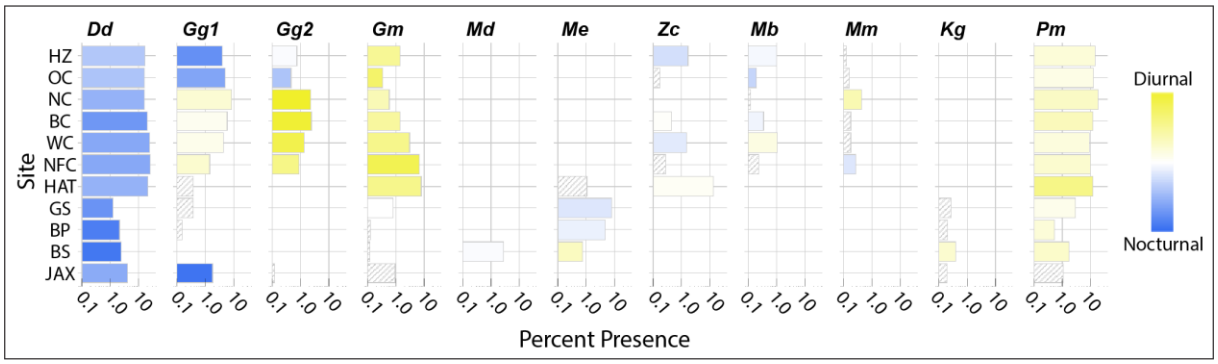

Figure 3.6: Partitioning of acoustic presence between day and night: white indicates an even 50/50 split; bright yellow indicates 100% of presence occurring in the daytime; dark blue indicates 100% of presence occurring in the nighttime. Gray fill indicates that normalized time of day was not significant; stripes indicate no model due to insufficient presence or poor model performance. Bar heights as in Figure 2; site and species abbreviations as in Table 3.1.

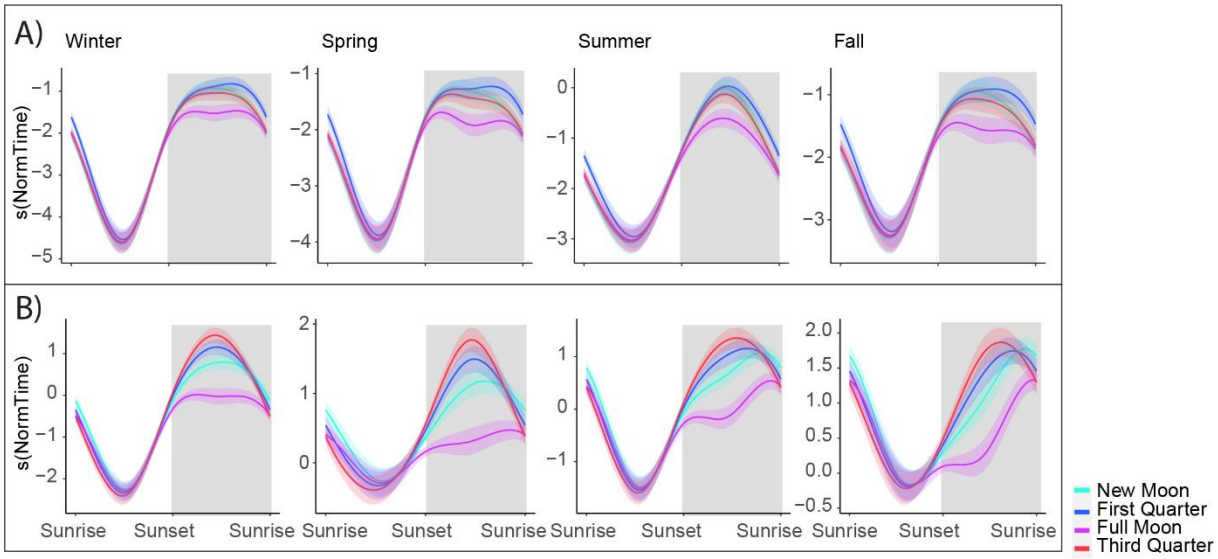

Figure 3.7: Diel activity patterns for short-beaked common dolphins at a) OC, and b) HAT showing differing impacts of the lunar cycle between sites and throughout the year. Each panel represents the interaction between normalized time of day (NT) and Julian Day (JD) at a different point in the seasonal cycle; colors in each panel show the interaction between NT and moon phase (MPh); gray shading shows nighttime. Site and species abbreviations as in Table 3.1.

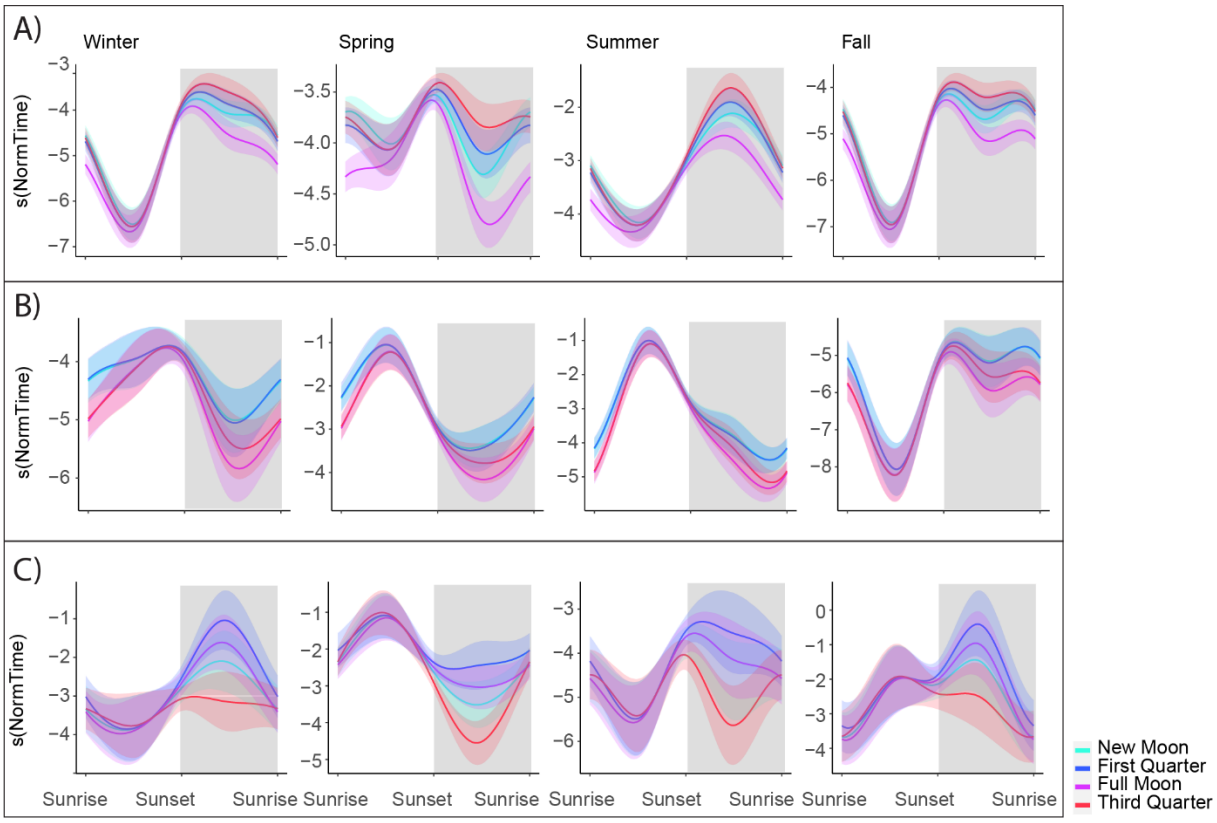

Figure 3.8: Diel activity patterns for the Risso's dolphin click types Gg1 (A) and Gg2 (B) at BC showing temporal separation; C) diel activity patterns of Gg2 at NFC showing substantial lunar modulation. Panels, colors, and shading as in
Figure 3.7.

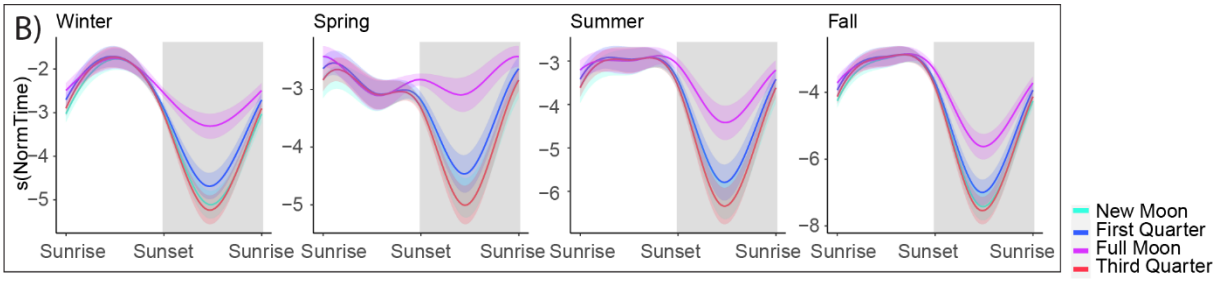

Figure 3.9: Diel activity patterns for short-finned pilot whales at HAT showing differing impact of the lunar cycle throughout the year. Panels colors, and shading as in
Figure 3.7.

3.8 APPENDIX

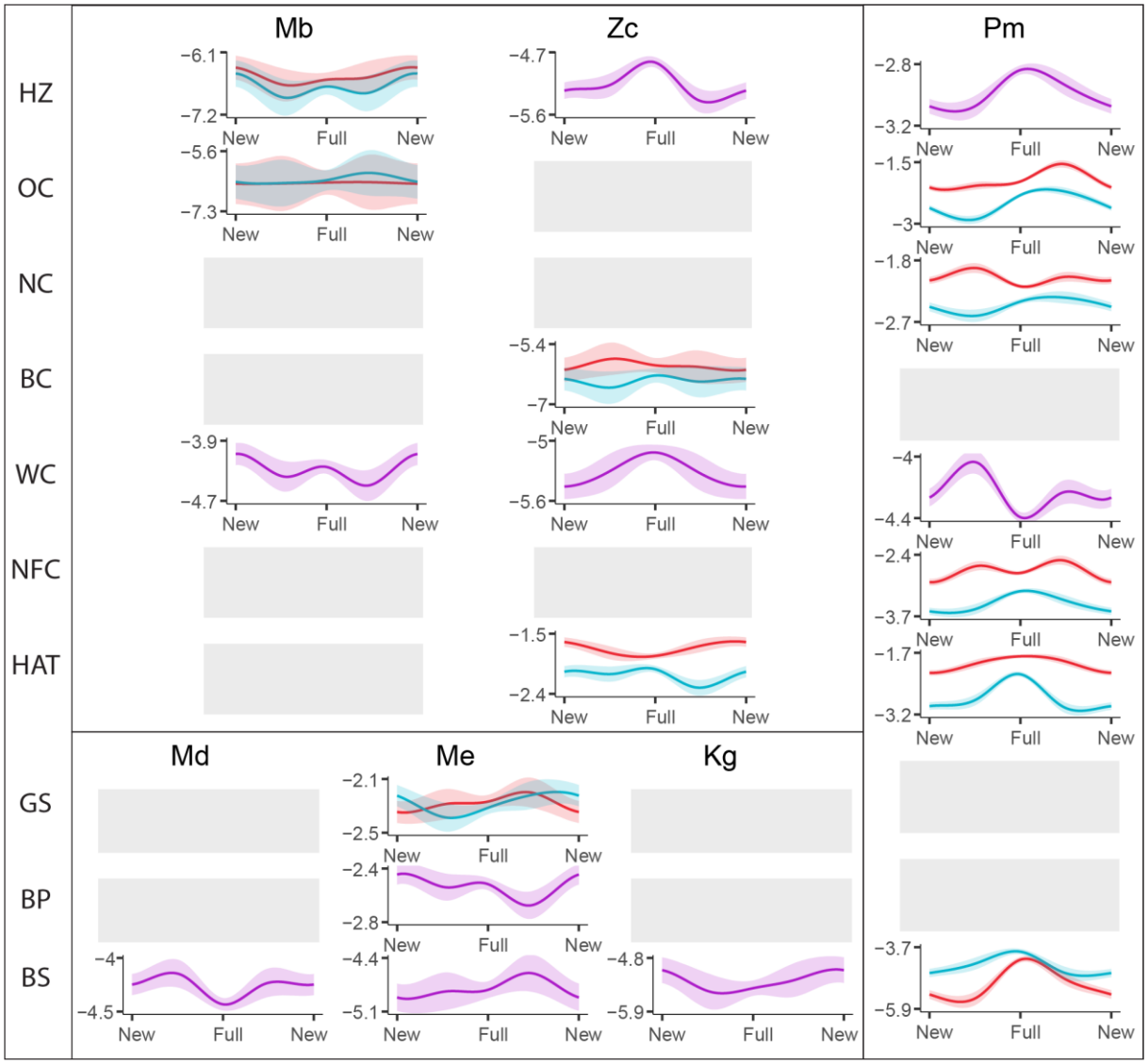

Figure 3.10: Partial fits of moon phase (MP) for the deep diving species; other terms held constant at their mean values. Shaded regions give 95% confidence intervals; gray blocks indicate no model due to low presence and/or poor performance. Plots showing a single curve (purple) depict the lunar pattern in the absence of significant interactions; plots with two curves depict the lunar patterns in the daytime (red) and nighttime (blue) when there was a significant interaction between MP and normalized time of day (NT). Site and species abbreviations as in Table 3.1.

Figure 3.11: Diel activity patterns for short-beaked common dolphins. At sites with 4 panels, each panel represents the interaction between normalized time of day (NT) and Julian Day (JD) at a different point in the seasonal cycle; colors in each panel show the interaction between NT and moon phase (MPh). At sites GS and BP there was no significant interaction between NT and MPh, so only the NT:JD interaction is shown. Site and species abbreviations as in Table 3.1.

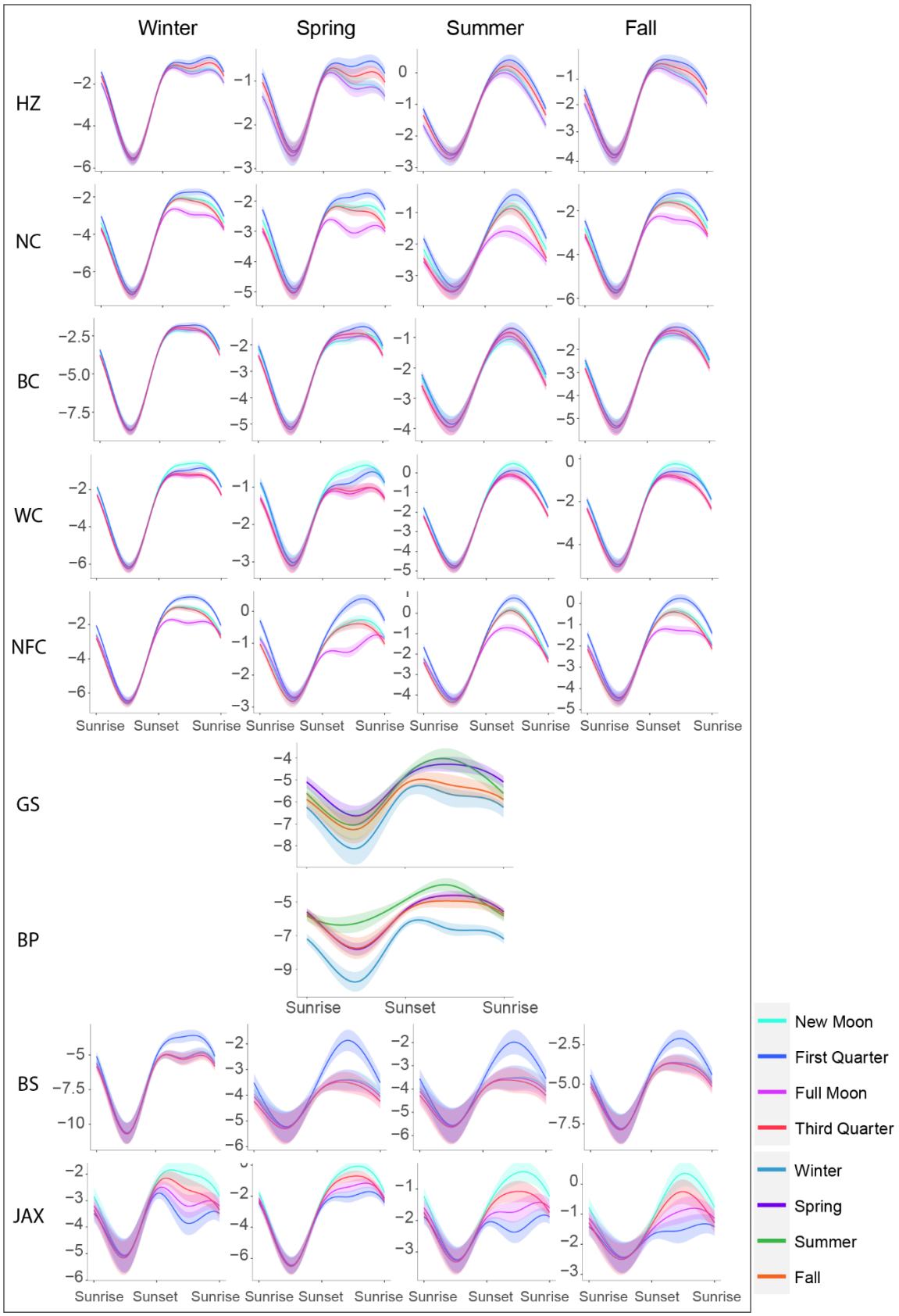
Winter
Spring
Summer
Fall
HZ
NC
BC
WC
NFC
GS
BP
BS
JAX
Sunrise
Sunset
Sunrise
New Moon
First Quarter
Full Moon
Third Quarter
Winter
Spring
Summer
Fall

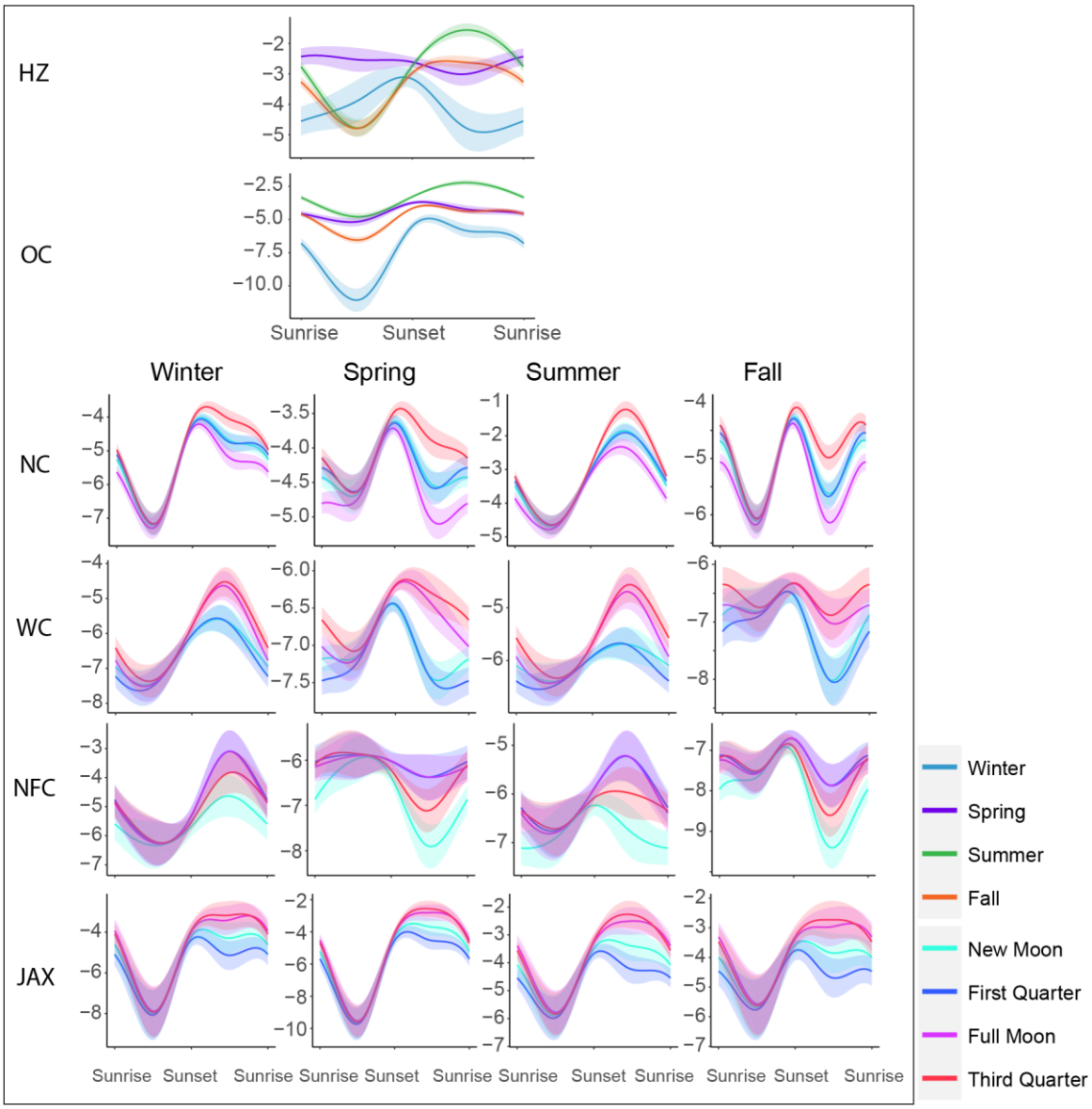

Figure 3.12: Diel activity patterns for Risso's dolphin click type Gg1. At sites with 4 panels, each panel represents the interaction between normalized time of day (NT) and Julian Day (JD) at a different point in the seasonal cycle; colors in each panel show the interaction between NT and moon phase (MPh). At sites HZ and OC there was no significant interaction between NT and MPh, so only the NT:JD interaction is shown. Site and species abbreviations as in Table 3.1

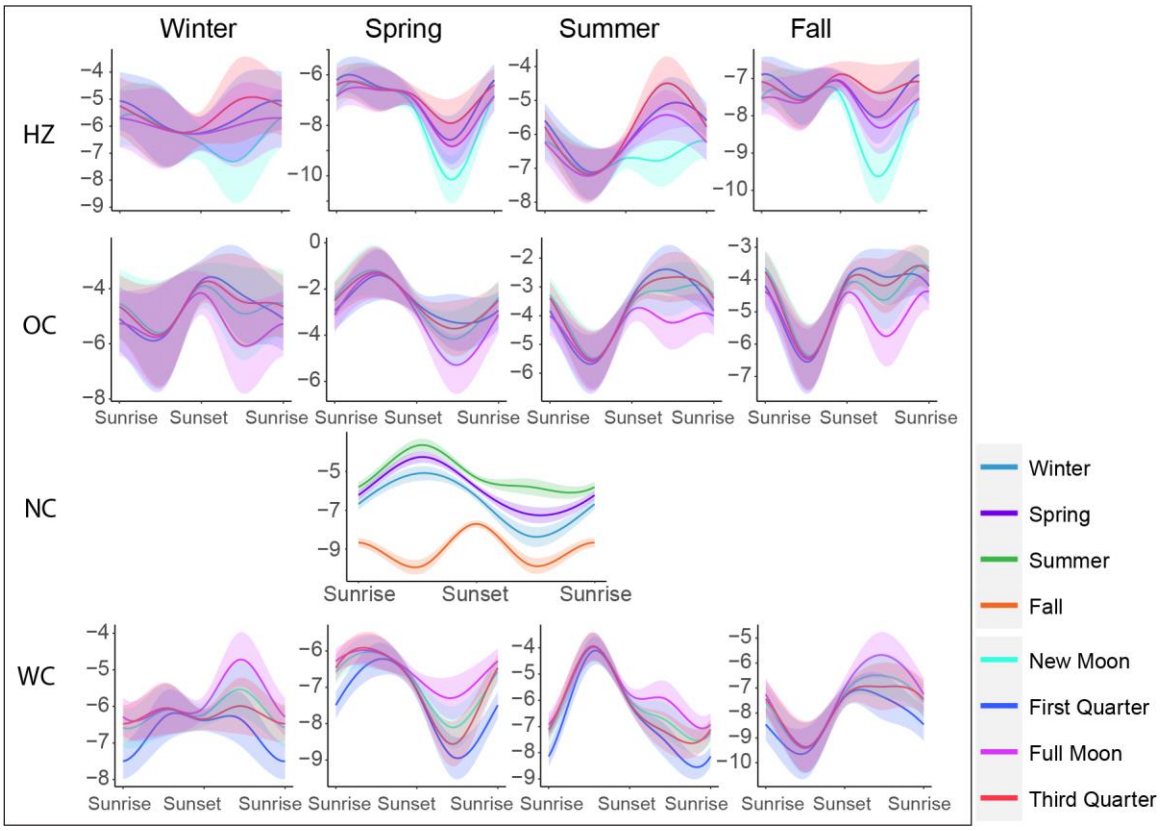

Figure 3.13: Diel activity patterns for Risso's dolphin click type Gg2. At sites with 4 panels, each panel represents the interaction between normalized time of day (NT) and Julian Day (JD) at a different point in the seasonal cycle; colors in each panel show the interaction between NT and moon phase (MPh). At site NC there was no significant interaction between NT and MPh, so only the NT:JD interaction is shown. Site and species abbreviations as in Table 3.1

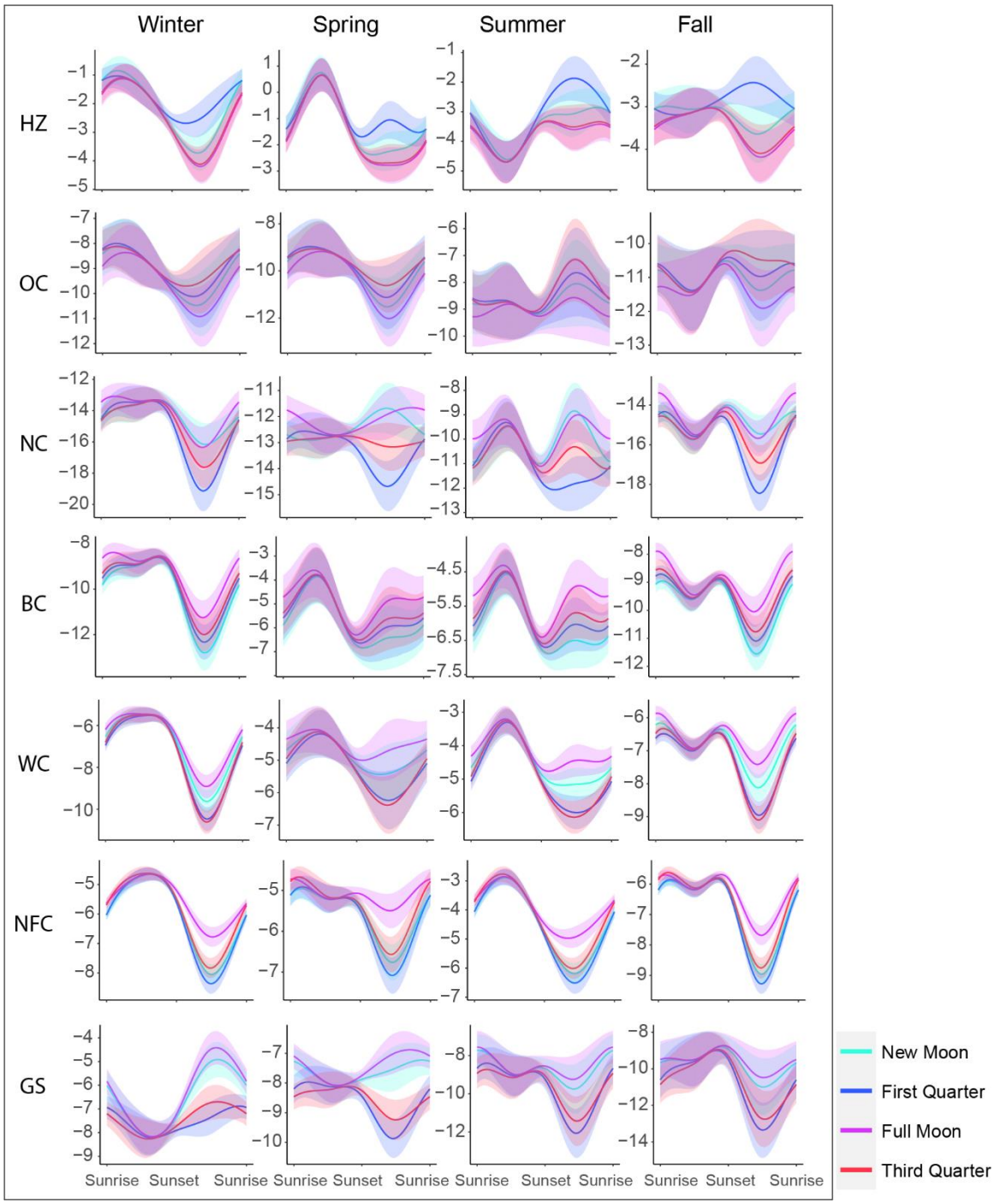

Figure 3.14: Diel activity patterns for short-finned pilot whales. Each panel represents the interaction between normalized time of day (NT) and Julian Day (JD) at a different point in the seasonal cycle; colors in each panel show the interaction between NT and moon phase (MPh). Site and species abbreviations as in Table 3.1

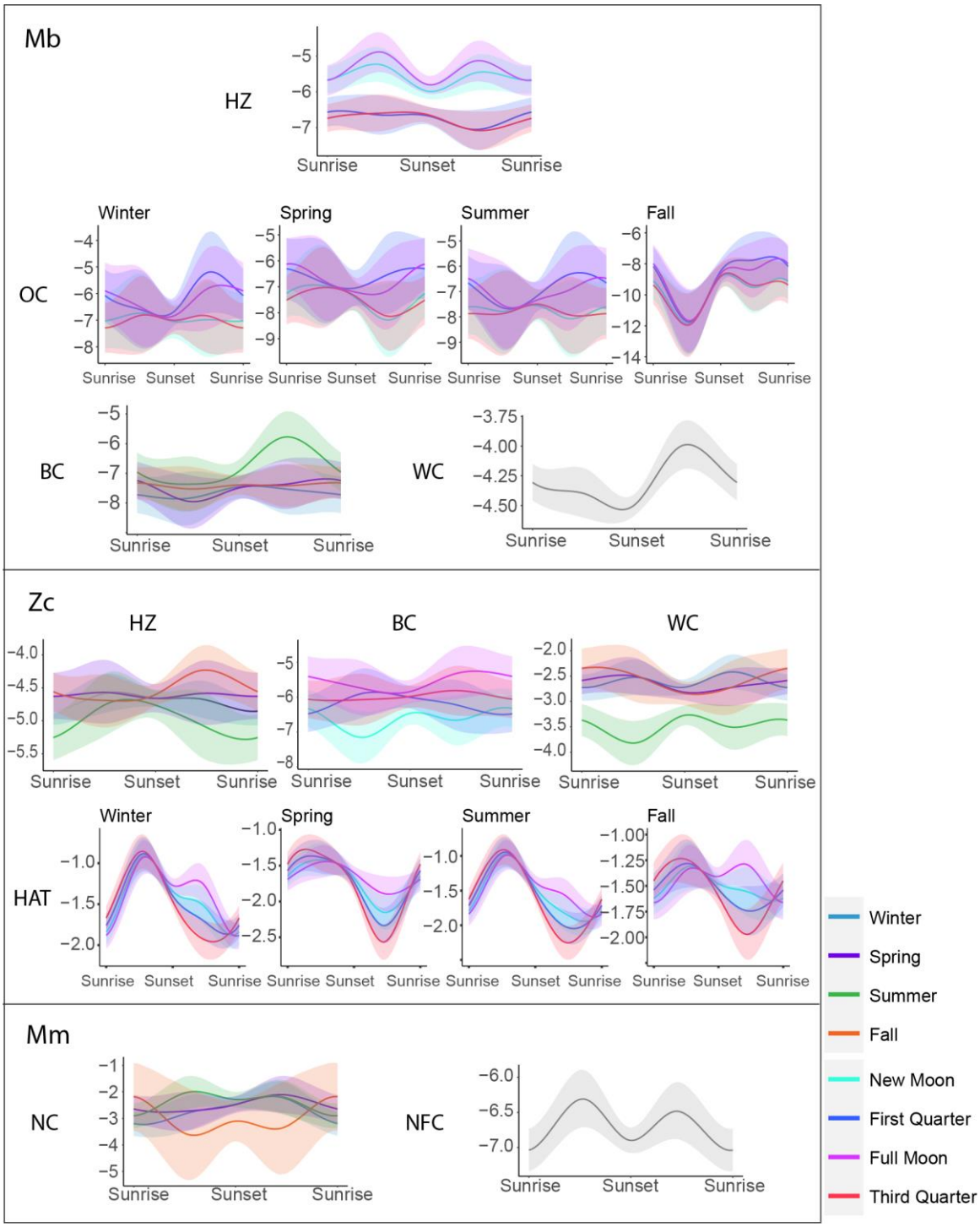

Figure 3.15: Diel activity patterns for Sowerby's (*Mb*), Cuvier's (*Zc*), and True's (*Mm*) beaked whales. For sites with 4 panels, each panel represents the interaction between normalized time of day (NT) and Julian Day (JD) at a different point in the seasonal cycle; colors in each panel show the interaction between NT and moon phase (MPh). At sites with a single panel there was no significant interaction between NT and MPh; if it was significant the NT:JD interaction is shown by color; if there were no significant interactions the NT pattern is shown in grey. Site and species abbreviations as in Table 3.1

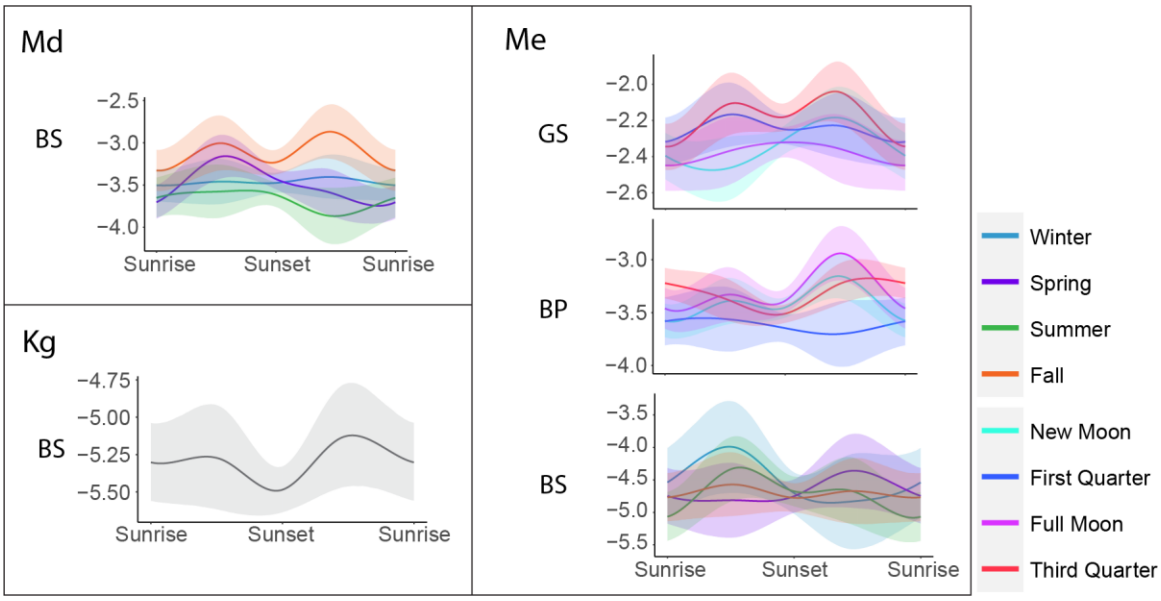

Figure 3.16: Diel activity patterns for Blainville's (*Md*) and Gervais' (*Me*) beaked whales and *Kogia* spp. (Kg). Colors in each panel show the interaction between either normalized time of day (NT) and Julian day (JD), or NT and moon phase (MPh). If there were no significant interactions the NT pattern is shown in grey. Site and species abbreviations as in Table 3.1

Figure 3.17: Diel activity patterns for sperm whales (*Pm*). At sites with 4 panels, each panel represents the interaction between normalized time of day (NT) and Julian Day (JD) at a different point in the seasonal cycle; colors in each panel show the interaction between NT and moon phase (MPh). At sites with a single panel there was no significant interaction between NT and MPh, so only the NT:JD interaction is shown. Site and species abbreviations as in Table 3.1

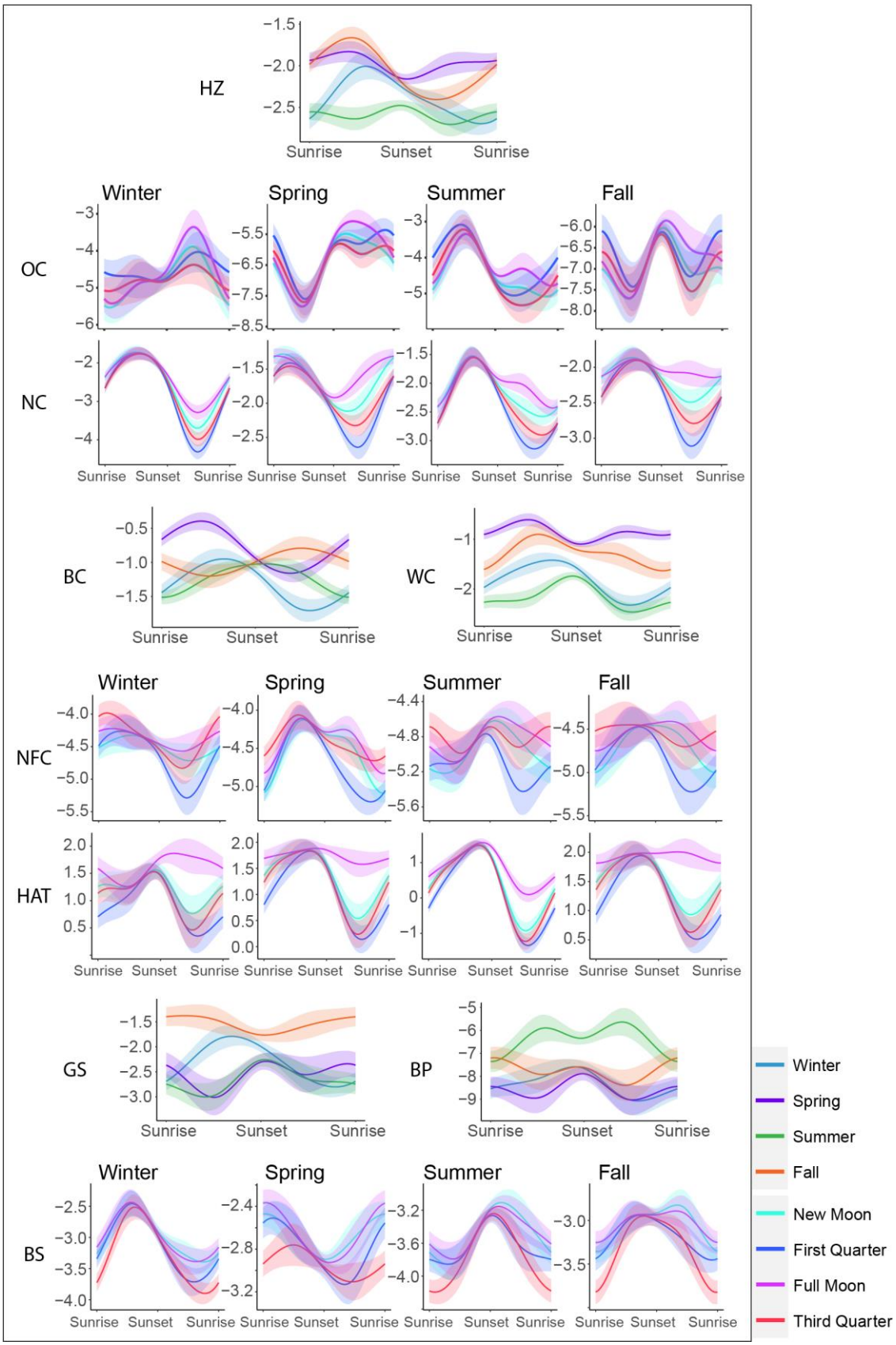
HZ
Winter
Spring
Summer
Fall
OC
NC
BC
WC
NFC
HAT
GS
BP
BS
Sunrise
Sunset
Sunrise
Winter
Spring
Summer
Fall
New Moon
First Quarter
Full Moon
Third Quarter

3.9 ACKNOWLEDGEMENTS

Chapter 3, in full, has been submitted for publication of the material as it may appear in Science Advances. Cohen, R.E., Frasier, K.E., Baumann-Pickering, S., Hildebrand, J.A. Spatial and temporal separation of toothed whales in the western North Atlantic. The dissertation author was the primary researcher and author of this paper.

4 THE ROLE OF THE GULF STREAM IN NICHE PARTITIONING OF TOOTHED WHALES IN THE WESTERN NORTH ATLANTIC

4.1 ABSTRACT

The western North Atlantic is home to more than two dozen odontocete species, all top predators relying on patchy resources of mid and upper-trophic level prey. Niche partitioning is expected under such circumstances of overlapping resource use, but little work has been done to characterize the differences in realized niche of these apparent competitors. Past efforts at modeling habitat suitability for odontocete species in this region have relied primarily on the visual sighting record, which is sparse for many odontocete species and must be aggregated across many years to get some measure of statistical power. This is largely due to the difficulty of observing and discriminating highly mobile species distributed with low density over vast pelagic ranges, especially those that spend significant time at depth or which have cryptic surface behaviors. The result of these shortcomings is that our knowledge of habitat preferences for odontocetes in this region is often limited in terms of both species and temporal resolution. To address some of these knowledge gaps we investigated habitat preferences for ten odontocete species using time series of species presence derived from passive acoustic data collected continuously across a three-year study period at monitoring sites spanning a latitudinal habitat gradient. We were specifically interested in the role of the Gulf Stream current and its mesoscale rings in shaping habitats and segregating species. We hypothesized that co-occurring odontocete species would select for differing environmental conditions, minimizing direct competition for resources via niche partitioning. We identified three distinct oceanic regimes occurring across our shelf break monitoring sites, and observed that species presence was clearly segregated along the lines of these regimes. Gulf Stream rings were found to be only modestly correlated with oceanic conditions at our monitoring sites, but ring vicinity was still a strong predictor of presence for most species. For species with similar foraging ecologies occurring in a given regime, we found distinctly different preferences for temperature and salinity ranges. We used

these insights to predict habitat suitability across the region for each species in each season. Our results demonstrate clear niche partitioning of odontocete species in this region, and provide insights into habitat preferences which can be used to predict distributional shifts in odontocete species presence in response to anthropogenically-driven ocean change.

4.2 INTRODUCTION

A diverse guild of cetacean top predators inhabits the western North Atlantic, most being species in the parvorder Odontoceti, or toothed whales. As shown in Chapters 2 and 3, the distributions of odontocete species in this region clearly reflect the Gulf Stream boundary and exhibit periodicity on multiple temporal scales. Ecological niche theory posits that when there is overlap between the ecological niches of two or more species, these species will differentiate their realized resource niches to reduce competition [215,216]. Previously we demonstrated spatiotemporal separation between odontocete species in this region with similar foraging ecology, which may be a means of minimizing direct competition for prey resources. However, the environmental factors driving these observed patterns in habitat utilization, and which define the ecological niches occupied by each odontocete species and their preferred prey, are poorly understood.

The North Atlantic is characterized by the powerful Gulf Stream western boundary current which transports large volumes of equatorial water northeast across the basin. In the west, the northern wall of the current acts as a dynamic boundary between two quite different ecoregions [46,116,117]. South of the Gulf Stream front, warm, salty, low-productivity waters originating in the Sargasso Sea dominate the water column. North of the Gulf Stream front, deep Labrador Sea water, as well as shallower water masses formed through the mixing of Labrador Current waters with Coastal Water (on the shelf) or Gulf Stream water (off the shelf) [47–49], provide habitats which are comparatively cool, fresh, and productive. Oceanographic conditions across this region fluctuate seasonally, are subject to short-term variability in response to transient Gulf Stream meanders, rings, and filaments, and may

also be subject to broad-scale climate change-mediated shifts [217–221]. Insights into what dictates suitable habitat for each odontocete species in this dynamic environment, and how the species might be expected to respond to climate change-mediated habitat shifts, are of interest for management of these protected populations with respect to anthropogenic activities such as fisheries, commercial shipping, marine resource extraction, and naval exercises.

Habitat models for cetaceans have traditionally been developed using visual survey data [134–136,222], but the data-hungry nature of these statistical approaches, and the low encounter rates typical of many pelagic odontocete species, usually necessitate aggregating data over many years to obtain some measure of statistical power. Visual surveys are dependent upon sea state and visibility conditions, so effort is therefore restricted to daylight hours and biased towards the spring and summer months. This may result in underestimation of species present in a given region primarily in the fall or winter. Additionally, some species are unable to be reliably discriminated visually due to their highly similar physical appearances and/or cryptic surface behavior, and so are often grouped. The result is that habitat models built exclusively on visual data often lack temporal and species resolution, and are ill-suited to predicting habitat suitability at all points throughout the year.

More recently, species presence inferred from marine passive acoustic data has begun to be incorporated into these modeling efforts [151,172]. Autonomous passive acoustic monitoring offers some advantages over visual surveys, as the acoustic data can be collected continuously in all seasons and sea states. Autonomous platforms such as moorings and drifters offer the added advantage of being noninvasive, and therefore may enable assessment of animal behavior unaltered by tagging activities or the vicinity of a scientific vessel. Here we utilized the time series of acoustic presence for ten odontocete species derived from passive acoustic data in Chapters 2 and 3 to characterize relationships between species presence and environmental covariates with an eye to the influence of the Gulf Stream. We hypothesized that species occupying similar regions, and exhibiting similar foraging ecologies, would minimize potential competition for prey resources via niche partitioning.

Lacking concrete data on exactly which prey species are being targeted by each odontocete species, we used environmental covariates as proxies for prey availability, with the assumption that each odontocete species would target conditions associated with presence of their preferred prey species. We found clear separation of odontocete species habitat preferences along the lines of several physical, chemical, and biological covariates, and used these insights to predict seasonal presence of each species across the region. Results are discussed in the context of the influence of the Gulf Stream and predicted climate change scenarios. These findings substantially advance our understanding of odontocete habitat utilization in this region, especially with regard to the cryptic beaked whale and *Kogia* species.

4.3 METHODS

All analyses were carried out in the R computing environment [143]. We utilized time series of odontocete species presence derived from passive acoustic data recorded at eleven (11) shelf-break and slope monitoring sites in the western North Atlantic (Figure 2.1) by [142] using a combination of automated algorithms and expert analyst review. The acoustically-differentiable odontocete species included in this analysis were: Risso's dolphins (*Grampus griseus*), identified by two different click types; short-beaked common dolphins (*Delphinus delphis*); short-finned pilot whales (*Globicephala macrorhynchus*); Blainville's beaked whales (*Mesoplodon densirostris*); Sowerby's beaked whales (*Mesoplodon bidens*); Gervais' beaked whales (*Mesoplodon europaeus*); True's beaked whales (*Mesoplodon mirus*); Cuvier's beaked whales (*Ziphius cavirostris*); and sperm whales (*Physeter macrocephalus)*. *Kogia* spp., which are not acoustically differentiable based on current knowledge, were included as a genus-level group. For this analysis the two Risso's dolphin click types were combined for a single time series of Risso's dolphin presence. Species acoustic presence/absence at each monitoring site during the period of May 1, 2016, to April 30, 2019, was classified in 5-minute

intervals, and subsequently summed to daily resolution quantified as the number of 5-minute bins with presence each day.

4.3.1 Environmental Covariate Data

Relevant environmental covariates were identified from previous odontocete habitat modelling efforts [110,136,148,222,223] and obtained from publicly-available databases of remotely-sensed and modeled oceanographic data at daily resolution (Table 3.1). For the Hybrid Ocean Coordinate Model (HYCOM; [224]) data, which were available with 3-hourly resolution during our study period, we obtained the model output for noon of each day. The HYCOM products and finite-size Lyapunov exponent (FSLE) data were re-gridded to a consistent spatial resolution of 0.08° using the *regrid* function in the *EFDR* package [225]; data from the grid point nearest each HARP site were then extracted. Water u-velocity (eastward) and v-velocity (northward) from HYCOM were not related directly to species presence, but rather were combined to calculate water velocity magnitude (VelMag; m/s) and direction (VelAsp; °, with north set to 0°) for each depth layer, as well as eddy kinetic energy (EKE) at the surface. EKE is a measure of energetic anomaly and as such is sensitive to the definition of the time mean relative to which the anomaly is computed. Following the method of [226], we calculated EKE as $EKE = 0.5*(u'^2 + v'^2)$, where u' and v' are the u and v velocity fluctuations obtained by subtracting calendar year velocity averages from 5-day rolling means of u and v. EKE values were averaged over the four grid points nearest to each HARP site in order to better capture the mesoscale energetics. Distances to the center of the nearest cyclonic and anticyclonic eddies (C/AEddyDist) were derived from Aviso's Mesoscale Eddy Trajectory Atlas product (META3.2 DT allsat, DOI:10.24400/527896/a01-2022.005.210802, [227]), which was produced by SSALTO/DUACS and distributed by AVISO+ (https://www.aviso.altimetry.fr/) with support from CNES, in collaboration with IMEDEA. This atlas was downloaded on 4 April, 2022, and covers the period from January 1993 to August 2021. Several of the covariates considered here quantify various aspects of the energetics of the Gulf Stream and related mesoscale features (e.g. FSLE, C/AEddyDist,

EKE, water velocity magnitude and direction), and were included to test the hypothesis that target species may either prefer or avoid such features.

The chlorophyll (Chl) record suffered from loss of data due to cloud cover, so re-gridding in the same fashion as the other covariates would have resulted in interpolating over very large spatial gaps. Instead we chose to average Chl values from the four grid points nearest to each monitoring site on each day, before linearly interpolating remaining gaps in the time series at each site. This likely resulted in considerable smoothing of the Chl time series, but we considered this acceptable in light of the trophic separation between primary productivity and the target species.

Examination of covariate data distributions showed that data from HYCOM contained spurious marginal values where the model interacted with the continental mask at depth. Many of the target species in this analysis were deep divers [210,228–231], and so we were interested in exploring relationships between species presence and conditions at or near foraging depths. Therefore we chose to use data from the grid points adjacent to each site but one step east and south, i.e. further off the shelf break where the continental mask was deeper, to enable inclusion of covariates down to 700 m. Data for a few non-consecutive days in our study period were not available from HYCOM; resultant gaps in the covariate time series at each site were linearly interpolated.

4.3.2 Exploration of Oceanic Conditions

The oceanic conditions experienced at each site were characterized by visualizing distributions of covariate values as kernel density plots and carrying out principal component analysis (PCA) to identify groupings of similar conditions which might represent distinct oceanic regimes. To assess the influence of Gulf Stream rings on conditions at our sites we calculated Pearson's correlation between distance to the nearest cyclonic/anticyclonic eddy and covariate values, as well as covariate anomalies. Anomalies were calculated by subtracting a monthly mean centered on each observation to get a measure of deviation from regular seasonal fluctuations. We then investigated the relationships

between species presence and these oceanic conditions several ways: 1) by calculating Pearson's correlation between presence and covariate values on a per-species and per-site basis; 2) by visualizing distributions of covariate values observed simultaneous to each species' presence as violin plots; 3) by performing Kolmogorov-Smirnov tests comparing the distributions of covariate values observed during species presence to the null background distribution, both across the whole region and on a per-site basis; 4) by visualizing mean weekly presence in discrete covariate value bins on a per-species and per-site basis and comparing the apparent preferences of spatially overlapping species; and 5) by modeling species presence relative to the covariates.

4.3.3 Statistical Modeling

Generalized additive models (GAMs) [145] were chosen to characterize the shapes of relationships between species presence and environmental covariates. GAMs are an extension of generalized linear models (GLMs) which relate a smooth function of the response variable to an additive predictor of covariates, which may include smooth functions of covariates. These smooth functions of covariates can capture highly complex non-linear relationships, making GAMs much more flexible than GLMs. The GAM approach has been extensively used and validated for cetacean habitat models in this study region and elsewhere [110,134,136,147–151,222,232]. To compute these models we used the *gam* function within the *mgcv* package [233].

An underlying assumption of GAMs is that the response data are independent, an assumption which is often violated by spatiotemporal autocorrelation in species presence data. We tested this assumption by examining the residual autocorrelation of models relating species presence at each site to the candidate covariates identified by correlation coefficients, and found that the shapes of the autocorrelation functions indicated autoregressive dependence. The points at which the autocorrelation values dropped within the confidence intervals varied from 4-43 lags (days). To reduce this temporal autocorrelation, we decided to coarsen the temporal resolution by summing presence, and averaging covariate values, in each week. Re-testing of the residual correlation of the weekly data in the same

manner as above showed that this substantially reduced residual autocorrelation to 2-7 lags (weeks) which we considered to be an acceptable trade-off between temporal resolution and data independence. We also tested for overdispersion in the species presence data and found that none of the presence time series met the criteria for Poisson distribution (variance = mean); therefore we elected to use the Tweedie distribution, which enables full-likelihood model fitting while accounting for overdispersion and zero-inflation.

Covariates exhibiting substantial correlation with a given species' presence (>0.2 at one or more sites) were considered during the model selection process. For the covariates available at multiple depth layers, conditions at the surface as well as conditions at a depth layer relevant to each species' foraging ecology were considered. To determine whether covariates should be included as linear or smooth terms, and with how many knots in the case of smooth terms, we compared Akaike Information Criterion (AIC) [234] values of single-predictor models in which each covariate was included as a linear term or as a smooth with three to five knots; the maximum of five knots, resulting in up to four degrees of freedom, and a smoothing parameter (gamma) of 1.4, were chosen to avoid overfitting and in the interest of describing ecologically-interpretable relationships. Cubic regression shrinkage splines were used for the smooth terms, except for water velocity direction, which was modeled as a cyclic cubic spline to impose continuity between 0° and 360° (both due north).

Species presence timeseries, and corresponding observations for all candidate covariates, were pooled across sites to fit a single regional GAM per species using the restricted maximum likelihood method. For *Kogia* spp., only observations from Cape Hatteras and southwards were used, as the sampling frequency of 200 kHz only enabled partial resolution of *Kogia* spp. click spectra and impeded discrimination between *Kogia* spp. and harbor porpoise at the northern sites, where they co-occur [164]. Concurvity, a generalization of collinearity to smooth terms, was quantified between candidate covariates using the *concurvity* function in the *mgcv* package [233]. In cases of highly concurved covariates (>0.5), terms were removed from the model and concurvity retested iteratively to

arrive at a set of more or less independent predictors. This generally resulted in each covariates being represented in the model only at a single depth layer, as conditions at the surface and at depth were often, though not always, correlated. The *dredge* function from the *MuMIn* package [235] was used to carry out model selection by comparing models built on different combinations of terms based on Akaike Information Criterion (AIC) [234] values to find the most parsimonious model.

Model goodness-of-fit was quantified by overall deviance explained, as well as Spearman's rank correlation and mean absolute error calculated for model predictions versus actual observations, both for instances of non-zero presence and for all data. Mean absolute error for each species was also calculated as a percentage of the 90th percentile – 10th percentile range of the data, to allow direct comparisons of model error between species with presence ranging over very different scales (e.g. 1-10s bins/week for *Kogia* spp. vs. 100-1000s bins/week for sperm whales). The diagnostic tests were carried out on non-zero data to determine if the error rates were being inflated by very low, but non-zero, predictions of presence during observations of no presence. Most of the species considered here were present for only a small percent of the total recording effort, resulting in zero-inflated presence data distributions. Model predictions of extremely low levels of presence (e.g. 1e-10 bins/week, negligible for our purposes) during the many observations of actual zero presence could bias the error rates simply by being so numerous.

4.3.4 Model Predictions

In the interest of predicting habitat suitability using widely available oceanographic data, models containing solely surface covariates were built for each species (referred to hereafter as "surface models"). For the deep diving species (all but common dolphins and Risso's dolphins), we chose to restrict predictions to water depths >200m to avoid making predictions in very shallow habitats which were not represented in our model training data, and which previous work has shown is not utilized by these species. Change in deviance explained as a result of removing deep covariates from the optimal models was quantified and found to be between 0% and 5% for all species except

Risso's dolphins, for which removal of salinity at 400 m resulted in a reduction in deviance explained of 15.8%. The surface models were used to predict seasonal habitat suitability for each species using climatologies computed by averaging all daily observations within a single month representative of each season (winter = January, spring = April, summer = July, fall = October) and across all three study years.

4.4 RESULTS

4.4.1 Characterization of Oceanic Regimes

Kernel density plots of the weekly averaged covariate observations at each site showed clear separation between the northern sites and the southern sites along the lines of temperature, salinity, SSH, and chlorophyll (Figure 4.1). Observations of SST, surface salinity, and Chl at HAT were more similar to the southern sites, while the range of SSH values at both HAT and GS were intermediate between the northern and southern regions. The sites in the direct path of the Gulf Stream (GS and HAT) were distinct for their large magnitude water velocities, low variability in direction of water flow, and to a lesser extent for more extreme FSLE values. The other southern sites did not exhibit these characteristics of highly energetic flow.

PCA of the oceanographic covariates revealed tight clustering of the northern sites and separation between the northern sites and those from HAT southwards (Figure 4.2). PC1 accounted for 50.9% of the variance between observations, while PC2 accounted for an additional 11.2%. The PCA showed that GS was more closely associated with BP and BS than with HAT, while GS and HAT were clearly distinct from BP and BS in the kernel density plots of SSH, surface water velocity, and surface water direction. On the basis of these observations we propose that the conditions experienced at the monitoring sites considered here can be divided into 3 regimes: Northerly, Gulf Stream Direct (GSD) influence, and Gulf Stream Indirect (GSI) influence (Table 4.2). The Northerly regime was characterized by SST ranging from 5º C to 23º C, surface salinity <35 PPT, negative SSH values, Chl

>0.3 mg/m^3, water velocities <0.5 m/s, and highly variable direction of water flow. The Gulf Stream Indirect influence regime (GSI) was characterized by SST >23º C, surface salinity >36 PPT, SSH >0.2 m, Chl <0.25 mg/m^3, water velocities <0.6 m/s, and highly variable direction of water flow. The Gulf Stream Direct influence regime (GSD) had high SST and surface salinity values similar to the GSI regime, but SSH and Chl values intermediate between the Northerly and the GSI regimes. Further, this regime was particularly distinguished by water velocities >0.5 m/s and water flow directed almost exclusively to the northeast.

We found few cases of strong correlation between distance to the nearest cyclonic/anticyclonic eddy and covariate values or covariate anomalies. The small magnitude of most of the correlations with both absolute covariate values and covariate anomalies may suggest that the oceanographic conditions at our sites are not primarily driven by the influence of Gulf Stream rings, or that this approach was not well-suited to quantifying their influence.

4.4.2 Odontocete Species Regime Preferences

The odontocete species considered here were divided into distinct groups by differences in the ranges of covariate values in which each was present, i.e. the ecological niches they occupied (Figure 4.1). The beaked whale species could clearly be separated between Northerly (Cuvier's, Sowerby's, and True's) and GSD/GSI (Blainville's, Gervais'). Risso's dolphins and short-finned pilot whales exhibited a primarily Northerly signature, but low levels of presence at the central-southern sites extended the range of covariate values at which they were present. *Kogia* spp. were the reverse of these dolphins, with a strong GSD/GSI preference, but long tails in the covariate distributions driven by low levels of presence in the Northerly regime. Short-beaked common dolphin and sperm whale presence reflected presence across all sites, with no significant differences between the distributions of covariate values in which they were present and the background distributions of those variables across the region.

Blainville's beaked whales preferred the GSI regime, with selection for high SST, surface salinity, and SSH values, and very low Chl concentrations. The distribution of water velocity values in which they were present did not differ significantly from background conditions, indicating that they were not selective for water velocity. Gervais' beaked whales exhibited many of the same preferences as Blainville's, though with more variability in SST, surface salinity, SSH, and Chl values due to their presence at HAT. However, high levels of Gervais' presence at GS imparted a distinctive signature of high water velocities, primarily northeastern water flow, and larger magnitude FSLE values, demonstrating their preference for the GSD regime. Cuvier's, Sowerby's, and True's beaked whales, on the other hand, exhibited preference for the Northerly regime, with SST and salinity ranging into lower values, negative SSH values, high Chl concentrations, and direction of water flow distribution centered around 200º (southwest). Cuvier's abundant presence at HAT could be seen in more observations of presence at higher SSH and surface salinity values and in northeasterly water flows compared to Sowerby's and True's.

Covariate distributions for Risso's dolphins and short-finned pilot whales were similar to those of short-beaked common dolphins, but the former two were significantly different than background conditions in most cases, while common dolphins were not. The root of this difference lies in Risso's and pilot whales' presence primarily from HAT northwards, in the GSD and Northerly regimes, while common dolphins were present across all three regimes. In the SSH violin plot (Figure 4.1) this can be seen in the slightly greater proportion of Risso's and pilot whale presence observations associated with negative SSH values than is seen for common dolphins. Pilot whales were not selective for water velocity or direction of water flow. This was somewhat surprising given their locus of presence at HAT, which had the fastest and most narrowly directed flow of any of our sites, but may just be a result of looking at binary presence/absence without taking into account magnitude of presence. Sperm whales were very similar to the short-beaked common dolphins in their apparent tolerance for variable conditions across regimes. Kogia spp. exhibited many similarities to Blainville's

and Gervais' beaked whales in their oceanographic preferences, but with a much wider spread of SST, salinity, and SSH values as a result of low levels of presence at the northern sites. Interpretation of these seemingly Northerly preferences should be made with caution, as some proportion of Kogia spp. presence at the northern sites may in fact be confusion with harbor porpoise [164]. Despite this Northerly influence, their locus of presence at BS drove an overall preference for low Chl concentration.

4.4.3 Habitat Models

The most parsimonious models retained 3-6 covariates and explained between 40.4% and 86.9% of the deviance of the null model (Table 4.3). SST was the most common covariate, retained in models for all species except *Kogia* spp., followed by SSH, salinity at foraging depth, and distance to cyclonic eddy (all retained in 7/10 models). The covariates available for model comparison were determined largely by how much concurvity was present. SST, temperature at depth, surface salinity, and salinity at depth were all frequently concurved with one another to varying extents; in these cases removal of temperature at depth and surface salinity was effective at reducing concurvity. The opposite choice – removal of salinity and depth and surface temperature - would have been equally effective, and therefore the final decision was arbitrary, but consistent across models. As a result, the infrequent retention of these covariates in the final models cannot be interpreted as an indication of unimportance, but rather the limitations of the modeling approach. On the other hand, water velocity, EKE, water direction, FSLE, and AEddyDist were not generally concurved with other terms, so their retention in just 1-3 models may be interpreted as an indication that they were not very impactful for the species considered here, at the spatial and temporal scales utilized.

Models were generally well-fit to the training data, as shown by the high values for deviance explained (Table 4.3), and Spearman's rank correlation and relative MAE values falling mostly in the "fair to good" and "excellent" ranges laid out by [236] (Table 4.4).

4.4.4 Niche Partitioning of Presumed Competitors

Within the broad oceanic regime preferences identified here, we looked for evidence of niche partitioning among the species which were present across similar ranges of covariate values and are known to have similar foraging ecology. Specifically, we considered apparent niche overlap between Blainville's and Gervais' beaked whales in the south, between Cuvier's, Sowerby's and True's beaked whales in the north, and between Risso's dolphins and short-finned pilot whales in the north. We found that while the presence-covariate relationships indicated by the regional GAMs didn't always vary substantially between direct competitors, there was always clear separation according to preferred values of at least one covariate on a per-site basis. The particular covariates driving separation sometimes varied between sites. We do not expect these species to be actively selecting for particular ranges of salinity, SSH, Chl, etc., but rather we expect that they will preferentially seek out and forage in conditions optimal for their preferred prey species. Further work will need to be done to identify these prey species and their optimal niches.

The regional models for Blainville's and Gervais's beaked whales only had SST and direction of surface water flow as common terms (Table 4.3). The model output showed a preference for higher SST for both species, but Blainville's were associated with water flow to the southwest, while Gervais' were associated with flow to the northeast (Figures 4.3, 4.4). For Gervais' this preference was likely driven by their high levels of presence at GS, where the direction of water flow is largely invariant. At BS, where these species co-occur the most, the distributions of Chl, surface salinity, SST, temperature at foraging depth, and direction of water flow at the surface associated with presence of each species were significantly different between species (Table 4.5). Kernel density plots showed that at BS Gervais' selected for higher water temperatures both at the surface and (less so) at depth, lower surface salinity values, and lower chlorophyll values (Figure 4.5). The only selectivity apparent for Blainville's at this site was for lower SST; otherwise Blainville's presence was associated with covariate distributions indistinguishable from the background conditions (i.e. not selective). This may

suggest that Blainville's preferred prey in this region are consistently available at BS, while the preferred prey of Gervais' beaked whales may be more abundantly present or more accessible during warmer water conditions at BS.

When considering level of each species' presence associated with different oceanographic conditions at site BS, there was a clear separation along the lines of SSH, SST, temperature at foraging depth, surface salinity, and salinity at foraging depth (Figure 4.6). Blainville's exhibited higher levels of presence at higher SSH, higher salinity both at the surface and at depth, and lower SST, but higher temperatures at foraging depth, and smaller magnitude FSLE values. Gervais' exhibited higher levels of presence associated with lower SSH values and larger magnitude FSLE values at BS; these preferences were consistent with the conditions at GS, their site of primary occupancy, which has moderate SSH values and large FSLE values.

The Cuvier's and Sowerby's beaked whale regional models both retained SSH, SST, and CEddyDist, in addition to other terms in the Cuvier's model (Table 4.3). These species showed similar, broadly negative relationships to these overlapping terms, though Cuvier's exhibited higher specificity for low SSH values than Sowerby's did (Figures 4.7-4.8). Cuvier's also exhibited a slight uptick in presence at SST values >25º C which was not seen in the corresponding relationship for Sowerby's. At the three sites where they overlap (HZ, BC, WC), considering covariate distributions during species presence, irrespective of level of presence, did not yield insights into how these two species partition the niche space. Cuvier's and Sowerby's did not exhibit much selectivity for the covariates considered, and the distributions of covariate values over which each was present did not differ significantly between species, or generally from background conditions (Table 4.6). In terms of level of presence, Cuvier's and Sowerby's were best separated by salinity, either at the surface or at depth, and to a lesser extent by temperature at depth and by FSLE; the particular range of values targeted by each species varied between the three sites (Figure 4.9). At HZ Cuvier's exhibited a strong

preference for low salinity conditions at depth, with highest levels of presence at salinity values <33 PPT and much lower levels of presence at higher salinity values; Sowerby's presence was fairly consistent across a broad range of deep salinity values at HZ. At BC and WC surface salinity was a better separator. At BC Cuvier's had highest presence at surface salinity values >35 PPT, while Sowerby's showed a strong preference for values <33 PPT, and at WC Cuvier's once again preferred high salinity values, though with less specificity, while Sowerby's didn't seem to be selective. Cuvier's exhibited much higher levels of presence in low temperatures at depth at HZ and WC, while Sowerby's were present across a wider range of values. At WC Cuvier's also higher levels of presence at larger magnitude FSLE values, with Sowerby's exhibiting little preference. The variability in oceanographic conditions associated with highest levels of presence of each odontocete species between sites may indicate that these species are targeting different prey at each of these sites.

True's beaked whales were predominantly present at site NC in the north, a site where both Cuvier's and Sowerby's beaked whales had very low levels of presence despite occupying the adjacent sites. SSH and SST were retained in the regional models for all three species, and showed broadly similar patterns for SSH, but quite different patterns for SST (Figures 4.7, 4.8, 4.10). Both Cuvier's and Sowerby's exhibited a generally negative relationship with SST, with highest presence predicted at the lowest temperatures, while True's exhibited lowest presence at low SST values. The True's model also retained salinity at depth, which showed an opposite pattern (negative) to the one indicated by the Cuvier's model (positive).

At NC the three species each exhibited some selectivity for particular conditions, but True's was never associated with a distribution of covariate values which differed from both Sowerby's and Cuvier's (Table 4.7, Figure 4.11). All three selected for values of SSH significantly more negative than the background conditions, but not significantly different from one another. All three species also selected for cooler SST conditions, though to differing degrees; the distribution of temperatures associated with Sowerby's presence was most clearly shifted towards colder temperatures, and

differed significantly from the distributions associated with both Cuvier's and True's presence, which did not significantly differ from one another. A similar pattern was seen for the distribution of Chl values associated with each species' presence: all three selected for significantly higher Chl values than the background conditions, with Sowerby's showing the most substantial shift, and significant differences between the distribution associated with Sowerby's and those associated with both Cuvier's and True's, but not between Cuvier's and True's. Sowerby's were also more selective for salinity, both at the surface and at depth, than Cuvier's or True's.

In terms of level of presence, neither SSH, nor SST, nor salinity at depth were effective at separating the three species, though FSLE and temperature at depth were (Figure 4.12). True's exhibited a strong preference for small magnitude FSLE values, while Sowerby's and Cuvier's exhibited highest levels of presence associated with more strongly negative values. This may indicate that the preferred prey of Sowerby's and Cuvier's at NC are associated with mesoscale structures such as filaments and rings, while True's exploits prey associated with less energetic flows. Cuvier's and Sowerby's exhibited opposite preferences for temperature at depth, with Cuvier's preferring the warmer temperatures and Sowerby's preferring the cooler temperatures, while True's mostly occupied the values in between.

Risso's dolphins and short-finned pilot whales both occupy all of the northern sites (see Chapter 3) and are known to be primarily teuthophagus moderately-deep and deep divers ([181–183,185]). The regional models for these two species retained many of the same terms, including SST, salinity at 400m, Chl concentration, and CEddyDist (Table 4.3). The shapes of the relationships estimated for each of these covariates showed that short-finned pilot whales had much narrower preferred ranges of SST and salinity at 400m, while the relationship with cyclonic eddies were opposite between the two species—pilot whales appear to prefer the vicinity of cyclonic eddies, while Risso's dolphins presence increased with increasing distance to the nearest cyclonic eddy (Figures 4.13-4.14).

When considering the distributions of covariate values associated with each species' presence, most covariate distributions were not significantly different during either species' presence than background conditions (**Error! Reference source not found.**). For the few covariates which did exhibit selectivity, direction of selection varied between sites (Figure 4.15). At the northernmost site, HZ, Risso's dolphins selected for significantly warmer surface temperatures than the background distribution, while pilot whales were not selective; the same pattern was seen at OC, though lower amplitude and not significant. From BC to NFC the trend switched, with pilot whales selecting for significantly warmer surface waters, and Risso's dolphins either not showing selectivity (BC & WC) or else selecting for cooler surface waters (NFC). The two species also traded preferences for SSH conditions, with pilot whales selecting for less negative SSH values at BC and WC, where Risso's dolphins were not selective, while Risso's selected for more negative SSH at NFC, and less negative SSH at HAT, both sites where pilot whales were not selective.

Level of presence across the range of SST and SSH reaffirmed the preferences suggested by these patterns in selectivity (Figure 4.16). At HZ and OC Risso's preferred higher SSH and warmer SST, but at NC this pattern switched, and from NC to NFC Risso's preferred lower SSH and cooler waters; pilot whales exhibited the opposite pattern at every site. At HAT Risso's switched back to a preference for high SSH and high SST, with pilot whales again showing the opposite preference. Very similar patterns were seen for temperature at foraging 400m. Occasionally other covariates neatly separated the two species at a given site, but no other covariates were consistently good separators across sites. This variability in preferred conditions between sites may indicate prey switching between sites, or may also be evidence of distinct populations of Risso's dolphins and short-finned pilot whales which occupy a subset of the monitoring sites and whose foraging behaviors are specialized for targeting the prey species occupying these smaller subregions.

4.4.5 Predicted Seasonal Habitat Suitability

The regional habitat suitability indicated for each species by alternate model predictions captured the zonal differences in species' distributions. Some finer temporal scale features were aligned with the patterns in acoustic presence and sighting data identified in Chapters 2 and 3, but there were also some predictions of presence which suggested novel hotspots, and should be interpreted with caution. For example, estimates of high presence for some deep diving species (Blainville's beaked whales, sperm whales) in relatively shallow shelf waters on George's Bank were probably driven by low SST and very high Chl values in those grid cells. Knowledge of these species' diving ecology suggests it is highly unlikely that they would be found in such shallow waters. Inclusion of depth- and slope-related covariates in these models would likely help to constrain predictions of presence to areas suitable for the diving ecology of each species, but this was not feasible here due to the limited depth distribution of the acoustic monitoring sites.

The common dolphin and short-finned pilot whale model predictions reproduced seasonal peaks in presence which were observed in the acoustic record in Chapters 2 and 3. Common dolphins were predicted to have higher presence in the winter and spring, particularly between the shelf break of the mid-Atlantic Bight and southern New England and the northern wall of the Gulf Stream (Figure 4.17). Predictions of common dolphin presence showed a sharp drop-off across the Gulf Stream front, with presence predicted almost exclusively east and north of the Gulf Stream waters. The short-finned pilot whale model captured the fall increase in presence near HAT, but missed the wintertime peak (Figure 4.18).

In the north the Risso's dolphin predictions suggested a slight contraction of presence along the shelf break in the spring, and highest levels of presence on the shelf near southern New England in the fall (Figure 4.19). This aligns with the fall peaks at HZ and OC identified for Risso's dolphins in Chapter 3, but from NC south to HAT the actual seasonal peak in presence observed in the acoustic data occurred in the spring. The Risso's dolphin model also predicted very high levels of presence

hugging the coast at Cape Hatteras and in the south Atlantic bight, likely driven by high Chl and low EKE values in these grid cells, but such high levels of presence in these areas is not supported by the sighting record (Figure 2.22).

The Cuvier's beaked whale model predicted a narrow band of relatively high habitat suitability running along the northern wall of the Gulf Stream front across the entire study region (Figure 4.20). Hotspots were predicted near site WC and near the New England seamount chain in the winter and spring. The hotspot near WC matched the seasonal peak in Cuvier's beaked whale presence at WC identified in Chapter 3 (Figure 3.4), while the hotspot near the seamounts seems reasonable given the known association between deep diving mammals and regions of steep topographic relief [136,237,238]. Cuvier's presence at HAT, their site of primary occupancy according to the acoustic data (Figure 3.2), was underestimated by the model and predicted to peak in the summer, but missed the winter peak observed in the acoustic data (Figure 3.4). Sowerby's beaked whales were predicted to have low levels of presence north of the Gulf Stream front, with seasonal increases predicted in the winter and spring (Figure 4.21). This aligned with the winter peaks in presence seen at HZ and OC, but not the fall and summer presence peaks seen in the acoustic data from BC and WC, respectively (Figure 3.4). The Sowerby's presence predicted on Georges' Bank was likely driven by the cold water temperatures in those grid cells, but is unlikely to be accurate given the shallow water depths. The True's beaked whale model predicted very low levels of presence north of the Gulf Stream front with a slight increase in the winter and spring (Figure 4.22). High levels of presence were predicted in a few grid cells on George's Bank, likely driven by the very small FSLE and EKE values in these grid cells, but as with Sowerby's these are probably not reliable given what is known of True's beaked whales' deep diving ecology. The Gervais' beaked whale model identified the core of the Gulf Stream as the most favorable habitat, which was in keeping with the oceanographic preferences observed here for this species (Figures 4.1, 4.23).

The model predictions for Blainville's beaked whales exhibited some peculiarities. Despite very low levels of presence in our acoustic data, the Blainville's model predicted very high levels of presence in a large offshore region southeast of Bermuda in the summer and fall (Figure 4.24). To the best of our knowledge there has been no survey effort for Blainville's in the waters far offshore of the southeastern U.S., so the data to verify/disprove this predicted hotspot are not available. It is interesting to note that no particular hotspot for Blainville's was predicted at site BS, despite their clear locus of acoustic presence there in our data (Figure 3.2). Similar to Blainville's, the *Kogia* spp. model predictions did not capture presence at BS, and also suggested a large region of relatively favorable habitat west of the Bahamas and south of Bermuda (Figure 4.25). Habitat suitability in this area was predicted to peak in the summer, which is in keeping with the summertime peak in *Kogia* spp. presence at site BS observed in Chapter 3 (Figure 3.2).

The sperm whale model indicated higher habitat suitability north and east of the Gulf Stream, with increased presence in the winter and spring (Figure 4.26). This is partially in keeping with the spring peaks in sperm whale presence observed at the northern sites in Chapter 3 (Figure 3.4). Very high presence predicted on George's Bank and east of Nova Scotia was likely driven by high Chl values in those grid cells.

4.5 DISCUSSION

This study sheds new light on the drivers of habitat selection and niche partitioning, and seasonal patterns in habitat suitability, for a diverse group of toothed whale species occupying an oceanographically dynamic region. Kernel density plots and PCA revealed clear groupings of oceanic conditions which appear to be representative of distinct oceanic regimes. Most of the target species considered here exhibited pronounced preferences for one particular regime, though the presence of some species in two, or even all three, regimes influenced the shapes of the distributions shown in

Figure 4.1 4.1 and the significance of differences between presence conditions and background conditions. Habitat suitability models and seasonal predictions of presence for each species revealed areas of high habitat suitability which could be explored for further insights into species' presence, correlation with favorable prey fields, and potentially targeted for protection.

By utilizing passive acoustic data collected at sites arranged across a latitudinal habitat gradient we were able to sample species presence across a large region almost continuously throughout the 3-year study period. Thanks to previous works on acoustic discrimination of odontocete species [28,29,32,33,142], and seasonally unbiased training data, the resultant habitat models offer improved species resolution of beaked whales and delphinids in addition to more reliable predictions of year-round presence over models previously built for this region from aggregated visual survey data. Additionally, effort at the southern sites BP and BS extend our understanding of odontocete species presence along the edge of the Blake Plateau, an area with practically no visual survey effort (see sighting data maps from Chapter 2, Figures 2.2-2.9, 2.18-2.21).

The primary limitation of the data utilized here was the limited range of depths at which observations were made (450-1200m, Table 2.1). Since the acoustic monitoring sites did not capture much variability in depth or slope we were not able to investigate how these aspects of the environment influenced odontocete presence. Therefore predictions of animal presence in water depths very different from where the acoustic observations were made, especially much shallower water, should be interpreted with caution. One way to address this limitation would be to quantitatively compare these presence predictions to the visual data as a means of cross-validation. Another approach would be to train models on a combination of observations from both fixed passive acoustic sensors and mobile shipboard and aerial visual surveys, which cover a broad range of depth conditions and sample much more extensively on the shelf. There are a number of challenges associated with combining these two very different sensing modalities, but one pilot study in the Gulf of Mexico

suggests that this approach can reduce model error for species with a rich visual sighting record, i.e. dolphins [151].

4.5.1 Influence of the Gulf Stream

At the continental shelf break and slope monitoring sites considered here, we observed that the influence of the Gulf Stream in shaping the oceanic environment was more clearly seen through the delineation of broad scale ecoregions than through the immediate presence of mesoscale rings. We identified three distinct oceanic regimes experienced at our monitoring sites—Northerly, Gulf Stream direct influence, and Gulf Stream indirect influence—which separated out based on both the temporally-pooled distributions of covariate values experienced at each site (kernel density plots), as well as the instantaneous combinations of covariate values observed at each time step (PCA). The vicinity of mesoscale Gulf Stream rings did not strongly correlate with either absolute conditions or variability in conditions experienced at each site, which we took to mean that individual rings do not directly drive oceanic conditions at our sites. This could also indicate that our approach to quantifying the impact of rings was not well-suited to the task. While the characteristics of the water constituting a ring edge may be quite different from the surrounding water mass, and from the water constituting the ring core, the core itself is fairly homogeneous. Therefore, the passing of an eddy edge over one of our sites may well be detectable as a change in oceanographic conditions, but once a ring edge has passed conditions in the core are not likely to vary much with decreasing distance to the eddy center. Mesoscale ring radii vary between 50-150 km, so the distance at which the edge versus the core occupies a given site is not consistent from one ring to another. We did not account for this in our correlation analysis, instead assuming that conditions would change smoothly with decreasing distance to eddy center. An approach which identifies the edge of each individual ring and compares changes in conditions associated with the edge versus the core might yield further insights into the impacts of these features on shelf-break sites.

Irrespective of the influence of individual rings on our monitoring sites, the role of Gulf Stream and its rings in defining oceanic conditions in the western North Atlantic should not be understated. In addition to acting as a dynamic habitat boundary, it has been long known that the Gulf Stream is a major path for heat transport from the equator poleward, offsetting the radiative loss of heat from the higher latitudes [44]. Mixing of Gulf Stream waters with Labrador Slope Water, accomplished largely by warm core rings, contributes to the formation of surface Warm Slope Water between the northern wall of the Gulf Stream and the continental shelf break [49], while winter subduction of Gulf Stream waters forms the basis for North Atlantic Central Water at intermediate depths [239,240]. A major regime shift in 2000 led to increased annual formation of anticyclonic rings, without a corresponding increase in the annual formation of cold-core rings, resulting in excess heat transfer to the Slope Sea and increased warming of surface waters, particularly in the summers [217,218]. Additionally, the interactions of warm-core rings with the slope and shelf waters of southern New England and the mid-Atlantic Bight, and of cold-core rings with the slope and shelf waters of the southeastern U.S. seaboard, have important implications for the physical, chemical, and biological conditions in these areas, including heat and energy transfer, entrapment and transport of high- or low-productivity waters and their entrained flora and fauna, Ekman-induced upwelling, and new production in response to upwelled nutrients [219–221,241–246].

It is clear, therefore, that the habitats in our study region, and indeed throughout most of the North Atlantic basin, are shaped largely by the Gulf Stream. Changes in state and behavior of the Gulf Stream, either as a result of natural variability or mediated by climate change, are thereby likely to have profound impacts on the communities occupying these habitats. The odontocete habitat preferences identified here provide new insights which can be applied to manage these species in the face of such oceanographic shifts.

Despite apparently having little effect on the instantaneous conditions at our sites, at least one metric of eddy vicinity was retained in 70% of models, indicating some importance of these features

for many of the species considered here. Vicinity of cyclonic eddies was retained more than twice as frequently as vicinity of anticyclonic eddies (70% vs. 30%), and both were retained in 30% of models. Both types of eddy are observed to enhance primary productivity, though the exact mechanisms continue to be debated [247–252]. Associations between odontocetes and eddies have been previously reported and are believed to be driven by higher concentrations of mid-trophic level organisms associated with eddies [238,253–256].

4.5.2 Niche partitioning

We found clear evidence of ecological niche partitioning at multiple spatial scales among potential competitors for similar prey resources. At the regional level, beaked whale species presence was sharply bifurcated by the Gulf Stream, with three species strongly associated with the Northerly regime found north of the Gulf Stream front (Cuvier's, Sowerby's, and True's), and two species present almost exclusively in the GSD and GSI regimes south of the Gulf Stream front (Blainville's and Gervais'). However these results must be interpreted with the zonally-limited scope of the data in mind. As seen in [142], the visual survey record does show occasional encounters with Gervais' beaked whales north of Hatteras (Figure 2.5), though mostly beyond the shelf break where they may still be tracking Gulf Stream waters. Blainville's beaked whales, on the other hand, are sometimes observed at the shelf break sites of southern New England (Figure 2.4), which experience quite different oceanic conditions than site BS, their locus of primary presence in this analysis. This may suggest that Blainville's are targeting different prey species at these sites with divergent oceanic conditions. It may alternatively, or additionally, suggest that there are distinct populations of Blainville's occupying the northern vs. southern sites, which might be separated by their prey, and thereby environmental, preferences. Genetic analyses and investigation of acoustic differences between the Blainville's beaked whales encountered in each region may shed more light on this.

It is interesting to note that the dolphin species analyzed here all exhibited presence over much wider ranges of conditions than the beaked whale species. While there was some preference for the Northerly regime, all three dolphin species were also present, though in lower levels, at the sites in the GSD and GSI regimes. At first glance this contrast seems to suggest differences between the habitat specificity of shallower diving dolphins (relatively speaking) and extreme deep divers, but attempts at such a division break down when sperm whales are considered. Sperm whales were the second most widely distributed species in this analysis, after common dolphins, but are equally as specialized for pursuit of bathypelagic prey as the beaked whales. The reasons for this difference in habitat specificity are not clear, though perhaps investigation of prey specificity might reveal some insights.

At a finer spatial scale, we found that presumed competitors occupying the same site were always separated by their site-specific preferences for at least one covariate. This suggests subtle differences in each species' preferred niche, preferences which sometimes exhibited variability between sites. While it is convenient to situate these monitoring sites in the context of the major oceanic regimes identified here, conditions within each regime also exhibited variability, which likely translate to different foraging opportunities across sites in a given regime, and through time. Most frequently species were observed to be selective for particular water temperature, salinity, or SSH conditions, both when considering binary presence/absence and when considering level of presence. These oceanographic properties are known to drive patterns in the distribution and abundance of lower-trophic level organisms and their mid-trophic level predators ([53,257–259]). Given odontocete's ability to thermo- and osmoregulate, and most species' presence across a wide range of conditions in this region (Figure 4.1), site-specific differences in odontocete preferred thermal or salinity ranges may be a reflection of their selection for conditions optimal to particular prey species on a site-by-site basis. It has been suggested that odontocetes use knowledge of past foraging success to plan future foraging and optimize foraging efficiency [36,260], and that baleen whales integrate memory of foraging conditions in the previous year to make decisions about timing of migration to

feeding grounds [261], so familiarity with the periodic cycles in prey availability at sites of regular use are not unthinkable for these species.

4.5.3 Habitat suitability predictions would likely benefit from depth data

The regional and seasonal patterns in predicted habitat suitability for most of the species analyzed here were generally aligned with the regional distribution of each species inferred from both passive acoustic and sighting data (see Chapters 2 and 3). However, these predictions were limited by the absence of any depth- or slope-related covariates, resulting in unlikely predictions of high presence for some deep divers in shallow shelf waters. Distance to particular isobaths, distance to seamounts, and metrics of topographic relief have been found significant for a number of the deep diving species analyzed here, which are thought to target heightened productivity associated with bathymetrically-induced upwelling ([148,222,223,262–265]), and might improve predictive models for these species.

Hotspots identified for some species in regions with little to no visual or acoustic survey effort (e.g. the New England seamount chain for Cuvier's beaked whales; east of the Bahamas and south of Bermuda for Blainville's beaked whales and *Kogia* spp.), may suggest new regions in which to survey for presence of these species. One approach to accessing these far-offshore regions would be to equip autonomous surface or underwater vehicles with acoustic data acquisition systems. Transects run by such a vehicle could cover a large area for a fraction of the expense of a fully staffed scientific survey. Such methods have begun to be explored and hold much promise for assessment of remote regions and study of rare or cryptic animals [266].

4.6 CONCLUSION

Odontocete species in the western North Atlantic have been clearly shown to be well separated in terms of habitat preference, at both large (regional) and small (site-specific) spatial scales. The Gulf Stream is influential in structuring these habitats, both by delineating major ecoregions and by contributing to the formation of temperate water masses north of the Gulf Stream front. Changes in

Gulf Stream position and activity as a result of natural variability or anthropogenically-induced climate change are likely to translate into changes in odontocete species distributions. The predictive habitat suitability maps included here are a first step towards characterizing odontocete habitat shifts in this region and can be further improved by the addition of sighting data collected at a range of depths, and depth-related oceanographic covariates.

4.7 FIGURES

Table 4.1: Environmental covariates investigated as potential drivers of patterns in odontocete distribution and relative abundance.

Covariate	Units	Original Spatial Resolution	Description
Sea Surface Height (SSH) Water Temperature Salinity Water U-Velocity Water V-Velocity Water Velocity Magnitude Water Velocity Direction Eddy Kinetic Energy (EKE)	m °C PPT m/s m/s m/s ° m^2/s^2	0.08° lat x 0.08° lon between 40N-40S; 0.08° lat x 0.04° lon poleward of 40N/40S	Hybrid Coordinate Ocean Model (HYCOM; [224]) Derived from HYCOM u- and v-Velocity
Chl	mg/m^3	0.04°	Surface chlorophyll; ESA CCI Ocean Color Product [267]
Finite Size Lyapunov Exponent (FSLE)		0.04°	Aviso product, DOI: 10.24400/527896/a01-2022.002; derived from SSALTO/Duacs DT MADT UV products.
AEddyDist CEddyDist	km		Distance to nearest anticyclonic/cyclonic eddy; calculated from Aviso's Mesoscale Eddy Trajectory Atlas product [227]

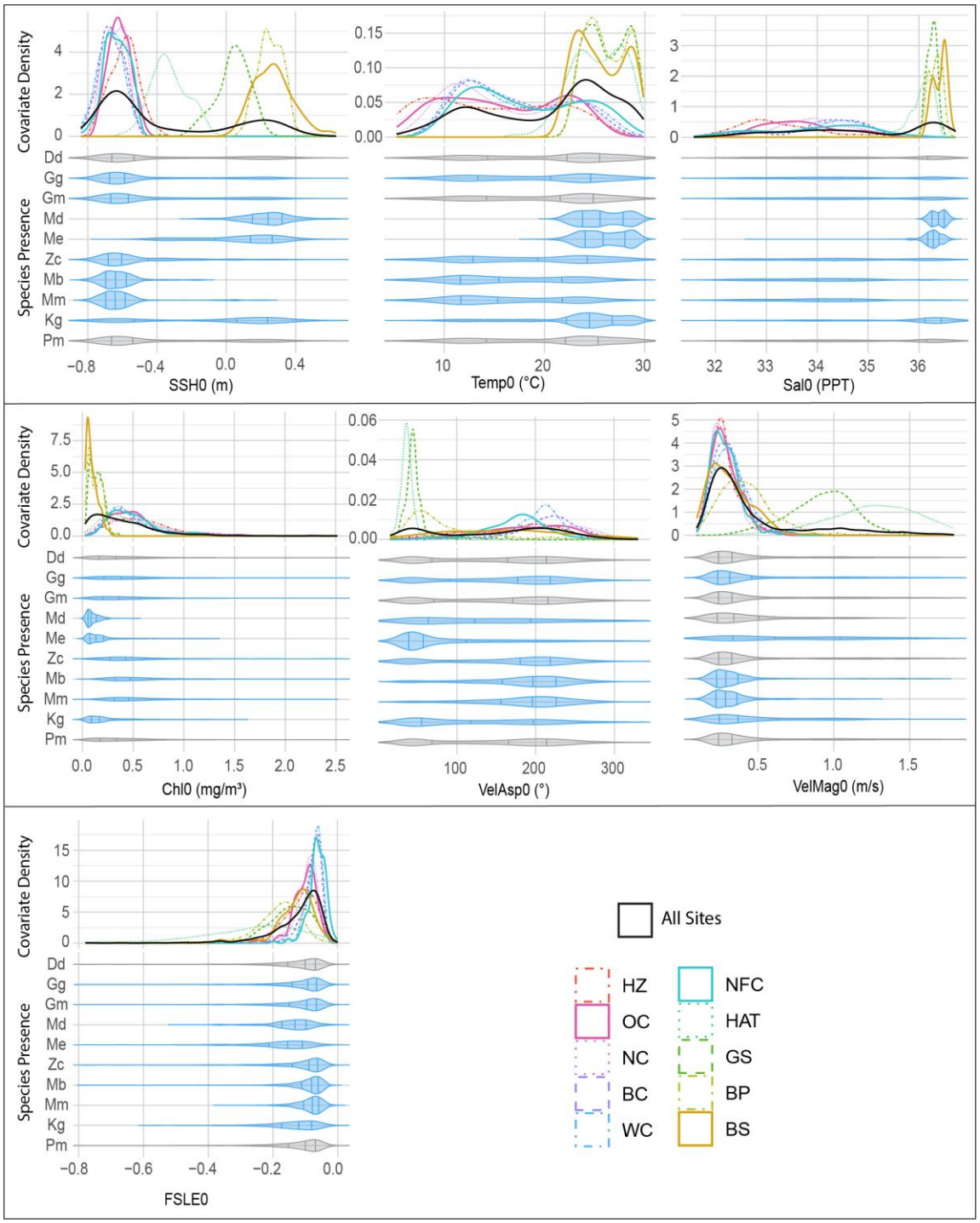

Figure 4.1: Distributions of values observed for oceanographic variables at the acoustic monitoring sites, and distributions of these same covariates observed when each species was present. In the violin plots, blue indicates the distribution was significantly different from the background conditions (black kernel density line; KS test, alpha = 0.05); grey indicates no significant difference. SSH: Sea surface height; SST: sea surface temperature; Sal0: surface salinity; Chl: chlorophyll concentration; Vel: water velocity; Dir: direction of water flow; FSLE: finite size Lyapunov exponent.

Table 4.2: Oceanic regimes identified according to distinct patterns in distributions of oceanographic conditions at each of the monitoring sites.

Regime	**Conditions**	**Sites**
Northerly	SST: 5º - 23º C Surface salinity: <35 PPT SSH: <0.4 m Chl: >0.3 mg/m^{3}_{3} Water Velocity: <0.5 m/s Water Direction: highly variable	HZ OC NC BC WC NFC
Gulf Stream Direct Path (GSD)	SST: >23º C Surface salinity: >36 PPT SSH: -0.4 - 0.2 m Chl: variable (low at GS, higher at HAT) Water Velocity: >0.5 m/s Water Direction: northeast	HAT GS
Gulf Stream Indirect Influence (GSI)	SST: >23º C Surface salinity: >36 PPT SSH: >0.2 m Chl: <0.25 mg/m^{3}_{3} Water Velocity: <0.6 m/s Water Direction: highly variable	BP BS

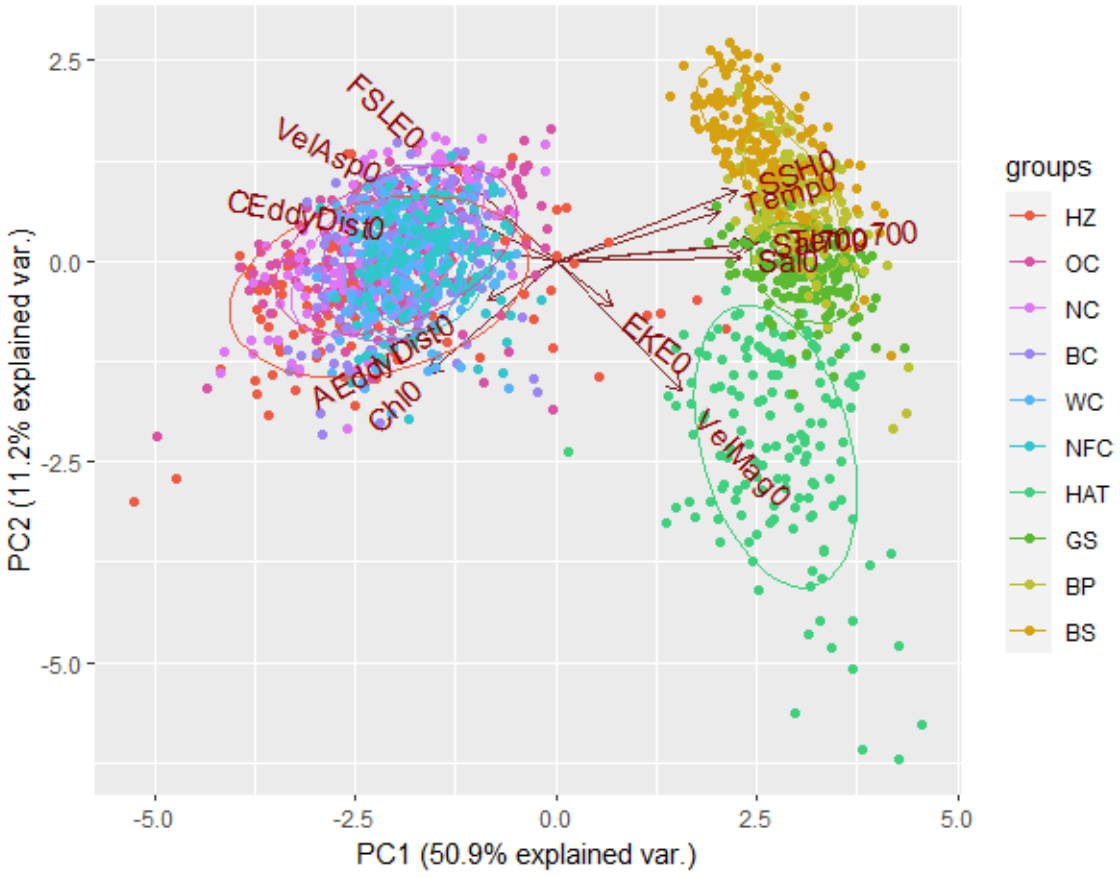

Figure 4.2: PCA analysis of the oceanographic conditions at the monitoring sites showed clear separation between the northern (HZ to NFC) and the southern (HAT to BS) sites.

Table 4.3: Terms retained in optimal habitat models for each species, as well as overall deviance explained for the model.

Species		*Dd*	*Gg*	*Gm*	*Md*	*Me*	*Zc*	*Mb*	*Mm*	*Kg*	*Pm*
Total DE (%)		73.5	49.2	45	78.7	86.9	61.7	50.5	43.6	40.4	40.6
GAM Terms	**SSH**	x				x	x	x	x	x	x
	SST	x	x	x	x	x	x	x	x		x
	Temp at Depth				x					x	
	Surface Salinity				x					x	
	Salinity at Depth	x	x	x		x	x		x		x
	Chl	x	x	x		x				x	x
	EKE		x						x		
	FSLE		x		x				x		
	Water Velocity								x		
	Water Direction				x	x	x				
	CEddyDist	x	x	x			x	x		x	x
	AEddyDist	x		x						x	

Table 4.4: Model fit diagnostics comparing model predicted presence to observed presence for non-zero data and all data. Rho: Spearman's rank correlation; MAE: mean absolute error; Rel.MAE: mean absolute error expressed as a percentage of the 90th percentile – 10th percentile range of the data. MAE is on the scale of the presence data for each species, and therefore not directly comparable between species; Rel.MAE is appropriate for comparing error between species. Goodness of fit thresholds, taken from [236], are: Rho: poor = $x < 0.05$, fair to good = $0.05 \leq x < 0.3$, excellent = $x \geq 0.3$; Rel.MAE: poor = $x > 100\%$, fair to good = $100\% \geq x > 25\%$, excellent = $x \leq 25\%$.

Species:	**Non-Zero Data**			**All Data**		
	Rho	**MAE**	**Rel.MAE**	**Rho**	**MAE**	**Rel.MAE**
Dd	0.878	101.364	0.148	0.872	101.804	0.148
Gg	0.684	62.382	0.269	0.746	53.329	0.256
Gm	0.617	35.127	0.230	0.655	30.441	0.224
Md	0.613	42.254	0.440	0.568	6.939	1.119
Me	0.724	45.121	0.223	0.846	17.605	0.168
Zc	0.525	29.942	0.179	0.601	19.457	0.324
Mb	0.268	8.745	0.312	0.680	5.441	0.302
Mm	0.345	4.901	0.306	0.581	2.765	0.395
Kg	0.589	3.058	0.306	0.576	1.476	0.211
Pm	0.648	126.631	0.270	0.664	124.086	0.269

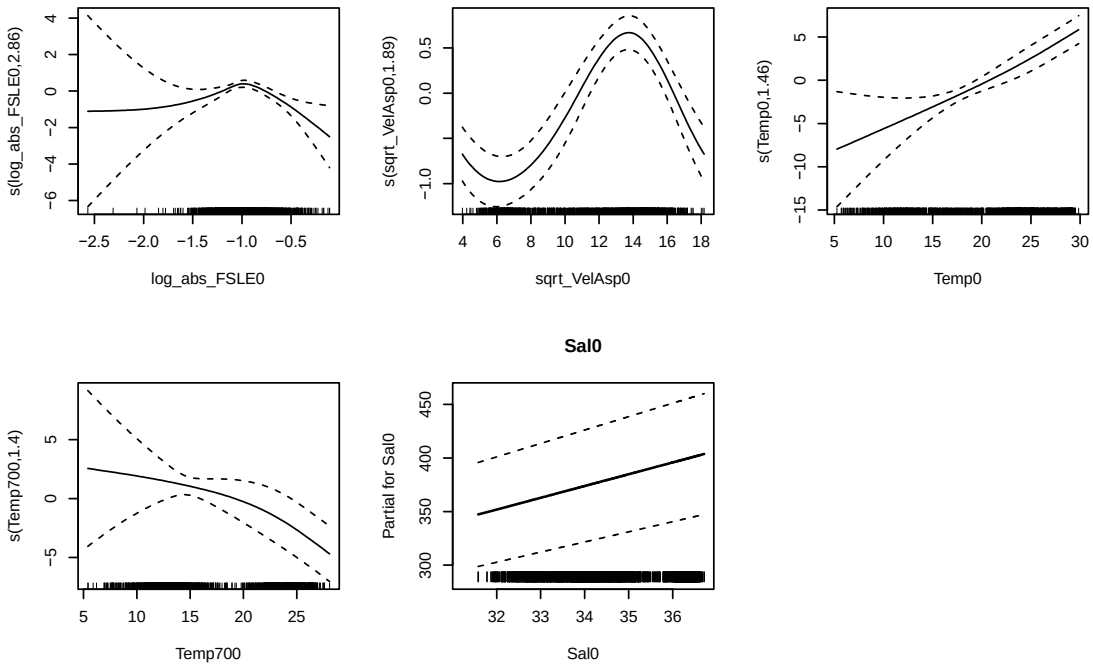

Figure 4.3: Relationships between environmental covariates and Blainville's beaked whale presence indicated by optimal habitat model.

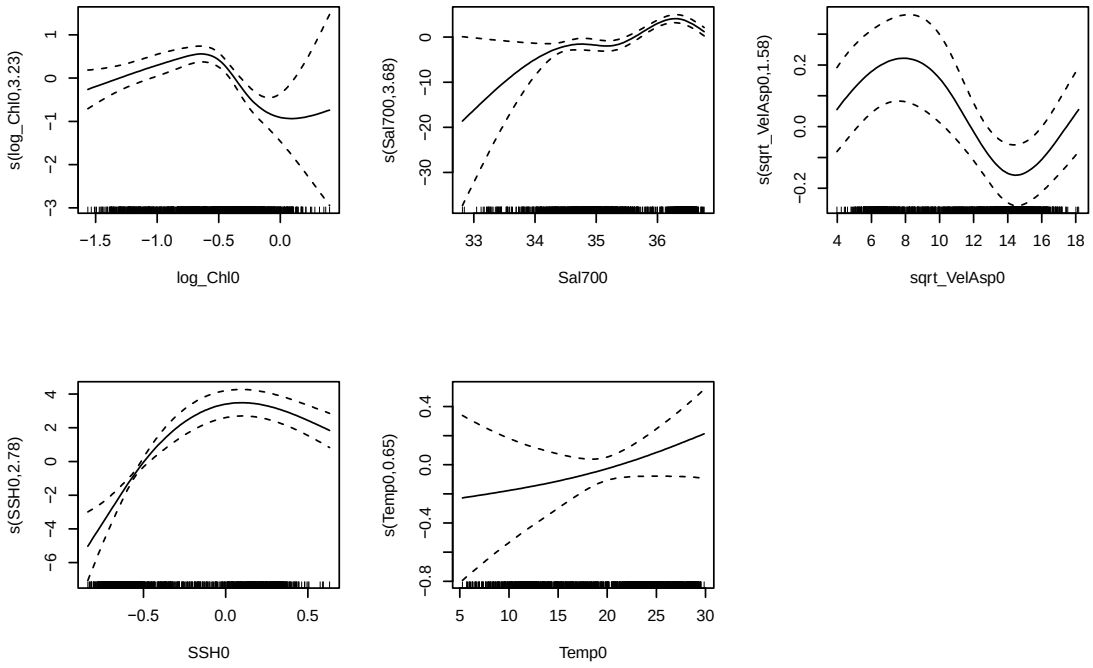

Figure 4.4: Relationships between environmental covariates and Gervais' beaked whale presence indicated by optimal habitat model.

Table 4.5: Significance of p-values from KS tests comparing distributions of covariate values observed during presence of Blainville's (*Md*) and Gervais' (*Me*) beaked whales at site BS to the null background distributions, and to one another.

	BS		
Covariate	***Md* vs Null**	***Me* vs Null**	***Md* vs *Me***
Chl0	NS	***	***
FLSE0	NS	NS	NS
SSH0	NS	NS	NS
Sal0	NS	***	***
Sal700	NS	NS	NS
Temp0	*	***	***
Temp700	NS	NS	**
VelAsp0	NS	NS	*
VelAsp700	NS	NS	NS
VelMag0	NS	NS	NS
VelMag700	NS	NS	NS
AEddyDist0	NS	NS	NS
CEddyDist0	NS	NS	NS

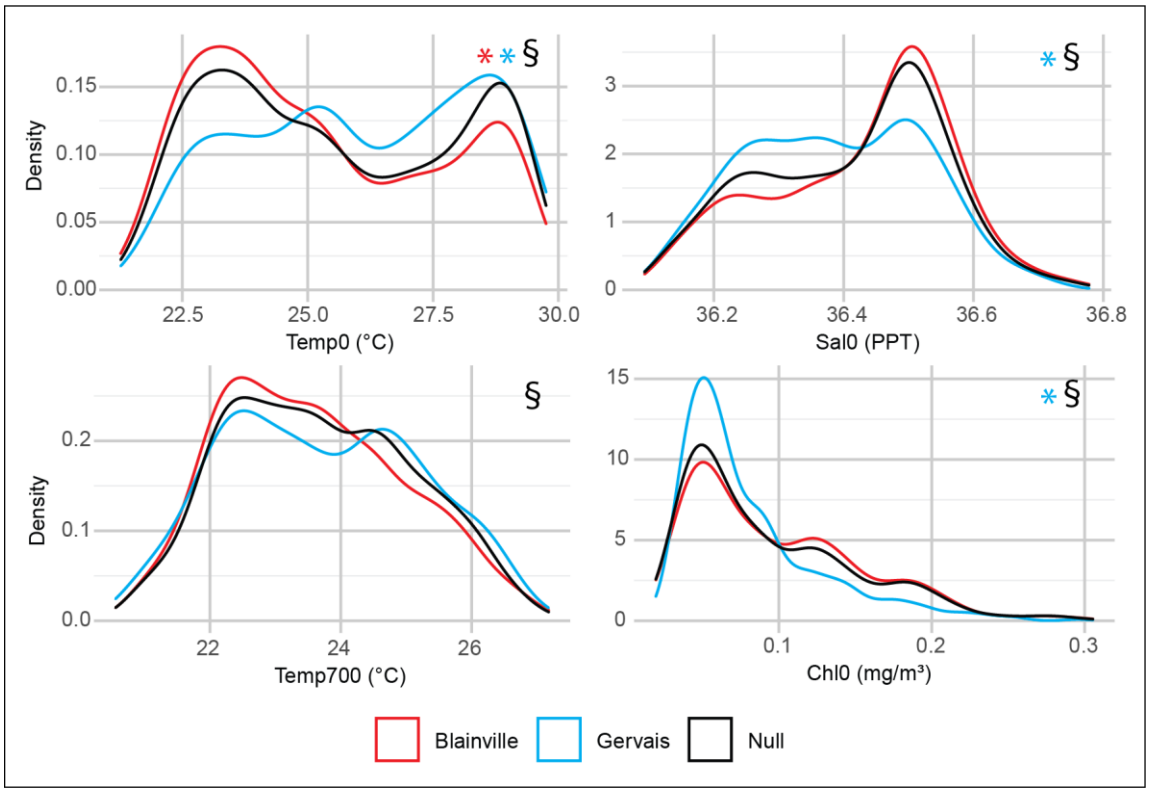

Figure 4.5: Kernel density plots comparing the distributions of covariate values associated with Blainville's and Gervais' beaked whale presence at site BS to background conditions. *: species' distribution significantly differed from the null distribution; §: species distributions significantly differed from one another. Gervais' exhibited selectivity for temperature, salinity, and chlorophyll, while Blainville's did not.

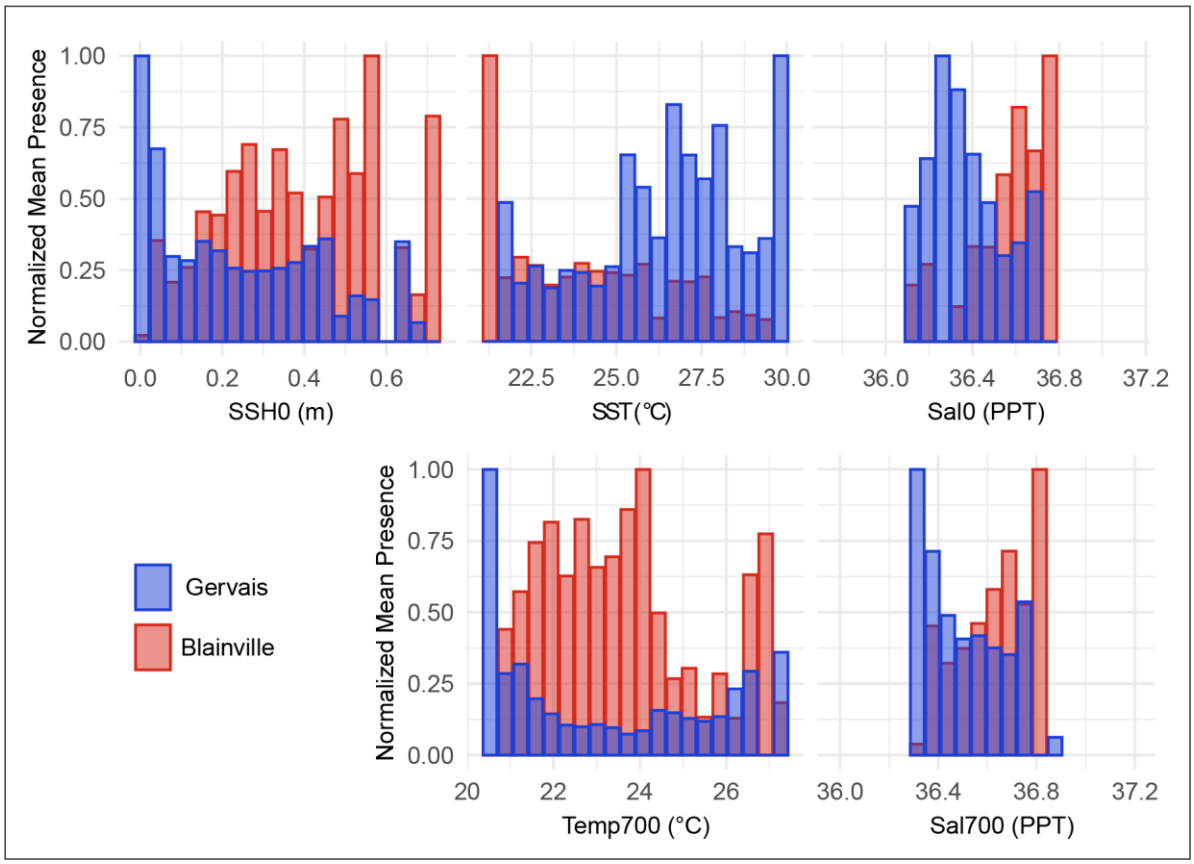

Figure 4.6: Mean presence of Blainville's and Gervais' beaked whales as a function of covariate values at site BS. Based on level of presence, Blainville's and Gervais' beaked whales exhibited quite different preferences for SSH, and salinity and temperature at the surface as well as at foraging depth.

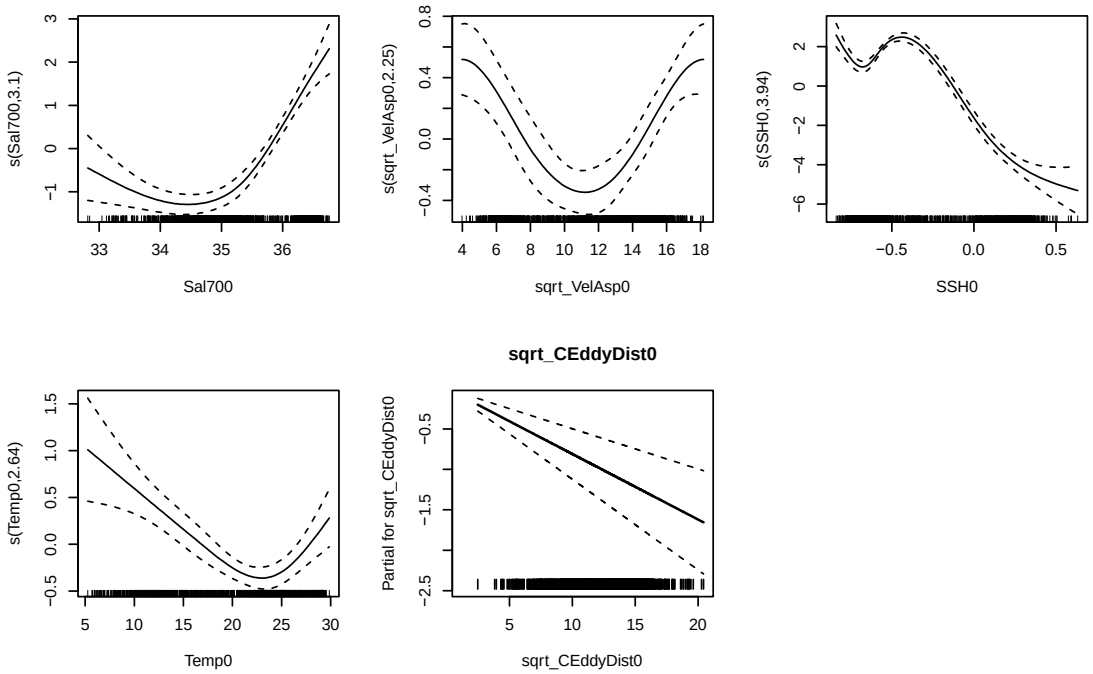

Figure 4.7: Relationships between environmental covariates and Cuvier's beaked whale presence indicated by optimal habitat model.

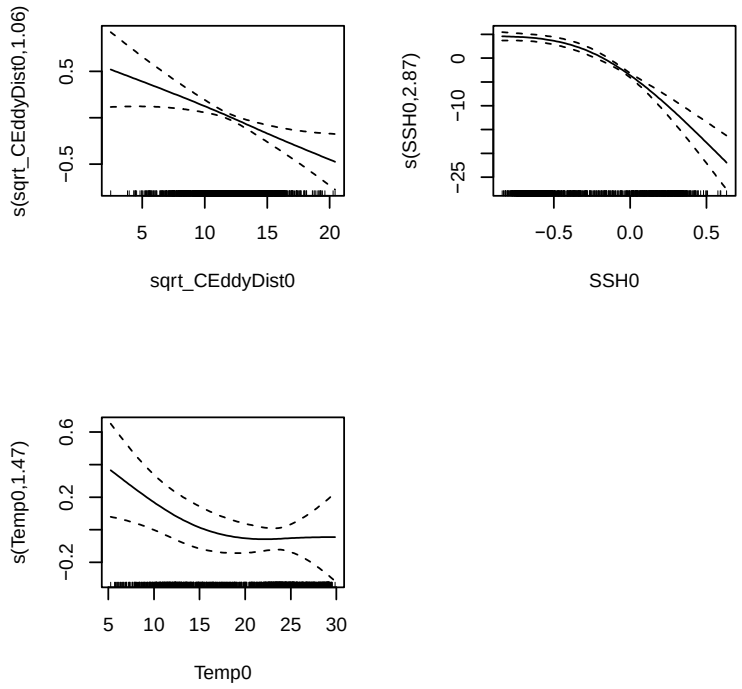

Figure 4.8: Relationships between environmental covariates and Sowerby's beaked whale presence indicated by optimal habitat model.

Table 4.6: Significance of p-values from KS tests comparing distributions of covariate values observed during presence of Sowerby's (*Mb)* and Cuvier's (*Zc*) beaked whales at sites HZ, BC, and WC to the null background distributions, and to one another.

	HZ			BC			WC		
Covariate	**Mb vs Null**	**Zc vs Null**	**Mb vs Zc**	**Mb vs Null**	**Zc vs Null**	**Mb vs Zc**	**Mb vs Null**	**Zc vs Null**	**Mb vs Zc**
Chl0	NS	NS	NS	NS	NS	NS	NS	NS	NS
FLSE0	NS	NS	NS	NS	NS	NS	NS	NS	NS
SSH0	**	NS	NS	NS	NS	NS	**	*	NS
Sal0	NS	NS	NS	NS	NS	NS	NS	NS	NS
Sal700	NS	NS	NS	NS	NS	NS	NS	NS	NS
Temp0	**	*	NS	NS	NS	NS	**	NS	NS
Temp700	NS	NS	NS	NS	NS	NS	NS	NS	NS
VelAsp0	NS	NS	NS	NS	NS	NS	NS	NS	NS
VelAsp700	NS	NS	NS	NS	NS	NS	NS	NS	NS
VelMag0	NS	NS	NS	NS	NS	NS	NS	NS	NS
VelMag700	NS	NS	NS	NS	NS	NS	NS	NS	NS
AEddyDist0	NS	NS	NS	NS	NS	NS	NS	NS	NS
CEddyDist0	NS	NS	NS	*	NS	NS	NS	NS	NS

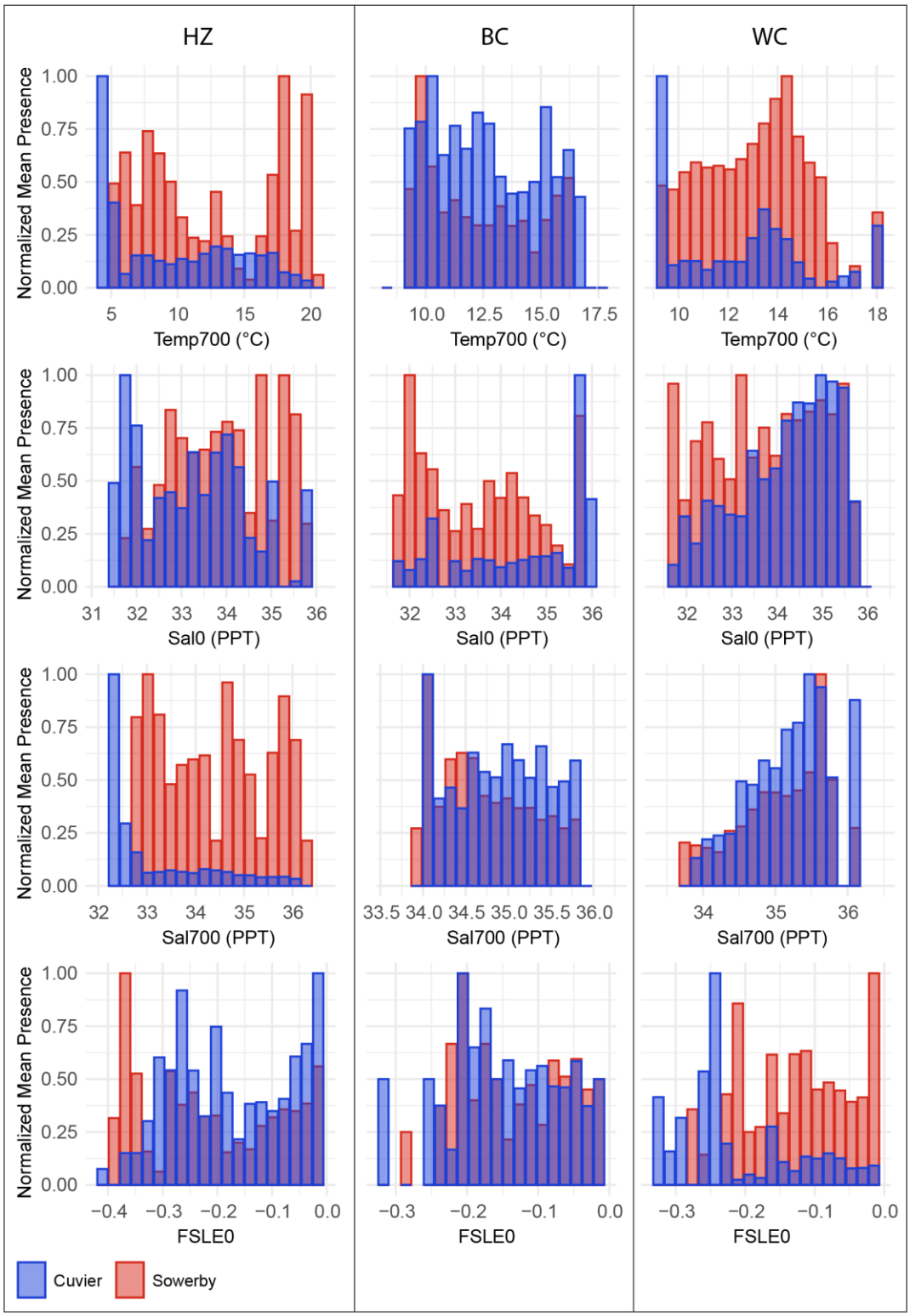

Figure 4.9: Mean presence of Sowerby's and Cuvier's beaked whales as a function of covariate vales at sites HZ, BC, and WC. Based on level of presence, Sowerby's and Cuvier's beaked whales were often separated by surface salinity, salinity and temperature at depth, and FSLE, but their preferred ranges for each of these covariates varied between sites HZ, BC, and WC.

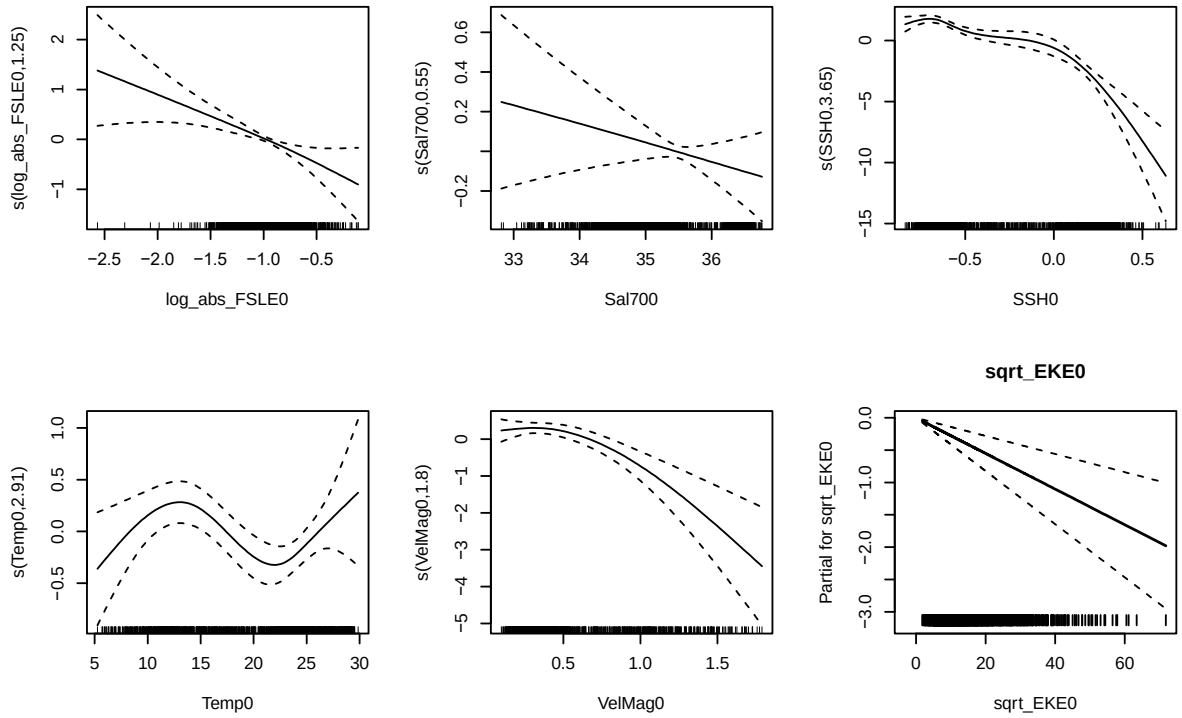

Figure 4.10: Relationships between environmental covariates and True's beaked whale presence indicated by optimal habitat model.

Table 4.7: Significance of p-values from KS tests comparing distributions of covariate values observed during presence of Sowerby's (*Mb)*, Cuvier's (*Zc*), and True's (*Mm*) beaked whales at site NC to the null background distributions, and to one another.

	NC					
Covariate	***Mb* vs Null**	***Zc* vs Null**	***Mm* vs Null**	***Mb* vs *Zc***	***Mb* vs *Mm***	***Zc* vs *Mm***
Chl0	***	**	*	*	***	NS
FLSE0	NS	NS	NS	NS	NS	NS
SSH0	***	***	***	NS	NS	NS
Sal0	**	NS	NS	***	**	NS
Sal700	**	NS	NS	***	**	NS
Temp0	***	**	***	**	***	NS
Temp700	***	NS	*	**	***	NS
VelAsp0	NS	NS	NS	NS	NS	NS
VelAsp700	NS	NS	NS	NS	NS	NS
VelMag0	NS	NS	NS	NS	NS	NS
VelMag700	NS	NS	NS	NS	NS	NS
AEddyDist0	NS	NS	NS	NS	NS	NS
CEddyDist0	NS	NS	NS	NS	NS	NS

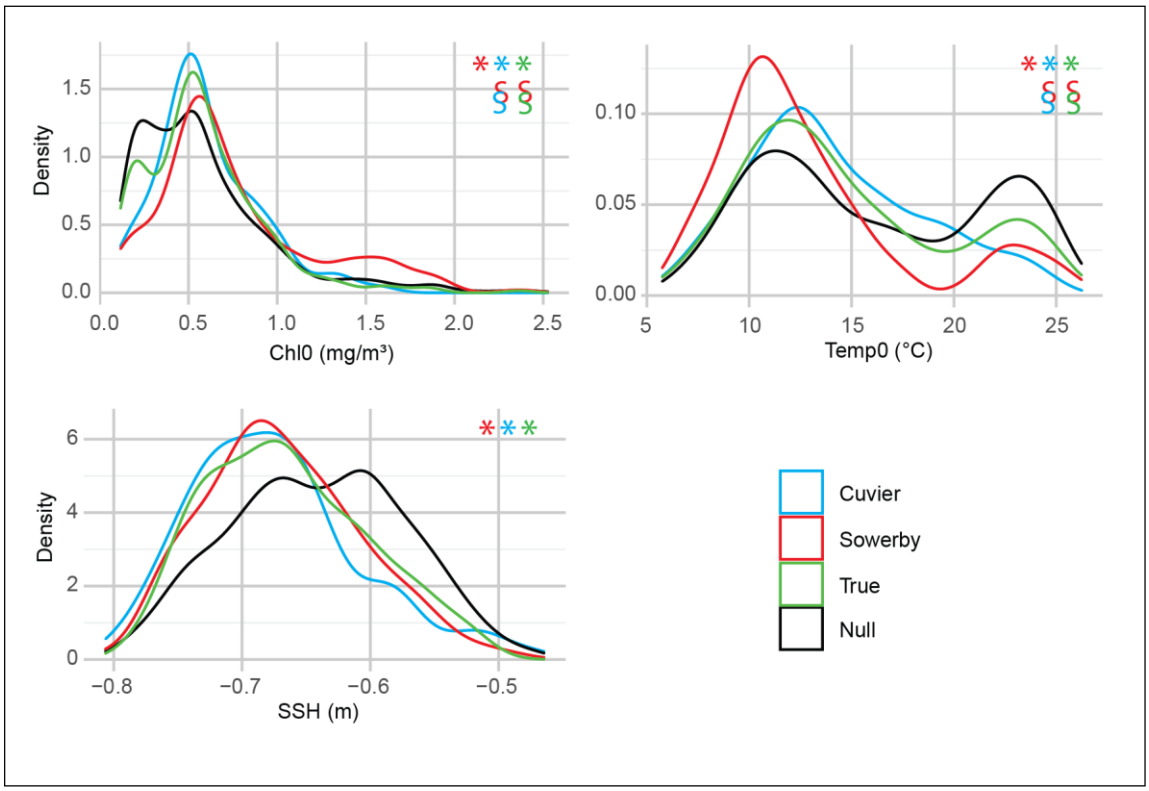

Figure 4.11: Kernel density plots comparing the distributions of covariate values associated with Cuvier's, Sowerby's, and True's beaked whale presence at site NC to background conditions. *: species' distribution significantly differed from the null distribution; §: species distributions significantly differed from one another. All three species exhibited selectivity, especially Sowerby's, but True's and Cuvier's did not significantly differ from one another.

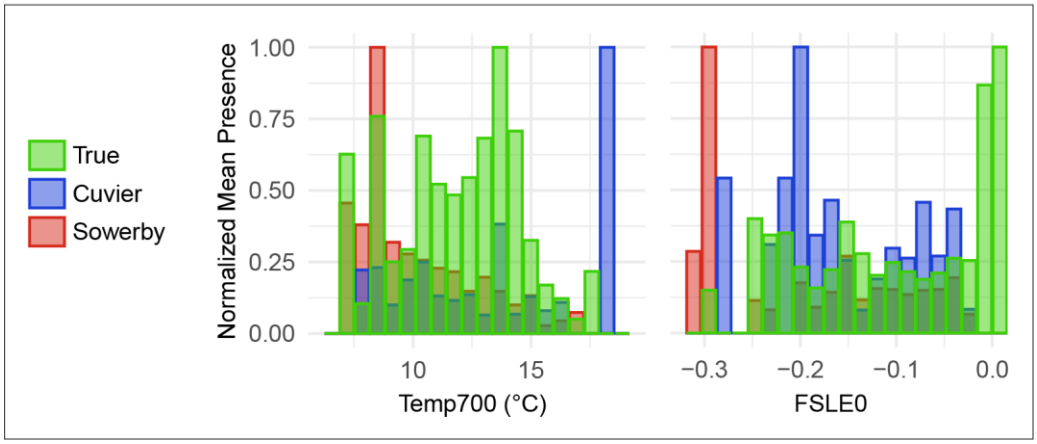

Figure 4.12: Mean presence of True's, Cuvier's and Sowerby's beaked whales as a function of covariate values at site NC, where they overlap to a small extent. The three species were well separated by their preferences for temperature at foraging depth and FSLE.

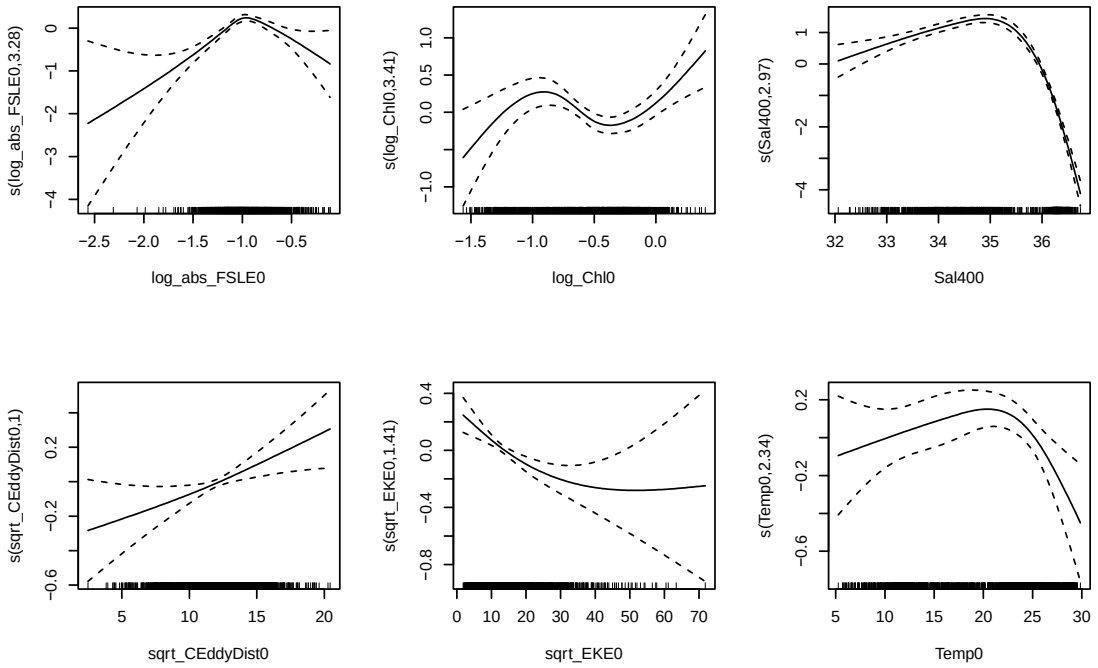

Figure 4.13: Relationships between environmental covariates and Risso's dolphin presence indicated by optimal habitat model.

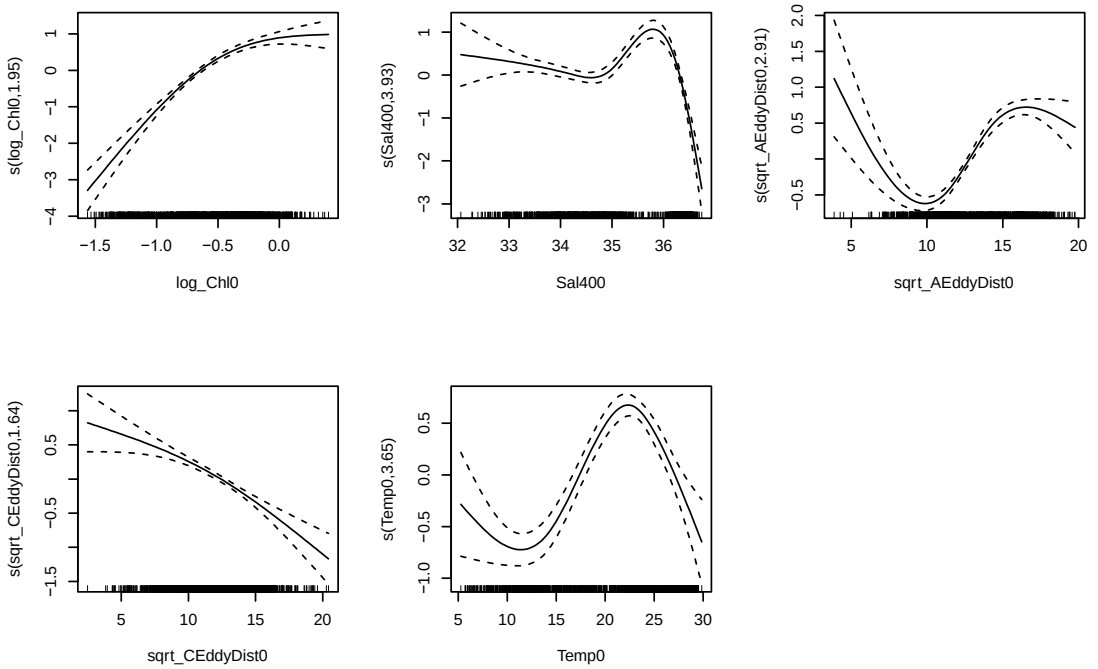

Figure 4.14: Relationships between environmental covariates and short-finned pilot whale presence indicated by optimal habitat model.

Table 4.8: Significance of p-values from KS tests comparing distributions of covariate values observed during presence of short-finned pilot whale (*Gm)* and Risso's dolphin (*Gg*) at the northern sites to the null background distributions, and to one another.

	HZ			**OC**			**NC**			**BC**		
Covariate	***Gm* vs Null**	***Gg* vs Null**	***Gm* vs *Gg***	***Gm* vs Null**	***Gg* vs Null**	***Gm* vs *Gg***	***Gm* vs Null**	***Gg* vs Null**	***Gm* vs *Gg***	***Gm* vs Null**	***Gg* vs Null**	***Gm* vs *Gg***
Chl0	NS	**	**	NS	**	NS	NS	NS	NS	**	NS	**
FLSE0	NS	NS	NS	NS	NS	NS	NS	NS	NS	NS	NS	NS
SSH0	NS	NS	NS	NS	NS	NS	NS	NS	NS	***	NS	***
Sal0	NS	NS	NS	NS	NS	NS	*	NS	NS	NS	NS	NS
Sal400	NS	NS	NS	NS	NS	NS	**	NS	NS	NS	NS	NS
Temp0	NS	***	**	NS	NS	***	NS	NS	NS	***	NS	***
Temp400	NS	*	NS	NS	NS	**	NS	NS	NS	***	NS	***
VelAsp0	NS	NS	NS	NS	NS	NS	NS	NS	NS	NS	NS	NS
VelAsp400	NS	NS	NS	NS	NS	NS	NS	NS	NS	NS	NS	NS
VelMag0	NS	NS	NS	NS	NS	NS	NS	NS	NS	NS	NS	NS
VelMag400	NS	NS	NS	NS	NS	NS	NS	NS	NS	NS	NS	NS
AEddyDist0	NS	NS	NS	NS	NS	*	NS	NS	NS	NS	NS	NS
CEddyDist0	NS	NS	NS	NS	NS	NS	NS	NS	NS	NS	NS	NS

Table 4.8 Continued: Significance of p-values from KS tests comparing distributions of covariate values observed during presence of short-finned pilot whale (*Gm)* and Risso's dolphin (*Gg*) at the northern sites to the null background distributions, and to one another.

	WC			**NFC**			**HAT**		
Covariate	***Gm* vs Null**	***Gg* vs Null**	***Gm* vs *Gg***	***Gm* vs Null**	***Gg* vs Null**	***Gm* vs *Gg***	***Gm* vs Null**	***Gg* vs Null**	***Gm* vs *Gg***
Chl0	**	NS	**	NS	*	**	NS	*	***
FLSE0	NS	NS	NS	NS	NS	NS	NS	NS	**
SSH0	***	NS	***	NS	*	***	NS	**	***
Sal0	**	NS	***	NS	NS	NS	NS	*	*
Sal400	**	NS	***	NS	NS	*	NS	NS	*
Temp0	***	NS	***	*	*	***	NS	NS	NS
Temp400	***	*	***	NS	NS	*	NS	NS	NS
VelAsp0	NS	NS	NS	NS	NS	NS	NS	NS	NS
VelAsp400	NS	NS	NS	NS	NS	NS	NS	NS	NS
VelMag0	NS	NS	NS	NS	NS	NS	NS	NS	NS
VelMag400	NS	NS	NS	NS	NS	NS	NS	NS	*
AEddyDist0	NS	NS	NS	NS	NS	NS	NS	NS	NS
CEddyDist0	**	NS	***	NS	NS	NS	NS	NS	NS

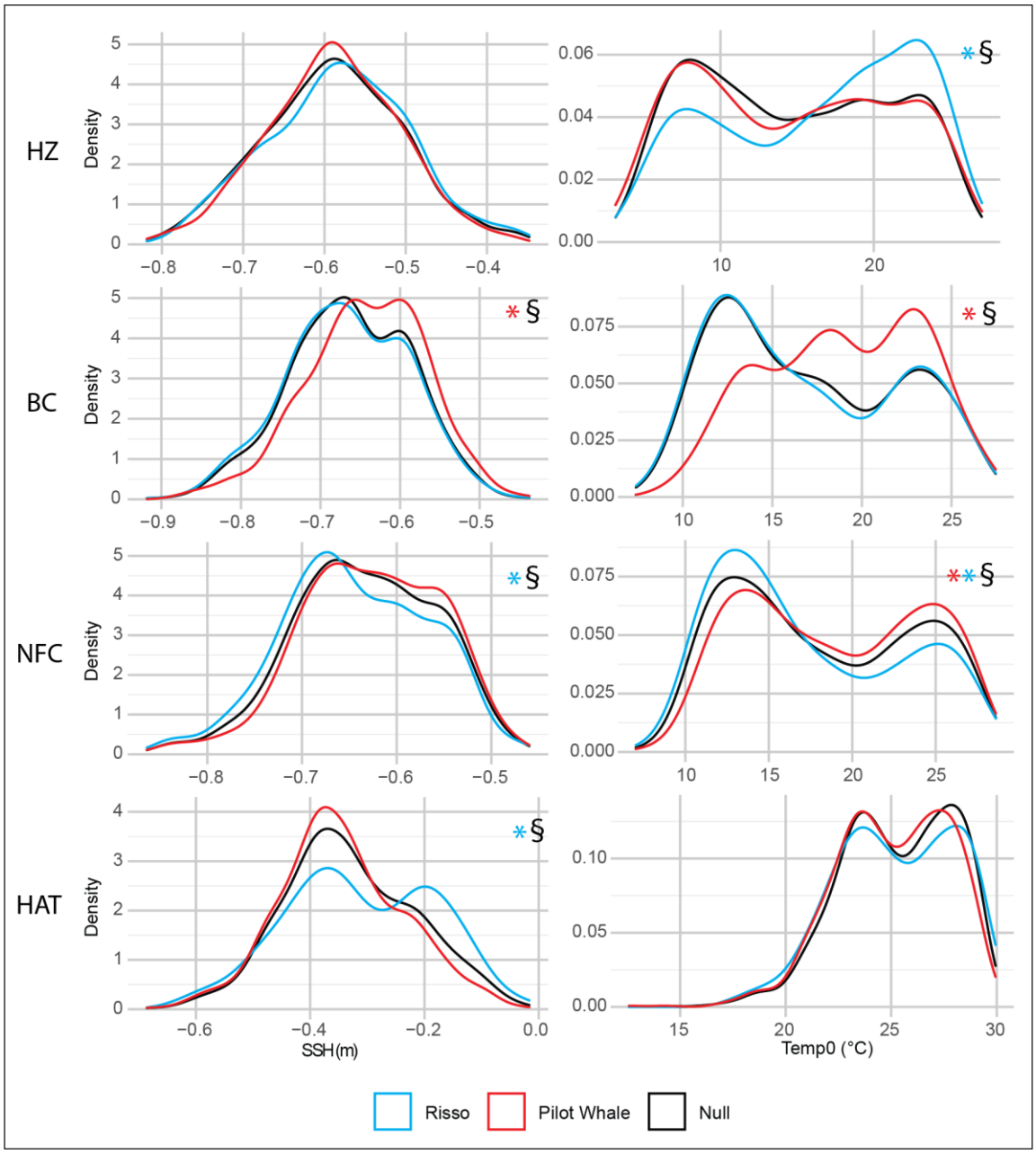

Figure 4.15: Kernel density plots comparing the distributions of covariate values associated with Risso's dolphin and short-finned pilot whale presence to background conditions. *: species' distribution significantly differed from the null distribution; §: species distributions significantly differed from one another. SST and SSH preferences exhibited by each species varied between sites.

Figure 4.16: Mean presence of Risso's dolphins and short-finned pilot whales as a function of covariate values. Risso's dolphins and short-finned pilot whales were both present at all of the sites from HAT northward, but could be consistently separated by their preferred ranges of SSH and temperature at foraging depth. Their preferences appear to change from one site to the next, which may be indicative of regional subpopulations or prey switching.

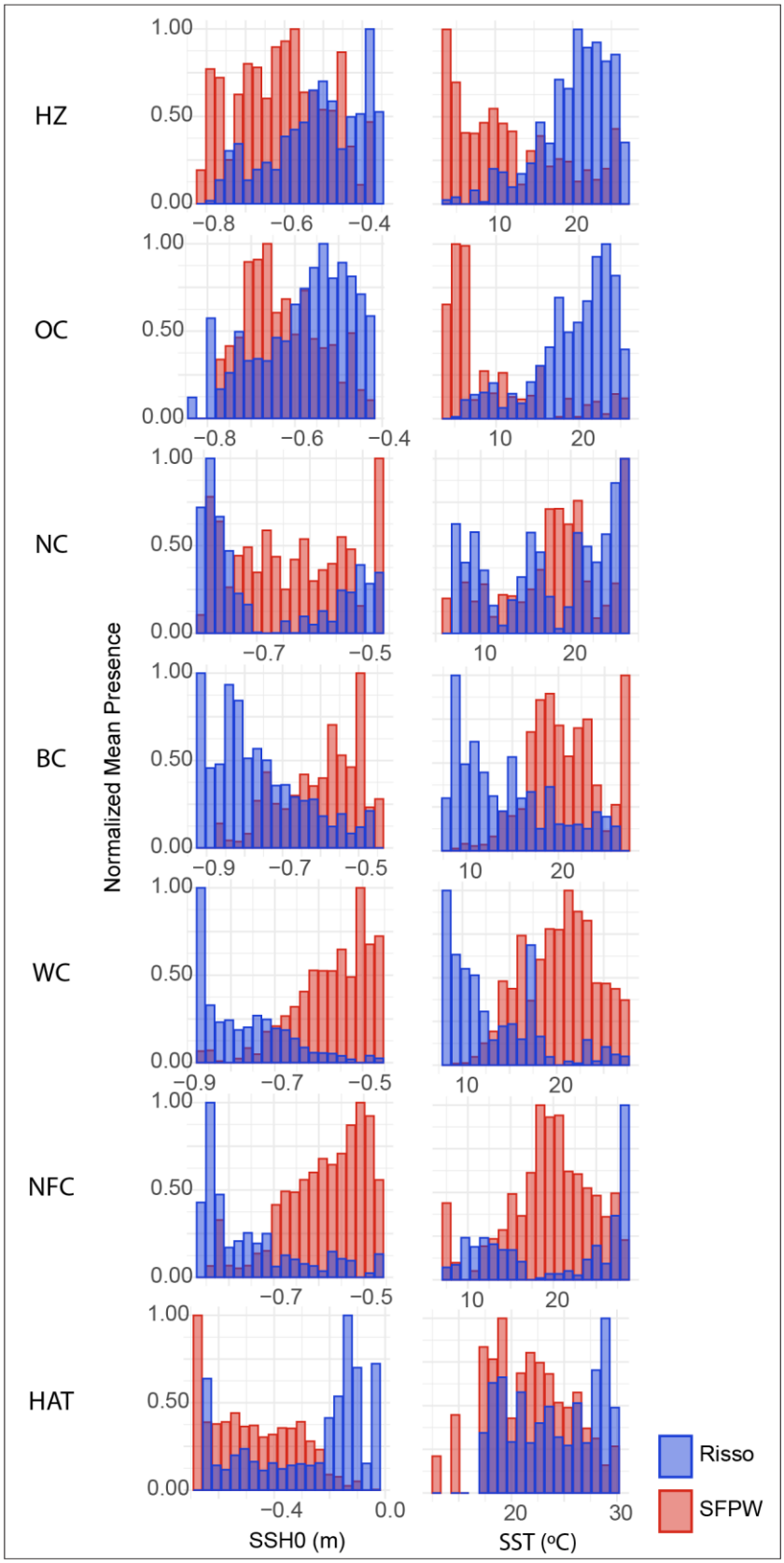
HZ
OC
NC
BC
WC
NFC
HAT
Normalized Mean Presence
1.00
0.50
0.00
−0.8
−0.6
−0.4
−0.7
−0.5
−0.9
−0.4
0.0
10
20
30
SSH0 (m)
SST (°C)
Risso
SFPW

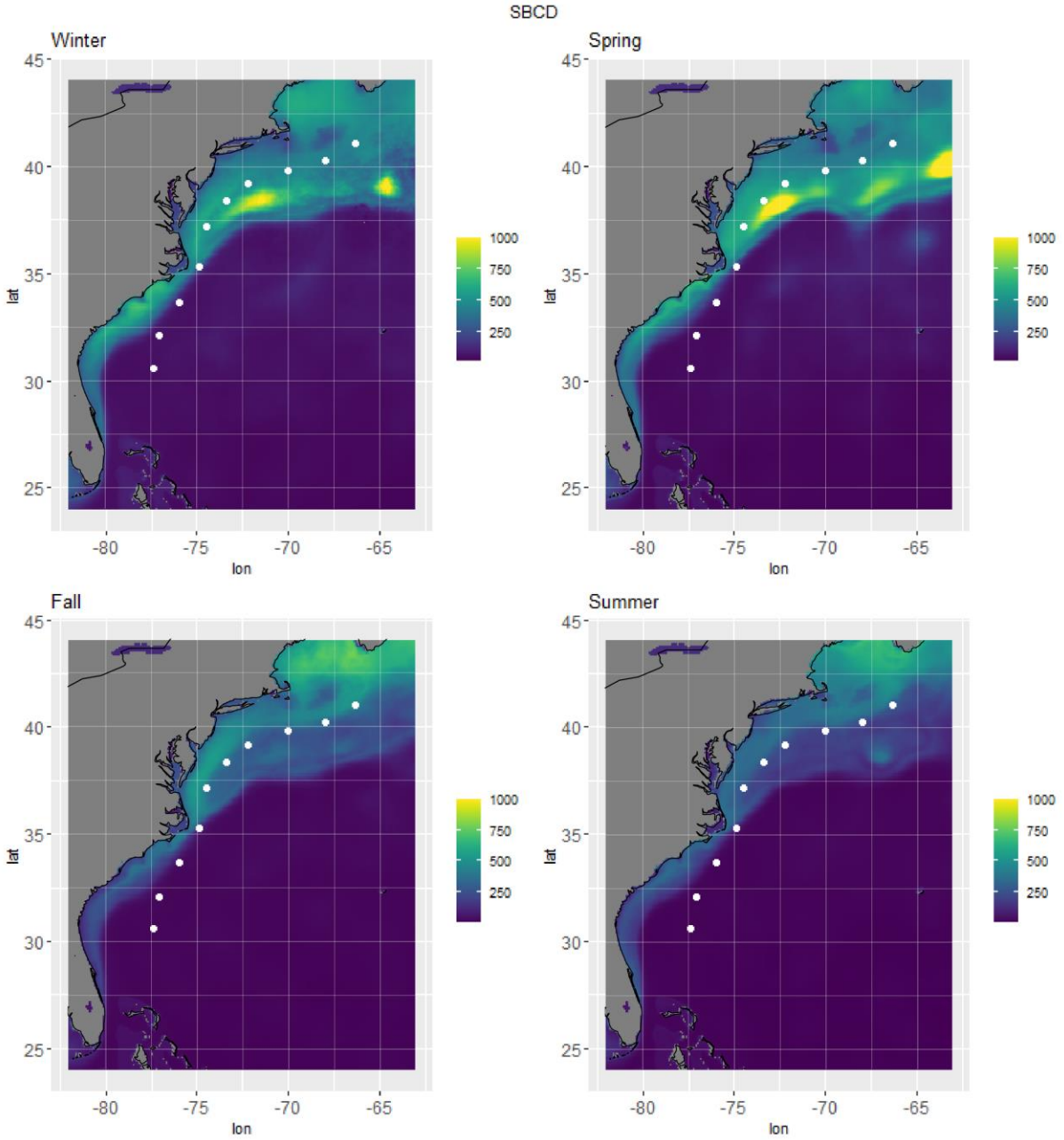

Figure 4.17: Surface model predictions of seasonal short-beaked common dolphin presence. Color scale shows predicted presence in units of 5-minute bins per week with presence.

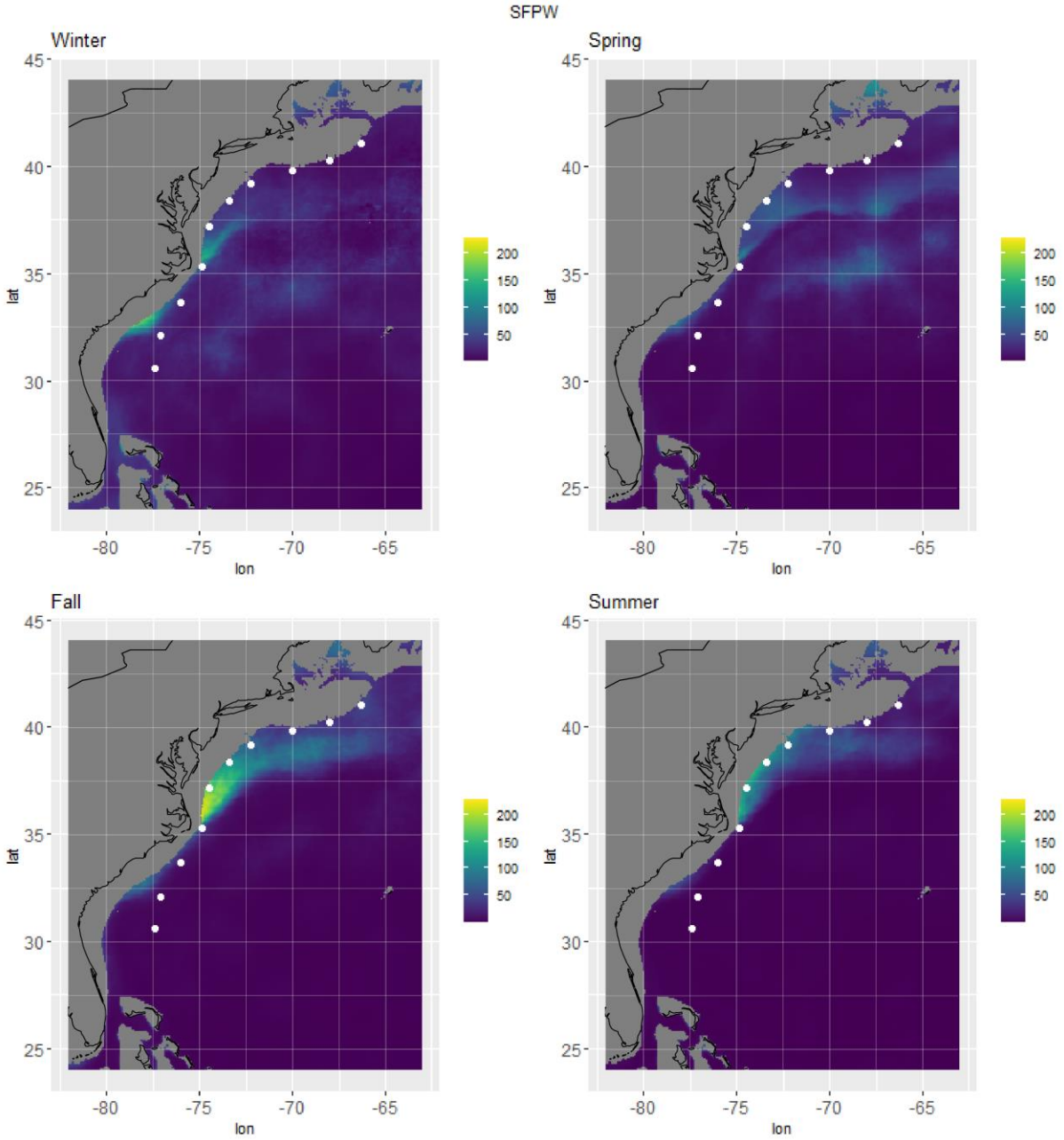

Figure 4.18: Surface model predictions of seasonal short-finned pilot whale presence. Color scale shows predicted presence in units of 5-minute bins per week with presence.

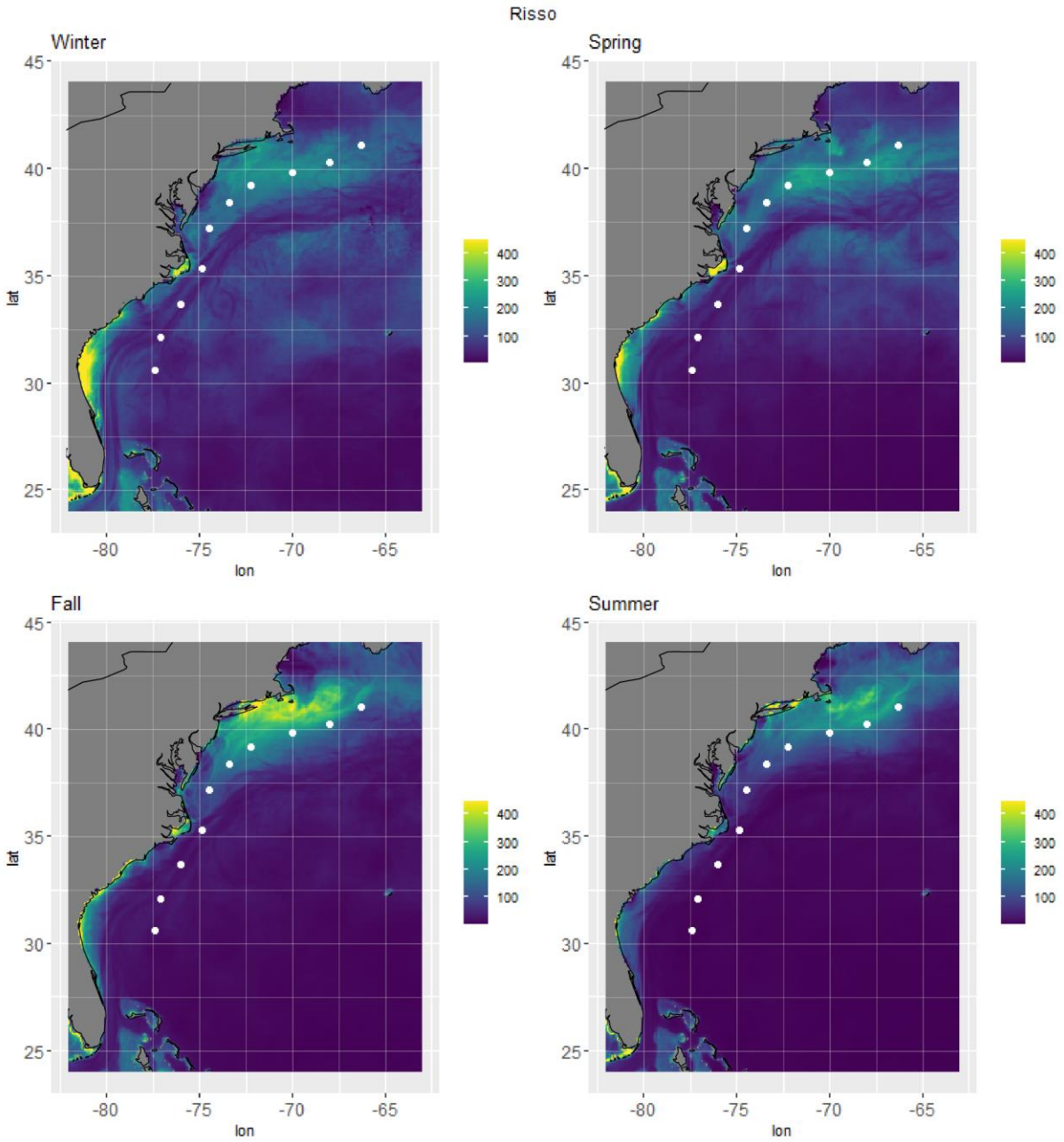

Figure 4.19: Surface model predictions of seasonal Risso's dolphin presence. Color scale shows predicted presence in units of 5-minute bins per week with presence.

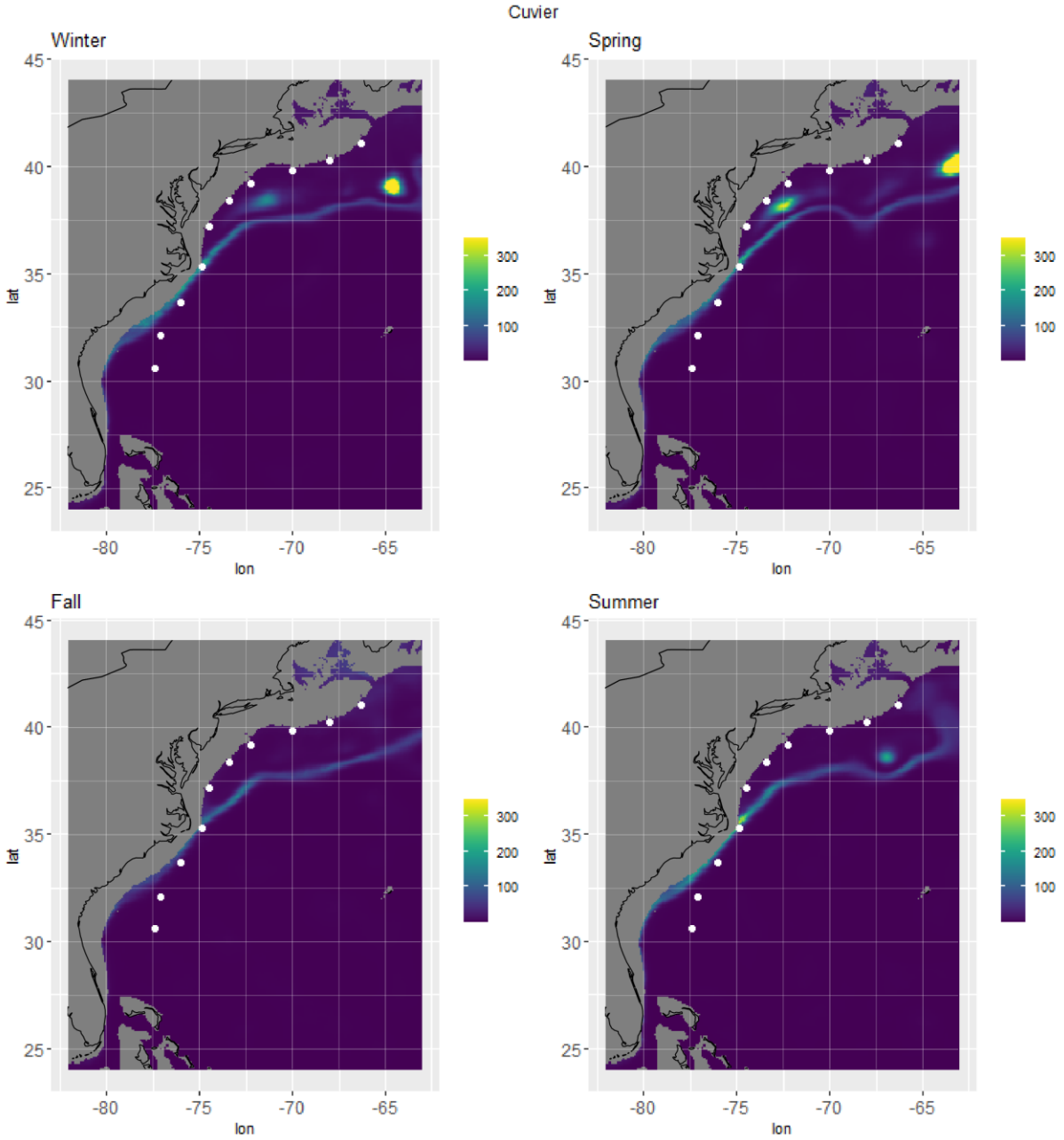

Figure 4.20: Surface model predictions of seasonal Cuvier's beaked whale presence. Color scale shows predicted presence in units of 5-minute bins per week with presence.

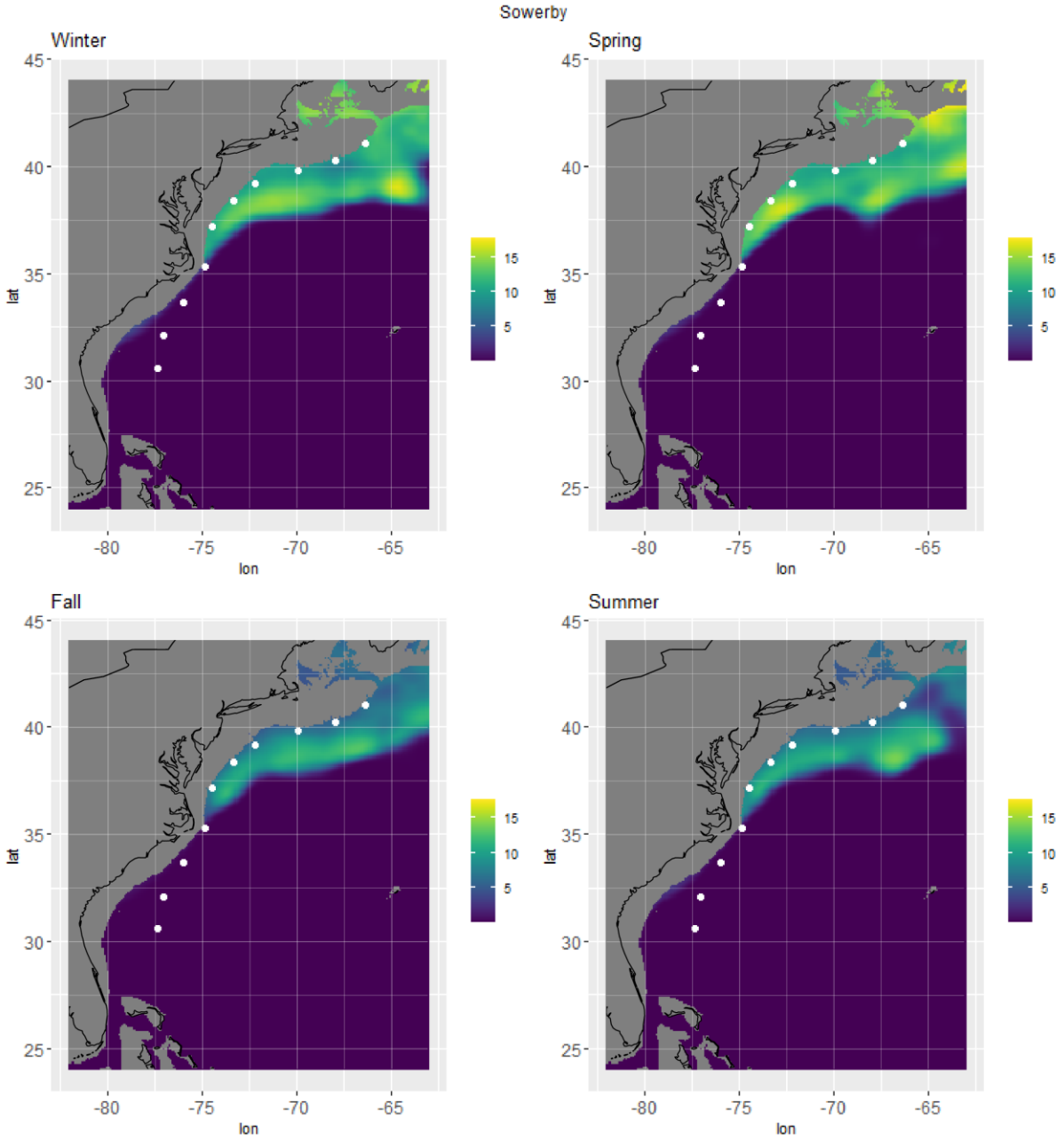

Figure 4.21: Surface model predictions of seasonal Sowerby's beaked whale presence. Color scale shows predicted presence in units of 5-minute bins per week with presence.

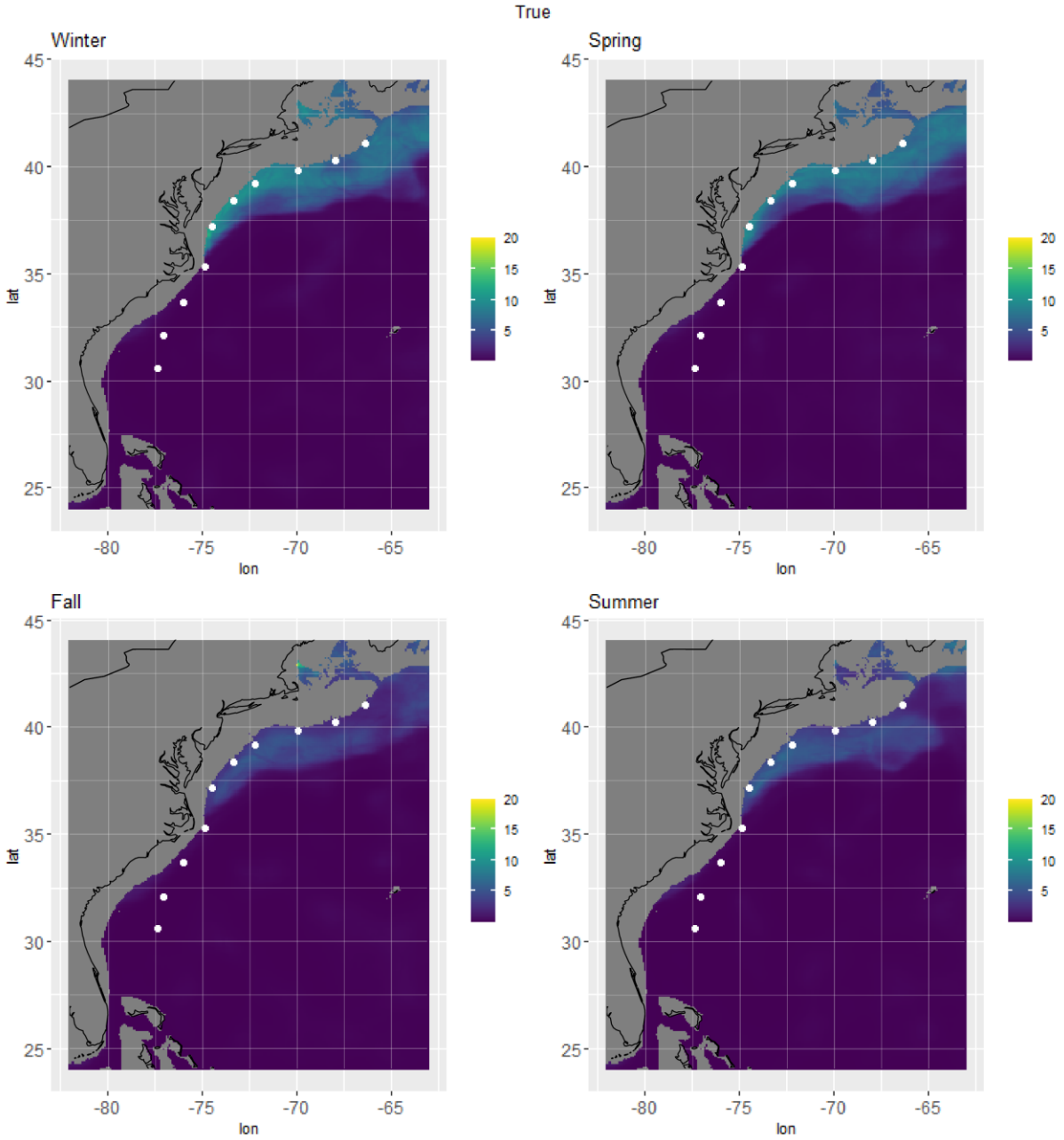

Figure 4.22: Surface model predictions of seasonal True's beaked whale presence. Color scale shows predicted presence in units of 5-minute bins per week with presence.

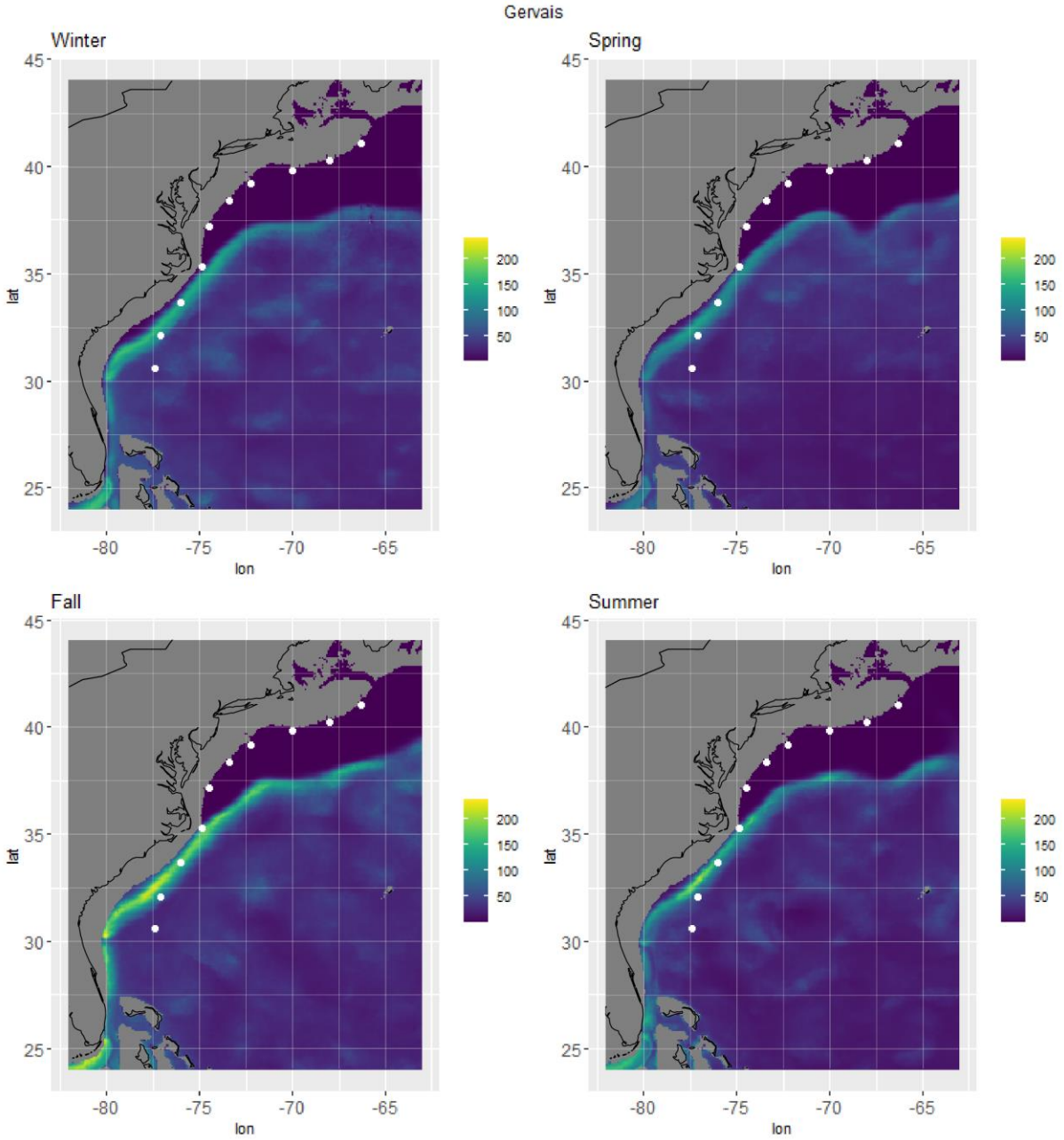

Figure 4.23: Surface model predictions of seasonal Gervais' beaked whale presence. Color scale shows predicted presence in units of 5-minute bins per week with presence.

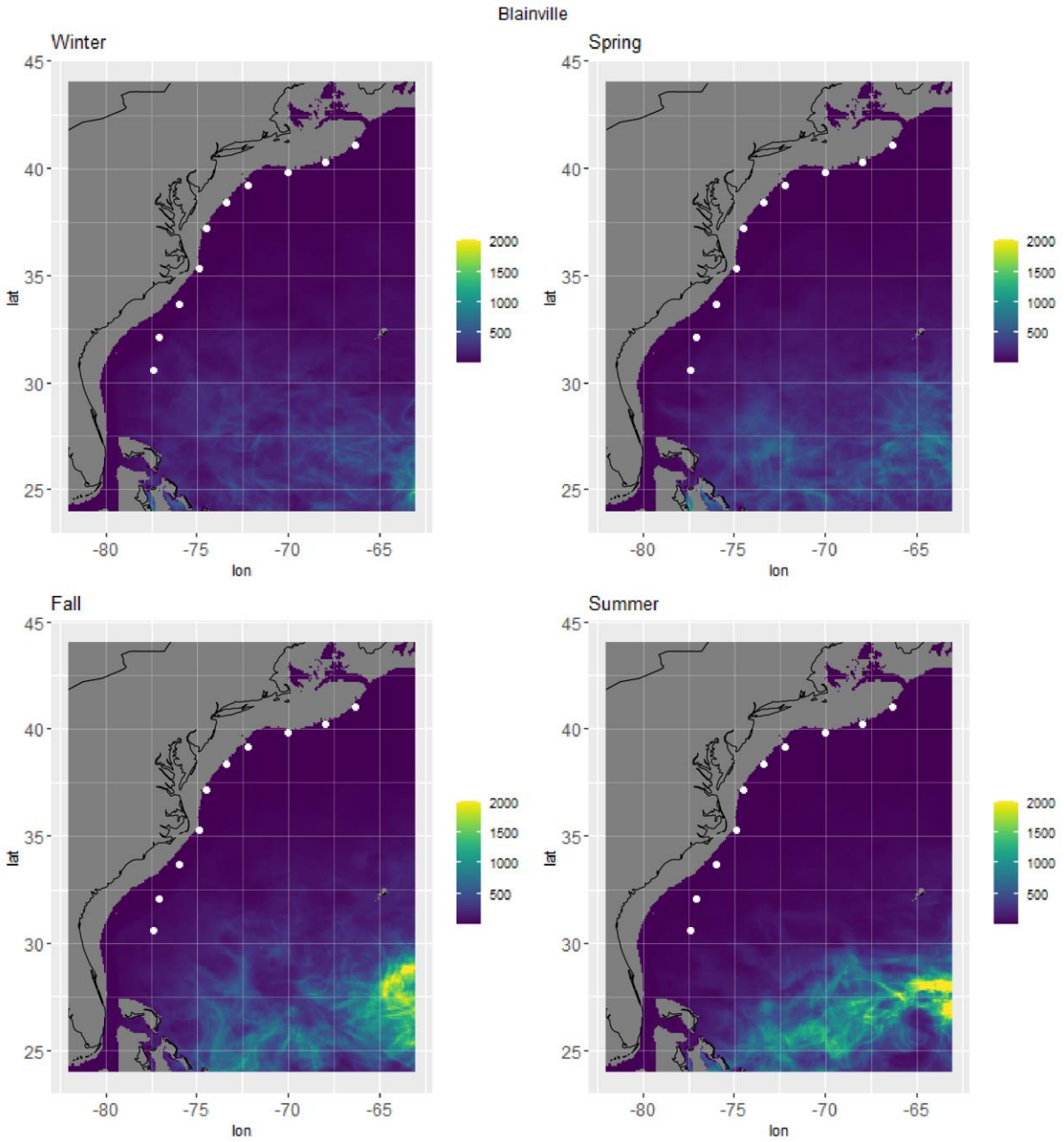

Figure 4.24: Surface model predictions of seasonal Blainville's beaked whale presence. Color scale shows predicted presence in units of 5-minute bins per week with presence.

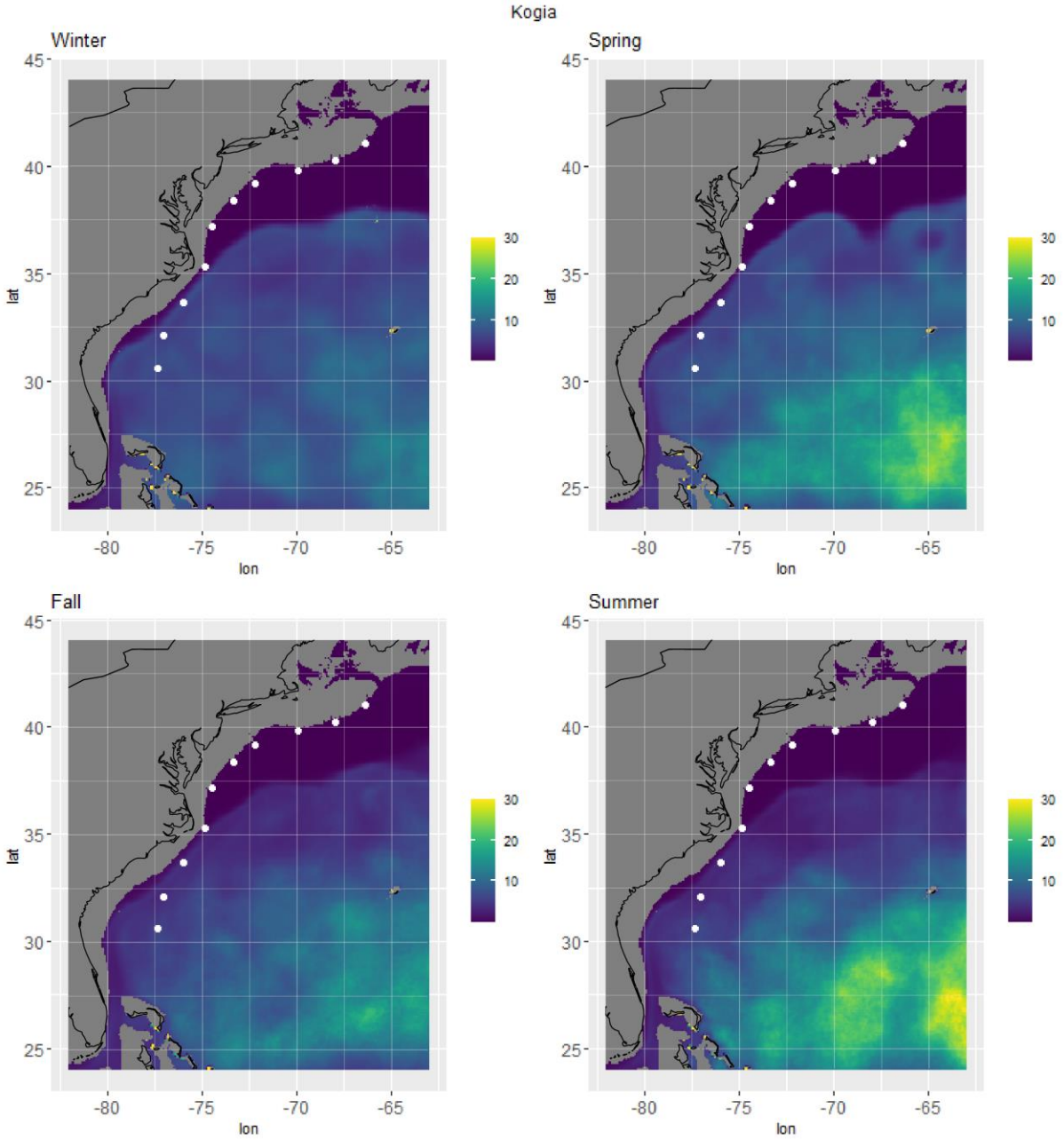

Figure 4.25: Surface model predictions of seasonal *Kogia* spp. presence. Color scale shows predicted presence in units of 5-minute bins per week with presence.

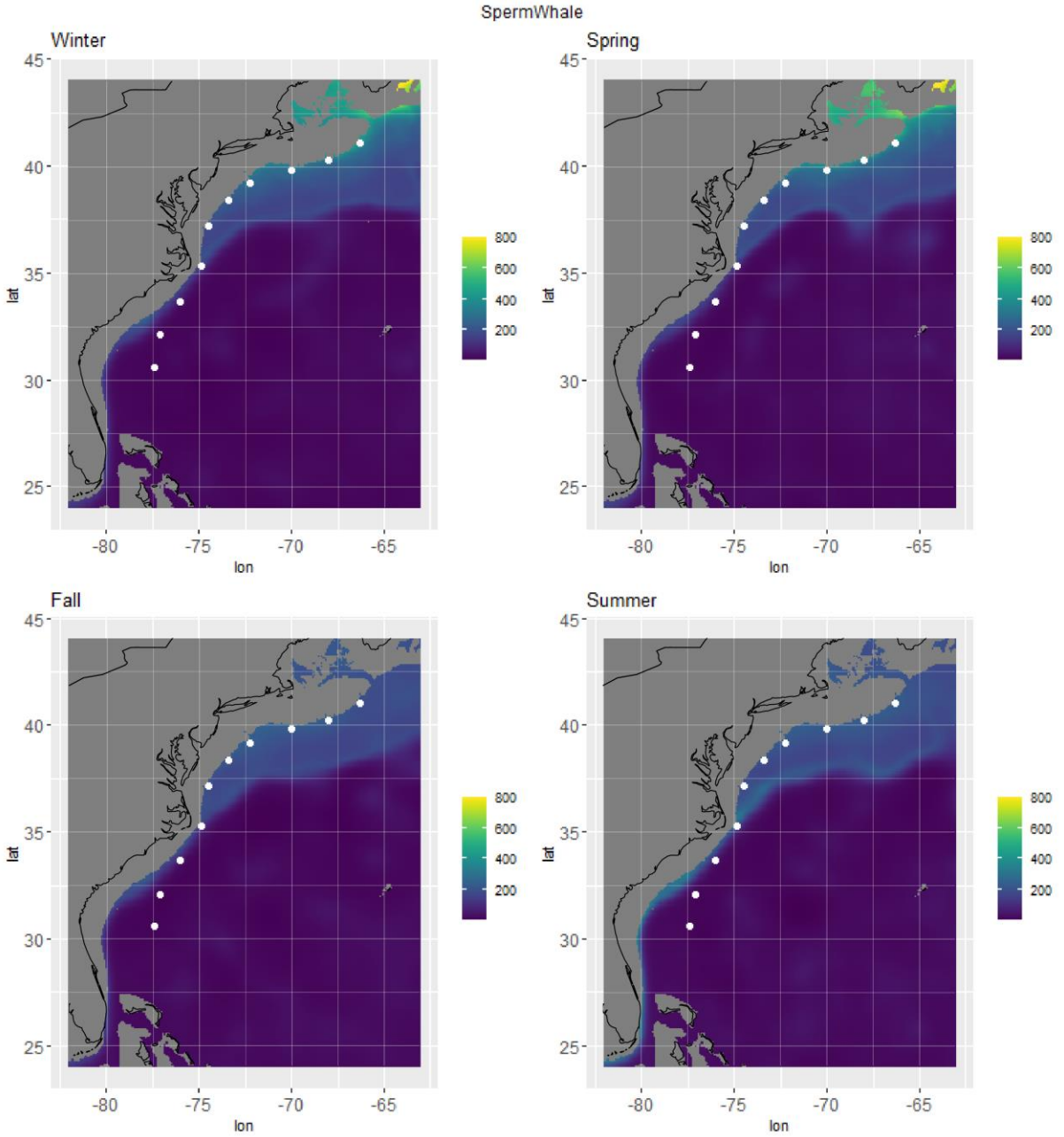

Figure 4.26: Surface model predictions of seasonal sperm whale presence. Color scale shows predicted presence in units of 5-minute bins per week with presence.

4.8 APPENDIX

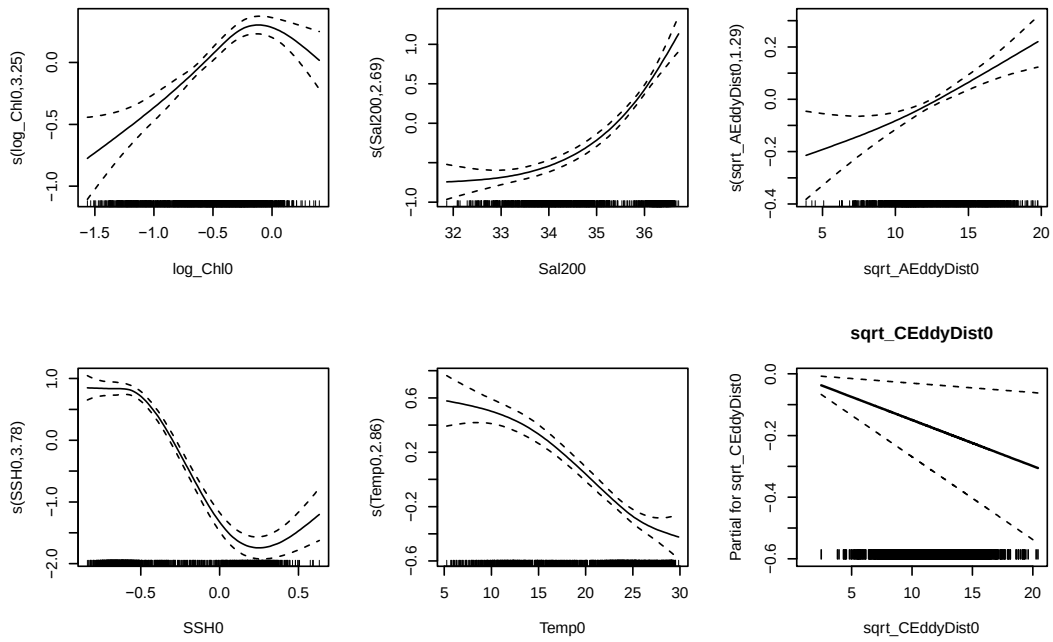

Figure 4.27: Relationships between environmental covariates and short-beaked common dolphin presence indicated by optimal habitat model.

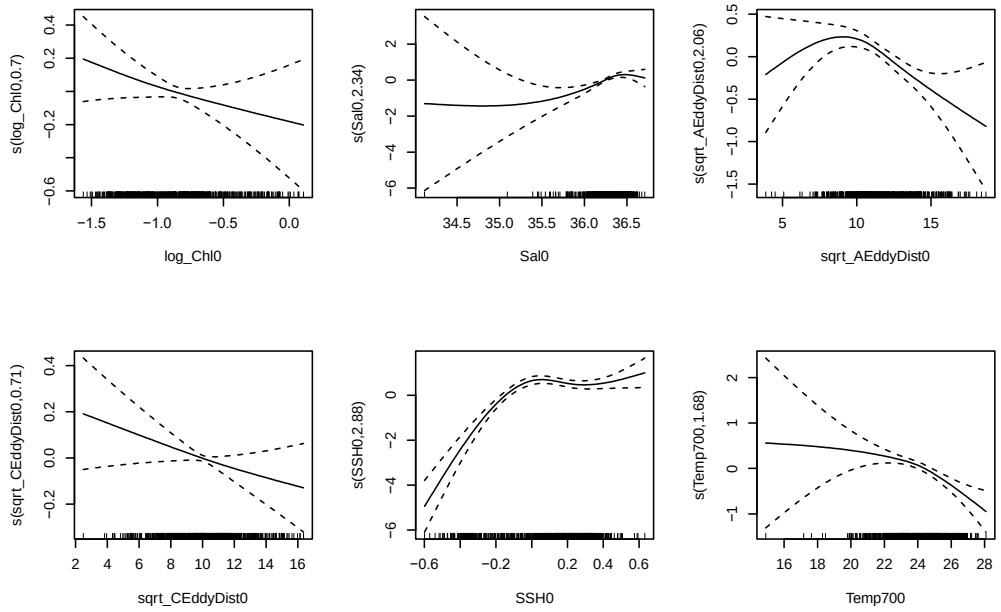

Figure 4.28: Relationships between environmental covariates and *Kogia* spp. presence indicated by optimal habitat model.

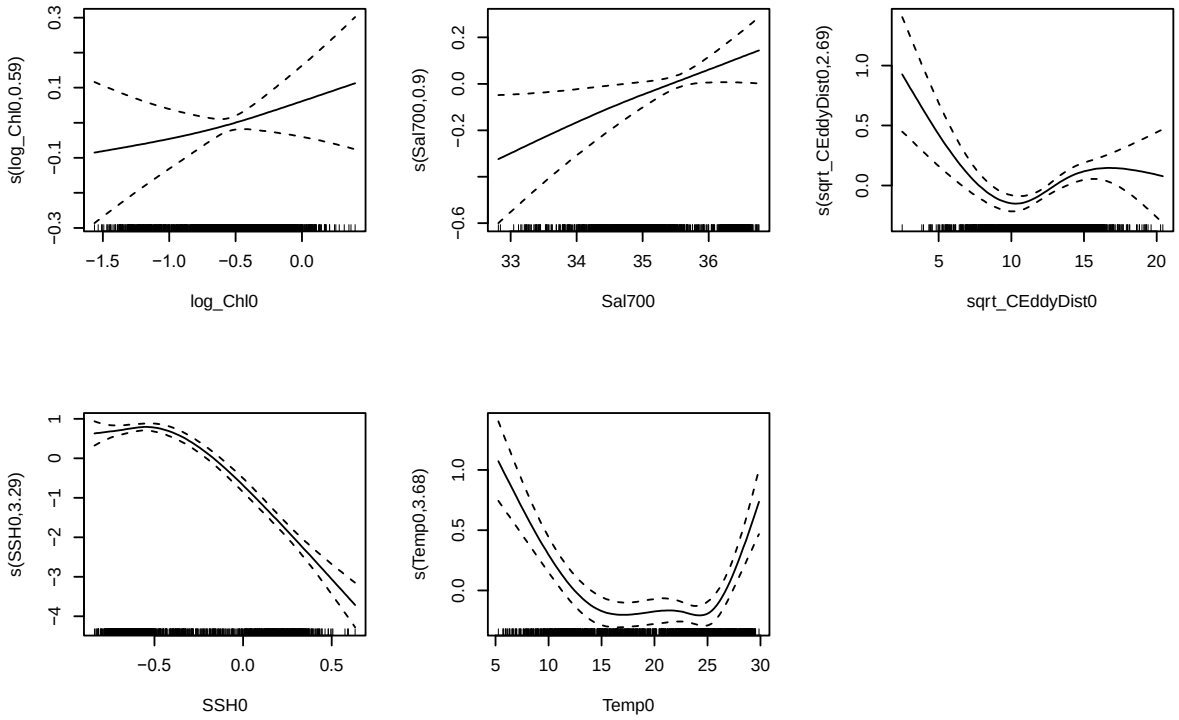

Figure 4.29: Relationships between environmental covariates and sperm whale presence indicated by optimal habitat model.

4.9 ACKNOWLEDGEMENTS

Chapter 4, in full, is currently being prepared for submission for publication of the material. Cohen, R.E., Baggett, L.M., Frasier, K.E., Baumann-Pickering, S., Hildebrand, J.A. The role of the Gulf Stream in niche partitioning of toothed whales in the western North Atlantic. The dissertation author was the primary researcher and author of this material.

REFERENCES

1. Payne RS, McVay S. Songs of Humpback Whales. Science (80-) [Internet]. 1971;173:587–97. Available from: http://www.icb.org.ar/descargas/Songs of Humpback Whales.pdf

2. Aldrich HL. Arctic Alaska and Siberia, or, Eight months with the Arctic whalemen. Chicago, New York: Rand, McNally & Company; 1889.

3. Schreiber OW. Some Sounds from Marine Life in the Hawaiian Area. J Acoust Soc Am. 1952;24(1):116–116.

4. Schevill WE. Underwater Sounds of Cetaceans. In: Tavolga WN, editor. Marine bioacoustics. Oxford, UK: Pergamon Press; 1964. p. 307–16.

5. Hastings MC, Au WWL. Marine bioacoustics and technology: The new world of marine acoustic ecology. AIP Conf Proc. 2012;1495(November):273–82.

6. Popper AN, Hawkins A, editors. The Effects of Noise on Aquatic Live. Advances in experimental medicine and biology. New York: Springer; 2012.

7. Fordyce RE. Cetacean Evolution. In: Encyclopedia of Marine Mammals. 2018. p. 180–5.

8. Gowans S. Grouping behaviors of dolphins and other toothed whales. In: Würsig B, editor. Ethology and Behavioral Ecology of Odontocetes. Springer; 2019. p. 3–24.

9. Connor RC, Mann J, Tyack PL, Whitehead H. Social evolution in toothed whales. Trends Ecol Evol. 1998;13(6):228–32.

10. Baird RW. Behavior and ecology of not-so-social odontocetes: Cuvier's and Blainville's beaked whales. In: Würsig B, editor. Ethology and Behavioral Ecology of Odontocetes. Springer; 2019. p. 305–29.

11. Smolker R, Richards A, Connor R, Mann J, Berggren P. Sponge carrying by dolphins (Delphinidae, Tursiops sp.): A foraging specialization involving tool use? Ethology. 1997;103(6):454–65.

12. Ohizumi H, Kuramochi T, Amano M, Miyazaki N. Prey switching of Dall's porpoise Phocoenoides dalli with population decline of Japanese pilchard Sardinops melanostictus around Hokkaido, Japan. Mar Ecol Prog Ser. 2000;200:265–75.

13. Au WWL. The Sonar of Dolphins. New York: Springer Verlag; 1993. 277 p.

14. Visser IN, Smith TG, Bullock ID, Green GD, Carlsson OGL, Imberti S. Antarctic peninsula killer whales (Orcinus orca) hunt seals and a penguin on floating ice. Mar Mammal Sci. 2008;24(1):225–34.

15. Ambrose ST, Froneman PW, Smale MJ, Cliff G, Plön S. Winter diet shift of long-beaked common dolphins (Delphinus capensis) feeding in the sardine run off KwaZulu-Natal, South Africa. Mar Biol. 2013;160(7):1543–61.

16. Simonis AE, Roch MA, Bailey B, Barlow J, Clemesha RES, Iacobellis S, Hildebrand JA, Baumann-Pickering S. Lunar cycles affect common dolphin Delphinus delphis foraging in the Southern California Bight. Mar Ecol Prog Ser. 2017;577:221–35.

17. Benoit-Bird KJ, Au WWL. Cooperative prey herding by the pelagic dolphin, Stenella longirostris . J Acoust Soc Am. 2009;125(1):125–37.

18. Zaeschmar JR, Dwyer SL, Stockin KA. Rare observations of false killer whales (Pseudorca crassidens) cooperatively feeding with common bottlenose dolphins (Tursiops truncatus) in the Hauraki Gulf, New Zealand. Mar Mammal Sci. 2013;29(3):555–62.

19. Taylor AR, Schacke JH, Speakman TR, Castleberry SB, Chandler RB. Factors related to common bottlenose dolphin (Tursiops truncatus) seasonal migration along South Carolina and Georgia coasts, USA. Anim Migr. 2016;3(1).

20. Norris KS, Prescott JH, Asa-Dorian PV, Perkins P. An experimental demonstration of echolocation behavior in the porpoise, Tursiops truncatus (Montagu). Biol Bull. 1961;120(2):163–76.

21. Berta A, Sumich JL, Kovacs KM. Marine Mammals: Evolutionary Biology. Academic Press; 1999.

22. Nemiroff L, Whitehead H. Structural characteristics of pulsed calls of long-finned pilot whales globicephala melas. Bioacoustics. 2009;19(1–2):67–92.

23. Dawson SM. Clicks and Communication: The Behavioural and Social Contexts of Hector's Dolphin Vocalizations. Ethology. 1991;88(4):265–76.

24. Watkins WA, Schevill WE. Sperm whale codas. J Acoust Soc Am. 1977;62(6):1485–90.

25. Clausen KT, Wahlberg M, Beedholm K, Deruiter S, Madsen PT. Click communication in harbour porpoises phocoena phocoena. Bioacoustics. 2011;20(1):1–28.

26. DeAngelis AI, Stanistreet JE, Baumann-Pickering S, Cholewiak DM. A description of echolocation clicks recorded in the presence of True's beaked whale (Mesoplodon mirus). J Acoust Soc Am. 2018;144(5):2691–700.

27. Baumann-Pickering S, Wiggins SM, Hildebrand JA, Roch MA, Schnitzler H-U. Discriminating features of echolocation clicks of melon-headed whales (Peponocephala electra), bottlenose dolphins (Tursiops truncatus), and Gray's spinner dolphins (Stenella longirostris longirostris). J Acoust Soc Am. 2010;128(4):2212–24.

28. Baumann-Pickering S, McDonald MA, Simonis AE, Solsona Berga A, Merkens KPB, Oleson EM, Roch MA, Wiggins SM, Rankin S, Yack TM, Hildebrand JA. Species-specific beaked whale echolocation signals. J Acoust Soc Am. 2013;134(3):2293–301.

29. Soldevilla MS, Henderson EE, Campbell GS, Wiggins SM, Hildebrand JA, Roch MA. Classification of Risso's and Pacific white-sided dolphins using spectral properties of echolocation clicks. J Acoust Soc Am. 2008;124(1):609–24.

30. Cholewiak D, Baumann-Pickering S, Van Parijs S. Description of sounds associated with Sowerby's beaked whales (Mesoplodon bidens) in the western North Atlantic Ocean. J Acoust Soc Am. 2013;134(5):3905–12.

31. Baumann-Pickering S, Yack TM, Barlow J, Wiggins SM, Hildebrand JA. Baird's beaked whale echolocation signals. J Acoust Soc Am. 2013;133(6):4321–31.

32. Marten K. Ultrasonic analysis of pygmy sperm whale (Kogia breviceps) and Hubbs' beaked whale (Mesoplodon carlhubbsi) clicks. Aquat Mamm. 2000;26(1):45–8.

33. Møhl B, Wahlberg M, Madsen PT, Miller LA, Surlykke A. Sperm whale clicks: Directionality and source level revisited. J Acoust Soc Am. 2000;107(1):638–48.

34. Gillespie D, Dunn C, Gordon J, Claridge D, Embling C, Boyd I. Field recordings of Gervais' beaked whales Mesoplodon europaeus from the Bahamas. J Acoust Soc Am. 2009;125(5):3428.

35. Benoit-Bird KJ. Prey caloric value and predator energy needs: Foraging predictions for wild spinner dolphins. Mar Biol. 2004;145(3):435–44.

36. Arranz P, de Soto NA, Madsen PT, Brito A, Bordes F, Johnson MP. Following a foraging fish-finder: Diel habitat use of Blainville's beaked whales revealed by echolocation. PLoS One. 2011;6(12).

37. New LF, Moretti DJ, Hooker SK, Costa DP, Simmons SE. Using Energetic Models to Investigate the Survival and Reproduction of Beaked Whales (family Ziphiidae). PLoS One. 2013;8(7).

38. Farmer NA, Noren DP, Fougères EM, Machernis A, Baker K. Resilience of the endangered sperm whale Physeter macrocephalus to foraging disturbance in the Gulf of Mexico, USA: A bioenergetic approach. Mar Ecol Prog Ser. 2018;589(Hoyt 2012):241–61.

39. Tamura T, Ohsumi S. Regional assessments of prey consumption by marine cetaceans in the world. International Whaling Commission, Scientific Committee Document SC/52/E. 2000.

40. Kenney RD, Scott GP, Thompson TJ, Winn HE. Estimates of prey consumption and trophic impacts of cetaceans in the USA northeast continental shelf ecosystem. J Northwest Atl Fish Sci. 1997;22(August 1995):155–71.

41. Roman J, Estes JA, Morissette L, Smith C, Costa D, McCarthy J, Nation JB, Nicol S, Pershing A, Smetacek V. Whales as marine ecosystem engineers. Front Ecol Environ. 2014;12(7):377–85.

42. Roman J, McCarthy JJ. The whale pump: Marine mammals enhance primary productivity in a coastal basin. PLoS One. 2010;5(10).

43. Lavery TJ, Roudnew B, Gill P, Seymour J, Seuront L, Johnson G, Mitchell JG, Smetacek V. Iron defecation by sperm whales stimulates carbon export in the Southern Ocean. Proc R Soc B Biol Sci. 2010;277(1699):3527–31.

44. Bryden HL, Hall M. Heat transports by currents across 25◦ N latitude in the Atlantic Ocean. Science (80-). 1980;207:884–6.

45. Palter JB. The role of the gulf stream in European climate. Ann Rev Mar Sci. 2015;7(September):113–37.

46. Bower AS, Rossby HT, Lillibridge J. The Gulf Stream--Barrier or Blender? J Phys Oceanogr. 1985;15.

47. McLellan HJ. On the distinctness and origin of the slope water off the Scotian Shelf and its easterly flow south of the Grand Banks. J Fish Board Canada. 1957;14(2).

48. Gatien MG. A study in the Slope Water region south of Halifax. J Fish Board Canada. 1976;33(10).

49. New AL, Smeed DA, Czaja A, Blaker AT, Mecking J V., Mathews JP, Sanchez-Franks A. Labrador Slope Water connects the subarctic with the Gulf Stream. Environ Res Lett. 2021;16(8).

50. Joyce TM, Zhang R. On the Path of the Gulf Stream and the Atlantic meridional overturning circulation. J Clim. 2010;23(11):3146–54.

51. Sanchez-Franks A, Zhang R. Impact of the Atlantic meridional overturning circulation on the decadal variability of the Gulf Stream path and regional chlorophyll and nutrient concentrations. Geophys Res Lett. 2015;42(22):9889–97.

52. Grice GD, Hart AD. The Abundance, Seasonal Occurrence and Distribution of the Epizooplankton between New York and Bermuda. Ecol Monogr. 1962;32(4):287–309.

53. Nye JA, Joyce TM, Kwon YO, Link JS. Silver hake tracks changes in Northwest Atlantic circulation. Nat Commun. 2011;2(1).

54. Taylor AH, Colebrook JM, Stephens JA, Baker NG. Latitudinal displacements of the Gulf Stream and the abundance of plankton in the north-east Atlantic. J Mar Biol Assoc United Kingdom. 1992;72(04):919–21.

55. Au WWL. The Sonar of Dolphins. Springer Verlag; 1993.

56. Johnson M, Madsen PT, Zimmer WMX, Aguilar De Soto N, Tyack PL. Foraging Blainville's beaked whales (Mesoplodon densirostris) produce distinct click types matched to different phases of echolocation. J Exp Biol. 2006;209(24):5038–50.

57. Johnson M, Hickmott LS, Aguilar Soto N, Madsen PT. Echolocation behaviour adapted to prey in foraging Blainville's beaked whale (Mesoplodon densirostris). Proc R Soc B Biol Sci. 2008;275(1631):133–9.

58. Madsen PT, Johnson M, Aguilar De Soto N, Zimmer WMX, Tyack P. Biosonar performance of foraging beaked whales (Mesoplodon densirostris). J Exp Biol. 2005;208(2):181–94.

59. Madsen PT, Kerr I, Payne R. Echolocation clicks of two free-ranging, oceanic delphinids with different food preferences: False killer whales Pseudorca crassidens and Risso's dolphins Grampus griseus. J Exp Biol. 2004;207(11):1811–23.

60. Nowacek DP. Acoustic ecology of foraging bottlenose dolphins (Tursiops truncatus), habitat-specific use of three sound types. Mar Mammal Sci. 2005;21(4):587–602.

61. Henderson EE, Hildebrand JA, Smith MH. Classification of behavior using vocalizations of Pacific white-sided dolphins (Lagenorhynchus obliquidens). J Acoust Soc Am. 2011;130(1):557–67.

62. Leroy EC, Thomisch K, Royer J-Y, Boebel O, Van Opzeeland I. On the reliability of acoustic annotations and automatic detections of Antarctic blue whale calls under different acoustic conditions. J Acoust Soc Am. 2018;144(2):740–54.

63. Frasier KE. A machine learning pipeline for classification of cetacean echolocation clicks in large underwater acoustic datasets. PLOS Comput Biol. 2021 Dec 3;17(12):e1009613.

64. Allen AN, Harvey M, Harrell L, Jansen A, Merkens KP, Wall CC, Cattiau J, Oleson EM. A Convolutional Neural Network for Automated Detection of Humpback Whale Song in a Diverse, Long-Term Passive Acoustic Dataset. Front Mar Sci. 2021;8(March).

65. Shiu Y, Palmer KJ, Roch MA, Fleishman E, Liu X, Nosal EM, Helble T, Cholewiak D, Gillespie D, Klinck H. Deep neural networks for automated detection of marine mammal species. Sci Rep. 2020;10(1):1–12.

66. Frasier KE, Henderson EE, Bassett HR, Roch MA. Automated identification and clustering of subunits within delphinid vocalizations. Mar Mammal Sci. 2016;32(3):911–30.

67. Frasier KE, Roch MA, Soldevilla MS, Wiggins SM, Garrison LP, Hildebrand JA. Automated classification of dolphin echolocation click types from the Gulf of Mexico. PLoS Comput Biol. 2017;13(12):1–23.

68. Rankin S, Archer F, Keating JL, Oswald JN, Oswald M, Curtis A, Barlow J. Acoustic classification of dolphins in the California Current using whistles, echolocation clicks, and burst pulses. Mar Mammal Sci. 2017;33(2):520–40.

69. Reyes Reyes MV, Iñíguez MA, Hevia M, Hildebrand JA, Melcón ML. Description and clustering of echolocation signals of Commerson's dolphins (Cephalorhynchus commersonii) in Bahía San Julián, Argentina. J Acoust Soc Am. 2015;138(4):2046–53.

70. Roch MA, Scott Brandes T, Patel B, Barkley Y, Baumann-Pickering S, Soldevilla MS. Automated extraction of odontocete whistle contours. J Acoust Soc Am. 2011;130(4):2212–23.

71. Roch MA, Soldevilla MS, Burtenshaw JC, Henderson EE, Hildebrand JA. Gaussian mixture model classification of odontocetes in the Southern California Bight and the Gulf of California. J Acoust Soc Am. 2007;121(3):1737–48.

72. Roch MA, Soldevilla MS, Hoenigman R, Wiggins SM, Hildebrand JA. Comparison of machine learning techniques for the classification of echolocation clicks from three species of

odontocetes. Can Acoust - Acoust Can. 2008;36(1):41–7.

73. Roch MA, Klinck H, Baumann-Pickering S, Mellinger DK, Qui S, Soldevilla MS, Hildebrand JA. Classification of echolocation clicks from odontocetes in the Southern California Bight. J Acoust Soc Am. 2011;129(1):467–75.

74. Hildebrand JA, Frasier KE, Helble TA, Roch MA. Performance metrics for marine mammal signal detection and classification. J Acoust Soc Am. 2022;Forthcoming.

75. Wiggins SM, Hildebrand JA. High-frequency Acoustic Recording Package (HARP) for broad-band, long-term marine mammal monitoring. Int Symp Underw Technol UT 2007 - Int Work Sci Use Submar Cables Relat Technol 2007. 2007;(April):551–7.

76. Halpin P., Read AJ, Fujioka E, Best BD, Donnelly B, Hazen LJ, Kot C, Urian K, LaBrecque E, Dimatteo A, Cleary J, Good C, Crowder LB, Hyrenbach KD. Obis-Seamap. Oceanography. 2011;22(2):104–15.

77. Frasier KE. Density estimation of delphinids using passive acoustics: A case study in the Gulf of Mexico. 2015 Oct;

78. Rankin S, Baumann-Pickering S, Yack T, Barlow J. Description of sounds recorded from Longman's beaked whale, Indopacetus pacificus . J Acoust Soc Am. 2011;130(5):EL339–44.

79. Baumann-Pickering S, Simonis AE, Oleson EM, Baird RW, Roch MA, Wiggins SM. False killer whale and short-finned pilot whale acoustic identification. Endanger Species Res. 2015;28(2):97–108.

80. Biemann C. Chinese whispers - An efficient graph clustering algorithm and its application to natural language processing problems. Proc TextGraphs 1st Work Graph-Based Methods Nat Lang Process. 2020;(June):73–80.

81. Goold JC, Jones SE. Time and frequency domain characteristics of sperm whale clicks. J Acoust Soc Am. 1995;98(3):1279–91.

82. Whitehead H, Weilgart L. Click rates from sperm whales. J Acoust Soc Am. 1990;87(4):1798–806.

83. Hildebrand JA, Baumann-Pickering S, Frasier KE, Trickey JS, Merkens KP, Wiggins SM, McDonald MA, Garrison LP, Harris D, Marques TA, Thomas L. Passive acoustic monitoring of beaked whale densities in the Gulf of Mexico. Sci Rep. 2015;5:1–15.

84. Au WWL, Banks K. The acoustics of the snapping shrimp Synalpheus parneomeris in Kaneohe Bay . J Acoust Soc Am. 1998;103(1):41–7.

85. Glorot X, Bordes A, Benigo Y. Deep Sparse Rectifier Neural Networks. In: Proceedings of the 14th International Conference on Artifical Intelligence and Statistics. 2011. p. 315–23.

86. Luce RD. Individual Choice Behavior; A Theoretical Analysis. New York: Wiley; 1959.

87. Frasier KE, Wiggins SM, Harris D, Marques TA, Thomas L, Hildebrand JA. Delphinid

echolocation click detection probability on near-seafloor sensors. J Acoust Soc Am. 2016;140(3):1918–30.

88. Kyhn LA, Jensen FH, Beedholm K, Tougaard J, Hansen M, Madsen PT. Echolocation in sympatric peale's dolphins (Lagenorhynchus australis) and commerson's dolphins (Cephalorhynchus commersonii) producing narrow-band high-frequency clicks. J Exp Biol. 2010;213(11):1940–9.

89. Madsen PT, Kerr I, Payne R. Source parameter estimates of echolocation clicks from wild pygmy killer whales (Feresa attenuata) (L). J Acoust Soc Am. 2004;116(4):1909–12.

90. Pedersen MB, Tønnesen P, Malinka CE, Ladegaard M, Johnson M, Aguilar de Soto N, Madsen PT. Echolocation click parameters of short-finned pilot whales (Globicephala macrorhynchus) in the wild. J Acoust Soc Am. 2021;149(3):1923–31.

91. Clarke E, Feyrer LJ, Moors-Murphy H, Stanistreet J. Click characteristics of northern bottlenose whales (Hyperoodon ampullatus) and Sowerby's beaked whales (Mesoplodon bidens) off eastern Canada. J Acoust Soc Am. 2019;146(1):307–15.

92. Johnson M, Madsen PT, Zimmer WMX, Aguilar De Soto N, Tyack PL. Beaked whales echolocate on prey. Proc R Soc B Biol Sci. 2004;271(SUPPL. 6):383–6.

93. Zimmer WMX, Johnson MP, Madsen PT, Tyack PL. Echolocation clicks of free-ranging Cuvier's beaked whales (Ziphius cavirostris). J Acoust Soc Am. 2005;117(6):3919–27.

94. Madsen PT, Carder DA, Bedholm K, Ridgway SH. Porpoise clicks from a sperm whale nose—convergent evolution of 130 khz pulses in toothed whale sonars? Bioacoustics. 2005;15(2):195–206.

95. Merkens K, Mann D, Janik VM, Claridge D, Hill M, Oleson E. Clicks of dwarf sperm whales (Kogia sima). Mar Mammal Sci. 2018;34(4):963–78.

96. Wahlberg M, Jensen FH, Aguilar Soto N, Beedholm K, Bejder L, Oliveira C, Rasmussen M, Simon M, Villadsgaard A, Madsen PT. Source parameters of echolocation clicks from wild bottlenose dolphins (Tursiops aduncus and Tursiops truncatus). J Acoust Soc Am. 2011;130(4):2263–74.

97. Soldevilla MS, Baumann-Pickering S, Cholewiak D, Hodge LEW, Oleson EM, Rankin S. Geographic variation in Risso's dolphin echolocation click spectra. J Acoust Soc Am. 2017;142(2):599–617.

98. Rendell LE, Matthews JN, Gill A, Gordon JCD, Macdonald DW. Quantitative analysis of tonal calls from five odontocete species, examining interspecific and intraspecific variation. J Zool. 1999;249(4):403–10.

99. Scheer M. Call vocalizations recorded among short-finned pilot Whales (globicep ala macrorhynchus) off tenerife, Canary Islands. Aquat Mamm. 2013;39(3):306–13.

100. Hodge LEW, Frasier KE, Hildebrand JA, Read AJ. Steps toward Classification of Unidentified Odontocete Clicks within Passive Acoustic Recordings. Final Report. Submitt to Nav Facil

Eng Command Atl Norfolk, Virginia, under Contract No N2470-15-D-8006, Task Order 006, issued to HDR Inc, Norfolk, Virginia July 2018.

101. Smith AB, Pacini AF, Nachtigall PE, Laule GE, Aragones L V., Magno C, Suarez LJA. Transmission beam pattern and dynamics of a spinner dolphin (Stenella longirostris). J Acoust Soc Am. 2019;145(6):3595–605.

102. Jensen FH, Johnson M, Ladegaard M, Wisniewska DM, Madsen PT. Narrow Acoustic Field of View Drives Frequency Scaling in Toothed Whale Biosonar. Curr Biol. 2018;28(23):3878-3885.e3.

103. Zimmer WMX, Madsen PT, Teloni V, Johnson MP, Tyack PL. Off-axis effects on the multipulse structure of sperm whale usual clicks with implications for sound production. J Acoust Soc Am. 2005;118(5):3337–45.

104. Moreno-Torres JG, Raeder T, Alaiz-Rodríguez R, Chawla N V., Herrera F. A unifying view on dataset shift in classification. Pattern Recognit. 2012;45(1):521–30.

105. Beijbom O, Hoffman J, Yao E, Darrell T, Rodriguez-Ramirez A, Gonzalez-Rivero M, Guldberg OH-. Quantification in-the-wild: data-sets and baselines. 2015;

106. González P, Álvarez E, Díez J, López-Urrutia Á, del Coz JJ. Validation methods for plankton image classification systems. Limnol Oceanogr Methods. 2017;15(3):221–37.

107. Orenstein EC, Kenitz KM, Roberts PLD, Franks PJS, Jaffe JS, Barton AD. Semi- and fully supervised quantification techniques to improve population estimates from machine classifiers. Limnol Oceanogr Methods. 2020;18(12):739–53.

108. Wenz GM. Acoustic Ambient Noise in the Ocean: Spectra and Sources. J Acoust Soc Am. 1962;34(12):1936–56.

109. Hildebrand JA. Anthropogenic and natural sources of ambient noise in the ocean. Mar Ecol Prog Ser. 2009;395:5–20.

110. Becker EA, Forney KA, Ferguson MC, Foley DG, Smith RC, Barlow J, Redfern J V. Comparing California current cetacean-habitat models developed using in situ and remotely sensed sea surface temperature data. Mar Ecol Prog Ser. 2010;413(August):163–83.

111. Conners MG, Hazen EL, Costa DP, Shaffer SA. Shadowed by scale: Subtle behavioral niche partitioning in two sympatric, tropical breeding albatross species. Mov Ecol [Internet]. 2015;3(1):1–20. Available from: http://dx.doi.org/10.1186/s40462-015-0060-7

112. Matich P, Ault JS, Boucek RE, Bryan DR, Gastrich KR, Harvey CL, Heithaus MR, Kiszka JJ, Paz V, Rehage JS, Rosenblatt AE. Ecological niche partitioning within a large predator guild in a nutrient-limited estuary. Limnol Oceanogr. 2017;62(3):934–53.

113. Iwahara Y, Shirakawa H, Miyashita K, Mitani Y. Spatial niche partitioning among three small cetaceans in the eastern coastal area of Hokkaido, Japan. Mar Ecol Prog Ser. 2020;637(Kadowaki 2016):209–23.

114. Lear KO, Whitney NM, Morris JJ, Gleiss AC. Temporal niche partitioning as a novel mechanism promoting co-existence of sympatric predators in marine systems. Proc R Soc B Biol Sci. 2021;288(1954).

115. Gao VD, Morley-Fletcher S, Maccari S, Vitaterna MH, Turek FW. Resource competition shapes biological rhythms and promotes temporal niche differentiation in a community simulation. Ecol Evol. 2020;10(20):11322–34.

116. Cavender-Bares KK, Karl DM, Chisholm SW. Nutrient gradients in the western North Atlantic Ocean: Relationship to microbial community structure and comparison to patterns in the Pacific Ocean. Deep Res Part I Oceanogr Res Pap. 2001;48(11):2373–95.

117. Wang S, Lin Y, Gifford S, Eveleth R, Cassar N. Linking patterns of net community production and marine microbial community structure in the western North Atlantic. ISME J [Internet]. 2018;12(11):2582–95. Available from: http://dx.doi.org/10.1038/s41396-018-0163-4

118. Schneider D, Piatt J. Scale-dependent correlation of seabirds with schooling fish in a coastal ecosystem. Mar Ecol Prog Ser. 1986;32(2):237–46.

119. Piatt JF, Methven DA. Threshold foraging behavior of baleen whales. Mar Ecol Prog Ser. 1992;84(3):205–10.

120. Hastie GD, Wilson B, Thompson PM. Fine-scale habitat selection by coastal bottlenose dolphins: Application of a new land-based video-montage technique. Can J Zool. 2003;81(3).

121. Kampa EM. Observations of a sonic-scattering layer during the total solar eclipse 30 June, 1973. Deep Res Oceanogr Abstr. 1975;22(6).

122. Last KS, Hobbs L, Berge J, Brierley AS, Cottier F. Moonlight Drives Ocean-Scale Mass Vertical Migration of Zooplankton during the Arctic Winter. Curr Biol [Internet]. 2016;26(2):244–51. Available from: http://dx.doi.org/10.1016/j.cub.2015.11.038

123. Martin AP, Richards KJ. Mechanisms for vertical nutrient transport within a North Atlantic mesoscale eddy. Deep Res Part II Top Stud Oceanogr. 2001;48(4–5):757–73.

124. Della Penna A, Gaube P. Mesoscale Eddies Structure Mesopelagic Communities. Front Mar Sci. 2020;7(July):1–9.

125. Legendre L. The significance of microalgal blooms for fisheries and for the export of particulate organic carbon in oceans. J Plankton Res. 1990;12(4):681–99.

126. Biktashev VN, Brindley J, Horwood JW. Phytoplankton blooms and fish recruitment rate. J Plankton Res. 2003;25(1):21–33.

127. Van De Wolfshaar KE, Daewel U, Hjøllo SS, Troost TA, Kreus M, Pätsch J, Ji R, Maar M. Sensitivity of the fish community to different prey fields and importance of spatial-seasonal patterns. Mar Ecol Prog Ser. 2021;680:79–95.

128. Houston AI, Carbone C. The optimal allocation of time during the diving cycle. Behav Ecol. 1992;3(3):255–65.

129. Macarthur RH, Pianka ER. On Optimal Use of a Patchy Environment Author (s): Robert H . MacArthur and Eric R . Pianka (Group E). 2011;100(916):603–9.

130. Haury L, Mcgowan J, Wiebe P. Spatial pattern in plankton communities. In: Steele JH, editor. Environmental Science. Boston, MA: Springer; 1978. p. 277–327.

131. Kotliar NB, Wiens JA. Nordic Society Oikos Multiple Scales of Patchiness and Patch Structure : A Hierarchical Framework for the Study of Heterogeneity Author (s): Natasha B . Kotliar and John A . Wiens Published by : Wiley on behalf of Nordic Society Oikos Stable URL : http: Oikos. 1990;59(2):253–60.

132. Rose GA, Leggett W. The Importance of Scale to Predator-Prey Spatial Correlations : An Example of Atlantic Fishes. Ecol Soc Am. 1990;71(1):33–43.

133. Bradbury IR, Snelgrove PVR, Pepin P. Passive and active behavioural contributions to patchiness and spatial pattern during the early life history of marine fishes. Mar Ecol Prog Ser. 2003;257:233–45.

134. Hamazaki T. Cetacean Habitats I N the Mid-Western. Mar Mammal Sci. 2002;18(4):920–39.

135. Best BD, Halpin PN, Read AJ, Fujioka E, Good CP, LaBrecque EA, Schick RS, Roberts JJ, Hazen LJ, Qian SS, Palka DL, Garrison LP, McLellan WA. Online cetacean habitat modeling system for the US East Coast and Gulf of Mexico. Endanger Species Res. 2012;18(1):1–15.

136. Roberts JJ, Best BD, Mannocci L, Fujioka E, Halpin PN, Palka DL, Garrison LP, Mullin KD, Cole TVN, Khan CB, McLellan WA, Pabst DA, Lockhart GG. Habitat-based cetacean density models for the U.S. Atlantic and Gulf of Mexico. Sci Rep [Internet]. 2016;6:1–12. Available from: http://dx.doi.org/10.1038/srep22615

137. Parks SE, Miksis-Olds JL, Denes SL. Assessing marine ecosystem acoustic diversity across ocean basins. Ecol Inform [Internet]. 2014;21:81–8. Available from: http://dx.doi.org/10.1016/j.ecoinf.2013.11.003

138. Campos-Cerqueira M, Aide TM. Improving distribution data of threatened species by combining acoustic monitoring and occupancy modelling. Methods Ecol Evol. 2016;7(11):1340–8.

139. Browning E, Gibb R, Glober-Kapfer P, Jones KE. Passive acoustic monitoring in ecology and conservation. Woking, UK: WWF-UK; 2017. 76 p.

140. Gibb R, Browning E, Glover-Kapfer P, Jones KE. Emerging opportunities and challenges for passive acoustics in ecological assessment and monitoring. Methods Ecol Evol. 2019;10(2):169–85.

141. Picciulin M, Kéver L, Parmentier E, Bolgan M. Listening to the unseen: Passive acoustic monitoring reveals the presence of a cryptic fish species. Aquat Conserv Mar Freshw Ecosyst. 2019;29(2):202–10.

142. Cohen RE, Frasier KE, Baumann-Pickering S, Wiggins SM, Rafter MA, Baggett LM,

Hildebrand JA. Identification of western North Atlantic odontocete echolocation click types using machine learning and spatiotemporal correlates [Internet]. Vol. 17, PLoS ONE. 2022. 1–37 p. Available from: http://dx.doi.org/10.1371/journal.pone.0264988

143. Core Team R. R: A language and environment for statistical computing. [Internet]. Vienna, Austria: R Foundation for Statistical Computing; 2020. Available from: https://www.r-project.org/

144. Thieurmel B, Elmarhraoui A. suncalc: Compute sun position, sunlight phases, moon position and lunar phase [Internet]. 2019. Available from: https://cran.r-project.org/package=suncal

145. Hastie TJ, Tibshirani RJ. Generalized additive models. Generalized Additive Models. 1986. p. 1–335.

146. Ferguson MC, Barlow J, Fiedler P, Reilly SB, Gerrodette T. Spatial models of delphinid (family Delphinidae) encounter rate and group size in the eastern tropical Pacific Ocean. Ecol Modell. 2006;193(3–4):645–62.

147. Redfern J V., Ferguson MC, Becker EA, Hyrenbach KD, Good C, Barlow J, Kaschner K, Baumgartner MF, Forney KA, Ballance LT, Fauchald P, Halpin P, Hamazaki T, Pershing AJ, Qian SS, Read A, Reilly SB, Torres L, Werner F. Techniques for cetacean-habitat modeling. Vol. 310, Marine Ecology Progress Series. 2006.

148. Forney KA, Ferguson MC, Becker EA, Fiedler PC, Redfern J V., Barlow J, Vilchis IL, Ballance LT. Habitat-based spatial models of cetacean density in the eastern Pacific Ocean. Endanger Species Res. 2012;16(2):113–33.

149. Forney KA, Becker EA, Foley DG, Barlow J, Oleson EM. Habitat-based models of cetacean density and distribution in the central North Pacific. Endanger Species Res. 2015;27(1).

150. Becker EA, Forney KA, Foley DG, Smith RC, Moore TJ, Barlow J. Predicting seasonal density patterns of California cetaceans based on habitat models. Endanger Species Res. 2014;23(1).

151. Frasier KE, Garrison LP, Soldevilla MS, Wiggins SM, Hildebrand JA. Cetacean distribution models based on visual and passive acoustic data. Sci Rep. 2021;11(1):1–16.

152. Liang KY, Zeger SL. Longitudinal data analysis using generalized linear models. Biometrika. 1986;73(1):13–22.

153. Pirotta E, Matthiopoulos J, MacKenzie M, Scott-Hayward L, Rendell L. Modelling sperm whale habitat preference: A novel approach combining transect and follow data. Mar Ecol Prog Ser. 2011;436(Whitehead 2003):257–72.

154. Benjamins S, van Geel N, Hastie G, Elliott J, Wilson B. Harbour porpoise distribution can vary at small spatiotemporal scales in energetic habitats. Deep Sea Res Part II Top Stud Oceanogr [Internet]. 2017 Jul;141:191–202. Available from: https://linkinghub.elsevier.com/retrieve/pii/S0967064516301849

155. Merkens KP, Simonis AE, Oleson EM. Geographic and temporal patterns in the acoustic detection of sperm whales Physeter macrocephalus in the central and western North Pacific

Ocean. Endanger Species Res. 2019;39:115–33.

156. Halekoh U, Højsgaard S, Yan J. The R package geepack for generalized estimating equations. J Stat Softw. 2006;15(2):1–11.

157. Wang W, Yan J. Shape-Restricted Regression Splines with R Package splines2. J Data Sci. 2021;19(July):498–517.

158. Pan W. Goodness-of-fit tests for GEE with correlated binary data. Scand J Stat. 2002;29(1):101–10.

159. Henderson EE, Martin SW, Manzano-Roth R, Matsuyama BM. Occurrence and Habitat Use of Foraging Blainville's Beaked Whales (Mesoplodon densirostris) on a U.S. Navy Range in Hawaii. Aquat Mamm [Internet]. 2016 Dec 1;42(4):549–62. Available from: http://www.aquaticmammalsjournal.org/index.php?option=com_content&view=article&id=1537:occurrence-and-habitat-use-of-foraging-blainville-s-beaked-whales-mesoplodon-densirostris-on-a-u-s-navy-range-in-hawaii&catid=150&Itemid=157

160. Owen K, Andrews RD, Baird RW, Schorr GS, Webster DL. Lunar cycles influence the diving behavior and habitat use of short-finned pilot whales around the main Hawaiian Islands. Mar Ecol Prog Ser. 2019;629:193–206.

161. van Haren H, Compton TJ. Diel Vertical Migration in Deep Sea Plankton Is Finely Tuned to Latitudinal and Seasonal Day Length. PLoS One. 2013;8(5).

162. Doya C, Aguzzi J, Pardo M, Matabos M, Company JB, Costa C, Mihaly S, Canals M. Diel behavioral rhythms in sablefish (Anoplopoma fimbria) and other benthic species, as recorded by the Deep-sea cabled observatories in Barkley canyon (NEPTUNE-Canada). J Mar Syst [Internet]. 2014;130:69–78. Available from: http://dx.doi.org/10.1016/j.jmarsys.2013.04.003

163. Hildebrand JA, Frasier KE, Baumann-Pickering S, Wiggins SM, Merkens KP, Garrison LP, Soldevilla MS, McDonald MA. Assessing seasonality and density from passive acoustic monitoring of signals presumed to be from pygmy and dwarf sperm whales in the gulf of Mexico. Front Mar Sci. 2019;6(FEB).

164. Gaskin DE. The harbor porpoise Phocoena phocoena (L.): Regional populations, status, and information on direct and indirect catches. 1984.

165. Gelman A, Hill J. Data analysis using regression and multilevel/hierarchical models. Cambridge, UK: Cambridge University Press; 2006.

166. Yack TM, Barlow J, Roch MA, Klinck H, Martin S, Mellinger DK, Gillespie D. Comparison of beaked whale detection algorithms. Appl Acoust [Internet]. 2010;71(11):1043–9. Available from: http://dx.doi.org/10.1016/j.apacoust.2010.04.010

167. Reilly SB, Fiedler PC. Interannual variability of dolphin habitats in the eastern tropical Pacific. I:Research vessel surveys, 1986-1990. Fish Bull. 1994;92(2):434–50.

168. Fullard KJ, Early G, Heide-JØrgensen MP, Bloch D, Rosing-Asvid A, Amos W. Population structure of long-finned pilot whales in the North Atlantic: A correlation with sea surface

temperature? Mol Ecol. 2000;9(7):949–58.

169. Doksæter L, Olsen E, Nøttestad L, Fernö A. Distribution and feeding ecology of dolphins along the Mid-Atlantic Ridge between Iceland and the Azores. Deep Res Part II Top Stud Oceanogr. 2008;55(1–2):243–53.

170. McCullough JLK, Wren JLK, Oleson EM, Allen AN, Siders ZA, Norris ES. An Acoustic Survey of Beaked Whales and Kogia spp. in the Mariana Archipelago Using Drifting Recorders. Front Mar Sci. 2021;8(June):1–15.

171. Baumann-Pickering S, Roch MA, Brownell RL, Simonis AE, McDonald MA, Solsona-Berga A, Oleson EM, Wiggins SM, Hildebrand JA. Spatio-temporal patterns of beaked whale echolocation signals in the North Pacific. PLoS One. 2014;9(1).

172. Stanistreet JE, Nowacek DP, Baumann-Pickering S, Bell JT, Cholewiak DM, Hildebrand JA, Hodge LEW, Moors-Murphy HB, Van Parijs SM, Read AJ. Using passive acoustic monitoring to document the distribution of beaked whale species in the western north atlantic ocean. Can J Fish Aquat Sci. 2017;74(12):2098–109.

173. Kowarski K, Delarue J, Martin B, O'Brien J, Meade R, Cadhla O, Berrow S. Signals from the deep: Spatial and temporal acoustic occurrence of beaked whales off western Ireland. PLoS One. 2018;13(6):1–26.

174. Rice A, Širović A, Trickey JS, Debich AJ, Gottlieb RS, Wiggins SM, Hildebrand JA, Baumann-Pickering S. Cetacean occurrence in the Gulf of Alaska from long-term passive acoustic monitoring. Mar Biol. 2021;168(5).

175. Bearzi M. Habitat Partitioning by Three Species of Dolphins in Santa Monica Bay, California. Bull South Calif Acad Sci. 2005;104(3):113–24.

176. Clarke MR, Pascoe PL. The stomach contents of a risso's dolphin (grampus griseus) stranded at thurlestone, South Devon. J Mar Biol Assoc United Kingdom. 1985;65(3):663–5.

177. Clarke MR. Cephalopods from the stomachs of a risso's dolphin (grampus griseus) from the mediterranean. J Mar Biol Assoc United Kingdom. 1992;72(4):861–7.

178. González, A. F., López, A., Guerra, A., Barreiro A. Fisheries Research Volume 21 issue 1-2 1994 [doi 10.1016_0165-7836(94)90103-1] A.F. González; A. López; A. Guerra; A. Barreiro - - Diets of marine mammals stranded on the northwestern Spanish Atl.pdf. 1994;21:179–91.

179. Blanco C, Raduán MÁ, Raga JA. <Blanco_etal_2006_Risso dolphin diet in Med.pdf>. 2006;70(September):407–11.

180. Wang MC, Shao KT, Huang SL, Chou LS. Food partitioning among three sympatric odontocetes (Grampus griseus, Lagenodelphis hosei, and Stenella attenuata). Mar Mammal Sci. 2012;28(2):143–57.

181. Plön S, Heyns-Veale ER, Smale MJ, Froneman PW. Life history parameters and diet of Risso's dolphins, Grampus griseus, from southeastern South Africa. Mar Mammal Sci. 2020;36(3):786–801.

182. Luna A, Sánchez P, Chicote C, Gazo M. Cephalopods in the diet of Risso's dolphin (Grampus griseus) from the Mediterranean Sea: A review. Mar Mammal Sci. 2022;38(2):725–41.

183. Mintzer VJ, Gannon DP, Barros NB, Read AJ. Stomach contents of mass-stranded short-finned pilot whales (Globicephala macrorhynchus) from North Carolina. Mar Mammal Sci. 2008;24(2):290–302.

184. Sinclair EH. Stomach Contents of Four Short-Finned Pilot Whales (Globicephala Macrorhynchus) From the Southern California Bight. Mar Mammal Sci. 1992;8(1):76–81.

185. Hernández-García V, Martín VM. Stomach Contents of two Short-finned Pilot Whale (Globicephala macrorhynchus Gray, 1846) (Cetacea, Delphinidae) off the Canary Islands: A Preliminary Note. Int Counc Explor Sea Mar Mamm Comm. 1994;16:1–9.

186. Barlow J, Schorr G, Falcone E, Moretti D. Variation in dive behavior of Cuvier's beaked whales with seafloor depth, time-of-day, and lunar illumination. Mar Ecol Prog Ser [Internet]. 2020 Jun 25;644:199–214. Available from: https://www.int-res.com/abstracts/meps/v644/p199-214/

187. West KL, Walker WA, Baird RW, Mead JG, Collins PW. Diet of Cuvier's beaked whales Ziphius cavirostris from the North Pacific and a comparison with their diet world-wide. Mar Ecol Prog Ser. 2017;574:227–42.

188. F. V, G. OM, A. KO, T. MP, M. J. Sowerby's beaked whale biosonar and movement strategy indicate deep-sea foraging niche differentiation in mesoplodont whales. J Exp Biol. 2022;

189. Ecology S, Aug N, Chesson P. Behavior , Heterogeneity , and the Dynamics of Interacting Species Author (s): Peter Chesson and Michael Rosenzweig Stable URL : http://www.jstor.org/stable/1941092 REFERENCES Linked references are available on JSTOR for this article : You may need to l. 2016;72(4):1187–95.

190. Arjo WM, Pletscher DH. Behavioral responses of coyotes to wolf recolonization in northwestern Montana. Can J Zool. 1999;77(12):1919–27.

191. Vanak AT, Fortin D, Thaker M, Ogden M, Owen C, Greatwood S, Slotow R. Moving to stay in place: Behavioral mechanisms for coexistence of African large carnivores. Ecology. 2013;94(11):2619–31.

192. Papastamatiou YP, Bodey TW, Friedlander AM, Lowe CG, Bradley D, Weng K, Priestley V, Caselle JE. Spatial separation without territoriality in shark communities. Oikos. 2018;127(6):767–79.

193. Perrin WF, Evans WE, Holts DB. Movements of pelagic dolphins (Stenella Spp .) in the eastern tropical Pacific as indicated by results of tagging, with summary of tagging operations, 1969-76. NOAA Tech Rep [Internet]. 1979;(1967):1–14. Available from: http://swfsc.noaa.gov/publications/CR/1979/7928.PDF

194. Reilly S. Seasonal changes in distribution and habitat differences among dolphins in the eastern tropical Pacific. Mar Ecol Prog Ser. 1990;66(1985):1–11.

195. Elwen S, Meÿer MA, Best PB, Kotze PGH, Thornton M, Swanson S. Range and movements of female heaviside's dolphins (Cephalorhynchus heavisidii), as determined by satellite-linked telemetry. J Mammal. 2006;87(5):866–77.

196. Abecassis M, Polovina J, Baird RW, Copeland A, Drazen JC, Domokos R, Oleson E, Jia Y, Schorr GS, Webster DL, Andrews RD. Characterizing a foraging hotspot for short-finned pilot whales and blainville's beaked whales located off the west side of Hawai'i island by using tagging and oceanographic data. PLoS One. 2015;10(11).

197. M Copeland A. Influences of Temporal Changes in Pelagic Scattering Layers on Short-Finned Pilot Whales Behavior. Oceanogr Fish Open access J. 2019;9(2):1–12.

198. Simonis AE. By the Light of the Moon: North Pacific Dolphins Optimize Foraging with the Lunar Cycle. UC San Diego Electron Theses Diss. 2017;117.

199. Benoit-Bird KJ, Southall BL, Moline MA. Dynamic foraging by Risso's dolphins revealed in four dimensions. Mar Ecol Prog Ser. 2019;632:221–34.

200. Jensen FH, Keller OA, Tyack PL, Visser F. Dynamic biosonar adjustment strategies in deep-diving Risso's dolphins driven partly by prey evasion. J Exp Biol. 2020;223(3).

201. Visser F, Keller OA, Oudejans MG, Nowacek DP, Kok ACM, Huisman J, Sterck EHM. Risso's dolphins perform spin dives to target deep-dwelling prey. R Soc Open Sci. 2021;8(12).

202. Soldevilla MS, Wiggins SM, Hildebrand JA. Spatio-temporal comparison of Pacific white-sided dolphin echolocation click types. Aquat Biol. 2010;9(1):49–62.

203. Aoki K, Amano M, Yoshioka M, Mori K, Tokuda D, Miyazaki N. Diel diving behavior of sperm whales off Japan. Mar Ecol Prog Ser [Internet]. 2007 Nov 8;349:277–87. Available from: http://www.int-res.com/abstracts/meps/v349/p277-287/

204. Baird RW, Webster DL, Schorr GS, McSweeney DJ, Barlow J. Diel variation in beaked whale diving behavior. Mar Mammal Sci. 2008;24(3):630–42.

205. van Haren H. Monthly periodicity in acoustic reflections and vertical motions in the deep ocean. Geophys Res Lett. 2007;34(12):1–5.

206. Plueddemann AJ, Pinkel R. Characterization of the patterns of diel migration using a Doppler sonar. Deep Sea Res Part A, Oceanogr Res Pap. 1989;36(4):509–30.

207. Stewart BS. Diving Behavior. In: Würsig B, Thewissen JGM, Kovacs KM, editors. Encyclopedia of Marine Mammals. 3rd ed. London, UK; 2018. p. 262–7.

208. Pusineri C, Magnin V, Meynier L, Spitz J, Hassani S, Ridoux V. Food and feeding ecology of the common dolphin (Delphinus delphis) in the oceanic Northeast Atlantic and comparison with its diet in neritic areas. Mar Mammal Sci. 2007;23(1):30–47.

209. Henderson EE, Hildebrand JA, Smith MH, Falcone EA. The behavioral context of common dolphin (Delphinus sp.) vocalizations. Mar Mammal Sci. 2012;28(3):439–60.

210. Aguilar Soto N, Johnson MP, Madsen PT, Díaz F, Domínguez I, Brito A, Tyack P. Cheetahs of the deep sea: Deep foraging sprints in short-finned pilot whales off Tenerife (Canary Islands). J Anim Ecol. 2008;77(5):936–47.

211. Quick NJ, Isojunno S, Sadykova Di, Bowers M, Nowacek DP, Read AJ. Hidden Markov models reveal complexity in the diving behaviour of short-finned pilot whales. Sci Rep. 2017;7:1–12.

212. Baird RW, McSweeney DJ, Heithaus MR, Marshall GJ. SHORT-FINNED PILOT WHALE DIVING BEHAVIOR: DEEP FEEDERS AND DAYTIME SOCIALITES. In: Abstract submitted to the 15th Biennial Conference on the Biology of Marine Mammals. Greensboro, NC; 2003.

213. Wells RS, Fougeres EM, Cooper AG, Stevens RO, Brodsky M, Lingenfelser R, Dold C, Douglas DC. Movements and Dive Patterns of Short-Finned Pilot Whales (Globicephala macrorhynchus) Released from a Mass Stranding in the Florida Keys. Aquat Mamm. 2013;39(1):61–72.

214. Tyson Moore RB, Douglas DC, Nollens HH, Croft L, Wells RS. Post-release monitoring of a stranded and rehabilitated short-finned pilot whale (Globicephala macrorhynchus) reveals current-assisted travel. Aquat Mamm. 2020;46(2):200–14.

215. Grinnell J. The Niche-Relationships of the California Thrasher Author (s): Joseph Grinnell Published by : Oxford University Press Stable URL : https://www.jstor.org/stable/4072271. Auk. 1917;34(4):427–33.

216. Hutchinson GE. Homage to Santa Rosalia or Why Are There So Many Kinds of Animals ? Published by : The University of Chicago Press for The American Society of Naturalists Stable URL : https://www.jstor.org/stable/2458768 REFERENCES Linked references are available on JSTO. Am Nat [Internet]. 1959;93(870):145–59. Available from: D-494

217. Gangopadhyay A, Gawarkiewicz G, Silva ENS, Monim M, Clark J. An Observed Regime Shift in the Formation of Warm Core Rings from the Gulf Stream. Sci Rep. 2019;9(1):1–9.

218. Silver A, Gangopadhyay A, Gawarkiewicz G, Silva ENS, Clark J. Interannual and seasonal asymmetries in Gulf Stream Ring Formations from 1980 to 2019. Sci Rep [Internet]. 2021;11(1):1–7. Available from: https://doi.org/10.1038/s41598-021-81827-y

219. Lee TN, Atkinson P. Low-frequency current and temperature variability from Gulf Stream frontal eddies and atmospheric forcing along the southeast U.S. outer continental shelf. J Geophys Res. 1983;88:4541–67.

220. Gangopadhyay A, Gawarkiewicz G, Silva ENS, Silver AM, Monim M, Clark J. A Census of the Warm-Core Rings of the Gulf Stream: 1980–2017. J Geophys Res Ocean. 2020;125(8):1–17.

221. Halliwell GR, Mooers CNK. The space time structure and variability of shelf water-slope water and Gulf stream temperatures fronts and associated warm-core eddies. J Geophys Res. 1979;84(C12, Dec.20, 1979):7707–25.

222. Chavez-Rosales S, Palka DL, Garrison LP, Josephson EA. Environmental predictors of habitat suitability and occurrence of cetaceans in the western North Atlantic Ocean. Sci Rep. 2019;9(1):1–11.

223. Correia AM, Tepsich P, Rosso M, Caldeira R, Sousa-Pinto I. Cetacean occurrence and spatial distribution: Habitat modelling for offshore waters in the Portuguese EEZ (NE Atlantic). J Mar Syst [Internet]. 2015;143:73–85. Available from: http://dx.doi.org/10.1016/j.jmarsys.2014.10.016

224. Metzger EJ, Helber RW, Hogan PJ, Posey PG, Thoppil PG, Townsend TL, Wallcraft AJ, Smedstad OM, Franklin DS. Global ocean Forecast System 3.1 Validation Testing. 2017.

225. Zammit-Mangion A, Huang H. Enhanced False Detection Rate of Images in the Wavelet Domain. 2014.

226. Rieck JK, Böning CW, Greatbatch RJ, Scheinert M. Seasonal variability of eddy kinetic energy in a global high-resolution ocean model. Geophys Res Lett. 2015;42(21):9379–86.

227. Pegliasco C, Delepoulle A, Mason E, Morrow R, Faugère Y, Dibarboure G. META3.1exp: a new global mesoscale eddy trajectory atlas derived from altimetry. Earth Syst Sci Data. 2022;14(3):1087–107.

228. Jensen FH, Perez JM, Johnson M, Soto NA, Madsen PT. Calling under pressure: Short-finned pilot whales make social calls during deep foraging dives. Proc R Soc B Biol Sci. 2011;278(1721):3017–25.

229. Tyack PL, Johnson M, Soto NA, Sturlese A, Madsen PT. Extreme diving of beaked whales. J Exp Biol. 2006;209(21):4238–53.

230. Watwood SL, Miller PJO, Johnson M, Madsen PT, Tyack PL. Deep-diving foraging behaviour of sperm whales (Physeter macrocephalus). J Anim Ecol. 2006;75(3):814–25.

231. Mcalpine DF, Murison LD, Hoberg EP. New records for the pygmy sperm whale, Kogia breviceps (physeteridae) from Atlantic Canada with notes on diet and parasites. Mar Mammal Sci. 1997;13(4):701–4.

232. Becker EA, Carretta J V., Forney KA, Barlow J, Brodie S, Hoopes R, Jacox MG, Maxwell SM, Redfern J V., Sisson NB, Welch H, Hazen EL. Performance evaluation of cetacean species distribution models developed using generalized additive models and boosted regression trees. Ecol Evol. 2020;10(12):5759–84.

233. Wood SN. Fast stable restricted maximum likelihood and marginal likelihood estimation of semiparametric generalized linear models. J R Stat Soc. 2011;73(1):3–36.

234. Akaike H. Information theory and an extension of the maximum likelihood principle. In: Petrov B., Csaki F, editors. The Second International Symposium on Information Theory. 1973. p. 267–81.

235. Bartoń K. MuMIn: Multi-Model Inference [Internet]. 2022. Available from: https://cran.r-

project.org/package=MuMIn

236. Menza C, Kinlan B, Dorfman DS, Poti M, Caldow C. A biogeographic assessment of seabirds, deep sea corals and ocean habitats of the New York Bight: science to support offshore spatial planning. NOAA. NOAA Tech Memo NOS NCCOS 141 [Internet]. 2012;224. Available from: http://ccma.nos.noaa.gov/ecosystems/coastalocean/ny_spatialplanning.aspx

237. Thorne LH, Foley HJ, Baird RW, Webster DL, Swaim ZT, Read AJ. Movement and foraging behavior of short-finned pilot whales in the Mid-Atlantic Bight: Importance of bathymetric features and implications for management. Mar Ecol Prog Ser. 2017;584:245–57.

238. Waring GT, Fairfield CP, Ruhsam CM, Sano M. Sperm whales associated with Gulf Stream features off the north-eastern USA shelf. Fish Oceanogr. 1993;2(2):101–5.

239. Worthington L V. The 18° water in the Sargasso Sea. Deep Sea Res. 1958;5(2–4):297–305.

240. Talley LD, Raymer ME. Eighteen degree water variability. J Mar Res. 1982;40.

241. Blanton JO, Atkinson LP, Pietrafesa LJ, Lee TN. The intrusion of Gulf Stream water across the continental shelf due to topographically-induced upwelling. Deep Sea Res Part A, Oceanogr Res Pap. 1981;28(4):393–405.

242. Yoder JA, Atkinson LP, Bishop SS, Blanton JO, Lee TN, Pietrafesa L. Phytoplankton dynamics within Gulf Stream intrusions on the southeastern United States continental shelf during summer 1981. Cont Shelf Res. 1985;4(6):611–35.

243. McClain CR, Atkinson LP. A note on the Charleston Gyre. J Geophys Res. 1985;90(C6):857–62.

244. Lee TN, Yoder JA, Atkinson LP. Gulf Stream frontal eddy influence on productivity of the southeast US Continental Shelf. J Geophys Res. 1991;96(C12):191–205.

245. Zhang WG, Gawarkiewicz GG. Dynamics of the direct intrusion of Gulf Stream ring water onto the Mid-Atlantic Bight shelf. Geophys Res Lett. 2015;42(18):7687–95.

246. Csanady GT. The birth and death of a warm core ring. J Geophys Res. 1979;84:777–80.

247. Dufois F, Hardman-Mountford NJ, Greenwood J, Richardson AJ, Feng M, Matear RJ. Anticyclonic eddies are more productive than cyclonic eddies in subtropical gyres because of winter mixing. Sci Adv. 2016;2(5):1–7.

248. Dufois F, Hardman-Mountford NJ, Greenwood J, Richardson AJ, Feng M, Herbette S, Matear R. Impact of eddies on surface chlorophyll in the South Indian Ocean. J Geophys Res Ocean [Internet]. 2014;(119):3868–82. Available from: http://onlinelibrary.wiley.com/doi/10.1002/jgrc.20353/abstract

249. Chelton DB, Gaube P, Schlax MG, Early JJ, Samelson RM. The influence of nonlinear mesoscale eddies on near-surface oceanic chlorophyll. Science (80-). 2011;334(6054):328–32.

250. McGillicuddy Jr. DJ, Anderson LA, Bates NR, Bibby T, Buesseler KO, Carlson CA, Davis DS,

Ewart C, Falkowski PG, Goldthwait SA, Hansell DA, Jenkins WJ, Johnson R, Kosnyrev VK, Ledwell JR, Li QP, Siegel DA, Steinberg DK. Eddy / Wind Interactions Stimulate Extraordinary Mid-Ocean Plankton Blooms. Science (80-). 2007;0(May):1021–6.

251. Falkowski PG, Ziemann D, Kolber Z, Bienfangt PK. Role of eddy pumping in enhancing primary production in the ocean. Nature. 1991;352(July):55–8.

252. McGillicuddy DJ. Mechanisms of Physical-Biological-Biogeochemical Interaction at the Oceanic Mesoscale. Vol. 8, Annual Review of Marine Science. 2016. 125–159 p.

253. Woodworth PA, Schorr GS, Baird RW, Webster DL, Mcsweeney DJ, Hanson MB, Andrews RD, Polovina JJ. Eddies as offshore foraging grounds for melon-headed whales (Peponocephala electra). Mar Mammal Sci. 2012;28(3):638–47.

254. Griffin RB. Sperm whale distributions and community ecology associated with a warm-core ring off Georges Bank. Mar Mammal Sci. 1999;15(1):33–51.

255. Tynan CT. Cetacean distributions and oceanographic features near the Kerguelen Plateau. Geophys Res Lett. 1997;24(22):2793–6.

256. Davis RW, Ortega-Ortiz JG, Ribic CA, Evans WE, Biggs DC, Ressler PH, Cady RB, Leben RR, Mullin KD, Würsig B. Cetacean habitat in the northern oceanic Gulf of Mexico. Deep Res Part I Oceanogr Res Pap. 2002;49(1):121–42.

257. Sabatés A, Martín P, Lloret J, Raya V. Sea warming and fish distribution: The case of the small pelagic fish, Sardinella aurita, in the Twestern Mediterranean. Glob Chang Biol. 2006;12(11):2209–19.

258. Genner MJ, Halliday NC, Simpson SD, Southward AJ, Hawkins SJ, Sims DW. Temperature-driven phenological changes within a marine larval fish assemblage. J Plankton Res. 2010;32(5):699–708.

259. Lei Y, Xu K, Ki Choi J, Pyo Hong H, Wickham SA. Community structure and seasonal dynamics of planktonic ciliates along salinity gradients. Eur J Protistol [Internet]. 2009;45(4):305–19. Available from: http://dx.doi.org/10.1016/j.ejop.2009.05.002

260. Arranz P, Benoit-Bird KJ, Southall BL, Calambokidis J, Friedlaender AS, Tyack PL. Risso's dolphins plan foraging dives. J Exp Biol. 2018;221(4).

261. Szesciorka AR, Ballance LT, Širović A, Rice A, Ohman MD, Hildebrand JA, Franks PJS. Timing is everything: Drivers of interannual variability in blue whale migration. Sci Rep. 2020;10(1):1–9.

262. Breen P, Brown S, Reid D, Rogan E. Modelling cetacean distribution and mapping overlap with fisheries in the northeast Atlantic. Ocean Coast Manag [Internet]. 2016;134:140–9. Available from: http://dx.doi.org/10.1016/j.ocecoaman.2016.09.004

263. Tepsich P, Rosso M, Halpin PN, Moulins A. Habitat preferences of two deep-diving cetacean species in the northern Ligurian Sea. Mar Ecol Prog Ser. 2014;508:247–60.

264. Moors-Murphy HB. Submarine canyons as important habitat for cetaceans, with special reference to the Gully: A review. Deep Res Part II Top Stud Oceanogr [Internet]. 2014;104:6–19. Available from: http://dx.doi.org/10.1016/j.dsr2.2013.12.016

265. Moulins A, Rosso M, Nani B, Würtz M. Aspects of the distribution of Cuvier's beaked whale (Ziphius cavirostris) in relation to topographic features in the Pelagos Sanctuary (north-western Mediterranean Sea). J Mar Biol Assoc United Kingdom. 2007;87(1):177–86.

266. Verfuss UK, Aniceto AS, Harris D V., Gillespie D, Fielding S, Jiménez G, Johnston P, Sinclair RR, Sivertsen A, Solbø SA, Storvold R, Biuw M, Wyatt R. A review of unmanned vehicles for the detection and monitoring of marine fauna. Mar Pollut Bull [Internet]. 2019;140(February 2018):17–29. Available from: https://doi.org/10.1016/j.marpolbul.2019.01.009

267. Sathyendranath S, Brewin RJW, Brockmann C, Brotas V, Calton B, Chuprin A, Cipollini P, Couto AB, Dingle J, Doerffer R, Donlon C, Dowell M, Farman A, Grant M, Groom S, Horseman A, Jackson T, Krasemann H, Lavender S, et al. An ocean-colour time series for use in climate studies: The experience of the ocean-colour climate change initiative (OC-CCI). Sensors (Switzerland). 2019;19(19).

SIGHTING DATA SOURCES

1. Ampela, K. and C. Bacon. 2018. VACAPES PAX Vessel Opportunistic Sightings July 2015 - Nov 2017. Data downloaded from OBIS-SEAMAP (http://seamap.env.duke.edu/dataset/1815) on 2018-09-18.

2. Ampela, K. and G. Miller-Francisco. 2016. JAX FIREX Aerial Surveys 5-8 September 2012. Data downloaded from OBIS-SEAMAP (http://seamap.env.duke.edu/dataset/880) on 2019-09-18.

3. Barco, S. 2013. Virginia Aquarium Marine Mammal Strandings 1988-2008. Data downloaded from OBIS-SEAMAP (http://seamap.env.duke.edu/dataset/502) on 2019-09-18 and 2021-03-04.

4. Barco, S. 2014. Virginia and Maryland Sea Turtle Research and Conservation Initiative Aerial Survey Sightings, May 2011 through July 2013. Data downloaded from OBIS-SEAMAP (http://seamap.env.duke.edu/dataset/1201) on 2019-09-18.

5. Barco, S. 2015. Marine Mammal and Sea Turtle Sightings in the Vicinity of the Maryland Wind Energy Area 2013-2015. Data downloaded from OBIS-SEAMAP (http://seamap.env.duke.edu/dataset/1340) on 2019-09-18.

6. Barco, S. 2015. Virginia CZM Wind Energy Area Survey - Left side - May 2014 through December 2014. Data downloaded from OBIS-SEAMAP (http://seamap.env.duke.edu/dataset/1229) on 2019-09-18.

7. Barco, S. 2015. Virginia CZM Wind Energy Area Survey - Right side - May 2014 through December 2014. Data downloaded from OBIS-SEAMAP (http://seamap.env.duke.edu/dataset/1231) on 2019-09-18.

8. Barco, S. 2015. Virginia CZM Wind Energy Area Survey- Right side - November 2012 through April 2014. Data downloaded from OBIS-SEAMAP (http://seamap.env.duke.edu/dataset/1194) on 2019-09-18.

9. Barco, S. 2016. Virginia CZM Wind Energy Area Survey- Left side - November 2012 through April 2014. Data downloaded from OBIS-SEAMAP (http://seamap.env.duke.edu/dataset/1192) on 2019-09-18.

10. Boisseau, O. 2014. Visual sightings from Song of the Whale 1993-2013. Data downloaded from OBIS-SEAMAP (http://seamap.env.duke.edu/dataset/1158) on 2019-09-18, 2019-10-11, and 2021-03-04.

11. Boisseau, O. 2019. Sightings from R/V Song of the Whale during the spring 2019 MAPS survey (NMFS permit 14809). Data downloaded from OBIS-SEAMAP (http://seamap.env.duke.edu/dataset/2001) on 2019-10-18 and 2021-03-04.

12. Boisseau, O. 2019. Sightings from R/V Song of the Whale during the winter 2019 MAPS survey (NMFS permit 14809). Data downloaded from OBIS-SEAMAP (http://seamap.env.duke.edu/dataset/1999) on 2019-09-18 and 2021-03-04.

13. Cole, T. and C. Khan. 2016. NEFSC Right Whale Aerial Survey. Data downloaded from OBIS-SEAMAP (http://seamap.env.duke.edu/dataset/513) on 2019-09-18, 2019-10-11, and 2021-03-04.

14. Contillo, J. 2013. SEFSC Dolphin Photo ID. Data downloaded from OBIS-SEAMAP (http://seamap.env.duke.edu/dataset/226) on 2019-09-18.

15. Cotter, M. P. 2020. VACAPES NFC Aerial Surveys 2018-2019. Data downloaded from OBIS-SEAMAP (http://seamap.env.duke.edu/dataset/2059) on 2021-03-04.

16. DFO. (2017). DFO Maritimes Region Cetacean Sightings. Version 7 In OBIS Canada Digital Collections. Bedford Institute of Oceanography, Dartmouth, NS, Canada. Published by OBIS, Digital http://www.iobis.org/. Accessed on 2021-03-04.

17. Dias, L. and L. Garrison. 2018. AMAPPS Southeast Aerial Cruise Fall 2016. Data downloaded from OBIS-SEAMAP (http://seamap.env.duke.edu/dataset/1854) on 2019-09-18.

18. Dias, L. and L. Garrison. 2018. AMAPPS Southeast Aerial Cruise Fall 2017. Data downloaded from OBIS-SEAMAP (http://seamap.env.duke.edu/dataset/1858) on 2019-09-18.

19. Dias, L. and L. Garrison. 2018. AMAPPS Southeast Aerial Cruise Spring 2014. Data downloaded from OBIS-SEAMAP (http://seamap.env.duke.edu/dataset/1850) on 2019-09-18 and 2021-03-04.

20. Dias, L. and L. Garrison. 2018. AMAPPS Southeast Aerial Cruise Spring 2017. Data downloaded from OBIS-SEAMAP (http://seamap.env.duke.edu/dataset/1860) on 2019-09-18 and 2021-03-04.

21. Dias, L. and L. Garrison. 2018. AMAPPS Southeast Aerial Cruise Summer 2016. Data downloaded from OBIS-SEAMAP (http://seamap.env.duke.edu/dataset/1856) on 2019-09-18 and 2021-03-04.

22. Dias, L. and L. Garrison. 2018. AMAPPS Southeast Aerial Cruise Winter 2015. Data downloaded from OBIS-SEAMAP (http://seamap.env.duke.edu/dataset/1852) on 2019-09-18.

23. Dias, L. and L. Garrison. 2019. AMAPPS Southeast Aerial Cruise Spring 2019. Data downloaded from OBIS-SEAMAP (http://seamap.env.duke.edu/dataset/2036) on 2019-09-18 and 2021-03-04.

24. Dias, L. and L. Garrison. 2019. AMAPPS Southeast Shipboard Cruise Summer 2016. Data downloaded from OBIS-SEAMAP (http://seamap.env.duke.edu/dataset/1974) on 2019-09-18, 2019-10-11, and 2021-03-04.

25. Dias, L. and L. Garrison. 2020. AMAPPS Southeast Aerial Cruise Winter 2019-2020. Data downloaded from OBIS-SEAMAP (http://seamap.env.duke.edu/dataset/2053) on 2019-09-18.

26. Diaz, G. 2011. NOAA Southeast Fishery Science Center (SEFSC) Commercial Pelagic Observer Program (POP) Data. Data downloaded from OBIS-SEAMAP (http://seamap.env.duke.edu/dataset/103151496) on 2019-09-18 and 2021-03-04 and originated from iOBIS (http:www.iobis.org).

27. DiMatteo, A. 2014. Christopher Newport University bottlenose dolphin sightings in Virginia estuaries 2000-2006. Data downloaded from OBIS-SEAMAP (http://seamap.env.duke.edu/dataset/1074) on 2019-09-18.

28. Dunn, C. 2006. Bahamas Marine Mammal Research Organisation Aerial Survey. Data downloaded from OBIS-SEAMAP (http://seamap.env.duke.edu/dataset/330) on 2019-09-18 and 2021-03-04.

29. Dunn, C. 2006. Bahamas Marine Mammal Research Organisation Strandings. Data downloaded from OBIS-SEAMAP (http://seamap.env.duke.edu/dataset/327) on 2019-09-18, 2019-10-11, and 2021-03-04.

30. Dunn, C. 2013. Bahamas Marine Mammal Research Organisation On-transect Sightings. Data downloaded from OBIS-SEAMAP (http://seamap.env.duke.edu/dataset/328) on 2019-09-18, 2019-10-11, and 2021-03-04.

31. Dunn, C. 2013. Bahamas Marine Mammal Research Organisation Opportunistic Sightings. Data downloaded from OBIS-SEAMAP (http://seamap.env.duke.edu/dataset/329) on 2019-09-18, 2019-10-11, and 2021-03-04.

32. Engelhaupt, A. 2019. VACAPES Vessel Nearshore Humpback Whale Monitoring 2015. Data downloaded from OBIS-SEAMAP (http://seamap.env.duke.edu/dataset/2003) on 2019-09-18.

33. Engelhaupt, A. 2020. VACAPES Offshore Study Area Observations 2015-2018. Data downloaded from OBIS-SEAMAP (http://seamap.env.duke.edu/dataset/2066) on 2019-09-18 and 2021-03-04.

34. Garrison, L. 2013. SEFSC Atlantic surveys 1992. Data downloaded from OBIS-SEAMAP (http://seamap.env.duke.edu/dataset/3) on 2019-09-18 and 2021-03-04.

35. Garrison, L. 2013. SEFSC Atlantic surveys 1999. Data downloaded from OBIS-SEAMAP (http://seamap.env.duke.edu/dataset/5) on 2019-09-18 and 2021-03-04.

36. Garrison, L. 2013. SEFSC Atlantic surveys, 1998 (3). Data downloaded from OBIS-SEAMAP (http://seamap.env.duke.edu/dataset/1) on 2019-09-18 and 2021-03-04.

37. Garrison, L. 2013. SEFSC Mid-Atlantic Tursiops Survey, 1995 (1). Data downloaded from OBIS-SEAMAP (http://seamap.env.duke.edu/dataset/90) on 2019-09-18.

38. Garrison, L. 2013. SEFSC Mid-Atlantic Tursiops Survey, 1995 2. Data downloaded from OBIS-SEAMAP (http://seamap.env.duke.edu/dataset/89) on 2019-09-18.

39. Garrison, L. 2013. SEFSC Mid-Atlantic Tursiops Survey, 1995 3. Data downloaded from OBIS-SEAMAP (http://seamap.env.duke.edu/dataset/88) on 2019-09-18.

40. Garrison, L. 2013. SEFSC Southeast Cetacean Aerial Survey 1992. Data downloaded from OBIS-SEAMAP (http://seamap.env.duke.edu/dataset/87) on 2019-09-18.

41. Garrison, L. 2013. SEFSC Southeast Cetacean Aerial Survey 1995. Data downloaded from OBIS-SEAMAP (http://seamap.env.duke.edu/dataset/86) on 2019-09-18 and 2021-03-04.

42. Gowan, T. 2019. SEUS Right Whale EWS Aerial Surveys 2016-17. Data downloaded from OBIS-SEAMAP (http://seamap.env.duke.edu/dataset/1990) on 2019-09-18.

43. Gowan, T. 2019. SEUS Right Whale EWS Aerial Surveys 2018-19. Data downloaded from OBIS-SEAMAP (http://seamap.env.duke.edu/dataset/2004) on 2019-09-18.

44. Gowan, T. and B. Zoodsma. 2019. SEUS Right Whale EWS Aerial Surveys 2017-18. Data downloaded from OBIS-SEAMAP (http://seamap.env.duke.edu/dataset/1992) on 2019-09-18 and 2021-03-04.

45. Happywhale. 2021. Happywhale - Atlantic White-sided Dolphin in North Atlantic Ocean. Data downloaded from OBIS-SEAMAP (http://seamap.env.duke.edu/dataset/1937) on 2019-09-18and originated from Happywhale.com.

46. Happywhale. 2021. Happywhale - Common Bottlenose Dolphin in North Atlantic Ocean. Data downloaded from OBIS-SEAMAP (http://seamap.env.duke.edu/dataset/1947) on 2019-09-18 and originated from Happywhale.com.

47. Harris, Lei E. 2015. DFO Maritimes Region Cetacean Sightings. Version 6 In OBIS Canada Digital Collections. Bedford Institute of Oceanography, Dartmouth, NS, Canada. Published by OBIS, Digital http://www.iobis.org/. Data downloaded from OBIS-SEAMAP (http://seamap.env.duke.edu/dataset/103152572) on 2019-09-18, 2019-10-11, and 2021-03-04.

48. Hartvedt, S. 2020. Incidental sightings of marine mammals. Data downloaded from OBIS-SEAMAP (http://seamap.env.duke.edu/dataset/103152572) on 2021-03-04 and originated from OBIS (https://obis.org/dataset/dd335e79-f580-44a1-bedc-1476437eb73e)

49. Hyrenbach, D. 2011. Hatteras Eddy Cruise 2004. Data downloaded from OBIS-SEAMAP (http://seamap.env.duke.edu/dataset/322) on 2019-09-18.

50. Hyrenbach, D. and H. Whitehead. 2008. Sargasso sperm whales 2004. Data downloaded from OBIS-SEAMAP (http://seamap.env.duke.edu/dataset/306) on 2021-03-04.

51. Hyrenbach, D. and H. Whitehead. 2013. Sargasso 2005 - cetacean sightings. Data downloaded from OBIS-SEAMAP (http://seamap.env.duke.edu/dataset/332) on 2019-09-18 and 2021-03-04.

52. Hyrenbach, D., F. Huettmann and J. Chardine. 2012. PIROP Northwest Atlantic 1965-1992. Data downloaded from OBIS-SEAMAP (http://seamap.env.duke.edu/dataset/280) on 2019-09-18 and 2021-03-04.

53. Johnston, D. and Z. Swaim. 2013. DUML vessel-based surveys for proposed JAX USWTR site 2009-2011. Data downloaded from OBIS-SEAMAP (http://seamap.env.duke.edu/dataset/582) on 2019-09-18.

54. Josephson, B. 2015. AMAPPS Northeast Aerial Cruise Fall 2012. Data downloaded from OBIS-SEAMAP (http://seamap.env.duke.edu/dataset/1245) on 2019-09-18 and 2021-03-04.

55. Josephson, B. 2015. AMAPPS Northeast Aerial Cruise Spring 2012. Data downloaded from OBIS-SEAMAP (http://seamap.env.duke.edu/dataset/1247) on 2019-09-18 and 2021-03-04.

56. Josephson, B. 2015. AMAPPS Northeast Aerial Cruise Summer 2010. Data downloaded from OBIS-SEAMAP (http://seamap.env.duke.edu/dataset/1249) on 2019-09-18 and 2021-03-04.

57. Josephson, B. 2015. AMAPPS Northeast Aerial Cruise Summer 2011. Data downloaded from OBIS-SEAMAP (http://seamap.env.duke.edu/dataset/1233) on 2019-09-18 and 2021-03-04.

58. Josephson, B. 2015. AMAPPS Northeast Aerial Cruise Winter 2011. Data downloaded from OBIS-SEAMAP (http://seamap.env.duke.edu/dataset/1243) on 2019-09-18.

59. Josephson, B. 2015. AMAPPS Northeast Shipboard Cruise Summer 2011. Data downloaded from OBIS-SEAMAP (http://seamap.env.duke.edu/dataset/1269) on 2019-09-18, 2019-10-11, and 2021-03-04.

60. Josephson, B. 2015. AMAPPS Northeast Shipboard Cruise Summer 2013. Data downloaded from OBIS-SEAMAP (http://seamap.env.duke.edu/dataset/1271) on 2019-09-18 and 2021-03-04.

61. Josephson, B. 2016. AMAPPS Northeast Aerial Cruise Spring 2014. Data downloaded from OBIS-SEAMAP (http://seamap.env.duke.edu/dataset/1379) on 2019-09-18.

62. Josephson, B. 2016. AMAPPS Northeast Aerial Cruise Winter 2014. Data downloaded from OBIS-SEAMAP (http://seamap.env.duke.edu/dataset/1381) on 2019-09-18.

63. Josephson, B. 2016. AMAPPS Northeast Shipboard Cruise Spring 2014. Data downloaded from OBIS-SEAMAP (http://seamap.env.duke.edu/dataset/1377) on 2019-09-18 and 2021-03-04.

64. Josephson, B. 2018. AMAPPS Northeast Aerial Cruise Summer 2016. Data downloaded from OBIS-SEAMAP (http://seamap.env.duke.edu/dataset/1676) on 2019-09-18 and 2021-03-04.

65. Josephson, B. 2018. AMAPPS Northeast Shipboard Cruise Summer 2016. Data downloaded from OBIS-SEAMAP (http://seamap.env.duke.edu/dataset/1678) on 2019-09-18 and 2021-03-04.

66. Josephson, B. and D. Palka. 2018. NEFSC Abundance of the Gulf of Maine and Bay of Fundy Harbor Porpoise Based on Aerial Surveys 1999. Data downloaded from OBIS-SEAMAP (http://seamap.env.duke.edu/dataset/1895) on 2019-09-18.

67. Josephson, B. and D. Palka. 2018. NEFSC Aerial Circle-Back Abundance Survey 2006. Data downloaded from OBIS-SEAMAP (http://seamap.env.duke.edu/dataset/1889) on 2019-09-18 and 2021-03-04.

68. Josephson, B. and D. Palka. 2018. NEFSC North Atlantic Marine Mammal and Turtle Aerial Abundance Survey 2007. Data downloaded from OBIS-SEAMAP (http://seamap.env.duke.edu/dataset/1891) on 2019-09-18 and 2021-03-04.

69. Josephson, B. and D. Palka. 2018. NEFSC Twin Otter Aerial Survey 2008. Data downloaded from OBIS-SEAMAP (http://seamap.env.duke.edu/dataset/1893) on 2019-09-18 and 2021-03-04.

70. Josephson, B. and L. Garrison. 2015. AMAPPS Southeast Aerial Cruise Fall 2012. Data downloaded from OBIS-SEAMAP (http://seamap.env.duke.edu/dataset/1288) on 2019-09-18.

71. Josephson, B. and L. Garrison. 2015. AMAPPS Southeast Aerial Cruise Spring 2012. Data downloaded from OBIS-SEAMAP (http://seamap.env.duke.edu/dataset/1259) on 2019-09-18 and 2021-03-04.

72. Josephson, B. and L. Garrison. 2015. AMAPPS Southeast Aerial Cruise Summer 2010. Data downloaded from OBIS-SEAMAP (http://seamap.env.duke.edu/dataset/1273) on 2019-09-18.

73. Josephson, B. and L. Garrison. 2015. AMAPPS Southeast Aerial Cruise Summer 2011. Data downloaded from OBIS-SEAMAP (http://seamap.env.duke.edu/dataset/1275) on 2019-09-18 and 2021-03-04.

74. Josephson, B. and L. Garrison. 2015. AMAPPS Southeast Aerial Cruise Winter 2011. Data downloaded from OBIS-SEAMAP (http://seamap.env.duke.edu/dataset/1277) on 2019-09-18 and 2021-03-04.

75. Josephson, B. and L. Garrison. 2015. AMAPPS Southeast Aerial Cruise Winter 2013. Data downloaded from OBIS-SEAMAP (http://seamap.env.duke.edu/dataset/1289) on 2019-09-18.

76. Kenney, R. 2013. BLM CETAP AIR Sightings. Data downloaded from OBIS-SEAMAP (http://seamap.env.duke.edu/dataset/283) on 2019-09-18, 2019-10-11, and 2021-03-04.

77. Kenney, R. 2013. BLM CETAP OPP Sightings. Data downloaded from OBIS-SEAMAP (http://seamap.env.duke.edu/dataset/284) on 2019-09-18, 2019-10-11, and 2021-03-04.

78. Kenney, R. 2013. BLM CETAP SHIP Sightings. Data downloaded from OBIS-SEAMAP (http://seamap.env.duke.edu/dataset/285) on 2019-09-18, 2019-10-11, and 2021-03-04.

79. Kopelman, A. 2013. Opportunistic marine mammal sightings from commercial whale watching vessels, Montauk, New York 1981-1994. Data downloaded from OBIS-SEAMAP (http://seamap.env.duke.edu/dataset/1006) on 2019-09-18 and 2021-03-04.

80. Kopelman, A. 2015. CRESLI marine mammal observations from whale watch cruises 2000-2014. Data downloaded from OBIS-SEAMAP (http://seamap.env.duke.edu/dataset/896) on 2019-09-18.

81. LaBrecque, E. 2011. Cape Hatteras 04-05. Data downloaded from OBIS-SEAMAP (http://seamap.env.duke.edu/dataset/298) on 2019-09-18 and 2021-03-04.

82. Lapolla, F. 2013. The Dolphin Project. Data downloaded from OBIS-SEAMAP (http://seamap.env.duke.edu/dataset/304) on 2019-09-18.

83. Lockhart, G. and S. Barco. 2017. Virginia aerial marine species monitoring 2016 by VAQF - Left side -. Data downloaded from OBIS-SEAMAP (http://seamap.env.duke.edu/dataset/1494) on 2019-09-18.

84. Lockhart, G. and S. Barco. 2017. Virginia aerial marine species monitoring 2016 by VAQF - Right side -. Data downloaded from OBIS-SEAMAP (http://seamap.env.duke.edu/dataset/1495) on 2019-09-18.

85. Mallette S.D., Lockhart G G., McAlarney R.J., Cummings E.W., Pabst D. A., McLellan W.A., Barco S.G. 2016. Offshore Energy Planning: Documenting Megafauna off Virginiaâ€™s Coast Using Aerial Surveys. VAQF Scientific Report. 2016-04.

86. Mallette S.D., Lockhart G G., McAlarney R.J., Cummings E.W., Pabst D. A., McLellan W.A., Barco S.G. 2016. Offshore Energy Planning: Documenting Megafauna off Virginiaâ€™s Coast Using Aerial Surveys. VAQF Scientific Report. 2016-04.

87. Maughan, B. and K. Arnold. 2010. UK Royal Navy Marine Mammal Observations. Data downloaded from OBIS-SEAMAP (http://seamap.env.duke.edu/dataset/64) on 2019-09-18.

88. McLellan, W. 2005. UNCW Aerial Survey 1998-1999. Data downloaded from OBIS-SEAMAP (http://seamap.env.duke.edu/dataset/272) on 2019-09-18 and 2021-03-04.

89. McLellan, W. 2006. UNCW Marine Mammal Sightings 1998-1999. Data downloaded from OBIS-SEAMAP (http://seamap.env.duke.edu/dataset/66) on 2019-09-18 and 2021-03-04.

90. McLellan, W. 2007. UNCW Marine Mammal Sightings 2002. Data downloaded from OBIS-SEAMAP (http://seamap.env.duke.edu/dataset/67) on 2019-09-18.

91. McLellan, W. 2010. UNCW Marine Mammal Sightings 2001. Data downloaded from OBIS-SEAMAP (http://seamap.env.duke.edu/dataset/65) on 2019-09-18.

92. McLellan, W. 2011. UNCW Aerial Surveys for monitoring of proposed Onslow Bay USWTR site - Left side -. Data downloaded from OBIS-SEAMAP (http://seamap.env.duke.edu/dataset/435) on 2019-09-18.

93. McLellan, W. 2011. UNCW Marine Mammal Aerial Surveys 2006-2007. Data downloaded from OBIS-SEAMAP (http://seamap.env.duke.edu/dataset/400) on 2019-09-18.

94. McLellan, W. 2011. UNCW Right Whale Aerial Survey 05-06. Data downloaded from OBIS-SEAMAP (http://seamap.env.duke.edu/dataset/360) on 2019-09-18 and 2021-03-04.

95. McLellan, W. 2011. UNCW USWTR JAX Aerial Surveys May - Oct 2010 - Left side. Data downloaded from OBIS-SEAMAP (http://seamap.env.duke.edu/dataset/687) on 2019-09-18 and 2021-03-04.

96. McLellan, W. 2011. UNCW USWTR JAX Aerial Surveys May - Oct 2010 - Right side. Data downloaded from OBIS-SEAMAP (http://seamap.env.duke.edu/dataset/688) on 2019-09-18.

97. McLellan, W. 2011. USWTR JAX Aerial Survey -Left side- 2009-2010. Data downloaded from OBIS-SEAMAP (http://seamap.env.duke.edu/dataset/590) on 2019-09-18.

98. McLellan, W. 2011. USWTR JAX Aerial Survey -Left side- 2010-2011. Data downloaded from OBIS-SEAMAP (http://seamap.env.duke.edu/dataset/745) on 2019-09-18.

99. McLellan, W. 2011. USWTR JAX Aerial Survey -Right side- 2010-2011. Data downloaded from OBIS-SEAMAP (http://seamap.env.duke.edu/dataset/747) on 2019-09-18 and 2021-03-04.

100. McLellan, W. 2011. USWTR Onslow Bay Aerial Survey -Left side- 2008-2010. Data downloaded from OBIS-SEAMAP (http://seamap.env.duke.edu/dataset/586) on 2019-09-18.

101. McLellan, W. 2011. USWTR Onslow Bay Aerial Survey -Left side- 2010-2011. Data downloaded from OBIS-SEAMAP (http://seamap.env.duke.edu/dataset/749) on 2019-09-18.

102. McLellan, W. 2011. USWTR Onslow Bay Aerial Survey -Right side- 2008-2010. Data downloaded from OBIS-SEAMAP (http://seamap.env.duke.edu/dataset/588) on 2019-09-18.

103. McLellan, W. 2011. USWTR Onslow Bay Aerial Survey -Right side- 2010-2011. Data downloaded from OBIS-SEAMAP (http://seamap.env.duke.edu/dataset/751) on 2019-09-18.

104. McLellan, W. 2012. USWTR JAX Aerial Survey -Left side- 2011-2012. Data downloaded from OBIS-SEAMAP (http://seamap.env.duke.edu/dataset/857) on 2019-09-18.

105. McLellan, W. 2012. USWTR JAX Aerial Survey -Right side- 2009-2010. Data downloaded from OBIS-SEAMAP (http://seamap.env.duke.edu/dataset/592) on 2019-09-18.

106. McLellan, W. 2012. USWTR JAX Aerial Survey -Right side- 2011-2012. Data downloaded from OBIS-SEAMAP (http://seamap.env.duke.edu/dataset/859) on 2019-09-18.

107. McLellan, W. 2013. UNCW Aerial Surveys for monitoring of proposed Onslow Bay USWTR site - Right side -. Data downloaded from OBIS-SEAMAP (http://seamap.env.duke.edu/dataset/437) on 2019-09-18.

108. McLellan, W. 2013. UNCW Right Whale Aerial Surveys 2008. Data downloaded from OBIS-SEAMAP (http://seamap.env.duke.edu/dataset/464) on 2019-09-18 and 2021-03-04.

109. McLellan, W. 2014. AFAST Hatteras Aerial Survey -Left side- 2011-2012. Data downloaded from OBIS-SEAMAP (http://seamap.env.duke.edu/dataset/851) on 2019-09-18 and 2021-03-04.

110. McLellan, W. 2014. AFAST Hatteras Aerial Survey -Right side- 2011-2012. Data downloaded from OBIS-SEAMAP (http://seamap.env.duke.edu/dataset/855) on 2019-09-18 and 2021-03-04.

111. McLellan, W. 2014. AFTT Hatteras Aerial Survey -Left side- 2012-2013. Data downloaded from OBIS-SEAMAP (http://seamap.env.duke.edu/dataset/1138) on 2019-09-18 and 2021-03-04.

112. McLellan, W. 2014. AFTT Hatteras Aerial Survey -Right side- 2012-2013. Data downloaded from OBIS-SEAMAP (http://seamap.env.duke.edu/dataset/1140) on 2019-09-18 and 2021-03-04.

113. McLellan, W. 2014. AFTT JAX Aerial Survey -Left side- 2012-2013. Data downloaded from OBIS-SEAMAP (http://seamap.env.duke.edu/dataset/1128) on 2019-09-18.

114. McLellan, W. 2014. AFTT JAX Aerial Survey -Right side- 2012-2013. Data downloaded from OBIS-SEAMAP (http://seamap.env.duke.edu/dataset/1136) on 2019-09-18.

115. McLellan, W. 2015. AFTT Cape Hatteras Aerial Survey -Left side- 2014. Data downloaded from OBIS-SEAMAP (http://seamap.env.duke.edu/dataset/1237) on 2019-09-18 and 2021-03-04.

116. McLellan, W. 2015. AFTT Cape Hatteras Aerial Survey -Right side- 2014. Data downloaded from OBIS-SEAMAP (http://seamap.env.duke.edu/dataset/1235) on 2019-09-18 and 2021-03-04.

117. McLellan, W. 2015. AFTT JAX Aerial Survey -Left side- 2014. Data downloaded from OBIS-SEAMAP (http://seamap.env.duke.edu/dataset/1241) on 2019-09-18.

118. McLellan, W. 2015. AFTT JAX Aerial Survey -Right side- 2014. Data downloaded from OBIS-SEAMAP (http://seamap.env.duke.edu/dataset/1239) on 2019-09-18 and 2021-03-04.

119. McLellan, W. 2016. UNCW Hatteras Aerial Survey - Left side - 2015. Data downloaded from OBIS-SEAMAP (http://seamap.env.duke.edu/dataset/1350) on 2019-09-18 and 2021-03-04.

120. McLellan, W. 2016. UNCW Hatteras Aerial Survey - Right side - 2015. Data downloaded from OBIS-SEAMAP (http://seamap.env.duke.edu/dataset/1352) on 2019-09-18 and 2021-03-04.

121. McLellan, W. 2016. UNCW JAX Aerial Survey - Left side - 2015. Data downloaded from OBIS-SEAMAP (http://seamap.env.duke.edu/dataset/1362) on 2019-09-18.

122. McLellan, W. 2016. UNCW JAX Aerial Survey - Right side - 2015. Data downloaded from OBIS-SEAMAP (http://seamap.env.duke.edu/dataset/1364) on 2019-09-18.

123. McLellan, W. 2016. UNCW Norfolk Canyon Aerial Survey - Left side - 2015. Data downloaded from OBIS-SEAMAP (http://seamap.env.duke.edu/dataset/1354) on 2019-09-18 and 2021-03-04.

124. McLellan, W. 2016. UNCW Norfolk Canyon Aerial Survey - Right side - 2015. Data downloaded from OBIS-SEAMAP (http://seamap.env.duke.edu/dataset/1356) on 2019-09-18 and 2021-03-04.

125. McLellan, W. 2016. UNCW PAX Aerial Survey - Left side - 2015. Data downloaded from OBIS-SEAMAP (http://seamap.env.duke.edu/dataset/1358) on 2019-09-18.

126. McLellan, W. 2016. UNCW PAX Aerial Survey - Right side - 2015. Data downloaded from OBIS-SEAMAP (http://seamap.env.duke.edu/dataset/1360) on 2019-09-18.

127. McLellan, W. 2017. UNCW Hatteras Aerial Survey - Left side - 2016. Data downloaded from OBIS-SEAMAP (http://seamap.env.duke.edu/dataset/1471) on 2019-09-18 and 2021-03-04.

128. McLellan, W. 2017. UNCW Hatteras Aerial Survey - Right side - 2016. Data downloaded from OBIS-SEAMAP (http://seamap.env.duke.edu/dataset/1473) on 2019-09-18 and 2021-03-04.

129. McLellan, W. 2017. UNCW JAX Aerial Survey - Left side - 2016. Data downloaded from OBIS-SEAMAP (http://seamap.env.duke.edu/dataset/1475) on 2019-09-18.

130. McLellan, W. 2017. UNCW JAX Aerial Survey - Right side - 2016. Data downloaded from OBIS-SEAMAP (http://seamap.env.duke.edu/dataset/1477) on 2019-09-18.

131. McLellan, W. 2017. UNCW Norfolk Canyon Aerial Survey - Left side - 2016. Data downloaded from OBIS-SEAMAP (http://seamap.env.duke.edu/dataset/1479) on 2019-09-18 and 2021-03-04.

132. McLellan, W. 2017. UNCW Norfolk Canyon Aerial Survey - Right side - 2016. Data downloaded from OBIS-SEAMAP (http://seamap.env.duke.edu/dataset/1481) on 2019-09-18 and 2021-03-04.

133. McLellan, W. 2017. UNCW PAX Aerial Survey - Left side - 2017. Data downloaded from OBIS-SEAMAP (http://seamap.env.duke.edu/dataset/1652) on 2019-09-18.

134. McLellan, W. 2017. UNCW PAX Aerial Survey - Right side - 2017. Data downloaded from OBIS-SEAMAP (http://seamap.env.duke.edu/dataset/1654) on 2019-09-18.

135. McLellan, W. 2018. UNCW Hatteras Aerial Survey -Left side- 2017. Data downloaded from OBIS-SEAMAP (http://seamap.env.duke.edu/dataset/1668) on 2019-09-18 and 2021-03-04.

136. McLellan, W. 2018. UNCW Hatteras Aerial Survey -Right side- 2017. Data downloaded from OBIS-SEAMAP (http://seamap.env.duke.edu/dataset/1670) on 2019-09-18 and 2021-03-04.

137. McLellan, W. 2018. UNCW JAX Aerial Survey -Left side- 2017. Data downloaded from OBIS-SEAMAP (http://seamap.env.duke.edu/dataset/1662) on 2019-09-18 and 2021-03-04.

138. McLellan, W. 2018. UNCW JAX Aerial Survey -Right side- 2017. Data downloaded from OBIS-SEAMAP (http://seamap.env.duke.edu/dataset/1664) on 2019-09-18.

139. McLellan, W. 2018. UNCW Norfolk Canyon Aerial Survey -Left side- 2017. Data downloaded from OBIS-SEAMAP (http://seamap.env.duke.edu/dataset/1672) on 2019-09-18 and 2021-03-04.

140. McLellan, W. 2018. UNCW Norfolk Canyon Aerial Survey -Right side- 2017. Data downloaded from OBIS-SEAMAP (http://seamap.env.duke.edu/dataset/1674) on 2019-09-18 and 2021-03-04.

141. McLellan, W. 2018. UNCW PAX Aerial Survey - Left side - 2016. Data downloaded from OBIS-SEAMAP (http://seamap.env.duke.edu/dataset/1797) on 2019-09-18.

142. McLellan, W. 2018. UNCW PAX Aerial Survey - Right side - 2016. Data downloaded from OBIS-SEAMAP (http://seamap.env.duke.edu/dataset/1799) on 2019-09-18.

143. NEFSC. 2018. 2017 Annual Report of a Comprehensive Assessment of Marine Mammal, Marine Turtle, and Seabird Abundance and Spatial Distribution in US waters of the Western North Atlantic Ocean – AMAPPS II. Annual Report. Available at: https://www.fisheries.noaa.gov/resource/publication-database/atlantic-marine-assessment-program-protected-species.

144. NEFSC. 2020. 2019 Annual Report of a Comprehensive Assessment of Marine Mammal, Marine Turtle, and Seabird Abundance and Spatial Distribution in US waters of the Western North Atlantic Ocean – AMAPPS II. Annual Report. TO BE PUBLISHED.

145. NEFSC. 2020. 2019 Annual Report of a Comprehensive Assessment of Marine Mammal, Marine Turtle, and Seabird Abundance and Spatial Distribution in US waters of the Western North Atlantic Ocean – AMAPPS II. Annual Report. TO BE PUBLISHED.

146. Normandeau Associates and APEM data prepared for New York State Energy Research and Development Authority. 2019. Digital Aerial Baseline Survey of Marine Wildlife in Support of Offshore Wind Energy. NYSERDA.

147. Osman, R. 2011. A Biological Survey of the Waters of Woods Hole and Vacinity. Data downloaded from OBIS-SEAMAP (http://seamap.env.duke.edu/dataset/103150230) on 2019-10-11 and originated from iOBIS (http:www.iobis.org).

148. Palka, D. 2011. NEFSC 1995 AJ9501 (Part I). Data downloaded from OBIS-SEAMAP (http://seamap.env.duke.edu/dataset/56) on 2019-09-18 and 2021-03-04.

149. Palka, D. 2013. Harbor Porpoise Survey 1992 (AJ92-01). Data downloaded from OBIS-SEAMAP (http://seamap.env.duke.edu/dataset/302) on 2019-09-18.

150. Palka, D. 2013. NEFSC 1995 AJ9501 (Part II). Data downloaded from OBIS-SEAMAP (http://seamap.env.duke.edu/dataset/290) on 2019-09-18.

151. Palka, D. 2013. NEFSC 1995 pe9501. Data downloaded from OBIS-SEAMAP (http://seamap.env.duke.edu/dataset/296) on 2019-09-18 and 2021-03-04.

152. Palka, D. 2013. NEFSC 1995 pe9502. Data downloaded from OBIS-SEAMAP (http://seamap.env.duke.edu/dataset/294) on 2019-09-18 and 2021-03-04.

153. Palka, D. 2013. NEFSC 1999 aj9902. Data downloaded from OBIS-SEAMAP (http://seamap.env.duke.edu/dataset/300) on 2019-09-18 and 2019-10-11.

154. Palka, D. 2013. NEFSC Aerial Circle-Back Abundance Survey 2004. Data downloaded from OBIS-SEAMAP (http://seamap.env.duke.edu/dataset/398) on 2019-09-18.

155. Palka, D. 2013. NEFSC Aerial Survey - Experimental 2002. Data downloaded from OBIS-SEAMAP (http://seamap.env.duke.edu/dataset/107) on 2019-09-18 and 2021-03-04.

156. Palka, D. 2013. NEFSC Aerial Survey - Summer 1995. Data downloaded from OBIS-SEAMAP (http://seamap.env.duke.edu/dataset/109) on 2019-09-18 and 2021-03-04.

157. Palka, D. 2013. NEFSC Aerial Survey - Summer 1998. Data downloaded from OBIS-SEAMAP (http://seamap.env.duke.edu/dataset/113) on 2019-09-18 and 2021-03-04.

158. Palka, D. 2013. NEFSC Deepwater Marine Mammal 2002. Data downloaded from OBIS-SEAMAP (http://seamap.env.duke.edu/dataset/292) on 2019-09-18 and 2021-03-04.

159. Palka, D. 2013. NEFSC Harbor Porpoise 1991. Data downloaded from OBIS-SEAMAP (http://seamap.env.duke.edu/dataset/288) on 2019-09-18 and 2021-03-04.

160. Palka, D. 2013. NEFSC Mid-Atlantic Marine Mammal Abundance Survey 2004. Data downloaded from OBIS-SEAMAP (http://seamap.env.duke.edu/dataset/396) on 2019-09-18 and 2021-03-04.

161. Palka, D. 2013. NEFSC Survey 1997. Data downloaded from OBIS-SEAMAP (http://seamap.env.duke.edu/dataset/58) on 2019-09-18 and 2021-03-04.

162. Palka, D. 2013. NEFSC Survey 1998 1. Data downloaded from OBIS-SEAMAP (http://seamap.env.duke.edu/dataset/60) on 2019-09-18 and 2021-03-04.

163. Palka, D. 2013. NEFSC Survey 1998 2. Data downloaded from OBIS-SEAMAP (http://seamap.env.duke.edu/dataset/62) on 2019-09-18 and 2021-03-04.

164. Palka, D. 2014. NEFSC Survey 1991. Data downloaded from OBIS-SEAMAP (http://seamap.env.duke.edu/dataset/111) on 2019-09-18.

165. Rappucci, G. and L. Garrison. 2019. SEFSC GoMMAPPS 2017 Summer Aerial Survey. Data downloaded from OBIS-SEAMAP (http://seamap.env.duke.edu/dataset/1970) on 2019-09-18.

166. Rappucci, G. and L. Garrison. 2019. SEFSC GoMMAPPS 2018 Fall Aerial Survey. Data downloaded from OBIS-SEAMAP (http://seamap.env.duke.edu/dataset/1972) on 2019-09-18.

167. Read, A. 2011. Duke Cherry Point PopUps 2005-2006 Bottlenose dolphin whistle presence. Data downloaded from OBIS-SEAMAP (http://seamap.env.duke.edu/dataset/567) on 2019-09-18.

168. Smith, A. 2014. Mystic Aquarium's marine mammal and sea turtle stranding data 1976-2011. Data downloaded from OBIS-SEAMAP (http://seamap.env.duke.edu/dataset/945) on 2019-09-18 and 2021-03-04.

169. Speakman, T. 2011. NOAA Atlantic bottlenose dolphin sightings in the coastal and estuarine waters near Charleston, SC - 1994-2011. Data downloaded from OBIS-SEAMAP (http://seamap.env.duke.edu/dataset/737) on 2019-09-18.

170. Spontak, D. 2012. JAX ASWEX Aerial Monitoring 2011. Data downloaded from OBIS-SEAMAP (http://seamap.env.duke.edu/dataset/868) on 2019-09-18.

171. Spontak, D. 2012. JAX MAVEX Aerial Monitoring 2012. Data downloaded from OBIS-SEAMAP (http://seamap.env.duke.edu/dataset/875) on 2019-09-18.

172. Spontak, D. 2012. JAX MISSILEX Aerial Monitoring 2010. Data downloaded from OBIS-SEAMAP (http://seamap.env.duke.edu/dataset/874) on 2019-09-18.

173. Spontak, D. 2012. JAX SEASWITI Aerial Monitoring 2010 . Data downloaded from OBIS-SEAMAP (http://seamap.env.duke.edu/dataset/866) on 2019-09-18.

174. Spontak, D. 2012. JAX SEASWITI Vessel Monitoring 2010. Data downloaded from OBIS-SEAMAP (http://seamap.env.duke.edu/dataset/867) on 2019-09-18.

175. Spontak, D. 2012. VACAPES ASWEX Aerial Monitoring 2011. Data downloaded from OBIS-SEAMAP (http://seamap.env.duke.edu/dataset/869) on 2019-09-18.

176. Spontak, D. 2012. VACAPES FIREX Aerial Monitoring 2011. Data downloaded from OBIS-SEAMAP (http://seamap.env.duke.edu/dataset/871) on 2019-09-18.

177. Spontak, D. 2013. JAX GUNEX Aerial Monitoring Surveys October 2010. Data downloaded from OBIS-SEAMAP (http://seamap.env.duke.edu/dataset/893) on 2019-09-18.

178. Spontak, D. 2013. JAX MAVEX September 2012. Data downloaded from OBIS-SEAMAP (http://seamap.env.duke.edu/dataset/895) on 2019-09-18.

179. Spontak, D. 2013. NSN Monitoring for Pier 1 Upgrades 2011-2012. Data downloaded from OBIS-SEAMAP (http://seamap.env.duke.edu/dataset/894) on 2019-09-18.

180. Spontak, D. 2013. VACAPES FIREX and ASW Aerial Monitoring 2010. Data downloaded from OBIS-SEAMAP (http://seamap.env.duke.edu/dataset/870) on 2019-09-18.

181. Spontak, D. 2013. VACAPES MISSELEX Aerial Monitoring March 2013. Data downloaded from OBIS-SEAMAP (http://seamap.env.duke.edu/dataset/1017) on 2019-09-18.

182. Spontak, D. 2014. Norfolk/VA Beach MINEX Vessel Surveys. Data downloaded from OBIS-SEAMAP (http://seamap.env.duke.edu/dataset/1072) on 2019-09-18.

183. Spontak, D. 2014. Norfolk/VA Beach Photo-ID Surveys Aug 2012-Sep 2013. Data downloaded from OBIS-SEAMAP (http://seamap.env.duke.edu/dataset/1166) on 2019-09-18.

184. Spontak, D. 2015. Norfolk/VA Beach Inshore Vessel Surveys Nov 2012- Nov 2013. Data downloaded from OBIS-SEAMAP (http://seamap.env.duke.edu/dataset/1071) on 2019-09-18.

185. Swaim, Z. 2016. DUML vessel-based photo-id and biopsy surveys for proposed JAX USWTR site 2012-2015. Data downloaded from OBIS-SEAMAP (http://seamap.env.duke.edu/dataset/906) on 2019-09-18.

186. Swaim, Z. 2016. DUML vessel-based photo-id and biopsy surveys in Onslow Bay CHPT OPAREA 2011-2015. Data downloaded from OBIS-SEAMAP (http://seamap.env.duke.edu/dataset/902) on 2019-09-18.

187. Swaim, Z. 2016. DUML vessel-based photo-id and biopsy surveys in VACAPES OPAREA off Hatteras 2009, 2011-2015. Data downloaded from OBIS-SEAMAP (http://seamap.env.duke.edu/dataset/907) on 2019-09-18 and 2021-03-04.

188. Taylor, J. 2015. Bottlenose dolphins off Outer Banks 2007-2012. Data downloaded from OBIS-SEAMAP (http://seamap.env.duke.edu/dataset/837) on 2019-09-18.

189. Urian, K. 2013. DUML New River surveys on the occurrence, distribution and density of marine mammals in Camp Lejeune 2010-2011. Data downloaded from OBIS-SEAMAP (http://seamap.env.duke.edu/dataset/959) on 2019-09-18.

190. Urian, K. 2013. DUML surveys for the stock discrimination of bottlenose dolphins along the Outer Banks of North Carolina 2011-2012. Data downloaded from OBIS-SEAMAP (http://seamap.env.duke.edu/dataset/1010) on 2019-09-18.

191. Urian, K. 2013. DUML vessel-based line transect surveys for proposed Onslow Bay USWTR site 2007-2010. Data downloaded from OBIS-SEAMAP (http://seamap.env.duke.edu/dataset/433) on 2019-09-18.

192. Urian, K. 2014. DUML coastal surveys on the occurrence, distribution and density of marine mammals in Camp Lejeune 2010-2013. Data downloaded from OBIS-SEAMAP (http://seamap.env.duke.edu/dataset/957) on 2019-09-18.

193. Vukovich, M. 2018. Digital Aerial Baseline Survey of Marine Wildlife in Support of Offshore Wind Energy - OPA 2016. Data downloaded from OBIS-SEAMAP (http://seamap.env.duke.edu/dataset/1817) on 2019-09-18 and 2021-03-04.

194. Vukovich, M. 2019. Digital Aerial Baseline Survey of Marine Wildlife in Support of Offshore Wind Energy - OPA 2017. Data downloaded from OBIS-SEAMAP (http://seamap.env.duke.edu/dataset/1994) on 2019-09-18 and 2021-03-04.

195. Whitt, A. 2015. Marine mammal records of Cuba. Data downloaded from OBIS-SEAMAP (http://seamap.env.duke.edu/dataset/1190) on 2019-10-11.

196. Wolff, N. 2011. Aerial survey of upper trophic level predators on PLatts Bank, Gulf of Maine. Data downloaded from OBIS-SEAMAP (http://seamap.env.duke.edu/dataset/103150267) on 2019-09-18 and originated from iOBIS (http:www.iobis.org).

197. Woolmer, G. 2013. Historical distribution of whales shown by logbook records 1785-1913. Data downloaded from OBIS-SEAMAP (http://seamap.env.duke.edu/dataset/885) on 2021-03-04.